5-2012

Computer Modeling of the Influence of Structure Plan Areas on Tornado Forces

Nashmi Hassan M Alrasheedi
University of Arkansas, Fayetteville

Computer Modeling of the Influence of Structure Plan Areas on Tornado Forces

Computer Modeling of the Influence of Structure Plan Areas on Tornado Forces

A dissertation submitted in partial fulfillment
of the requirements for the degree of
Doctor of Philosophy in Mechanical Engineering

By
Nashmi Hassan Alrasheedi
King Saud University
Bachelor of Science in Mechanical Engineering, 2005
California State University-Fullerton
Master of Science in Mechanical Engineering, 2009

May 2012
University of Arkansas

ABSTRACT

The study of the conventional Straight Line (SL) wind flow dominates research into wind loads on structures. Most structure design takes into account only research into SL flow. Few researchers have studied tornado forces on buildings and attempted to distinguish between tornadic wind loads and SL flow loads. Using a computer simulation, this research addresses and distinguishes between the tornadic forces and SL forces on structures. In the numerical simulation, tornado forces and SL forces will be compared on large structure plan areas and on thin structure plan areas. Additionally this research investigates how the increase in the vortex strength (α) affects tornado forces on a cubic structure. The large structure plan areas are dimensionalized by the structure height: (1h x 1h, 2h x 2h, 4h x 4h and 8h x 8h) where h is 20.3 (m) and tornado maximum radius (r_{max}) is 61(m). The structure plan areas are a multiple of factor two. The thin structure plan areas are obtained by dividing the large structure plan areas by a factor of ten.

This research has three key findings. First, when the same maximum reference velocity ($V_{trans.}$) was used and when the large structure plan area characteristic length was approximately twice the tornado maximum diameter, the force and pressure coefficients had the same values as Straight Line (SL) flow. Second, the thin structure plan areas are more likely collapse faster in the presence of a tornado compared to SL flow due to the high differentials pressure in tornado between the windward wall and the leeward wall. In addition, on the thin structure plan areas, the tornado force coefficients were twice the SL flow force coefficients. The final key finding is that when the vortex strength (α) increased, the tornado force coefficients increased exponentially.

Keywords: Tornado, LES, Structure plan areas, vortex strength, forces, structures, SL flow

This dissertation is approved for recommendation
to the Graduate Council.

Dissertation Director:

_____
Dr. R. Panneer Selvam

Dissertation Committee:

_____
Dr. Rick J. Couvillion

_____
Dr. Darin W. Nutter

_____
Dr. Uchechukwu C. Wejinya

_____
Dr. Richard A. Coffman

DISSERTATION DUPLICATION RELEASE

I hereby authorize the University of Arkansas Libraries to duplicate this dissertation when needed for research and/or scholarship.

Agreed _____

Nashmi Hassan Alrasheedi

Refused _____

Nashmi Hassan Alrasheedi

ACKNOWLEDGMENTS

First, special thanks to my advisor Prof. R. Panneer Selvam for his guidance and his inspiration in the completion of this dissertation. In addition, his generous support Fall 2010 and Spring 2011 was appreciated. I am very pleased to have an advisor who has the knowledge and enthusiasm to make this dissertation unique, and allow me to contribute a new idea to the field of wind engineering. His inspiration throughout the past two years has largely impacted what I have achieved. I am confident to say his support has been invaluable. Thanks for introducing me to the wonderful field of computation and allow me to contribute a new idea to the field of wind engineering.

Second, special thanks to the dissertation committee members: Dr. Rick J. Couvillion, Dr. Darin W. Nutter, Dr. Uchechukwu C. Wejinya and Dr. Richard A. Coffman. Their time spent reviewing and commenting on the first part of this research enhanced the quality of this dissertation.

Third, special thanks to the University of Arkansas Quality Writing Center and especially Ramey Moore whose assistance in revising was enlightening.

Fourth, special thanks to my lab mates Scott Ragan and Matt Strasser for their wonderful friendship and help throughout the year of 2011 and 2012.

Five, special thanks to the government of Saudi Arabia for their financial support through my Master and Doctoral Degrees.

Finally, special thanks to my family and friends. Thank you, Mom, brothers, and sisters for your support and love. Special thanks to my oldest brother: Swealim Hassan Alrasheedi whose financial, emotional and mental support was a key to my current success.

TABLE OF CONTENTS

LIST OF TABLES

LIST OF FIGURES

NOMENCLATURE

A	The projected cross-sectional area
P	computed pressure in time
t	Time
Cp	Pressure coefficient
Cx	Force coefficient in the x-direction
Cy	Force coefficient in the y-direction
Cz	Force coefficient in the z-direction
Fx	Force in the x-direction
Fy	Force in the y-direction
Fz	Force in the z-direction
P_{ref}	Reference pressure
r_{max}	Tornado inner maximum core radius
u*	Frictional velocity
V_x	Velocity component in the x-direction
V_y	Velocity component in the y-direction
V_θ	Tangential velocity component
$V_{trans.}$	Translation velocity component
V_{max}	Maximum velocity component in tornado
z_0	Ground roughness length
Zf	Building height
LSPA	Large structure plan area
TSPL	Thin structure plan area

SPA	Structure plan area
LSPACLR	Large structure plan area characteristic length ratio
LSPACDL	Large structure plan areas characteristic diagonal length
TSPACLR	Thin structure plan area characteristic length ratio
TSPACDL	Thin structure plan areas characteristic diagonal length
TMCD	Tornado maximum characteristic diameter
ρ	Air density
α	Vortex strength
β	Tornado angle of attack

CHAPTER 1

INTRODUCTION

1.1 INTRODUCTION

Every year in the United States, billions of dollars of property damages, and rebuilding and reparation expenditures are associated with tornados. A major challenge of mitigating tornado damages is a properly understanding the forces created on a structure as a result of a tornado. Frequently, these forces produced within a tornado are from a combination of translational and rotational velocities. The tornado is defined as a column of air which has a short life span, a violent rotating vortex and high translating wind speed. The column of air can be visible as a variably shaped and sized funnel, which stretches from the parent cloud to the ground (Davies-Jones, 1986). The shape of the funnel is classified as a thin rope-like profile, a large cone-shaped profile or multiple vortices spinning around a center axis (Davies-Jones, 1986). Ying and Chang (1970) in the earlier study of tornado like vortices identified five useful tornado features in terms of fluid dynamics if:

1. a tornado appears as a huge vortex column of air which has low pressure and moves along the ground with centrifugal force and high rotational velocity;
2. the tornado vortex circulation is sustained not only by the earth's Coriolis force but also by the cloud's rotations;
3. a low density near the ground surface formed from the warm humid air causes the updraft in the tornado vortex core. The reverse condensation flow is visualized as column of air;

4. an inward circulation of the warm humid air resides in the ground boundary layer and is sucked towards the vortex core base where the pressure drops significantly. Most tornado damage occurs inside this highly turbulent layer;
5. the main wind, normally at the mid-tropospheric level, drives the rotating clouds tilting the tornado vortex column forward. A tension along the vortex develops through a pulling process as pressure drops in the core;

Tornado funnels appear in different sizes and shapes during tornado life cycle. Davies-Jones (1986) describes the life cycle of a tornado in five stages if:

1. the initial indication of noticeable rotation is called the dust-whirl stage, when a funnel pendant extends from the cloud base and the dust rises from the ground. There is a light damage in this stage;
2. the increase of the tornado intensity and the movement of the funnel to the surface make up the organizing stage;
3. the funnel's vertical extension with a maximum width is defined the mature stage. There is an intense damage in this stage;
4. the decay in the funnel width and increase in the funnel slope characterize the shrinking stage. A small damage belt is in this stage;
5. in the decay stage the vertical shear and drag surface stretch the vortex into a rope shape; Before dissipating, the funnel becomes significantly distorted;

Past research has focused on the influence of tornado forces on single structure plan areas, such as gable-roofed structures, rectangular structures, and cubic or tall buildings interacting with a translating or a stationary vortex. Selvam and Millett (2003, and 2005) have pioneered recent work on computer modeling simulations of tornado-interaction with a cubic

structure. They have shown by using computer visualization that the tornado produced twice the force coefficient on the cubic structure roof compared to the SL wind flow. On the other hand, Iowa State University (ISU) group has a laboratory simulator, which can simulate a translating tornado. The ISU group has investigated in the laboratory the interaction between a translating tornado and low rise gabled- roofed structure or tall structure with surrounding influence (Yang et al. 2009, Zang and Sarkar, 2010, Hann et al., 2010, and Hu et al., 2011). Their study has shown that the tornado produced twice to three times the force coefficient on the structure roof compared to the SL flow.

Until now in the literature (see Chapter 2), no one has attempted to study the interaction of a tornado with different structure plan areas which leaves several questions unanswered. 1. What would happen to the tornado forces on a structure with a plan area larger than the tornado size? 2. Do we expect the force and pressure coefficients to be higher, the same, or less than the SL wind loads? 3. Does the structure with large plan area subjected to higher force coefficients versus the thin (tall) structure plan areas? For these reasons, a numerical simulation will be conducted to study in detail the interaction of a tornado on these types of structures.

1.2 MOTIVATION AND OBJECTIVES

The past research has focused on gable-roofed, cubic or tall buildings interacting with a translating or a stationary vortex. It has been shown by the Computational Fluid Dynamic (CFD) group at the University of Arkansas (UofA), as well as researched at: Tokyo Polytechnic University (TPU), Oklahoma State University (OSU), Texas Tech University (TTU), and Iowa State University (ISU) that tornado forces on a structure are different from SL flow. The ISU group has investigated in the laboratory the interaction of a translating tornado with a structure (Yang et al., 2009, Zang and Sarkar, 2010, Hann et al., 2010, Thampi et al., 2010, Thampi et al.,

2011, and Hu et al., 2011). OSU, TPU and TTU have studied in tornado simulators the interaction of a stationary vortex with a structure (Sabareesh et.al 2009, Jischke et al, 1983, and Mishra et al., 2008a, 2008b). The CFD group has simulated the interaction of a translating tornado with a single structure (Wilson 1977, Selvam 1993, Selvam, 2002 a, Selvam et.al 2002b, Selvam and Millett, 2003, and Selvam and Millett 2005).

A literature review of Tornado-Structure Interaction (TSI) shows that a tornado creates two to three times the updraft force on a structure roof compare to SL wind. The investigations were for a tornado size larger than the structure. Therefore, an interaction of a tornado with different structure plan areas has not previously been studied as shown in the literature review (Chapter 2). It must also be noticed that no one has attempted to study the interaction of a tornado smaller than the structure plan area. The current literature review of TSI lacks the following:

1. Studying tornado forces on different structure plan areas.
2. Changing tornado parameters such as tornado angle of attack (β) and tornado vortex strength (α) for a fixed tornado size and studying the effect of these parameters on tornado force coefficients on different structure plan areas.
3. Comparing SL wind loads coefficients to tornado wind force coefficients for different structure plan areas.
4. Using the same maximum reference velocity in SL wind and tornado-like flow vortex to compare force coefficients on different structure plan areas.

Therefore, there is a need for studying tornado-interaction on different structure plan areas to examine tornado induced loads on these structures. A numerical simulation will carry out to investigate tornado wind loads on different structures plan areas and compare to the SL

flow. This research might lead us to save lives and mitigate tornado damages to structures. The following ideas are addressed in this research:

1. To study tornado forces on a flat roof structure. The structure has square plan areas ranging from 0.1h x 0.1h to 8h x 8h where h is the structure height. Tornado force coefficients will compare to SL force coefficients on the following structures plan areas:
    - Large structure plan areas (1h x 1h, 2h x 2h, 4h x 4h, and 8h x 8h)
    - Small structure plan areas (0.1h x 0.1h, 0.2h x 0.2h, 0.4h x 0.4h, and 0.8h x 0.8h)
2. To use the same maximum translating reference velocity in the SL wind and in the tornado-like flow vortex on these structure plan areas and compare tornado force coefficients to the SL force coefficients.
3. To change the tornado vortex strength (α) and study tornado forces on a cubic structure.

1.3 DISSERTATION ORGANIZATION

This dissertation is divided into eight chapters. Chapter 1 is an introduction and overview of the proposed research. Chapter 2 is a literature review on the past and current research on tornado forces on a structure. Chapter 3 discusses some of the existence of tornado mathematical models. Chapter 4 studies the effect of computational domain size changes on tornado forces. Chapter 5 discusses the influence of tornado forces on large structure plan areas and compares tornado force coefficients to SL flow force coefficient. Chapter 6 discusses the influence of tornado forces on thin structure plan areas and compares tornado force coefficients to SL flow force coefficient. Chapter 7 presents a discussion on how the vortex strength affects tornado forces on a structure. Chapter 8 summarizes the work that has been conducted in this research and provides a recommendation for future work.

CHAPTER 2

LITERATURE REVIEW

2.1 INTRODUCTION

Tornado model and Tornado-Structure Interaction (TSI) have been investigated by numerical simulations and laboratory simulators. Tornado models will be reviewed first and a discussion of TSI will follow. Many researchers were able to recreate the characteristics of a real tornado by using a computer model or in tornado laboratory simulators, as will be discussed in the first section in this chapter. Once a characteristic of a tornado was achieved either by numerical simulations or in laboratory simulators, a structure can be placed in the simulator or in the computational domain to study tornado forces on the structure.

The second part of the review begins by discussing the structure dynamic response due to a tornado interaction, the TSI in laboratory simulators and the TSI by using a computer modeling. The dynamic response of the structure was studied by using Finite Element Methods (FEM). Most of the TSI simulated in tornado simulators were for a stationary vortex. A scaled model was placed at different positions with respect to the tornado vortex. However, recently, at ISU, a translating tornado was simulated in the laboratory simulator. They studied TSI on a gable-roofed structure, gable-roofed structure with surrounding influence, and a high rise building. Velocities were measured by a digital particle image velocimetry, and force and moment were measured by high sensitivity load cells. The TSI is also studied by using numerical simulations. A translating tornado interaction with a structure is only modeled numerically by our Computational Mechanics Laboratory (CML) group at the University of Arkansas. The following flow chart illustrates the outline of literature reviews as show in Fig.2.1.

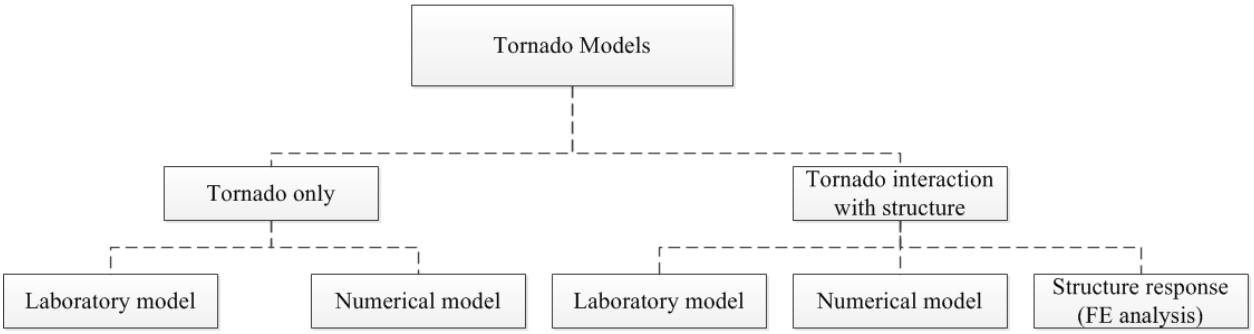

Figure 2.1 Literature review flow chart

2.2 TORNADO LABORATORY MODEL

Tornado experimental models have been refined in the past half century. Ying and Chang (1970) were the first researchers to simulate a tornado in the laboratory. Their model has a rotating screen at the top to produce the circulation and a suction fan to produce the updraft as shown in Fig.2.2. The mass of air passes through the rotating screen generates velocities components (tangential and rotational). The tornado-like vortex was generated by combining circulation, ground surface and tangential velocity together. Circulation strength was controlled by the speed of the rotating screen and the updraft was controlled by the amount of air passes through the suction fan. The distribution of the pressure and velocity was not accurate because of the core vortex was not stationary. Their model has the ability to capture a tornado-like vortex near the ground surface. Two years later Ward (1972) proposed a new tornado simulator which is similar to Ying's and Chang's (1970) tornado model. However, Ward succeeded in producing many types of tornado-like vortices encountered in nature. In Ward's tornado simulator, a fine mesh honeycomb material was placed at the top of the chamber to remove the tangential component from the outflow as shown in Fig.2.3. The simulator has an exhaust fan at the top to generate the updraft and two vanes at the bottom of the surface to provide the angular momentum.

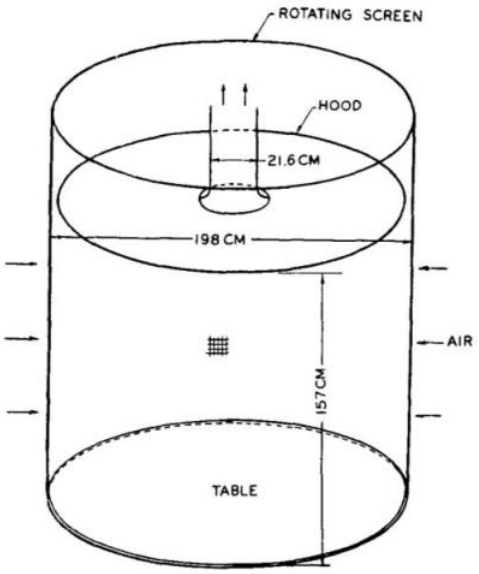

Figure 2.2 Ying and Chang mechanical simulator (1970)

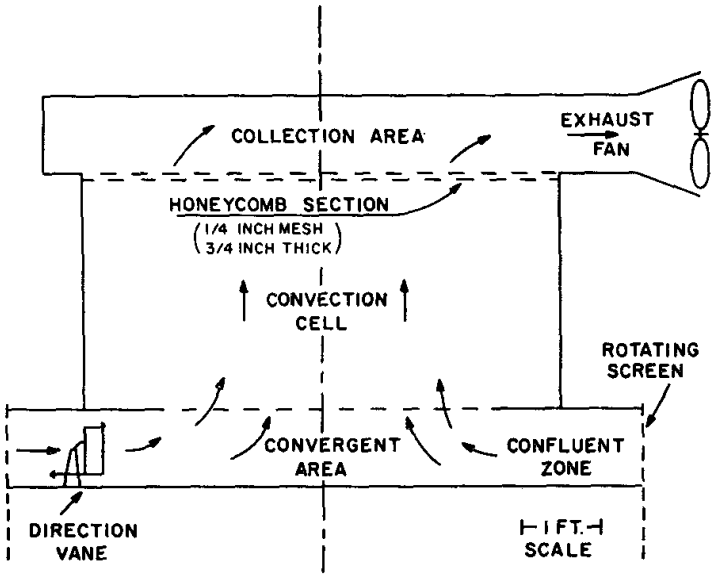

Figure 2.3 Ward tornado simulator (1972)

Similar to Ying's and Chang's (1970) tornado model, Wan and Chang (1972) were able to simulate a tornado on a smooth surface. Their simulator, in contrast, does not have a convection chamber but has an opening duct at the center to work as a sink. The model is shown in Fig.2.4. Two essential parameters were identified: Reynolds number (Re_t) and ε_c. where ε_c is the mean controlled parameter and is defined as:

$$\epsilon_c = \frac{Q}{\Gamma_\infty r_0} \tag{2.1}$$

Where Q is the sink strength and Γ_∞ is the free stream circulation and r_0 is the core radius. The simulator produced two-celled vortex for low ε_c and one-celled vortex for high ε_c. The tangential, vertical and radial velocities were measured by a three dimensional velocity prob. The vertical velocity found to be negative for low ε_c and positive for high ε_c.

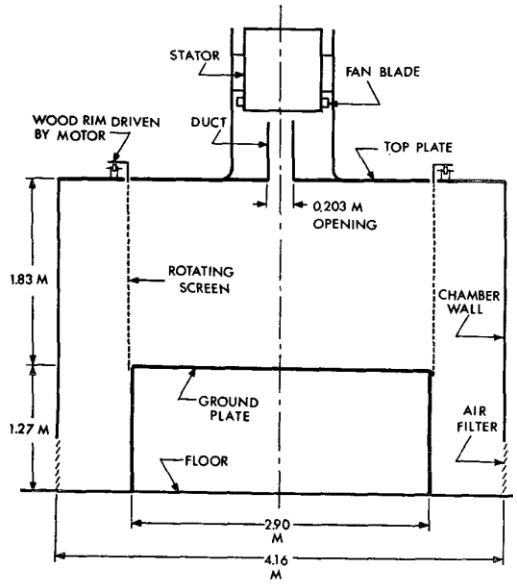

Figure 2.4 Wan and Chang (1972) tornado model

Davies–Jones (1973) analyzed the paper presented by Ward's (1964) and claimed that the radial momentum flux is not an important factor to produce vortices. The increase in the momentum flux was balanced by the outward pressure thrust. The volume flow rate should be the primary factor to produce the atmospheric vortices instead of the momentum flux. Church et al. (1977) modified Ward's simulator (1972) at Purdue University (PU) and the modified simulator is shown in Fig.2.5. The simulator has an exhaust suction fan through a flow straightening baffle. The flow straightening baffle with the suction fan was used to remove the rotational velocity and allow the axial flow. In addition, the simulator has a rotating mesh screen at the bottom to allow the flow to converge horizontally at the line of the symmetry. Four

essential parameters were found to control the vortex in the simulator and were combined into a single non-dimensionalized parameter, swirl ration (S). The swirl ratio is defined as:

$$S = \frac{V_\theta r_0}{2hV_r} \tag{2.2}$$

Where V_θ and V_r are the rotational and radial velocities; h is the axial distance and r_0 is the distance from the center of symmetry. The experiment concluded that the increase of S produces a multiple vortex.

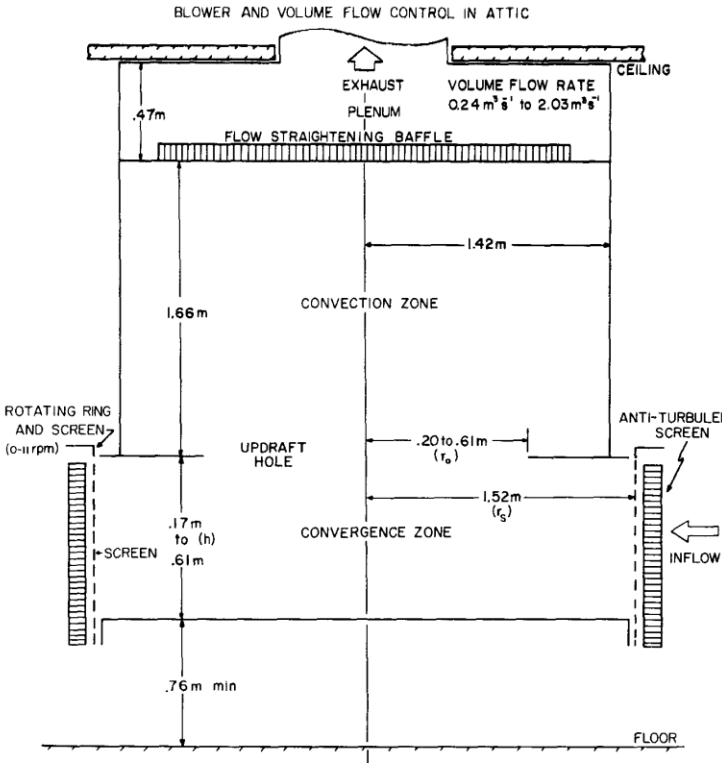

Figure 2.5 Schematic of Church et.al (1977) tornado simulator

Mitsuta and Monji (1984) at Kyoto University-Japan have developed small scale atmospheric vortices similar to Ward's simulator. The tornado simulator is illustrated in Fig.2.6. The simulator has fans to produce the circulation whereas in Ward's type simulator the circulation was provided by a rotating screen. The vortex core diameter depended only on the swirl ratio (S). The swirl ratio is defined as:

$$S = \frac{\mathrm{R}\tan(\theta)}{2H} \tag{2.3}$$

Where R is the updraft radius, θ is the inflow angle and H is the height. The transition between the one-celled vortex to two-celled vortex was occurred at a critical S close to unity and the maximum velocity found to be near the ground surface.

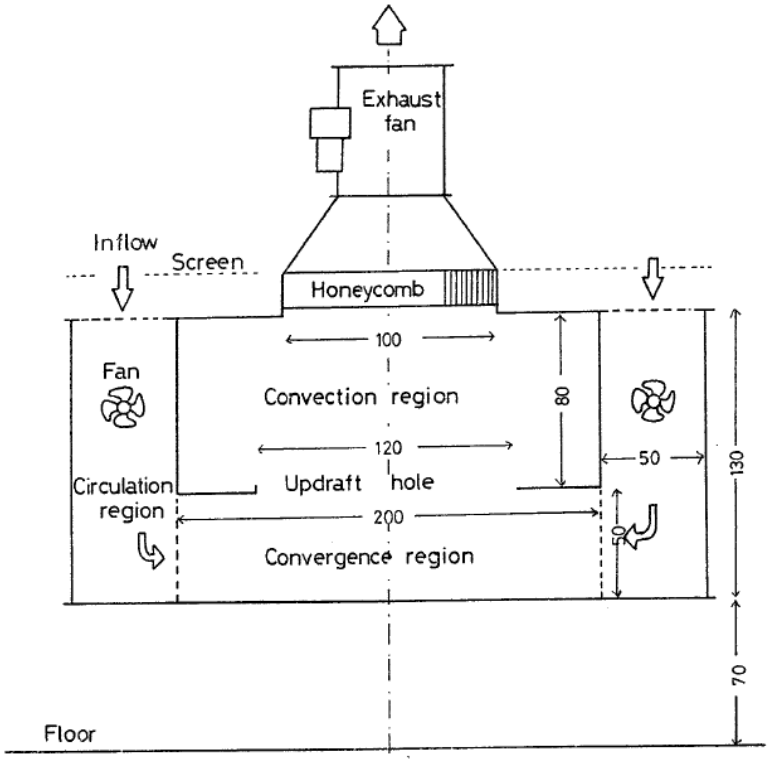

Figure 2.6 Schematic of Mitsuta and Monji(1984) tornado simulator

Recently, a group of ISU researchers has built a translating tornado simulator as shown in Fig.2.7. Sarkar et al. (2005) and Hann et al. (2008) measured flow field velocity in the laboratory and compared the results with mobile Doppler radar of two major tornados and a numerical simulation. The simulator was able to produce one-celled and two-celled vortices for a swirl ratio ranging from 0.08-1.14. Two elevation near the ground surface was investigated (Z=20 m, and 50 m). Observation found that the tangential velocity had the largest peak value among the simulator and the Doppler data result. Their experiment illustrate that the tornado simulator is

capable of capturing the characteristics of a real tornado, and it could be a useful tool to study tornado forces on structures.

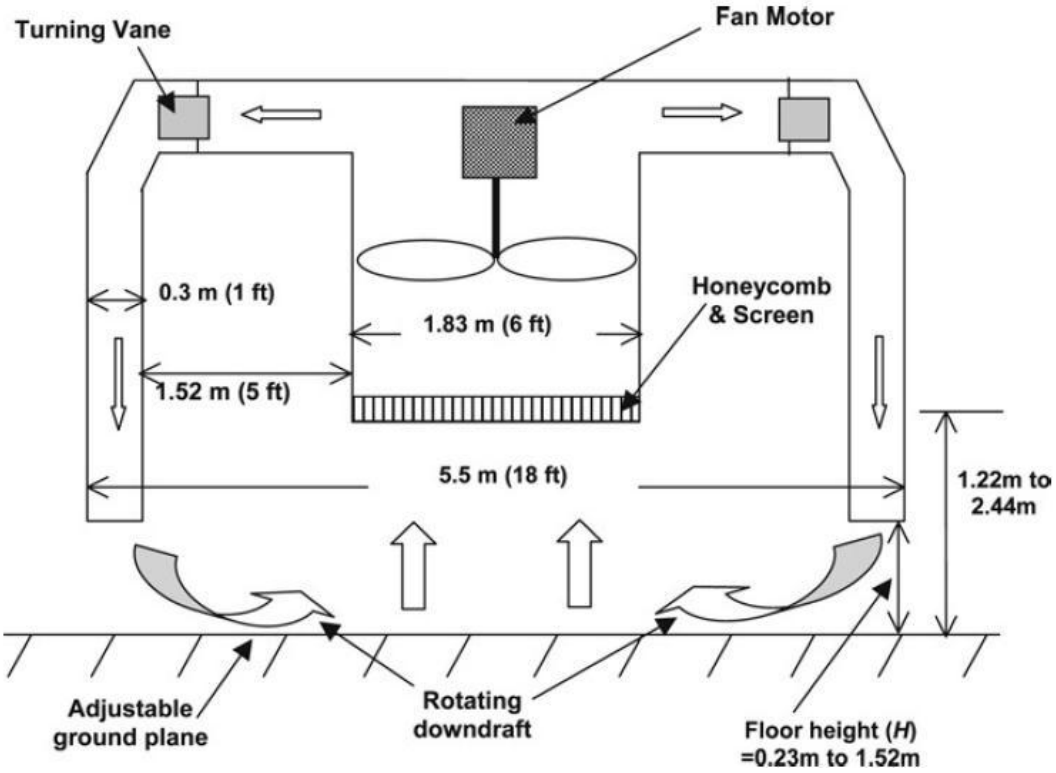

Figure 2.7 Schematic of ISU tornado simulator (Hann et.al 2008)

2.3 TORNADO NUMERICAL MODEL

Fiedler (1994) examined two-dimensional axisymmetric (r,z) numerical model to simulate a tornado-like vortex and the flow is incompressible. The vortices were developed in a domain with rigid boundaries by a rotating cylinder of fluid. A conclusion had been drawing from the study where it found that the tornado speed exceeded the thermodynamic speed limit by 5 times. The increase of the pressure gradient in the core with the distribution of the axial vortices provided an increase of the wind speed by 2% greater than the radial speed. Fiedler (1998) extended the two-dimensional model into three-dimensional (x,y,z) numerical model to simulate tornado like-vortices. The primary focus was on what happened at a high swirl ratio. At

a high swirl ratio it found that the three dimensional model produced multiple suction vortices. Nolan and Farrell (1999) did a further investigating by modifying Fiedler (1998) work, and they identified a new dimensionless parameter beside the Reynolds number (Re_c) and swirl ratio (S_d). The new dimensionless parameter is known as the vortex Reynolds number (Re_v), which is defined as the ratio of the far field circulation to the eddy viscosity as shown in Eq. (2.6).

$$Re_c = \frac{\mathrm{UL}}{\nu} \tag{2.4}$$

$$S_d = \frac{\Omega L}{U} \tag{2.5}$$

$$Re_v = \frac{Re_c}{S_d} = \frac{\Omega L^2}{\nu} \tag{2.6}$$

The Re_v is more useful than the Re_c and S_d because it predicts the characteristic of the flow in a tornado-like vortices. In Eq. (2.4), the Ω is the rotational rate, L is the length scale, U is the maximum convective velocity, and ν is the kinematic viscosity.

Lewellen et al. (1997) has simulated a lower portion of a tornado by using LES turbulent model to study the interaction of a tornado vortex with the surface. The computational domain was (1 km x 1 km x 2 km) and the minimum grid spacing was 1.5 m in the vertical and 2.5 m in the horizontal. Lewellen et al. investigated how a three dimensional unsteady numerical simulation of a tornado interacts with the surface. They found that the maximum swirl velocity exceeded the maximum quasi-cylindrical velocity by 60 % and localized within 50 (m) of the surface. Lewellen et al. (2000) extended his previous work (Lewellen et al. (1997)) to identify two essential parameters which controlled the size of the vortex. The parameters are the corner swirl ratio (S_c) and the outer swirl ratios (S_{outer}). These parameters are defined as:

$$\mathrm{S_c} = \frac{\mathrm{r_c \Gamma^2}_\infty}{\gamma} \tag{2.7}$$

$$S_{outer} = \frac{\Gamma_\infty}{r_o a_c h_{\mathrm{inf}}} \tag{2.8}$$

Here r_c ,Γ_∞,γ, r_o, a_c, and h_{inf} are core radius, angular momentum, total flux flowing in the corner flow region, starting radius average horizontal convergence and the height of the inflow layer. Their findings show that the mean swirl velocities near the surface were increased by 2.5 times the maximum swirl velocity aloft when S_c was decreased. Recently, Ishihara et al. (2011) used the LES turbulent model to study the flow fields of tornado-like vortices. A Ward-type simulator was numerically modeled for their study. Two swirl ratios were investigated (S=0.31 and 0.65). For a small ratio (S=0.31), the numerical result showed an existence of a one-celled vortex which has a peak vertical velocity at the center. On the other hand, the numerical simulation showed for a high swirl ratio (S=0.65) an occurrence of two-celled vortex with a maximum tangential velocity close to the ground surface. The numerical result was similar to Ward's simulator, producing one-and two-celled vortex for different swirl ratios.

2.4 TORNADO-STRUCTURE INTERACTION LABORATORY MODEL

Jischke et al. (1983) modified Ward's tornado simulator by adding an exhaust fan with a variable speed to generate the updraft and a convergent horizontal flow passing through the mesh wire as shown in Fig.2.8. They were able to control velocity components (tangential and radial) independently. A rectangular structure was placed in the simulator to study TSI. The structure plan area was 25.4 (cm) x 14.6 (cm) and 12.7 (cm) in height. The rectangular structure was moved in the simulator to three different locations. The tornado force and moment coefficients on the structure were calculated for two swirling flow angles (0^0 and 45^0). Three parameters were identified to characterize the tornadic flow fields. The three parameters are (r_u Γ/Q), (Γ/ν) and (h/r_c). Here r_u is the updraft radius, Γ is the imposed circulation, Q volumetric flow rate, h inflow layer depth,ν is the kinematic viscosity and r_c is the tornado core radius. The study concluded that the force and moment coefficients were sensitive to the swirl ratio compared to the SL wind

loads. In addition, the location of the tornado vortex to the structure was a significant factor in determining where the high force on the structure can be occurred.

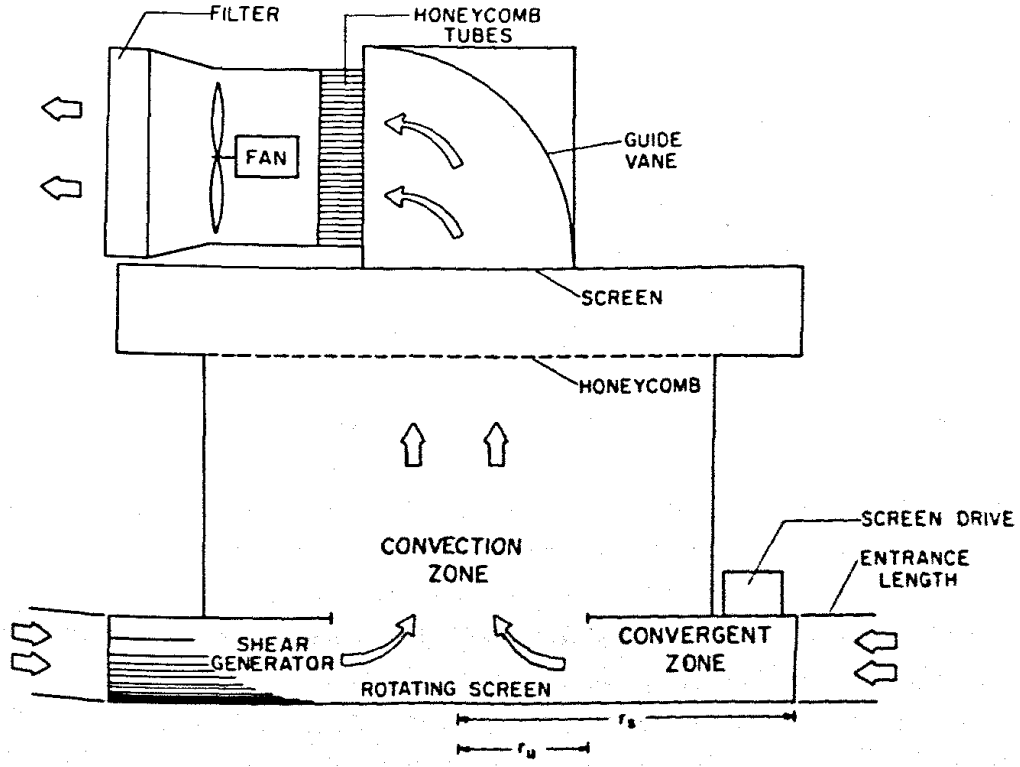

Figure 2.8 A modified of Ward's type tornado model (Jischke et.al, 1983)

Yang et al. (2009) modeled a high rise building in a wake vortex and studied the effect of changing the tornado angle with respect to the structure. The primary study was to calculate force and moment coefficients on a high rise structure at different location from the vortex core. Forces and moments on the structure were calculated by using a high sensitivity load cell, and a digital particle image velocimetry was used to measure the flow field. The wind loads (forces and moments) had a maximum value at the outer boundary of the tornado vortex core. In addition, the maximum wind loads on the structure found to be at 30^0 instead of 45^0 compared to SL wind loads. Velocity vectors were tangential with almost a zero radial component velocity. They concluded that the flow in a tornado rotates as a rigid column.

Sabareesh et al. (2009) analyzed the internal pressure on a cubic structure (100 mm) modeled in a stationary vortex in the laboratory simulator at Tokyo Polytechnic University, and compared the pressure with SL wind flow. Two swirl ratio were used (0.18 with an angle of 30^0 and S=0.54 with an angle of 60^0). The experiment showed that the pressure coefficients were different in tornado-like flow, and they had higher values than the SL wind. It also found that the mean pressure coefficients had positive and negative values on the roof when the swirl ratio was increased.

Haan et al. (2010) studied the effect of transient wind loads on a gable-roofed structure with a roof angel of 35^0 in the ISU tornado simulator (See Fig.2.9.). The study was on an open smooth terrain and for approximately F2 tornado. The force coefficients were compared to SL flow and found that the lateral force coefficients on the structure were 50% more than the SL wind. In addition, the updraft force coefficient was two to three times that of the force coefficients prescribed by ASCE 7-05 for SL flow.

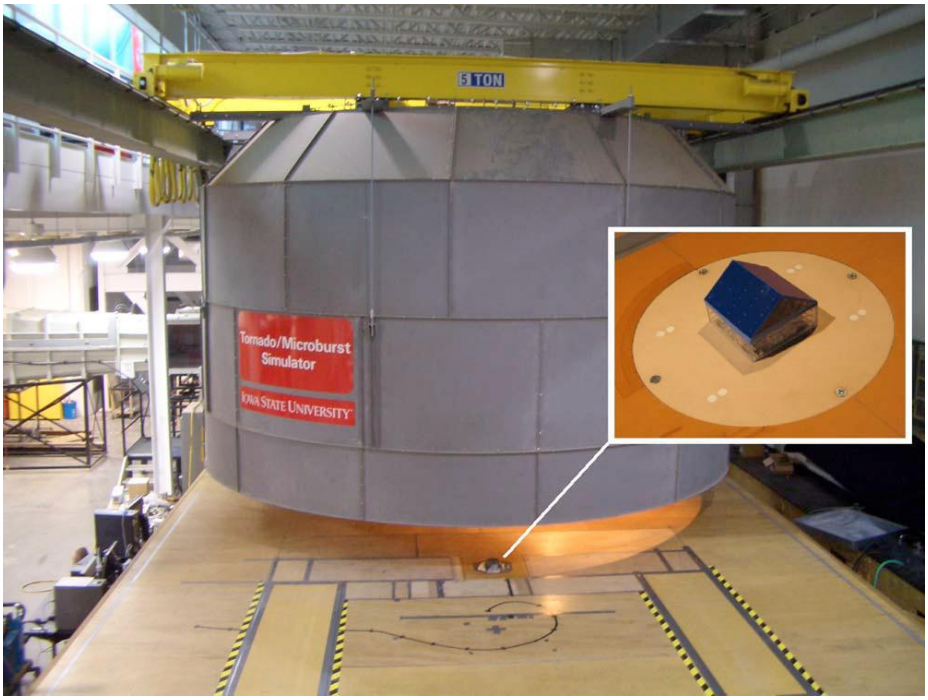

Figure 2.9 Photo of the ISU simulator (Hann,2010)

Zang and Sarkar (2010) conducted an experiment study on two-gable-roofed building with same surrounding structures. The influence or the interference of TSI with the surrounding structures was visually compared to SL flow. A tornado showed complicated vortices around the test model compared to the straight line flow.

Hu et al. (2011) conducted an experiment study on a low rise gable-roofed structure in the laboratory at ISU tornado simulator. The study was similar to Yang et.al (2008) in determining velocity vector components measurement, structure orientation and the location of the structure relatively to the tornado vortex. The study concluded that the updraft force coefficient was dominant and reached a maximum value at an angle ranging from 15^0 to 30^0 with respect to the model. Also, the value of the updraft force coefficient was at least three times the force coefficient obtained from a straight flow at all measured angles.

Mishra et al. (2008a, 2008b) also simulated the tornado in a laboratory and reported the pressure coefficients on a cubic building model when it is placed at different position with respect to the laboratory vortex model. They concluded that the pressure coefficients are different from the boundary layer wind tunnel measurements for straight wind. Sengupta et al. (2008) simulated the tornado in a laboratory and compared it with a computer model. Sengupta et al. concluded from their study on tornado vortex effects on a building, that the force coefficients are 1.5 times more than the suggested values by the ASCE 7-05.

2.5 TORNADO-STRUCTURE INTERACTION NUMERICAL MODEL

Wilson (1977) used a computer modeling to study the tornado-interaction with a structure. A two dimensional Eulerian hydrodynamic code was used to compute the force and pressure for seven runs. Four runs were for a translating tornado and the other were for stationary vortex. The RCV model was used as the tornado field model. There was no consideration for the kinematic viscosity or turbulence.in addition, a coarse grid was used and it is not sufficient to report an accurate result for the force and pressure coefficients.

Selvam (1993) was the first author to consider the effect of kinematic viscosity and turbulence to study the tornado flow interaction with the structure on a three dimensional structure. κ-ε turbulence model was used and found that the forces on the building roof were five times the SL wind loads in the force vortex region whereas in the free vortex region the forces were the same as the SL wind loads. Selvam et.al (2002b) did another study on a two dimensional cylinder. A lift and drag forces were calculated for a translating tornado. The result showed that when the tornado far away from the model the drag and lift coefficients were the same as the free stream flow. Also, they showed from flow visualizations vortices controlled the flow in the forced vortex region.

Selvam (2002 a) and Selvam and Millett (2002 c, 2003, and 2005) used LES turbulence model by filtering the NSEs. Selvam (2002 a) used 0.1D grid spacing close to the building and found that the force coefficients in the x and y-directions were less than the SL wind loads whereas the updraft force coefficient in the z-direction was higher than the SL wind loads. Selvam and Millett (2002 c) used a fine grid spacing 0.072H and found that the force coefficients in the x and y direction were less than the SL wind loads which in line with Selvam (2002a). However, the force coefficient in the z-direction was almost twice the SL wind loads. Selvam

and Millett (2003, and 2005) used a refine grid 0.0055H normal to the building and the tornado approached the building with 0^0 and 45^0 degrees. They concluded that the translating tornado generated about 200% force on the roof and about 45% more on the walls compared to SBL wind loads.

The literature on tornado-interaction with structures have focused on a single structure plan area, such as a gable-roofed structure, rectangular structure, and cubic or tall buildings interacting with a translating or a stationary vortex. Tornado-interaction with different structure plan areas has not been studied, which leaves several questions unanswered. What would happen to the tornado forces on a structure with a plan area larger than the tornado size? Do we expect the force and pressure coefficients to be higher, the same or less than the SL wind loads? Does the structure with large plan area subject to higher force coefficients versus the thin (tall) structure plan area? For these reasons, a numerical simulation is needed to study in detail the interaction of a translating tornado on different structures plan areas.

By answering these questions, we can begin to address the dynamic response of the structure to tornado-like vortex flow or SL wind flow. The next section will provide a short summary of the dynamic response of structure due to tornadic wind loads.

2.6 DYNAMIC RESPONSE OF STRUCTURE

Dutta et al. (2002) proposed a novel model of tornado dynamic response on a high rise building and small single-storied structure by using the FEM technique. The study was idealized to two dimensional with multidegrees of freedom and solved by FEM. The maximum and translating velocities were scaled from tornado records and used FEM techniques to obtain the structure mode shapes. They found that the structure response was controlled by the translating and lateral wind speeds.

Thampi et al. (2010 and 2011) used FEM technique to study the structure response due tornado strike. A scaled gabled-roofed timber structure was used for the study and the structure was similar to a partially destroyed structure by a real tornado. The structure plan area dimension is 15 (m) x 10 (m) and 3 (m) in height. The gable-roofed structure was placed inside the ISU simulator to collect a pressure measurement data and to use the FEM to predict structure failure. Two studies were applied to the model. The first study was on a sealed structure (windows and doors were closed), and the second was on an opened model (windows and doors were opened). The study concluded that the sealed structure experienced a lower negative internal pressure than the opened structure.

CHAPTER 3

TORNADO MATHEMATICAL MODELS

3.1 INTRODUCTION

This chapter introduces the tornado mathematical models which describe the characteristics of a tornado, in order to evaluate which of these existing models can reproduce a real tornado in the atmospheric environment. In addition, we will provide a discussion in order to identify which model is easy to numerically simulate and which model can reproduce a real tornado in the atmospheric environment. The models are the Rankine Combined Vortex (RCV), Burgers-Rott Vortex (BRV) and Sullivan Vortex (SV). These mathematical models satisfy the Navier-Stokes Equations (NSEs) of the fluid flow.

3.2 RANKINE COMBINED VORTEX MODEL

Rankine Combined Vortex model (RCV, 1882) satisfies the NSEs and it is the simplest model that can produce a vortex in the real atmospheric. The tangential velocity (V_θ) creates the vortex in a tornado. The RCV model combines two different flow fields. The force vortex region (inner flow field), the tangential velocity increases linearly from the center of the rotation to the maximum inner core radius (r_{max}). The free vortex region (outer flow fields), outside the range of the maximum inner core radius (r_{max}) the tangential velocity diminishes inversely with the increasing of the distance (r) from the center of rotation. Figure 3.1 illustrates the physical meaning of the RCV model.

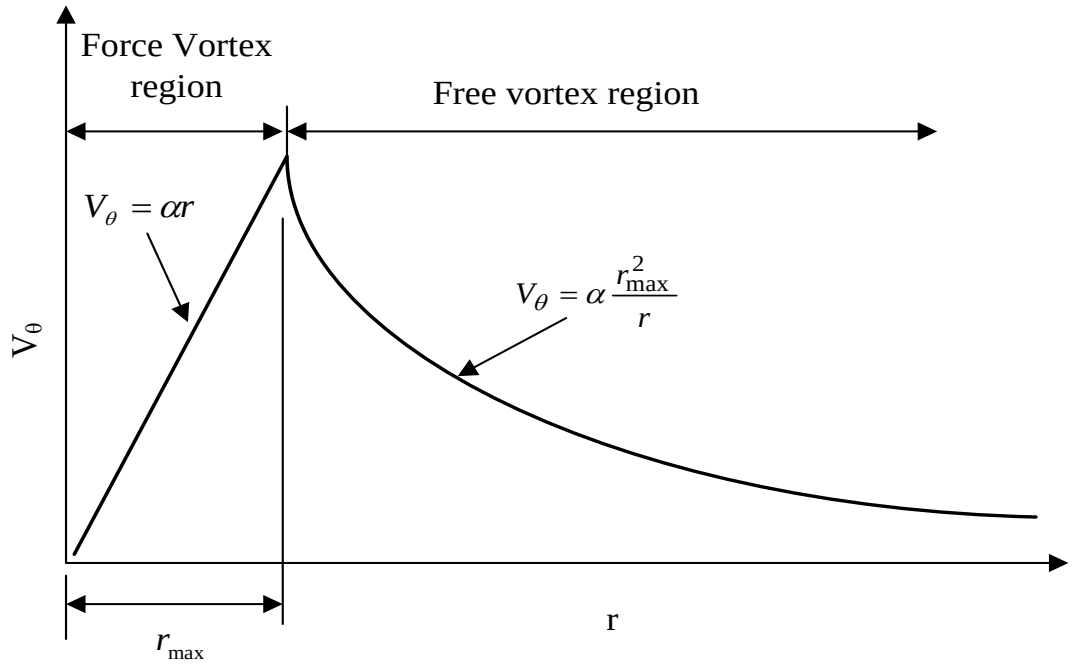

Figure 3.1 Rankine combined vortex model

The mathematical equation of the RCV model is defined as the follow:

$$V_\theta = \begin{cases} V_{max} \dfrac{r}{r_{max}} = \alpha \mathrm{r} & if\ 0 \le r \le r_{max} \\ V_{max} \dfrac{r_{max}}{r} = \alpha \dfrac{r_{max}^2}{r} & if\ r > r_{max} \end{cases}$$

Where V_{max} is the maximum flow intensity, α is the vortex strength, r is the distance from the center of rotation, r_{max} is the inner core maximum radius.

3.3 BURGERS AND ROTT VORTEX MODEL

Burgers and Rott Vortex (BRV) model satisfies the NSEs and matches the exact solution of the NSEs. Burger (1948) and Rott (1958) model is a one celled vortex. The tangential velocity (V_θ) in BRV model has similar flow patterns as the RCV model. However, the BRV model has a smooth peak at the center of rotation ($r = r_{max}$) compares to the RCV model. The BRV model has two other velocity components (vertical and radial velocities) besides the tangential velocity. The BRV model has an advantage over the RCV model in representing any

flow phenomena in a three dimensional vortex flow. Figure 3.2 illustrates the BRV model for the azimuthal velocity (V_θ).

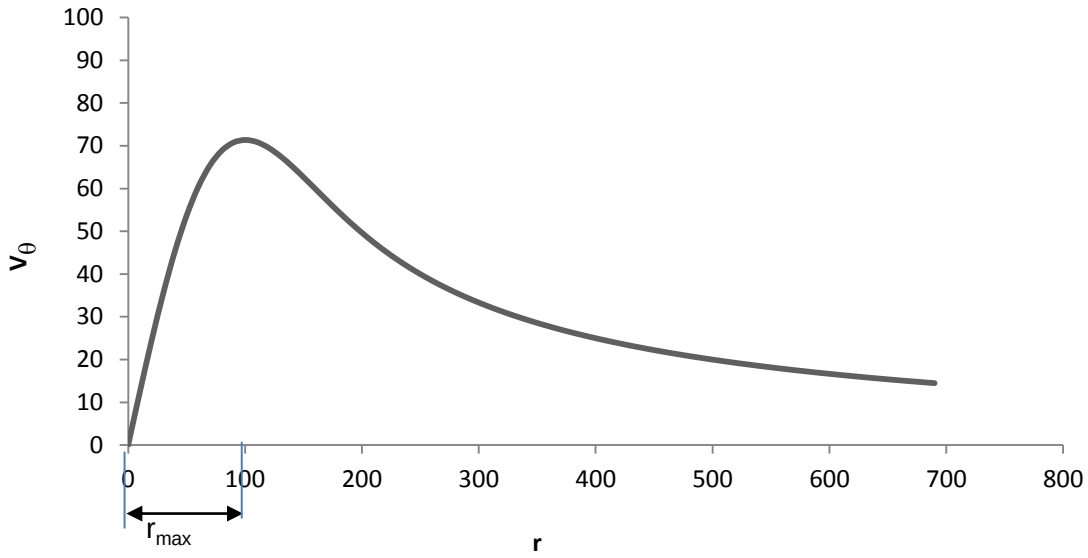

Figure 3.2 Burgers and Rott vortex model

The mathematical equations of BRV model are given bellow:

$$V_r = -ar$$

$$V_\theta = \frac{\Gamma}{2\pi r}\left(1 - e^{\frac{-ar^2}{2\upsilon}}\right)$$

$$V_z = 2az$$

$$P(r,z) = P_0 + \frac{\rho\Gamma^2 a}{\nu}\int_0^{\frac{ar^2}{2\upsilon}}(1-e^{-x})^2 dx - \frac{\rho a^2}{2}(r^2 + 4z^2) - \rho g z$$

Where V_r is the radial velocity component, V_θ is the tangential velocity component and V_z is the vertical velocity component. Γ is the vortex strength and a is the suction strength. P represents the atmospheric pressure distribution as a function of r and z only.

3.4 SULLIVAN VORTEX MODEL

Sullivan Vortex (SV, 1959) model also produces the exact solution to the NSEs. The model has three velocity components (radial, tangential and vertical) velocities similar to the BRV model. The SV model can produce a one or two celled vortex. The vertical velocity (V_z) is a function of the height (z) and the radius (r).

The mathematical equations of SVM define as follow:

$$V_r = -ar + 6\left(\frac{v}{r}\right)\left(1 - e^{\frac{-ar^2}{2\upsilon}}\right)$$

$$V_\theta = \frac{\Gamma}{2\pi r}\frac{H\left(a\frac{r^2}{2v}\right)}{H(\infty)}$$

$$V_z(z,r) = 2az - \left(1 - 3e^{\frac{-ar^2}{2\upsilon}}\right)$$

Where V_r is the radial velocity component, V_θ is the tangential velocity component and $V_z(z,r)$is the vertical velocity component in the z and r only. Γ is the vortex strength and a is the suction strength. ν is the eddy viscosity. H is a function integral in time. Figure 3.3 illustrates the SV model for two cell vortex.

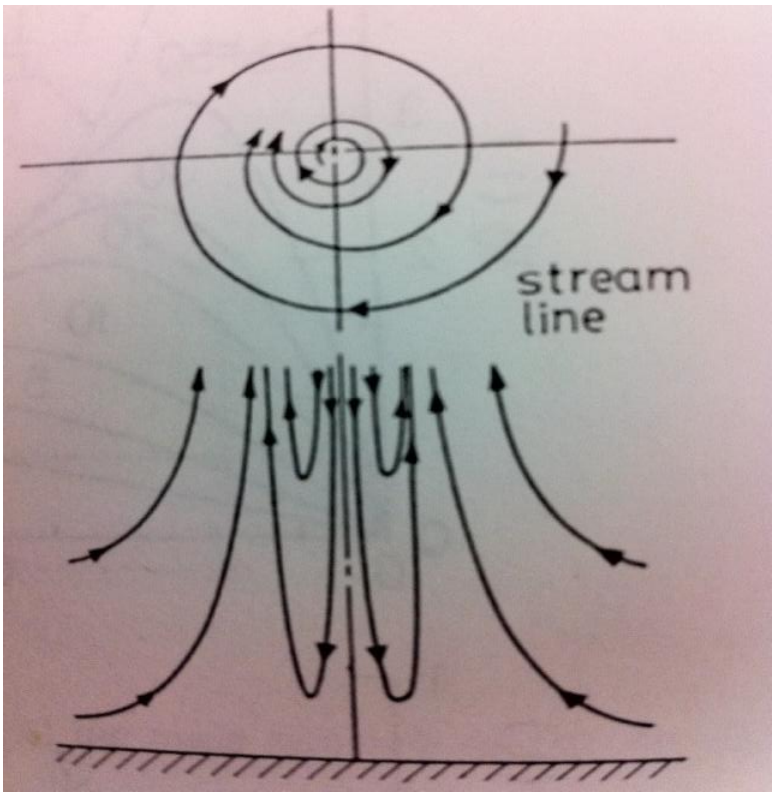

Figure 3.3 Two cell vortex Sullivan model (Akira Ogawa, 1993)

3.5 TORNADO MODEL COMPARISONS

The RCV model, the BV model and the SV model satisfy the NSEs and use to model a real tornado in the atmospheric air. The RCV model has the tangential velocity (V_θ) which produces a vortex and represents an actual tornado in the atmospheric air. The RCV model does not have a vertical velocity component but it does simulate the real tornado in the atmospheric. However, The RCV model has a bound limit to tornado peaks as described in the RCV velocities. In addition, the RCV model has the simplest mathematical equations and it is easy to numerically apply. The BV model can represent a real tornado and it is symmetric. However, a disadvantage of using this model is that there is no bound on the radius (r) to localize the vortex. Also, the vertical velocity (V_z) is a function of the height (z) and increases without bound limits with the height. The SV model is symmetric and the vertical velocity is a function of the radius

(r) and the height (z). Therefore, the vertical velocity in the SV model has also no bound limit on either the radius (r) or the height (z). The BV model and the SV model can represent a lower portion of a tornado and can extend to represent a thunderstorm. Hence, we are interested in a model which can represent a real tornado in the atmospheric and easy to apply numerically. Therefore, the RCV model is chosen for this research.

CHAPTER 4

COMPUTATIONAL DOMAIN SIZE EFFECT ON TORNADO FORCES

4.1 INTRODUCTION

The focus of this chapter is to change the computational domain size and do convergences study on tornado forces for a cube structure. The computational domain size is designed based on the tornado maximum radius (r_{max}) and structure height (h). The NSEs are iterated at each grid point in the domain and solve for pressure and velocities. The LES turbulent model is employed by filtering the NSEs to account for the turbulence flow. The simulated flow in the computational domain is highly turbulent and the domain has to be large enough to allow the turbulent flow to be developed. The cube structure center is at the origin axis and the computational domain geometry changes in each direction from that axis. The next sections will discuss in detail the design of the computational domain, grid generation and tornado parameters, geometry and boundary conditions, force coefficients, and the computational domain results.

4.2 DESIGN OF THE COMPUTATIONAL DOMAIN

The modeled structure is a cube for design simplicity and it has the dimensions h for the length, the width and the height. The computational domain has the dimensions D for the length and the width and H for height. The structure and the computational domain are shown in Fig.4.1.

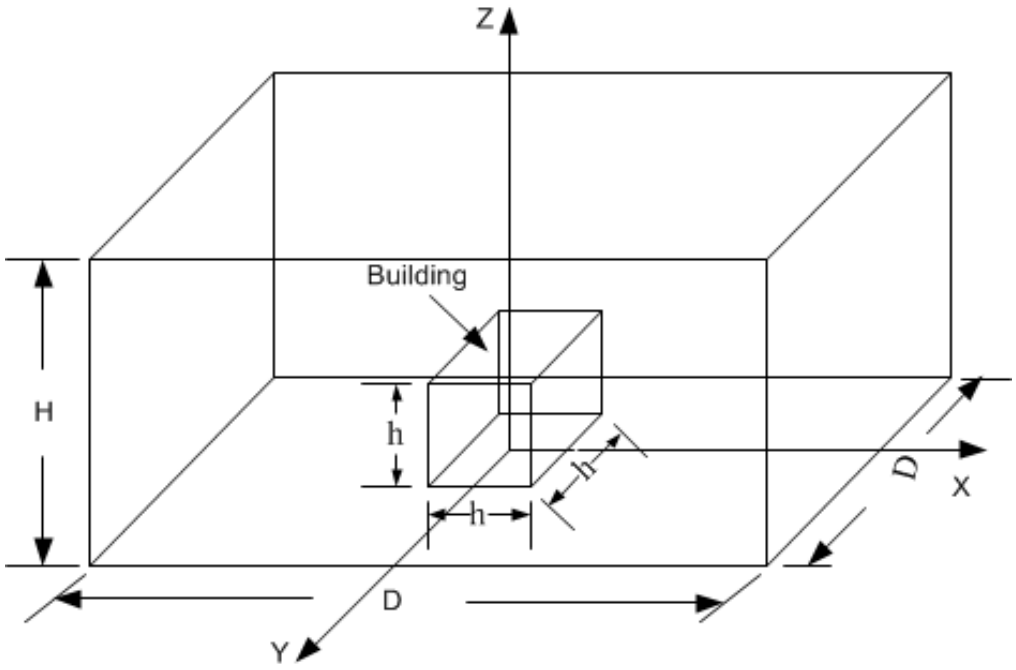

Figure 4.1 Isometric view of the computational domain

The increases in the domain size are based on how far the tornado center is from the origin which is represented by the distance (C). The schematic of the computational fluid domain (D x D), the modeled structure (h x h) and the simulated tornado in the domain in the x-y plane are illustrated in Fig. 4.2.

The fluid computational domain size (D x D x H) is calculated from Eq. (4.1), (4.2) and (4.3). A grid name is given to each computational domain size as specified in Table 4.1.

$$C = a \times r_{max} + \frac{h}{2} \tag{4.1}$$

$$D = 2 \times C + 2 \times r_{max} \tag{4.2}$$

$$H = \frac{D}{2} \tag{4.3}$$

Where:

C is a distance from the origin to tornado center

a is a constant parameter

r_{max} is the tornado inner maximum core radius

h is a unit length of the modeled structure geometry

D is the length or the width of the computational domain

H is the height of the computational domain

Table 4.1 Computational domain parameters design

Grid name	a	r_{max}	h	C	D	H
A1	2	3	1	6.5	16	8
A2	4	3	1	12.5	28	14
A3	6	3	1	18.5	40	20
A4	8	3	1	24.5	52	26
A5	10	3	1	30.5	64	32

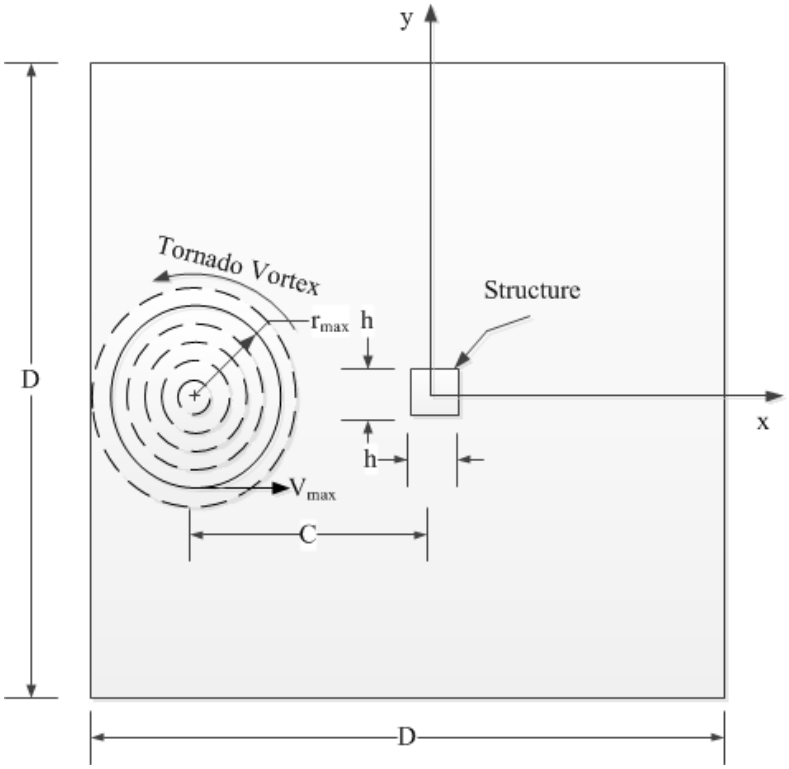

Figure 4.2 x-y Plane view of the fluid computational domain

4.3 GRID GENERATION AND TORNADO PARAMETERS

A discretization of a mesh, or grid points, can be generated for any physical model by using commercial packaging or writing a program code. In this dissertation, the grid points in the domain are generated by FORTRAN code. The minimum spacing normal to the structure in each direction is 0.01h and on the building edges is 0.1h. The grid spacing layout in the computational domain increases by 1.25 times the assigned minimum spacing. When the spacing between two nodes reaches the structure length, the spacing constrained to half of the structure's length in each direction. An illustration of the grid layout in the computational domain along the x- axis is presented in Fig. 4.3. The layout is the same for y-axis and z-axis.

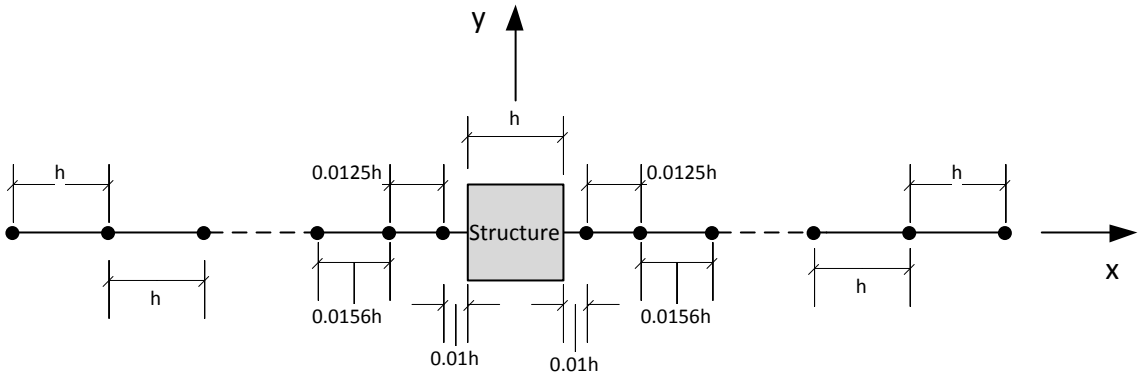

Figure 4.3 Grid layout illustrations along the x-axis

The grid properties are given in Table 4.2. Tecplot software is used to visualize the mesh in the computational domain. A z-y plane mesh for the structure (h x h x h) is shown in Fig.4.4. In addition, a x-y plane mesh for grid A1 is given in Fig.4.5.

Table 4.2 Grid properties

Grid name	Domain size in h	Grid Size	Grid spacing normal to bldg.	Total #of points in domain
A1	16 x 16 x 8	70 x 70 x 45	0.01 h	220,500
A2	28 x 28 x 14	74 x 74 x 50	0.01 h	273,800
A3	40 x 40 x 20	78 x 78 x 56	0.01 h	340,704
A4	52 x 52 x 26	80 x 80 x 62	0.01 h	396,800
A5	64 x 64 x 32	82 x 82 x 68	0.01 h	457,232

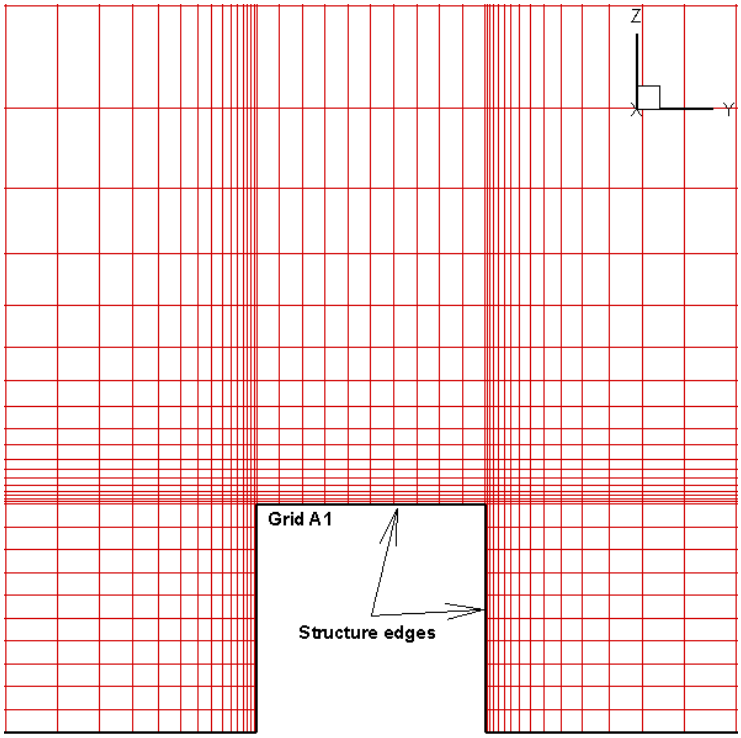

Figure 4.4 Structure (h x h x h) z-y plane mesh

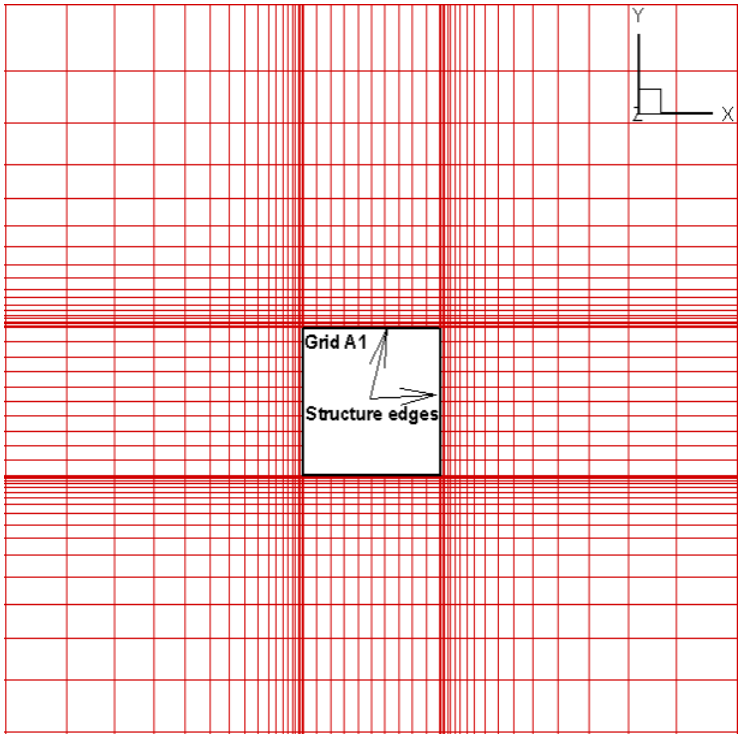

Figure 4.5 Structure (h x h x h) x-y plane grid points

A top view of a tornado path approaching a structure with 0^0 angle of attack is shown in Fig.4.6. The structure geometry is dimensionalized by the height of the structure (h) and the flow velocities filed are dimensionalized by the translation velocity (Vtrans.). The maximum velocity (V_{max}) in a tornado is the sum of two velocity components as shown in Eq. (4.4). The two velocity components are the tangential (V_θ) and the translation ($V_{trans.}$) velocities. In this research, the maximum velocity is calculated from the Rankine-Combined Vortex (RCV) velocities and an illustration is given in Fig.4.7. The strength of the vortex (α) in the tornado is kept constant. The physical parameters used in this study are summarized in Table 4.3.

$$V_{max} = V_{trans.} + V_\theta \tag{4.4}$$

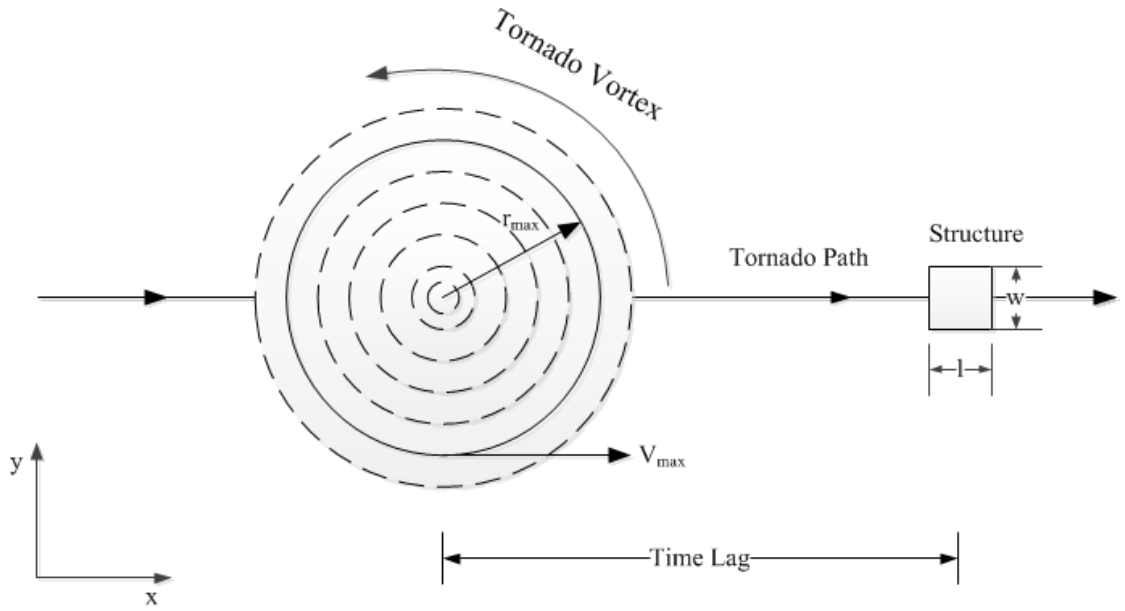

Figure 4.6 Top views of a tornado path and a structure

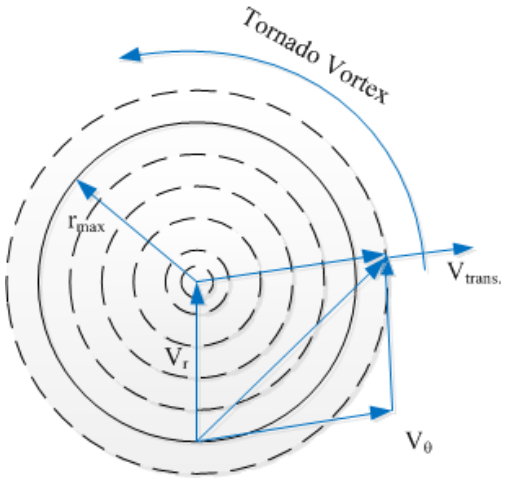

Figure 4.7 Schematic of RCV velocity components in a tornado

Table 4.3 Tornado parameters

	h	α	r_{max}	$V_{trans.}$	V_θ	V_{max}
English units	66.6 (ft)	1.5 (1/s)	200 (ft)	45.5 (mph)	205 (mph)	250.5 (mph)
SI units	20.3 (m)	1.5 (1/s)	61.0 (m)	20.3 (m/s)	91.5 (m/s)	111.8 (m/s)
Non-Dimensional units	1	1.5	3.0	1.0	4.5	5.5

4.4 GEOMETRY AND BOUNDARY CONDITIONS

The computational domain and the structure have the dimensions assigned in Table 4.4. The isometric computational domain with the modeled structure is again shown in Fig 4.8. The structure is assumed to be rigid and has a zero velocity on each face (no slip boundary condition).

Table 4.4 Computational domain and structure sizes

Grid name	Domain Size in h	Structure size
A1	16 x 16 x 8	h x h x h
A2	28 x 28 x 14	h x h x h
A3	40 x 40 x 20	h x h x h
A4	52 x 52 x 26	h x h x h
A5	64 x 64 x 32	h x h x h

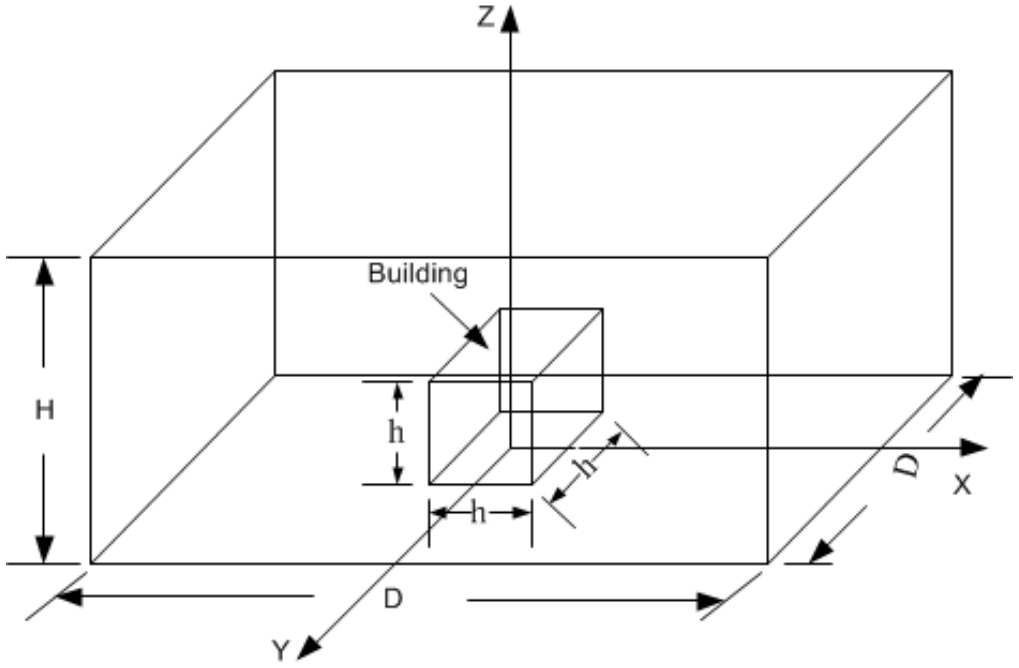

Figure 4.8 Isometric view of the computational domain

The boundary conditions applied on the exterior faces are the RCV model velocities. The RCV velocity components are given in a Cartesian form as described in Eq. (4.5, 4.6, 4.7 and 4.8). The RCV model velocities are applied for each grid point in the computational domain and these velocities change in time based on the location of the vortex core. The RCV model is discussed in detail in Chapter 3.

$$V_x = (V_t - y\alpha)Zf \qquad if\ r \le r_{max} \tag{4.5}$$

$$V_y = (x - V_t t)\alpha\ Zf \qquad if\ r \le r_{max} \tag{4.6}$$

$$V_x = (V_t - Cy)Zf \qquad if\ r > r_{max} \tag{4.7}$$

$$V_y = (x - V_t t)C\ Zf \qquad if\ r > r_{max} \tag{4.8}$$

Where:

$C = \alpha r^2_{max}/r^2$,

$r^2 = (x - V_t t)^2 + y^2$

$Z_f = u^* \ln ((h+h_0)/h_0)/\kappa$

The roughness length of the ground is h_0 and it is fixed at 0.00375 and κ is the turbulent kinetic energy and has an imperial constant value of 0.4 (Selvam, 1993). The height of the structure (h) has a non-dimensioned unit value. The frictional velocity is u* and it is calculated from a known velocity and height. Zf is an algorithm variation in the height to account for the boundary layer growth in the computational domain.

4.5 FORCE COEFFICIENTS

Forces on the structure are calculated by integrating the pressure over the surface area in x,y and z directions. The force coefficients are obtained from Eq. (4.9, 4.10 and 4.11). The reported force coefficients are for one time which is equal to the time lag. The time lag is the time from starting the simulation until the center of the tornado is coincided with the structure center.

$$Cx = \frac{F_x}{0.5\rho V^2 A} \tag{4.9}$$

$$Cy = \frac{F_y}{0.5\rho V^2 A} \tag{4.10}$$

$$Cz = \frac{F_z}{0.5\rho V^2 A} \tag{4.11}$$

C_x is the force coefficient in the x-direction, C_y is the force coefficient in the y-direction and C_z is the updraft force coefficient in the z-direction. ρ is the flow density and A is the projected area in which force is acting. Fx is the force in the x-direction, Fy is the force in the y-direction, and Fz is the force in the z-direction.

The reference velocity (V) has an assigned value based on the numerical study. If a tornado is simulated in the computational domain, the reference velocity is the maximum

velocity (V_{max}). On the other hand, if a SL wind flow is simulated in the computational domain, the reference velocity is the translating velocity ($V_{trans.}$).

4.6 TORNADO PROGRAM AND SOLUTION PROCEDURE

Our Computational Mechanics Laboratory group at the University of Arkansas (UA) has developed a CFD code, under the supervision of Prof. Selvam Panneer, to simulate a translating tornado and its interaction with a structure. The wind program is called the UA-CFD wind code. The LES turbulence model filters the incompressible NSEs and the semi-implicit Finite Difference (FE) technique is used to numerically solve the unknown three velocities and pressure as presented by Selvam (1997). The continuity and momentum equations in tensor notations are found in Appendix A.

4.7 COMPUTATIONAL DOMAIN STUDY RESULTS AND DISCUSSION

Five runs were simulated by using the UA-CFD wind program to study how increasing the computational domain size affects tornado forces. Each run was simulated for a cube structure with different computational domain sizes.

The computed force coefficients for each run and the delta (δ) convergence error are summarized in Table 4.5. The delta convergence error is evaluated for each force coefficient from Eqs. (4.12, 4.13 and 4.14). The computational domain convergence studies on tornado force coefficients in x, y and z directions are presented in Fig.4.9.

$$\delta x = \frac{Cx_{new} - Cx_{old}}{Cx_{new}} \times 100 \tag{4.12}$$

$$\delta y = \frac{Cy_{new} - Cy_{old}}{Cy_{new}} \times 100 \tag{4.13}$$

$$\delta z = \frac{Cz_{new} - Cz_{old}}{Cz_{new}} \times 100 \tag{4.14}$$

Table 4.5 Force coefficients and error convergence

Grid name	Cx	δx %	Cy	δy %	Cz	δz %
A1	0.59	------	0.73	------	1.36	------
A2	0.83	28.91	0.62	17.74	1.01	34.65
A3	0.53	56.60	0.54	14.81	0.81	24.69
A4	0.56	5.36	0.58	6.90	0.80	1.25
A5	0.58	3.44	0.60	3.33	0.82	2.44

Grid A1 and A2 had the highest values in force coefficients in the x, y and z direction and the highest error percentages among all other grid names. The increase in the force coefficients values and the high percentage of error is happened because the domain was not large enough to allow the turbulent flow to be developed and the tornado to be formed in that domain. To visualize the tornado formation around the structure and along the z-axis in the domain for each grid, a mid-plane section in the y-direction has been taking of the pressure contour plot as illustrated in Figs. (4.10, 4.11, 4.12, 4.13 and 4.14). The pressure contour plots for grid A1 and A2 showed that the tornado has not formed in the domain because it showed a discontinuity or a separation in the pressure contour plot along the z-axis. A mid-plane section in the y-direction of the pressure contour plot for grid A3 showed that the tornado has partially formed around the structure and along the z-axis. However, grid A4 and A5 showed that the tornado has completely formed around the structure and along the z-axis as demonstrated by the pressure contour plot. Figure 5.15 shows the three dimensional view of the formed tornado in the computational domain for grid A5.

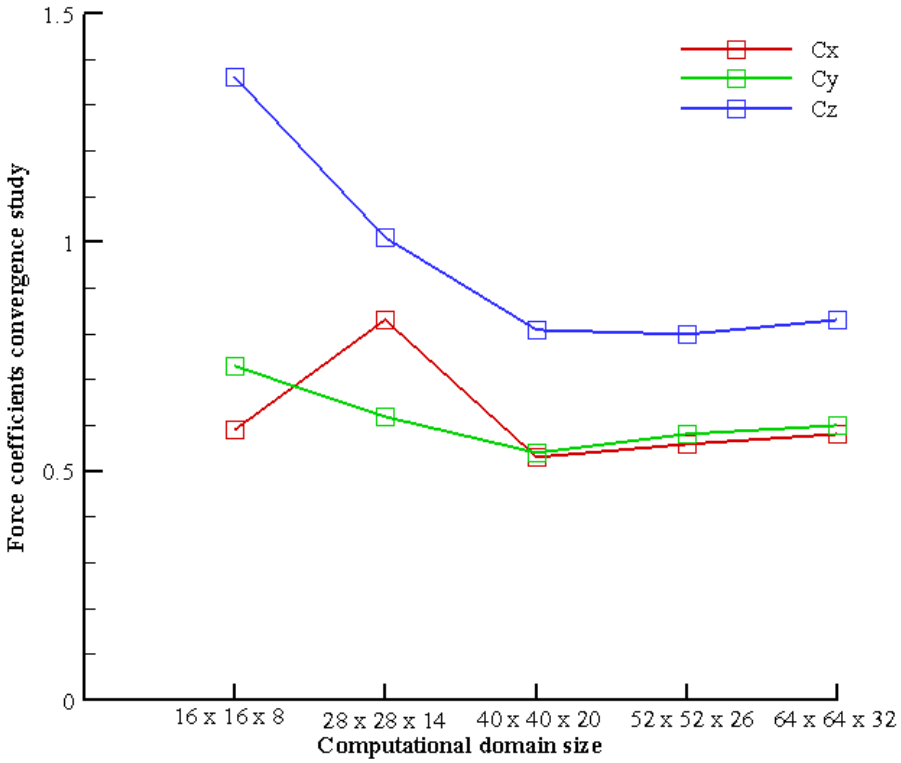

Figure 4.9 Force coefficients convergence studies

Force coefficients in time are plotted for each grid name in Figs.(4.16, 4.17, 4.18, 4.19 and 4.20). Grid A1 and A2 showed instability in time because the domain was not large enough to allow the turbulence fluctuations to converge before the tornado engulfed the structure. Grid A3, A4 and A5 showed a smooth transition in tornado force coefficients when the tornado engulfed the structure. The force coefficients for grid A3, A4 and A5 showed a single peak value when the tornado surrounded the model at the specified time lag whereas grid A1 and A2 showed multiple peaks values. The single peak value in the force coefficients is a signal to show that the tornado has been formed and with the highest strength in the domain.

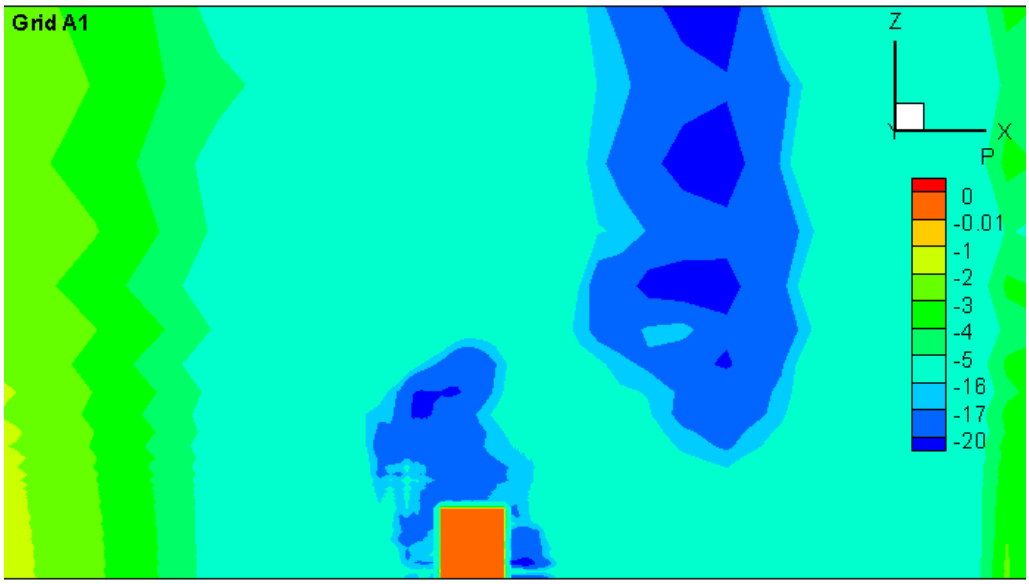

Figure 4.10 Grid A1 x-z plane pressure contour plots of a tornado

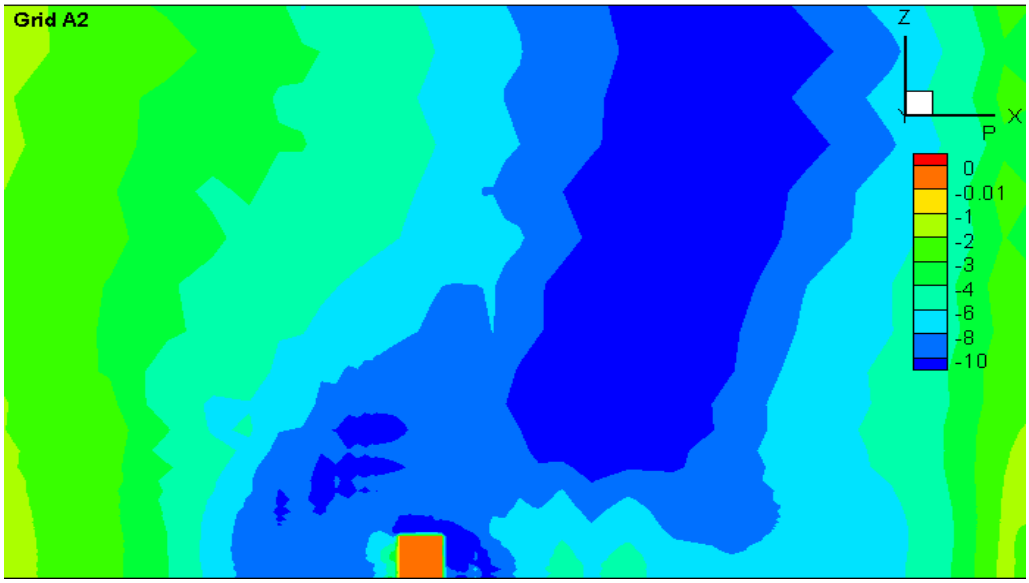

Figure 4.11 Grid A2 x-z plane pressure contour plots of a tornado

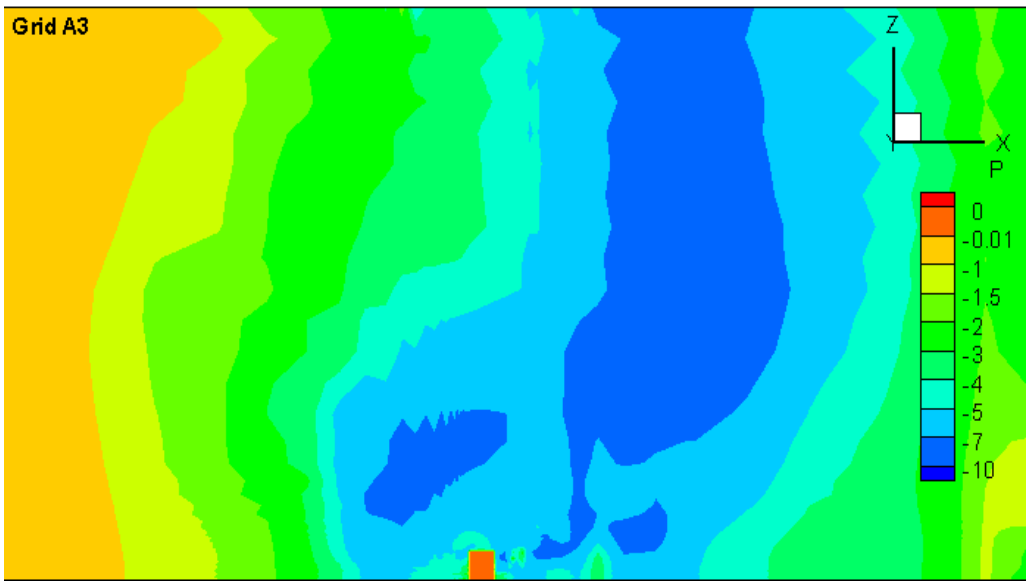

Figure 4.12 Grid A3 x-z plane pressure contour plots of a tornado

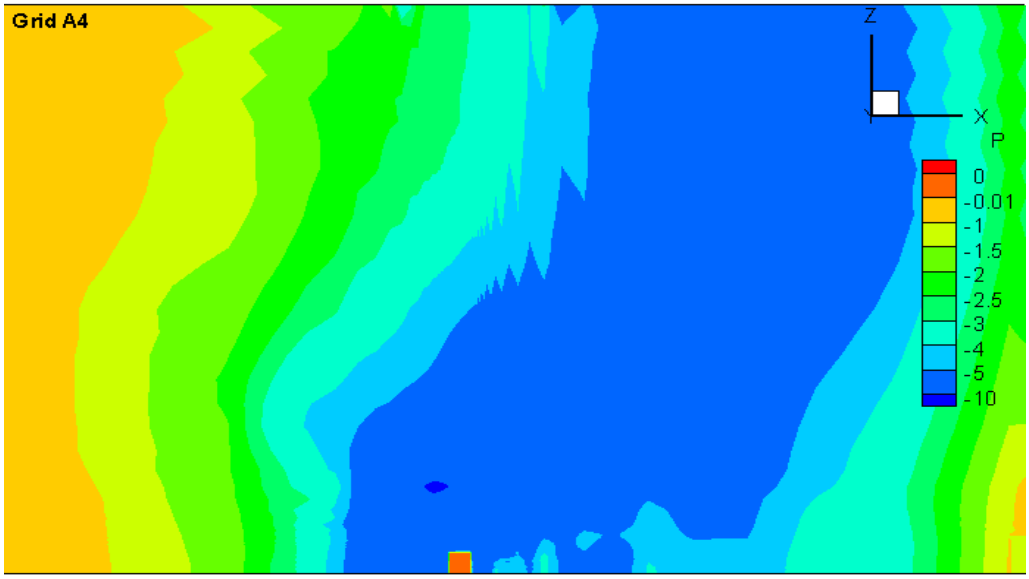

Figure 4.13 Grid A4 x-z plane pressure contour plots of a tornado

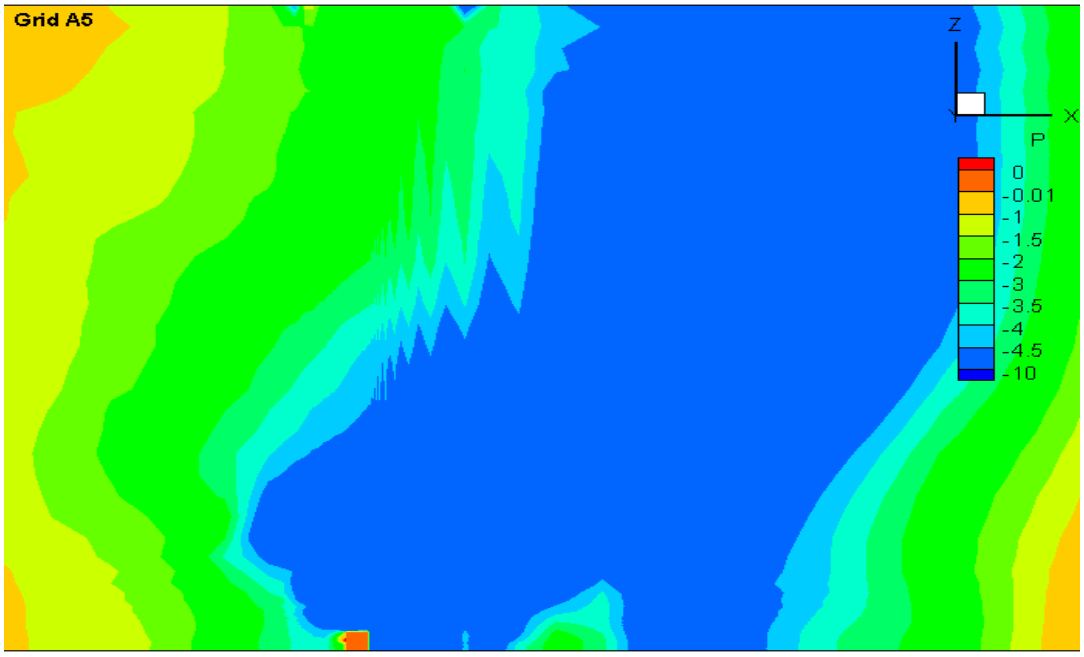

Figure 4.14 Grid A5 x-z plane pressure contour plots of a tornado

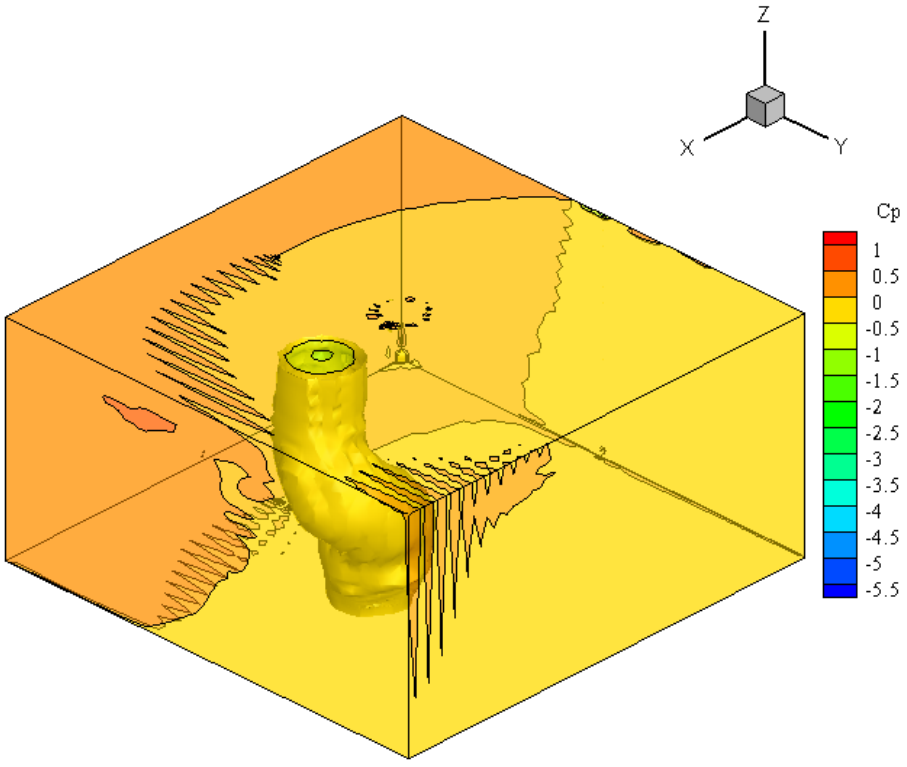

Figure 4.15 Grid A5, Three-dimensional view of the tornado

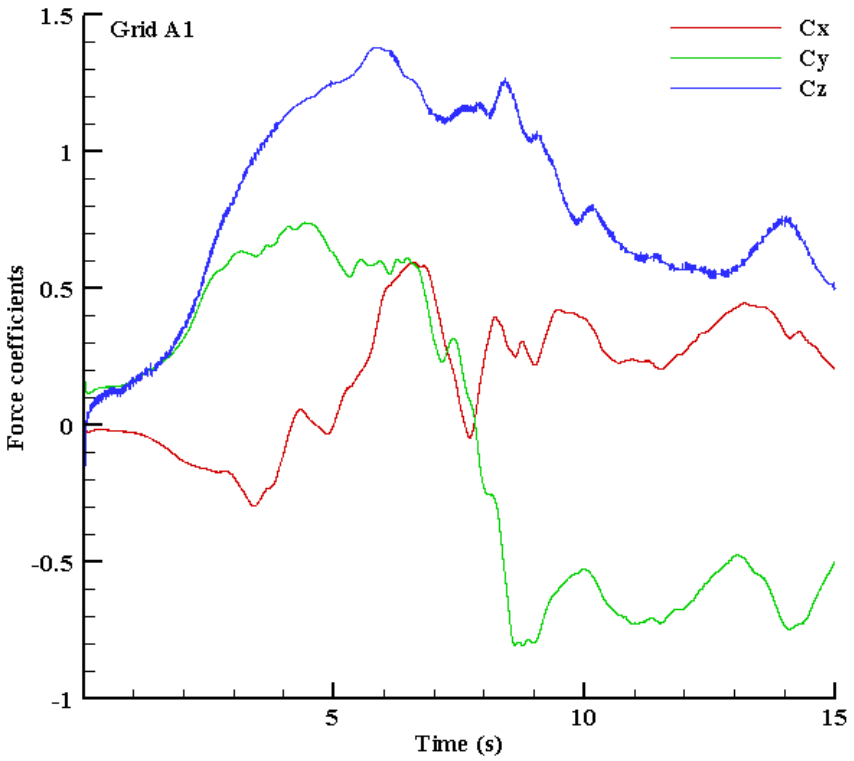

Figure 4.16 Computational domain (16 x 16 x 8), force coefficients

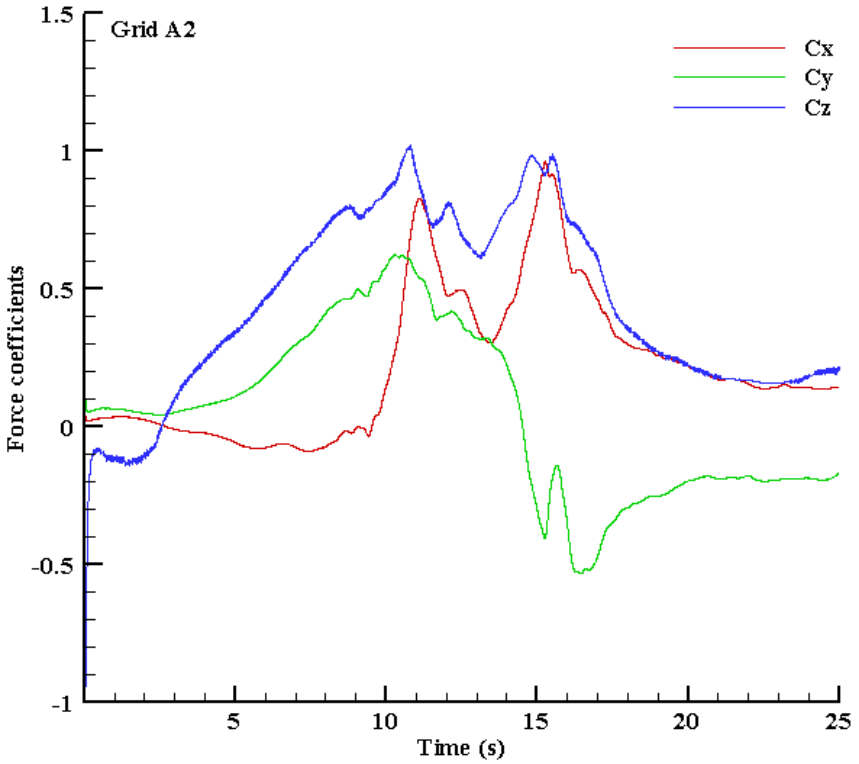

Figure 4.17 Computational domain (28 x 28 x 14), force coefficients

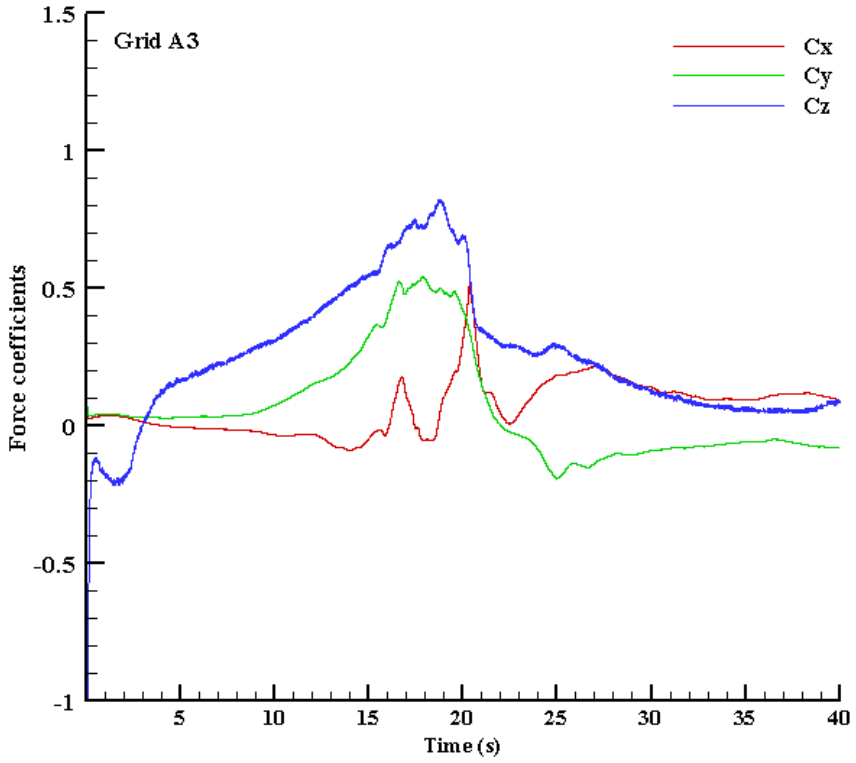

Figure 4.18 Computational domain (40 x 40 x 20), force coefficients

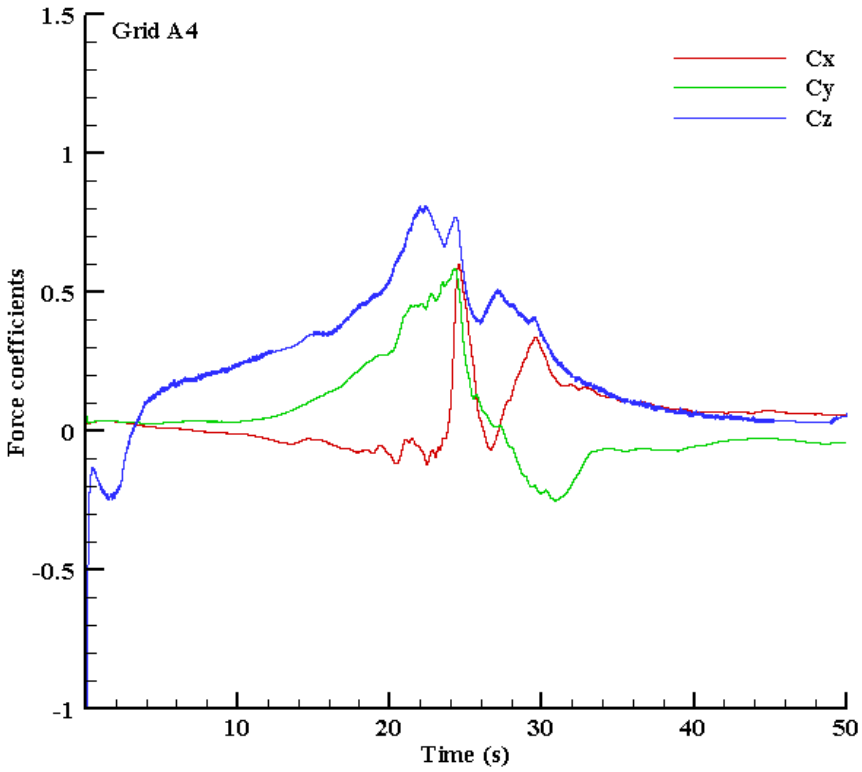

Figure 4.19 Computational domain (52 x 52 x 26), force coefficients

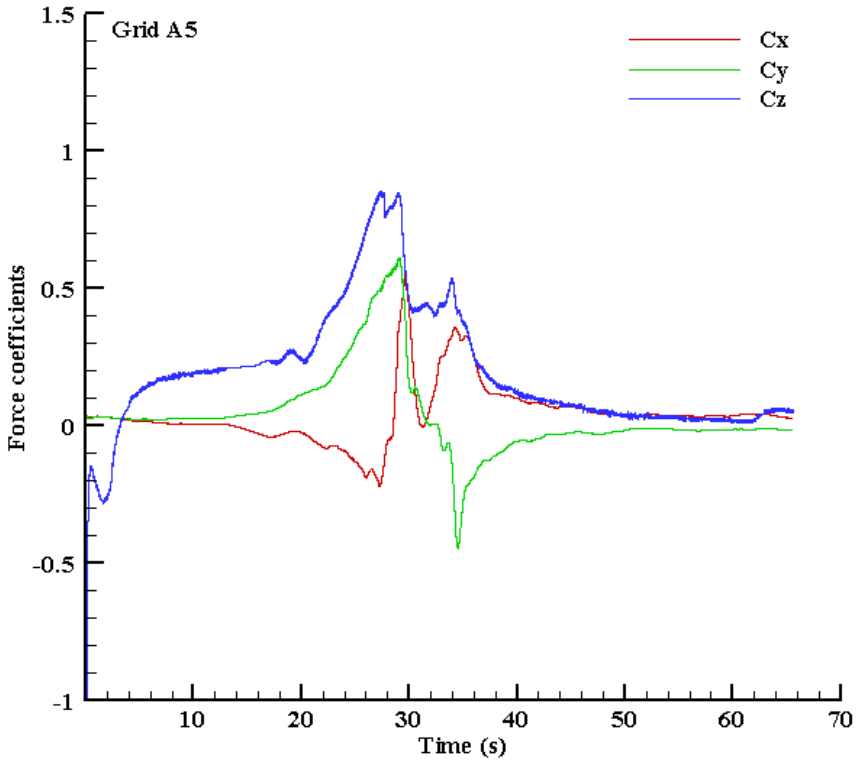

Figure 4.20 Computational domain (64 x 64 x 32), force coefficients

The computational domain size for grid A1, A2 and A3 were not sufficient enough to form a tornado in the computational domain. Grid A4 and A5 can be used to provide equitable result to the force coefficients induced by a tornado on a structure. The design of the computational fluid domain has to be at least 10 times the inner core tornado maximum radius in the x, y and z direction because the tornado has been completely form and the force coefficients did not change with increasing the computational domain size. Therefore, for future research, the computational fluid domain should be designed based on this study.

CHAPTER 5

COMPUTING TORNADO FORCES ON LARGE STRUCTURE PLAN AREAS

5.1 INTRODUCTION

The goal of this Chapter is to investigate tornado force coefficients on a square structure plan areas. The plan areas of the structure are set to be a square and a multiple of factor two for the same building height (h). The plan areas of the structure range from h x h to 8h x 8h. The tornado force coefficient comparison to the SL flow will more visible when comparing the structure plan area (h x h) to the largest structure plan area (8h x 8h).

In the numerical simulation, the tornado and SL flow approach the structure with two different angles of attack ($\beta = 0^0$ and $\beta = 45^0$). The tornado force coefficients are compared to the SL flow force coefficients for the same angle approaches. When the tornado approaches the structure with $\beta = 0^0$ and $\beta = 45^0$, the pressure coefficient (Cp) on the large structure plan area are compared. Besides the angles of attack, the same maximum translating ($V_{trans.}$) reference velocity will be used in both tornado and SL wind to compare the pressure coefficient (Cp) and the force coefficient (Cx) in the x-direction.

5.2 GRID PROPERTIES AND TORNADO PARAMETERS

Each grid name has the same grid properties layout in the x, y and z-directions and the grid has been generated by FORTRAN code. 0.005h minimum grid spacing normal to the structure and 0.05h spacing on the structure edges for all Large Structures Plan Areas (LSPA). The grid spacing layout in the computational domain increases by 1.25 times the assigned minimum grid spacing. When the spacing between two nodes reaches the half structure height in

each direction, the spacing is limited to half of the structure's height. The LSPA grid properties are given in Table 5.1.

Table 5.1 Large structure plan areas grid properties

Grid name	Structure plan areas	Grid size	Total # of points on Structure edges	Total # of points in domain
A	1h x 1h	88 x 88 x 69	21 x 21 x 21	534,336
B	2h x 2h	142 x 142 x 69	41 x 41 x 21	1,391,316
C	4h x 4h	208 x 208 x 69	81 x 81 x 21	2,985,216
D	8h x 8h	328 x 328 x 69	160 x 160 x 21	7,423,296

The mesh, or grid points, on the Structure Plan Area (SPA) is visualized by TecPlot software. The mesh on the SPA (1h x 1h) in the x-y plane is presented in Fig.5.1. Figure 5.2 shows a close up of the mesh for same structure plan area around the structure edges in x-y plane. The mesh of the rest of the LSPA are found in the Appendix (B-1).

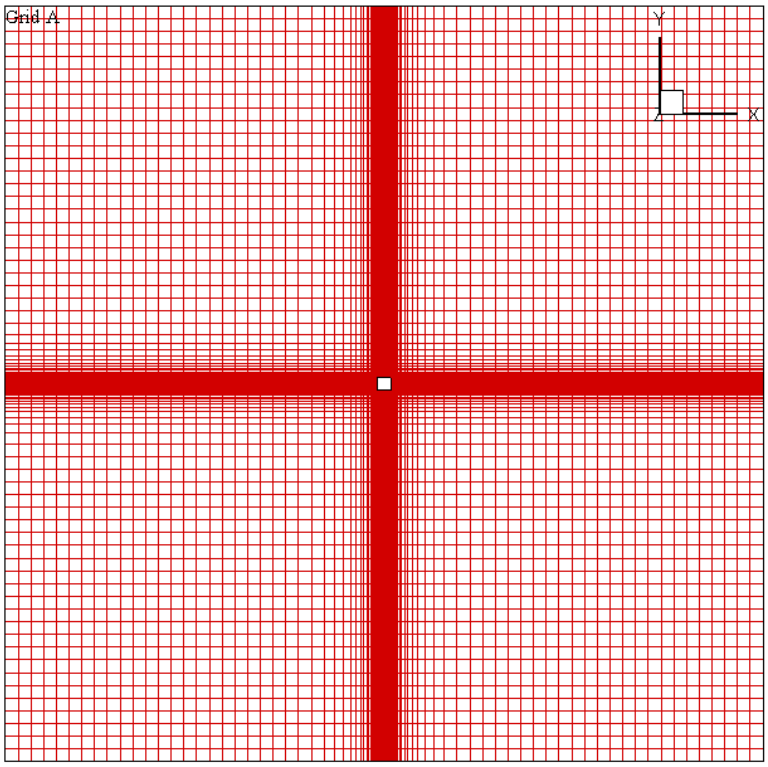

Figure 5.1 Structure plan area (1h x 1h), the x-y plane mesh

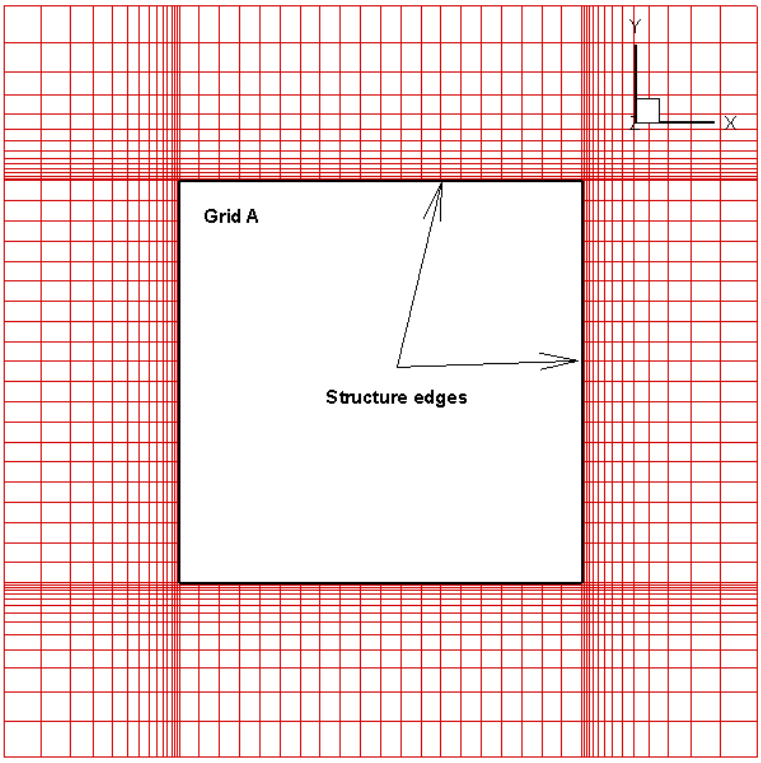

Figure 5.2 Structure plan area (1h x 1h), the x-y plane close up in the mesh

Top views of a tornado path approaching the LSPA with 0^0 and 45^0 angles of attack are illustrated in Figs.5.3 and 5.4 respectively. The structure geometry dimensionalizes by the height of the structure (h), and the translation velocity ($V_{trans.}$) dimensionalizes the flow velocity fields. The maximum velocity (V_{max}) in a tornado is the sum of two velocity components, and they are the tangential (V_θ) and the translation ($V_{trans.}$) velocities. The maximum velocity is calculated from the Rankine-Combined Vortex (RCV) velocities as described in Chapter 4. The tornado vortex strength (α) is the same for 0^0 and 45^0 angles of attack. The physical parameters used in this study are summarized in Table 5.2.

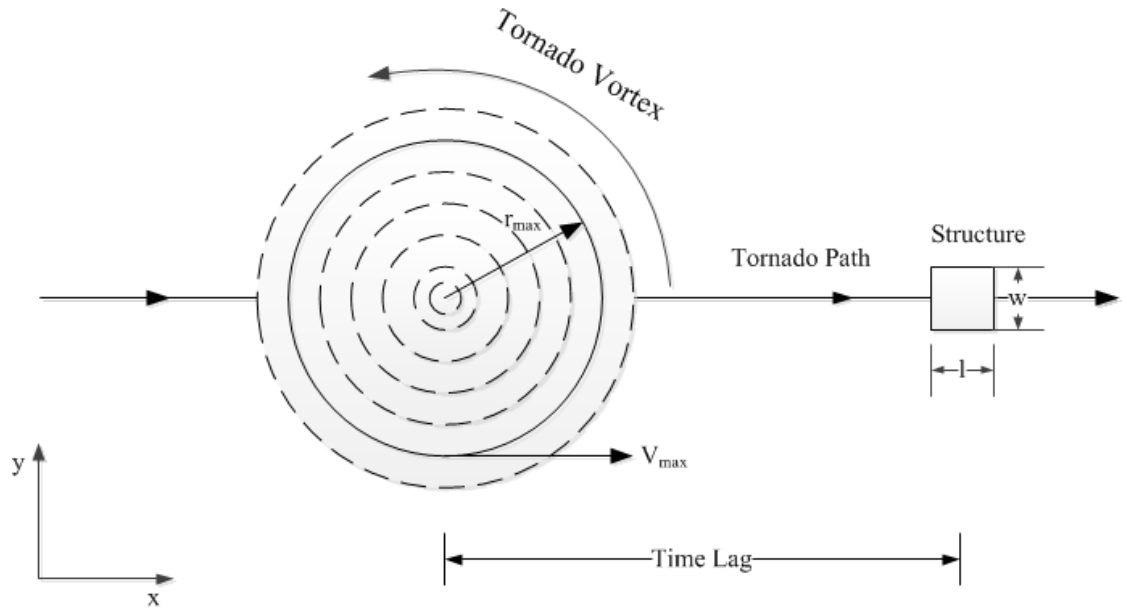

Figure 5.3 Top view of a tornado path approaches a structure with 0^0

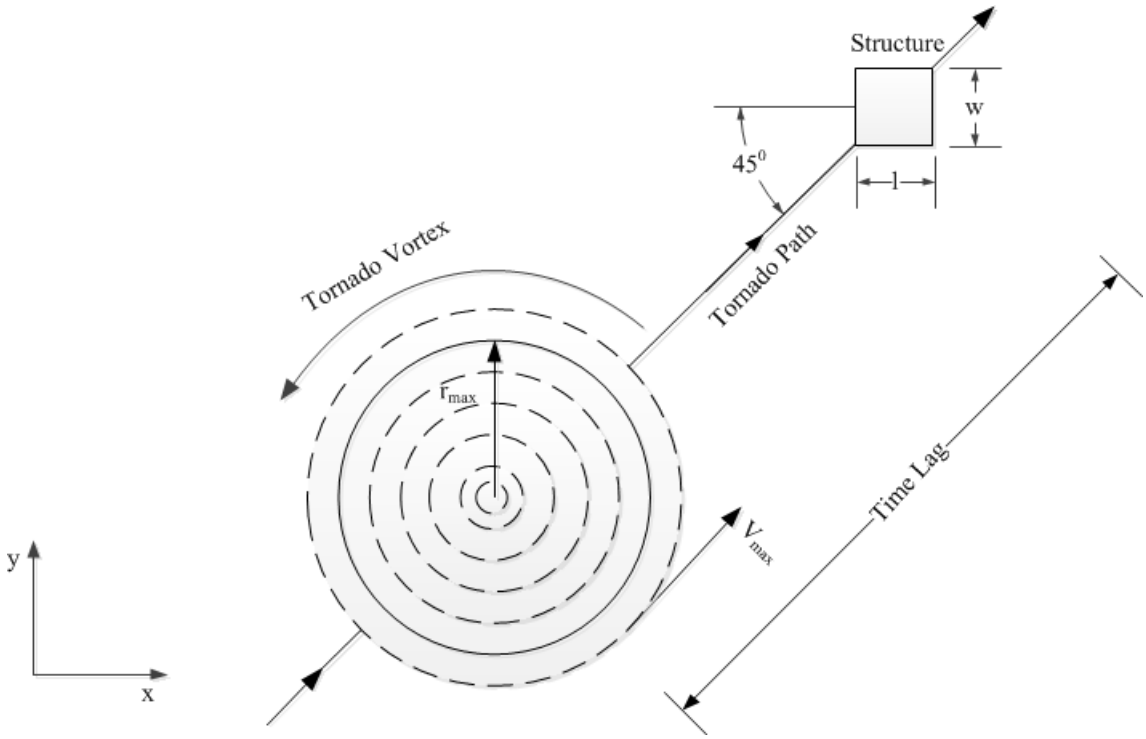

Figure 5.4 Top view of a tornado path approaches a structure with 45^0

Table 5.2 Large structure plan areas tornado parameters

	h	α	r_{max}	$V_{trans.}$	V_{θ}	V_{max}
English units	66.6 (ft)	1.5 (1/s)	200 (ft)	45.5 (mph)	205 (mph)	250.5 (mph)
SI units	20.3 (m)	1.5 (1/s)	61.0 (m)	20.3 (m/s)	91.5 (m/s)	111.8 (m/s)
Non-Dimensional units	1	1.5	3.0	1.0	4.5	5.5

5.3 GEOMETRY AND BOUNDARY CONDITIONS

The structure center starts at the origin axis and has the dimensions l for length, w for width and h for height. The computational fluid domain has the dimensions L for length, W for width and H for height. Figure 5.5 illustrates an isometric view of the structure and the computational fluid domain. The computational fluid domain is located approximately ten times the inner maximum tornado core radius (r_{max}) in each direction, as suggested by the design of the computational fluid domain in Chapter 4. The dimensions of the computational domain and the structure are specified in Table 5.3.

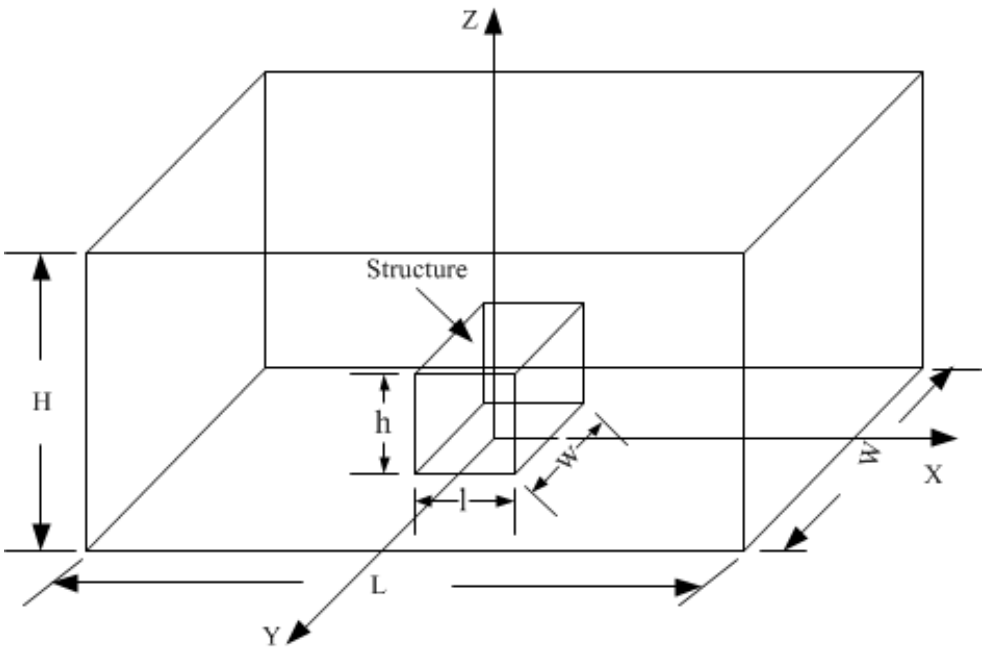

Figure 5.5 Isometric view of the computational fluid domain with the structure

Table 5.3 Computational domain and large structure plan area dimensions

Grid name	Domain size in h	Structure size
A	61 x 61 x 30.5	h x h x h
B	62 x 62 x 31	2h x 2h x h
C	64 x 64 x 32	4h x 4h x h
D	68 x 68 x 34	8h x 8h x h

On each face of the LSPA, zero velocities boundary conditions are applied (no slip boundary conditions). The boundary conditions applied on the exterior faces of the computational fluid domain are the RCV model velocities. The RCV velocity components are given in a Cartesian form as described in Eq. (5.1, 5.2, 5.3 and 5.4). The RCV model velocities are applied on each grid point in the computational domain, and these velocities change in time based on the location of the vortex core. The RCV model is discussed in detail in Chapters 3 and 4.

$$V_x = (V_t - y\alpha)Zf \qquad \text{if } r \le r_{max} \tag{5.1}$$

$$V_y = (x - V_t t)\alpha\, Zf \qquad if\ r \le r_{max} \tag{5.2}$$

$$V_x = (V_t - Cy)Zf \qquad \text{if } r > r_{max} \tag{5.3}$$

$$V_y = (x - V_t t)C\, Zf \qquad \text{if } r > r_{max} \tag{5.4}$$

The growth in the boundary layer along the z-axis (Zf) in the computational fluid domain is given in Eq.(5.5), as discussed in Chapter 4.

$$Zf = \frac{u}{k} \ln\left(\frac{h+h_0}{h_0}\right) \tag{5.5}$$

5.4 FORCE COEFFICIENTS AND PRESSURE COEFFICIENT

Forces on the LSPA are calculated by integrating the pressure on each surface area in x,y and z-directions. The force coefficients are obtained from Eq. (5.6, 5.7 and 5.8). The reported maximum tornado force coefficients on each structure are for the specified time lag. The time lag

is the period from the start of the simulation time and when the center of the tornado meets with the center of the structure. The pressure coefficient is calculated from Eq. (5.9).

$$Cx = \frac{F_x}{0.5\rho V^2 A} \tag{5.6}$$

$$Cy = \frac{F_y}{0.5\rho V^2 A} \tag{5.7}$$

$$Cz = \frac{F_z}{0.5\rho V^2 A} \tag{5.8}$$

$$Cp = \frac{\Delta p}{0.5\rho V^2} \tag{5.9}$$

The differential Pressure (Δp) is obtained from the computed pressure (p) subtracted from the reference (P_{ref}). P_{ref} is fixed at a constant value of 0. The force coefficients were defined in Chapter 4 (section 4.5).

The reference velocity (V) has an assigned value based on the numerical study. If a tornado is simulated in the computational domain, the reference velocity is the maximum velocity (V_{max}). On the other hand, if a SL wind flow is simulated in the computational domain, the reference velocity is the translating velocity ($V_{trans.}$).

5.5 LARGE STRUCTUE PLAN AREAS RESULTS AND DISCUSSION

The UA-CFD wind code was used to compute the tornado force coefficients on LSPA (h x h, 2h x 2h , 4h x 4h and 8h x 8h) and compare them to the SL flow force coefficients. The tornado approached the structure with 0^0 and 45^0 angles of attack. The force coefficient and pressure coefficients on the LSPA were computed when the tornado center was coincided with the structure center. The two centers coincide when the time is equal to the specified time lag in the numerical simulation. Figures 5.6 and 5.7 illustrate how the force coefficients and pressure coefficient are implemented in this Chapter.

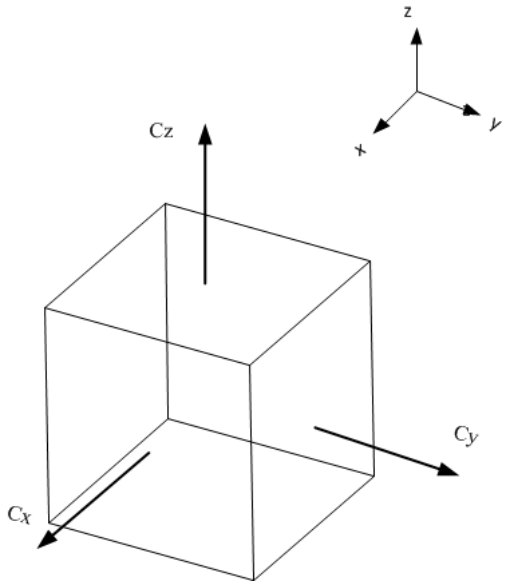

Figure 5.6 Force coefficients on the structure

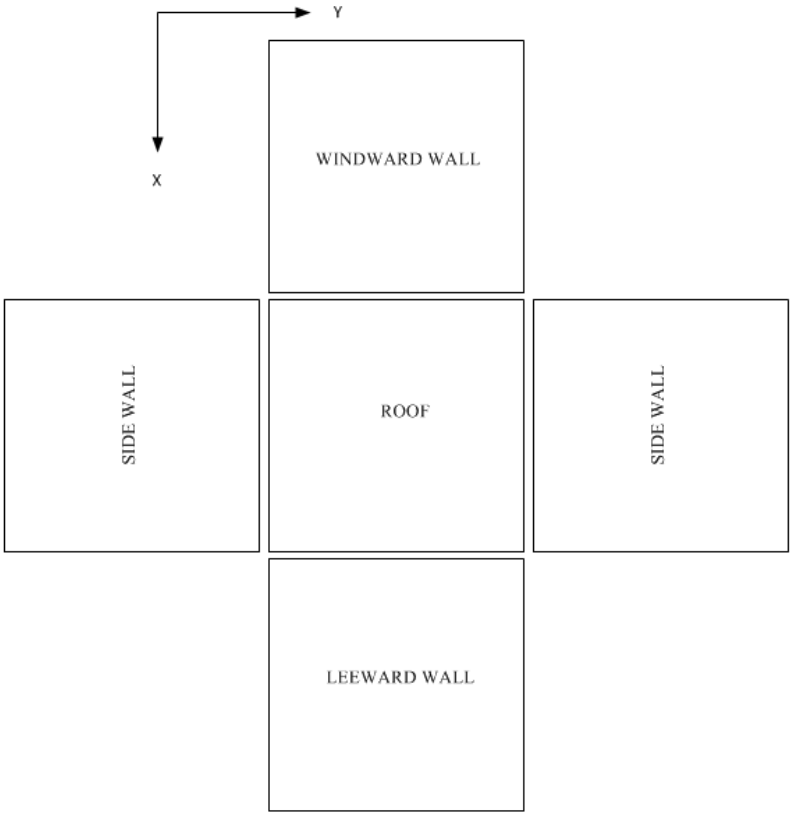

Figure 5.7 Layout of an exploded structure faces

Here we defined the Large Structure Plan Area Characteristic Length Ratio (LSPACLR) as d_{ratio} , the Large Structure Plan Areas Characteristic Diagonal Length (LSPACDL) as d_L, and the Tornado Maximum Characteristic Diameter (TMCD) as d_{max}. The LSPACLR is the ratio between the LSPACDL to TMCD. The LSPACLR is calculated form Eq. (5.10). Table 5.4 gives the values of the LSPACLR for each LSPA. Figure 5.8 illustrates the TMCD and the LSPACDL in the x-y plane for the LSPA.

$$d_{ratio} = \frac{d_L}{d_{max}} \tag{5.10}$$

Table 5.4 Tornado and structure plan areas characteristic length

Grid Name	Structure plan areas	d_L	d_{max}	d_{ratio}
A	1h x 1h	$\sqrt{2}$	6	0.24
B	2h x 2h	$2\sqrt{2}$	6	0.47
C	4h x 4h	$4\sqrt{2}$	6	0.94
D	8h x 8h	$8\sqrt{2}$	6	1.88

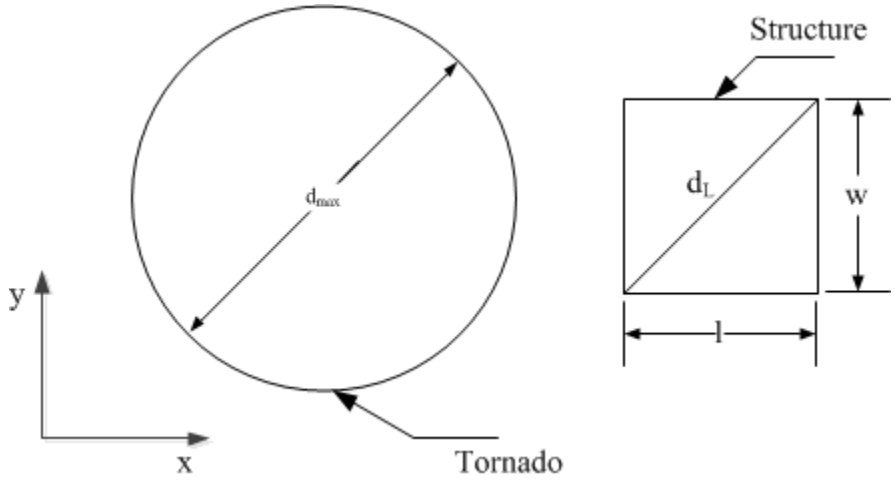

Figure 5.8 Tornado and structure characteristic length in x-y plane

The following sections will discuss first how the SPA has an influence on the tornado force coefficients compared to SL flow force coefficients, second the tornado pressure coefficient for two different angles approaches, and lastly the use of the same maximum

reference velocity ($V_{trans.}$) in both tornado and SL flow to compare the pressure coefficient on the structure roof and the force coefficient in the x-direction.

5.5.1 TORNADO FORCE COEFFICIENTS VS. SL FORCE COEFFICIENTS

Tornado and SL flow forces on a structure are computed by integrating the pressure on each surface of the LSPA. The force coefficients and pressure coefficient are calculated from Eqs. (5.6, 5.7, 5.8, and 5.9). As mentioned before, the reported maximum force coefficients are for the specified time lag in the simulation. At the specified time lag, the tornado center coincides with the structure center as shown in Fig. 5.9 for SPA (1h x 1h). The maximum force coefficients are reported in Table 5.5. The force coefficients in the x, y and z-directions showed that when the plan area is increased the force coefficient is decreased when the tornado approached the structure with $\beta = 0^0$ and $\beta = 45^0$ as shown in Table 5.5.

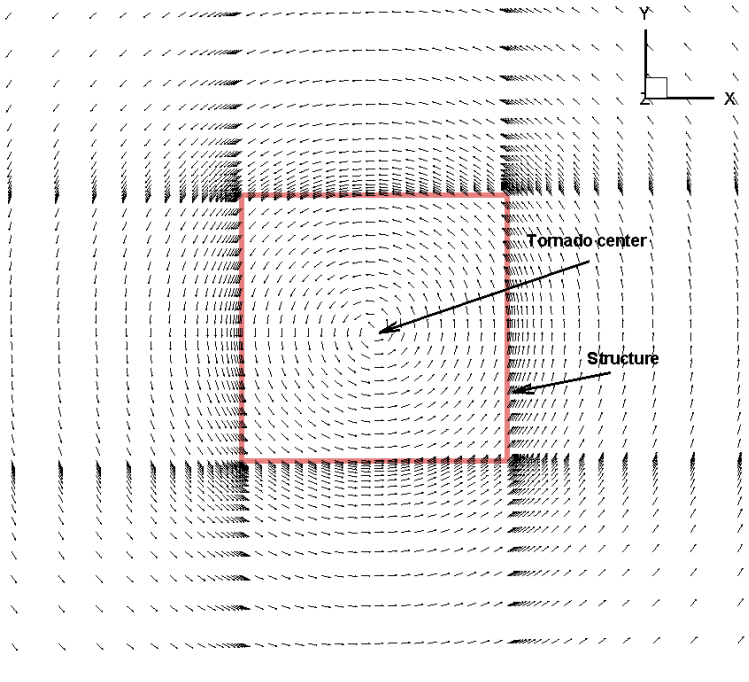

Figure 5.9 Tornado center and structure plan area (1h x 1h) center, 0.5h above the roof

The illustration of the force coefficients magnitude on the SPA (1h x 1h) is given in Fig 5.10 for $\beta = 0^0$. These force coefficients are the maximum force coefficients on the structure when the tornado center coincided with the structure center. same methodology can be applied on the SPA (2h x 2h , 4h x 4h and 8h x 8h) to visualize the force coefficients (see Table 5.4).

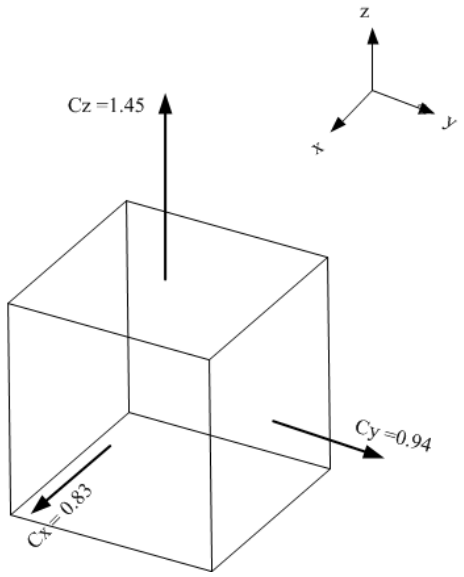

Figure 5.10 Force coefficients magnitude on the structure plan area (1h x 1h) for $\beta = 0^0$

Table 5.5 Tornado and SL flow absolute maximum force coefficients

Flow types	Grid Name	Structure plan areas	Angle of attack β	C_x	C_y	C_z
Tornado flow	A	h x h	0^0	0.83	0.94	1.45
			45^0	**0.91**	**0.60**	**1.46**
	B	2h x 2h	0^0	0.51	0.73	1.15
			45^0	**0.70**	**0.35**	**0.92**
	C	4h x 4h	0^0	0.14	0.20	0.27
			45^0	**0.27**	**0.10**	**0.31**
	D	8h x 8h	0^0	0.03	0.03	0.067
			45^0	**0.07**	**0.09**	**0.10**
SL flow	A	h x h	0^0	0.75	0.01	0.75
			45^0	**0.87**	**0.82**	**0.89**
	B	2h x 2h	0^0	0.74	0.002	0.62
			45^0	**0.81**	**0.72**	**0.70**
	C	4h x 4h	0^0	0.71	0.001	0.46
			45^0	**0.55**	**0.53**	**0.67**
	D	8h x 8h	0^0	0.69	0.01	0.47
			45^0	**0.29**	**0.28**	**0.74**

When the tornado approached the SPA (4h x 4h and 8h x 8h) with $\beta = 45^0$, it created approximately 20 % more force coefficients on the structure compared to $\beta = 0^0$. In this situation, the tornado covered more surface area and created high suction pressure on the roof and walls because of the angel of approach. The magnitude of the LSPCLR for SPA (8h x 8h) showed that the tornado covered nearly 50 % of the SPA. Therefore, on the SPA (4h x 4h and 8h x 8h), the tornado had a localized vortex effect on affected region whereas on the SPA (1h x 1h and 2h x 2h), the tornado vortex completely overlaid the SPA. From this, we conclude that the tornado force coefficients decreased when the SPA increased because the tornado did not affect portions of the SPA (8h x 8h).

On SPA (h x h), the tornado produced twice the force coefficient on the roof in the z-direction (C_z) compared to the SL wind for both angles of attack as shown in Figs. 5.11 and 5.12. The time history of the force coefficients on SPA (2h x 2h) for both tornado and SL flow are plotted in Figs. 5.13 and 5.14 for $\beta = 0^0$. Figure 5.13 indicated that when the tornado engulfed the LPA (2h x 2h) with $\beta = 0^0$, it exerted high suction force on all side walls and lifting force on the structure roof. However, Fig.5.14 illustrated that the SL flow force coefficient on the LPA (2h x 2h) showed a fluctuation for $\beta = 0^0$. Similar, from the time history force coefficient plot, the tornado generated high suction force on the roof and structure wall sides for $\beta = 45^0$. The force coefficients time history on the other LSPA are found in Appendix (B-2) for $\beta = 0^0$, $\beta = 45^0$.

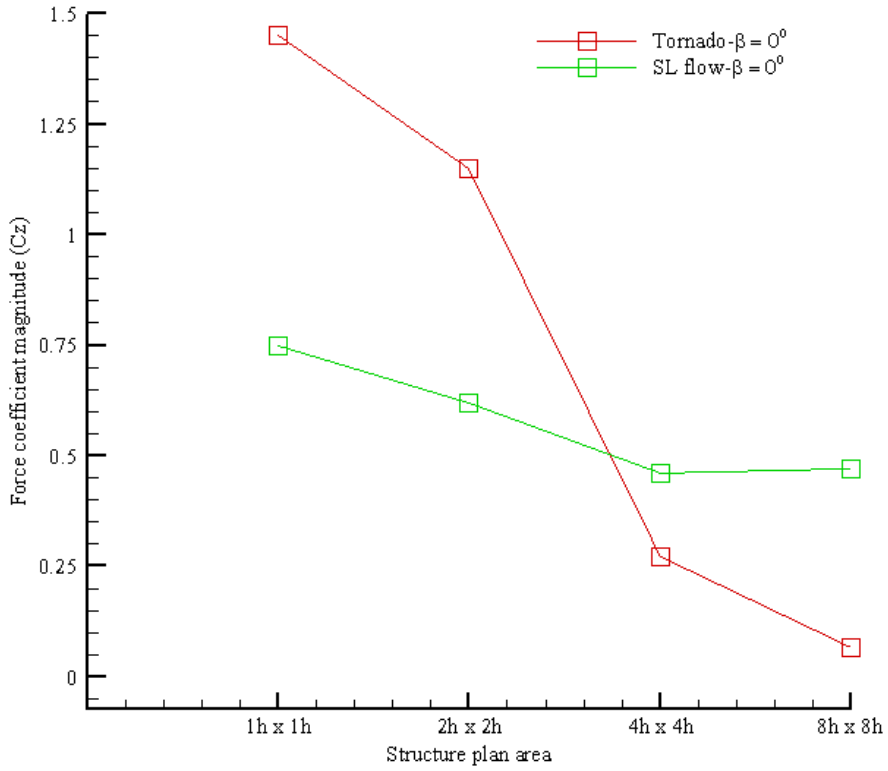

Figure 5.11 Large structure plan areas roof force coefficient comparison, $\beta=0^0$

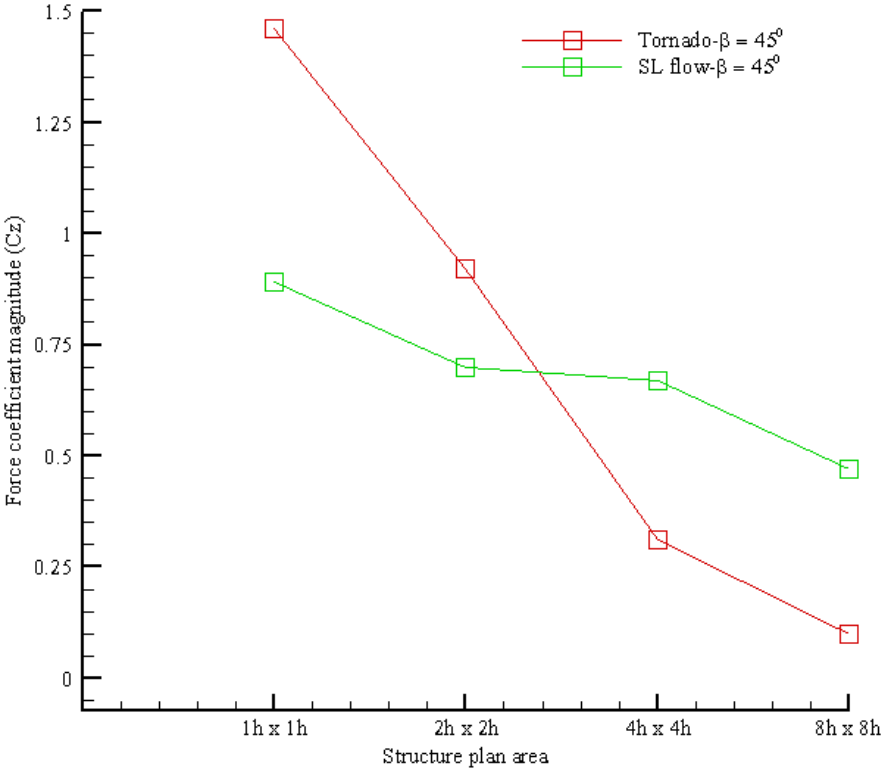

Figure 5.12 Large structure plan areas roof force coefficient comparison, $\beta=45^0$

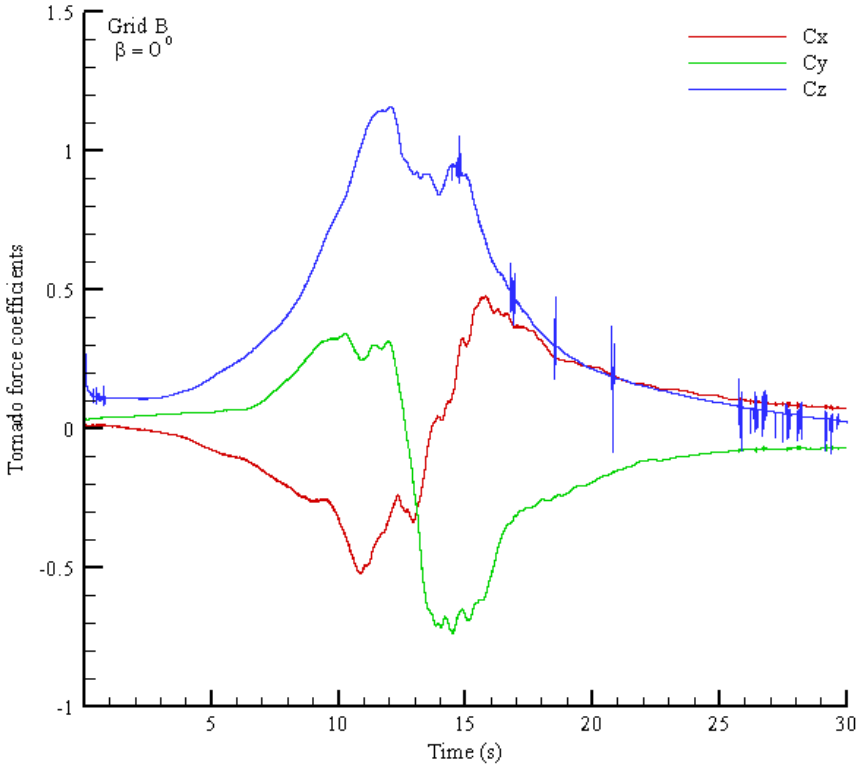

Figure 5.13 Structure plan area (2h x 2h), Tornado force coefficients, $\beta=0^0$

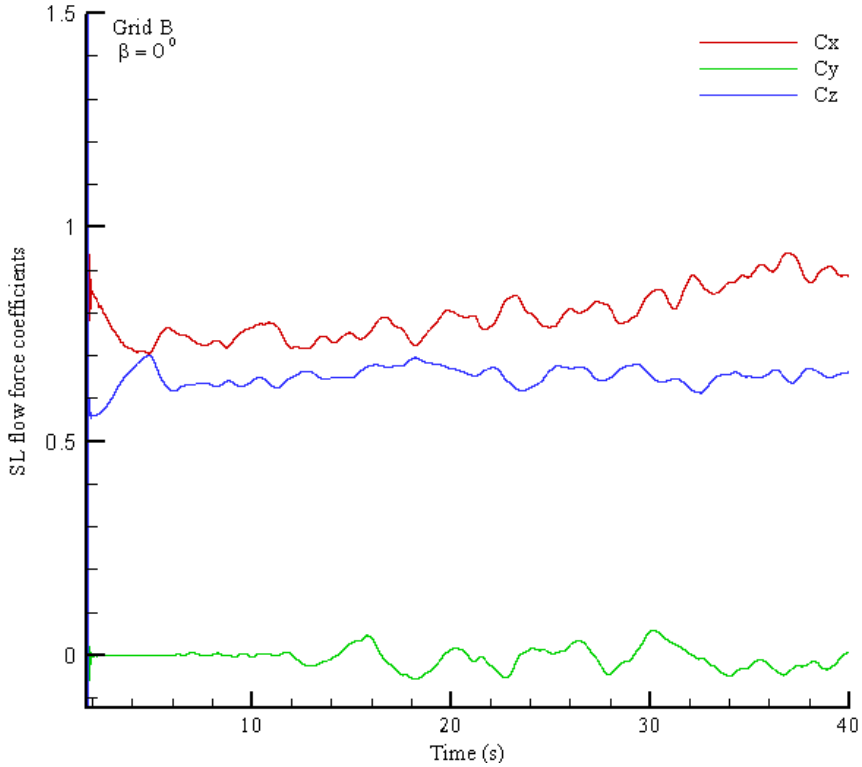

Figure 5.14 Structure plan area (2h x 2h), SL wind force coefficients, $\beta=0^0$

5.5.2 TORNADO PRESSURE COEFFICIENT

The pressure was iterated at each grid point by solving the NSEs numerically in the computational fluid domain in the x, y and z-directions. Consequently, the pressure was integrated on each grid cell, and the pressure coefficients (Cp) on the LSPA were computed from Eq. (5.9). The tornado maximum pressure coefficients (Cp) on the LSPA roof are tabulated in Table 5.6 for two angles' tornado approaching the structure. Figure 5.15 shows the tornado maximum pressure coefficient (Cp) comparison on LSPA.

Table 5.6 Tornado maximum pressure coefficient on large structure plan areas

Grid name	Structure plan areas	$C_{p,max}$ $\beta = 0^0$	$C_{p,max}$ $\beta = 45^0$
A	h x h	-1.8	-1.6
B	2h x 2h	-1.2	-1.1
C	4h x 4h	-0.35	-0.45
D	8h x 8h	-0.07	-0.16

When the Tornado approached the SPA (1h x 1h and 2h x 2h) with $\beta = 0^0$ and $\beta = 45^0$, it generated high suction pressure on the roof of the structure as shown in Fig.5.15 because the tornado vortex covered the SPA. When $\beta = 45^0$ and the SPA increase to (4h x 4h and 8h x 8h), the tornado created 10% suction pressure on the roof and corners compared to $\beta = 0^0$ as shown in Table 5.6. This increase occurred because the tornado vortex core covered a larger percentage of the SPA.

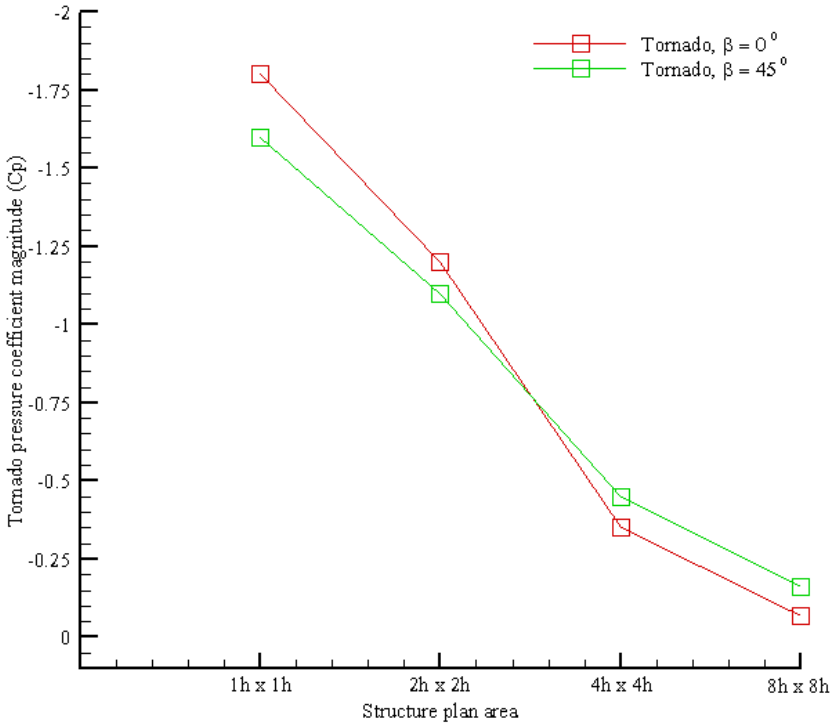

Figure 5.15 Tornado pressure coefficient (Cp) comparisons on large structure plan areas

Figures 5.16 and 5.17 show an x-y plane of the SPA (1h x 1h) compared to the tornado vortex size and the exploded faces of the pressure coefficients for $\beta = 0^0$. Figures 5.18 and 5.19 show the same illustration for $\beta = 45^0$. The LSPACL for SPA (1h x 1h) is nearly one quarter the tornado TMCD. The tornado is completely covered the SPA (1h x 1h) when the center of the tornado coincides with the structure center. When the tornado approached the SPA (1h x 1h) with $\beta = 0^0$ (Fig. 5.17), it generated high suction pressure on the windward, leeward and the roof, whereas when $\beta = 45^0$ (Fig 5.19) the tornado created high suction pressure on the structure corner and the roof.

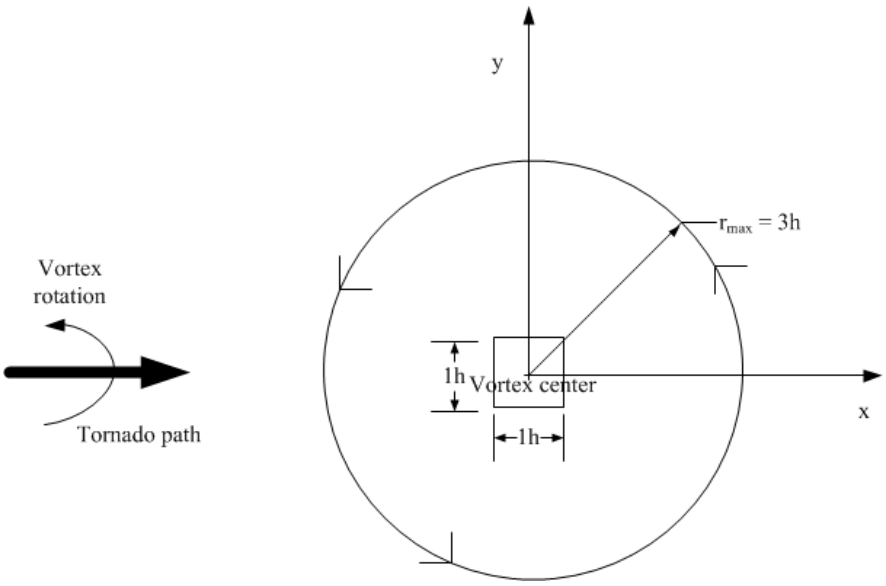

Figure 5.16 x-y plane schematic of the structure plan area (1h x1h) vs. tornado vortex ($\beta = 0^0$)

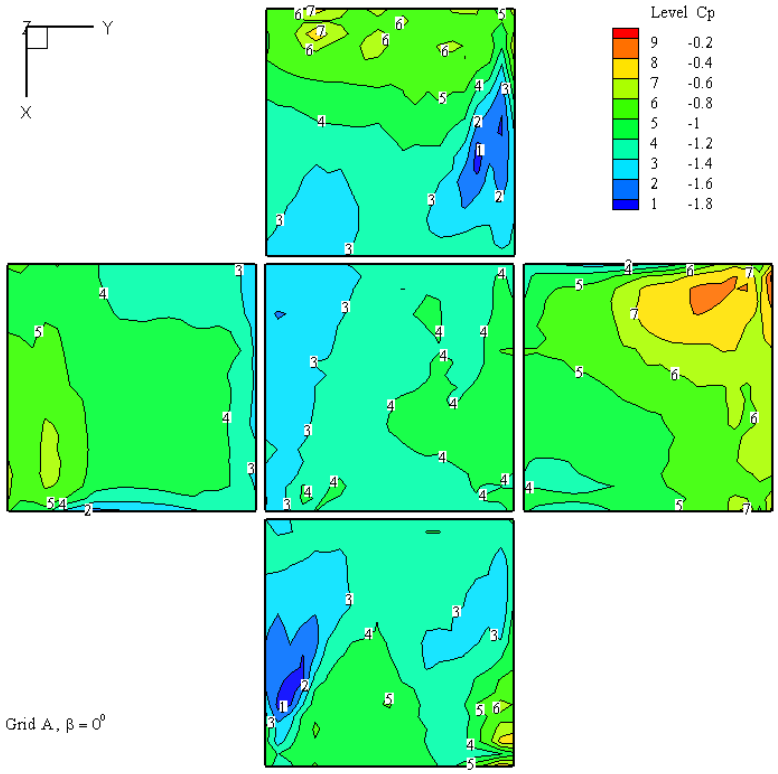

Figure 5.17 Structure plan area (1h x 1h), exploded faces of the pressure coefficients ($\beta = 0^0$)

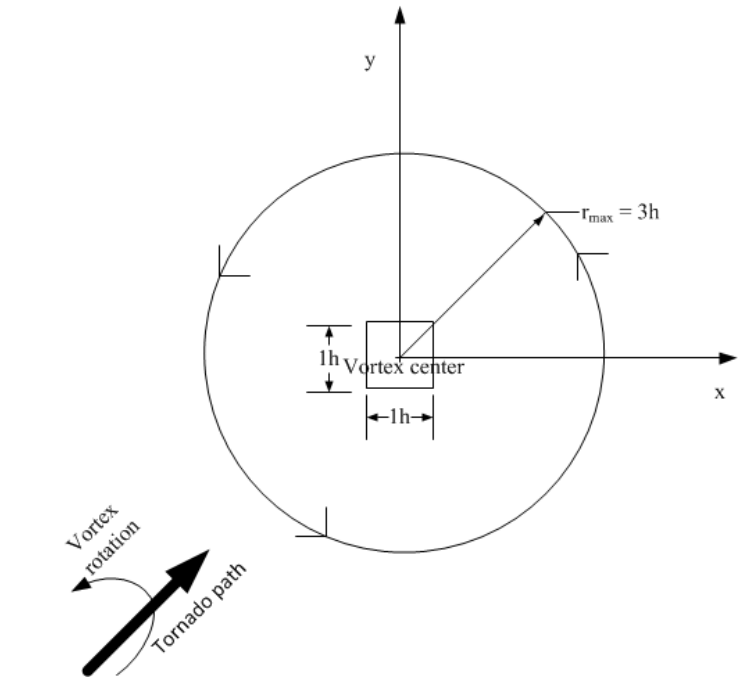

Figure 5.18 x-y plane schematic of the structure plan area (1h x1h) vs. tornado vortex (β= 45^0)

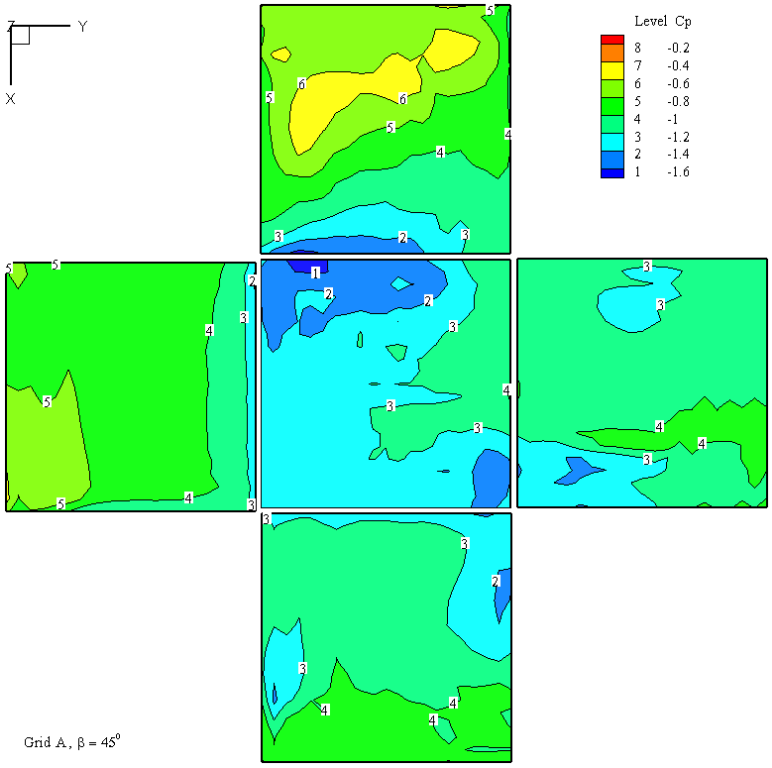

Figure 5.19 Structure plan area (1h x 1h), exploded faces of the pressure coefficients (β= 45^0)

Figure 5.20 shows an x-y plane schematic of the SPA (2h x 2h) compared to the tornado vortex size for $\beta = 0^0$. Figure 5.22 shows the same illustration for $\beta = 45^0$. The SPA (2h x 2h) characteristic length is approximately half the tornado characteristic vortex length. The distributions of the pressure coefficients on the structure exploded faces plan area (2h x 2h) are illustrated in Figs.5.21 and 5.23 for $\beta = 0^0$ and $\beta = 45^0$. When the tornado approaching the SPA (2h x 2h) with $\beta = 0^0$ (see Fig.5.21), it created high suction pressure on the roof, whereas when the tornado approaching the same SPA with $\beta = 45^0$ (see Fig.5.22), it generated high suction pressure on the roof, side walls and leeward wall.

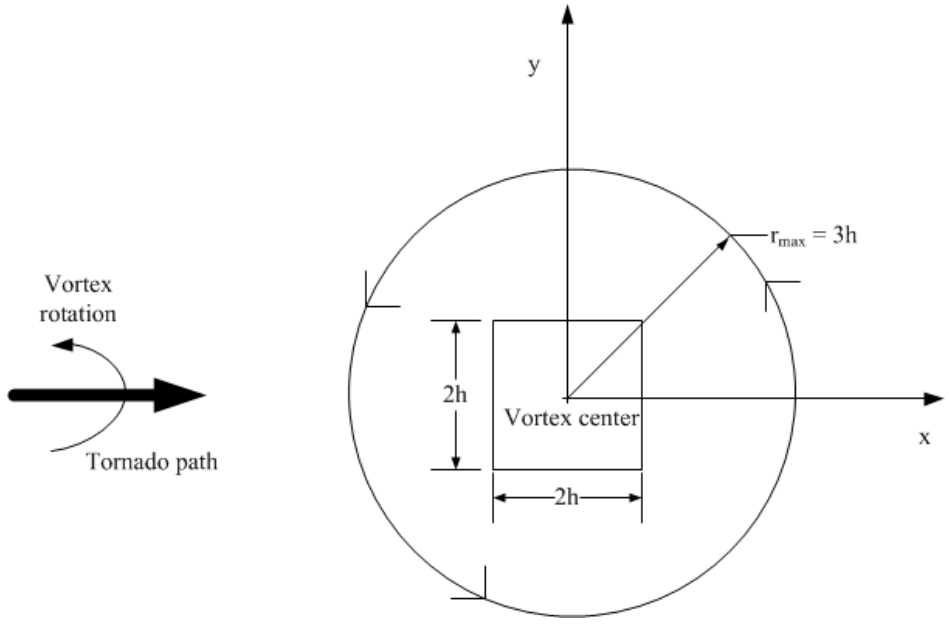

Figure 5.20 x-y plane schematic of the structure plan area (2h x2h) vs. tornado vortex ($\beta = 0^0$)

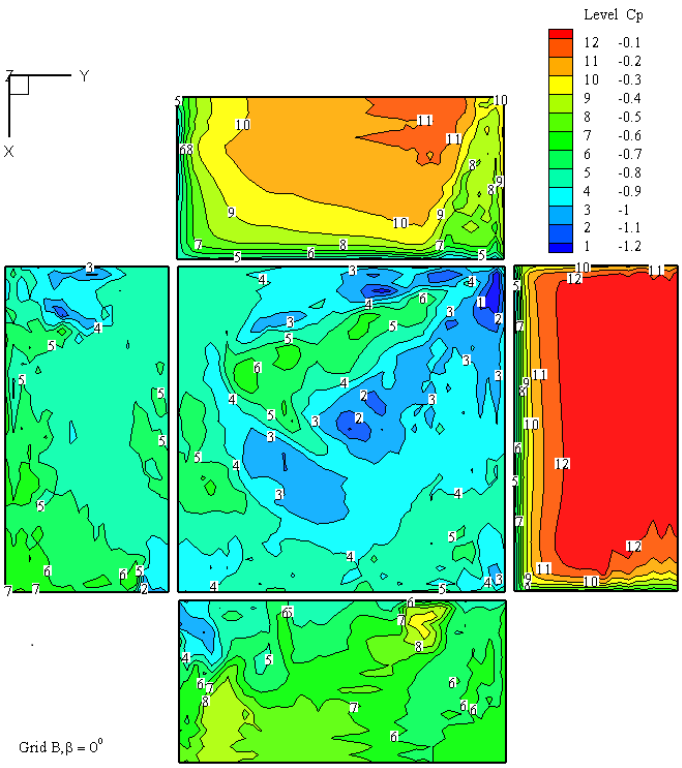

Figure 5.21 Structure plan area (2h x 2h), exploded faces of the pressure coefficients ($\beta = 0^0$)

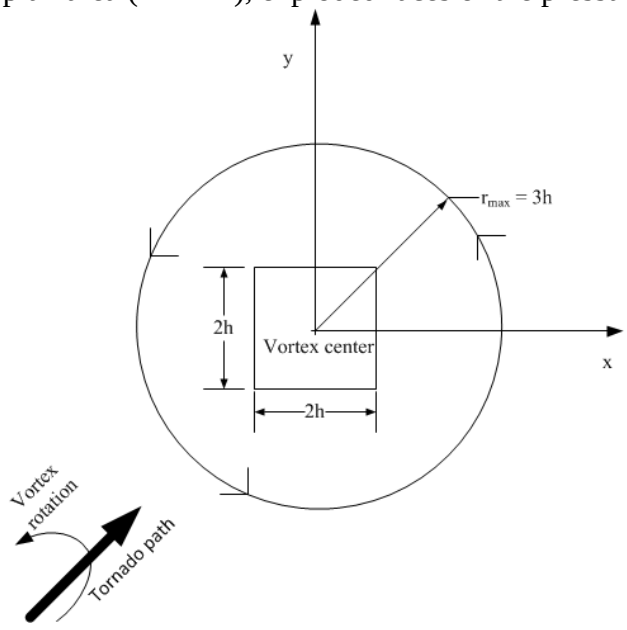

Figure 5.22 x-y plane schematic of the structure plan area (2h x2h) vs. tornado vortex ($\beta = 45^0$)

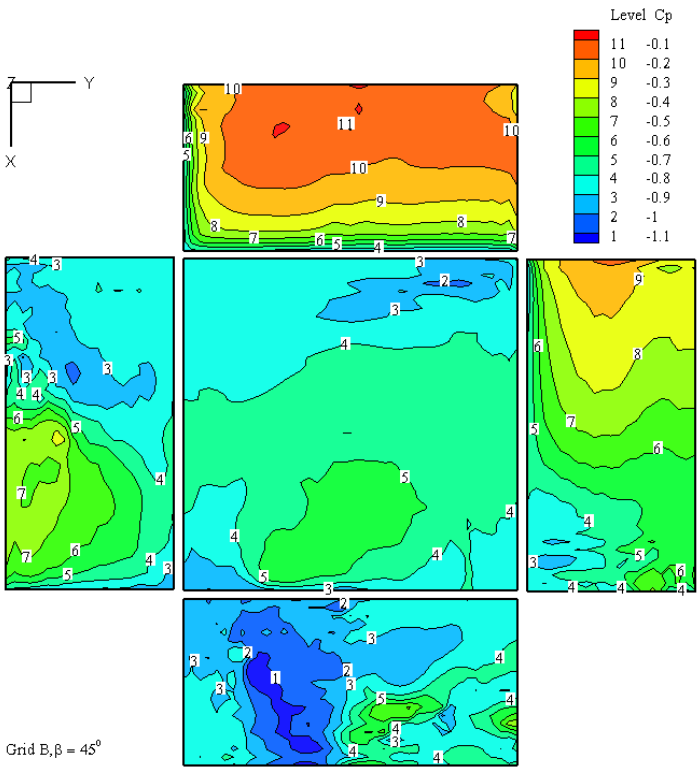

Figure 5.23 Structure plan area (2h x 2h), exploded faces of the pressure coefficients ($\beta = 45^0$)

The x-y plane schematic of the SPA (4h x 4h) compared to the tornado vortex size is illustrated in Figs. 5.24 and 5.26 for $\beta = 0^0$ and $\beta = 45^0$, respectively. The SPA (4h x 4h) characteristic length is approximately conterminous the tornado characteristic vortex length. The tornado vortices almost covered the SPA (4h x 4h). The distributions of the pressure coefficients on the structure exploded faces of SPA (4h x 4h) are illustrated in Figs.5.25 ($\beta = 0^0$) and 5.27($\beta = 45^0$). Figure 5.25 shows that when the tornado approaching the structure with $\beta = 0^0$, it engendered high suction pressure on the roof and side walls, whereas when the tornado approaching the same SPA with $\beta = 45^0$, it generated high suction pressure on the roof, side walls and leeward wall as shown in Fig.5.27.

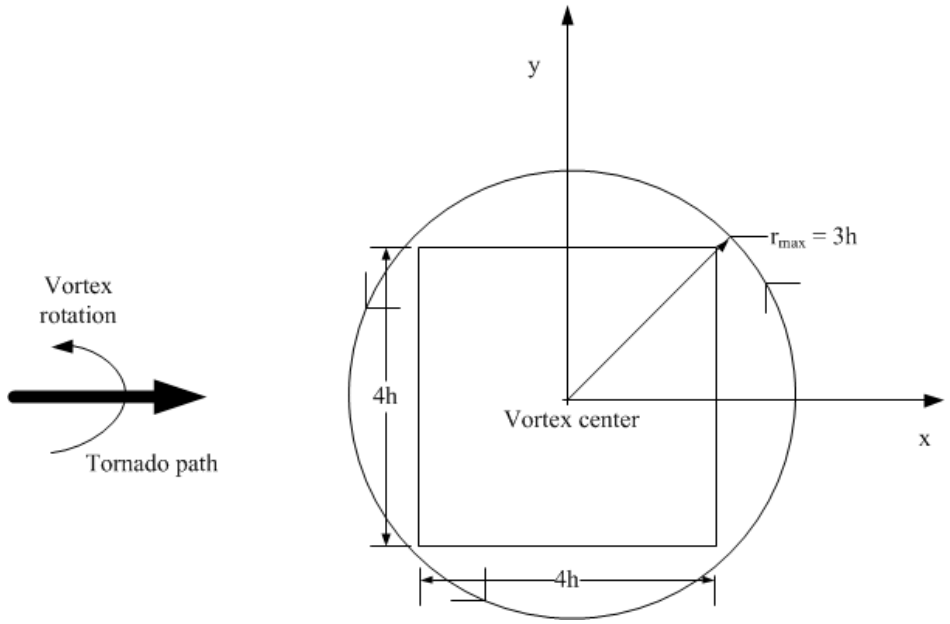

Figure 5.24 x-y plane schematic of the structure plan area (4h x4h) vs. tornado vortex ($\beta = 0^0$)

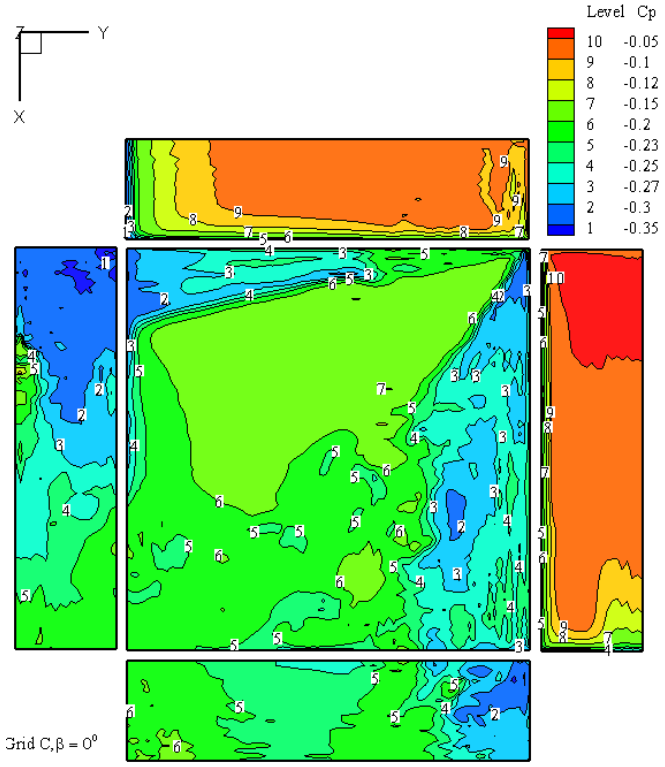

Figure 5.25 Structure plan area (4h x 4h), exploded faces of the pressure coefficients ($\beta = 0^0$)

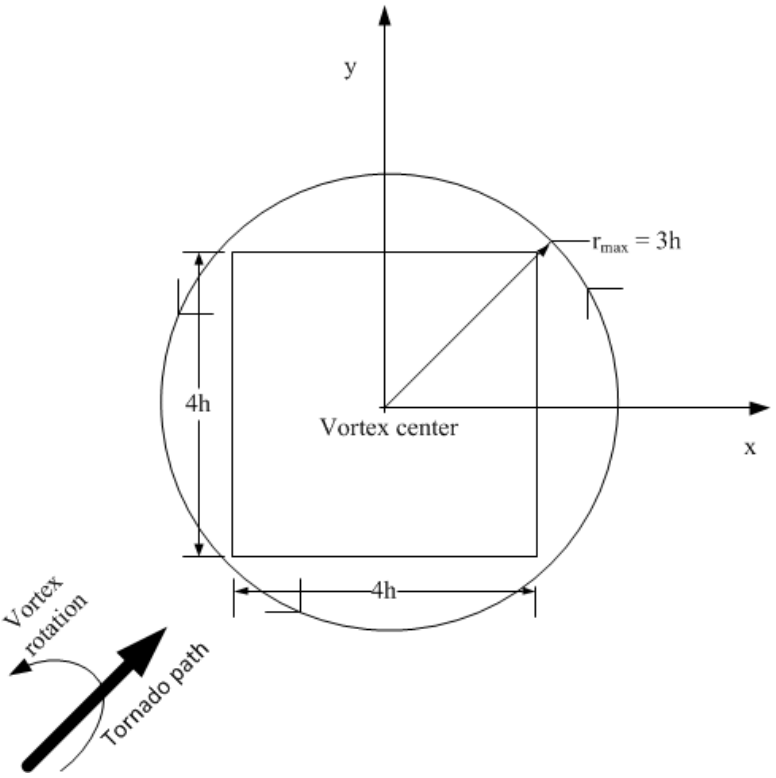

Figure 5.26 x-y plane schematic of the structure plan area (4h x4h) vs. tornado vortex (β= 45^0)

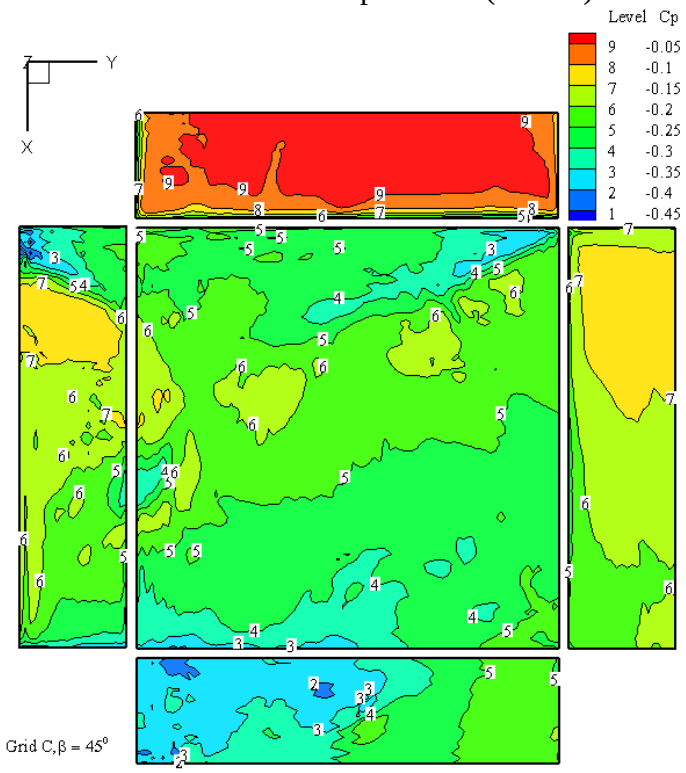

Figure 5.27 Structure plan area (4h x 4h), exploded faces of the pressure coefficients (β= 45^0)

Figures 5.28 (β= 0^0) and 5.30 (β= 45^0) show the x-y plane schematic of the SPA (8h x 8h) compared to the tornado vortex size. The SPA (8h x 8h) characteristic length is approximately twice the tornado characteristic vortex length. The tornado vortices are smaller than the SPA (8h x 8h) when the tornado completely engulfed the structure. The distributions of the pressure coefficients on the exploded faces on SPA (8h x 8h) are illustrated in Figs.5.29 (β= 0^0) and 5.31(β= 45^0). Figure 5.29 shows that when the tornado approaching the SPA (8h x 8h) with β= 0^0, it produced high suction pressure on the roof, whereas when β= 45^0 the tornado generated high suction pressure on the roof corners as shown in Fig.5.31.

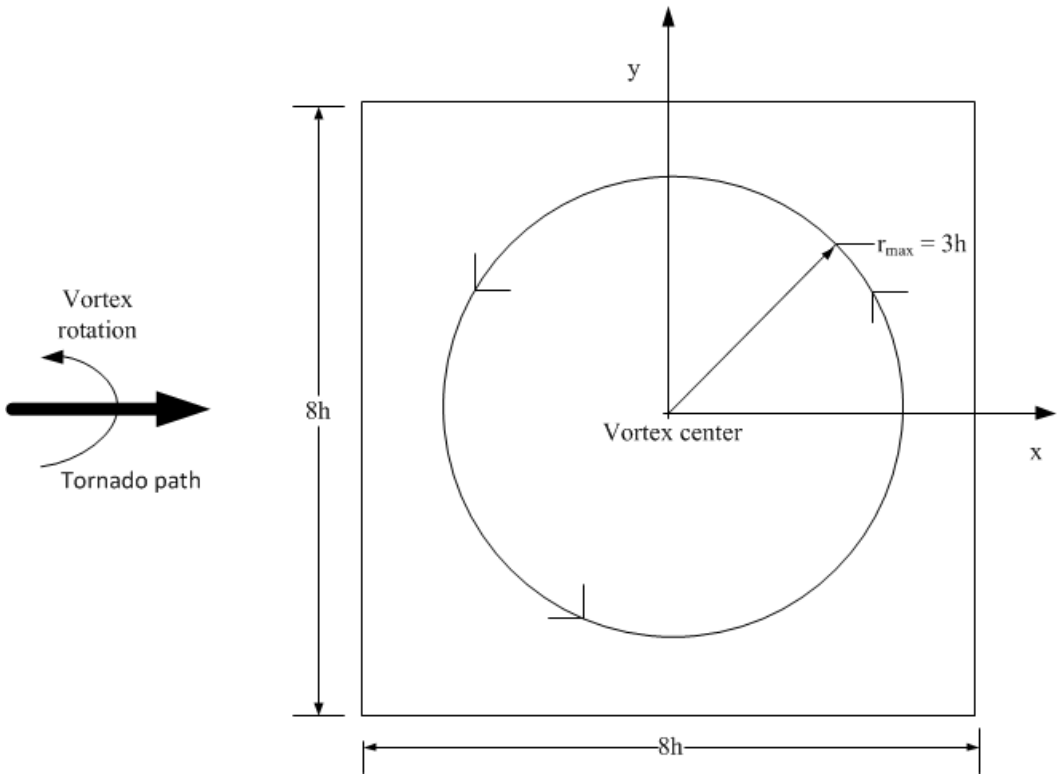

Figure 5.28 x-y plane schematic of the structure plan area (8h x8h) vs. tornado vortex (β= 0^0)

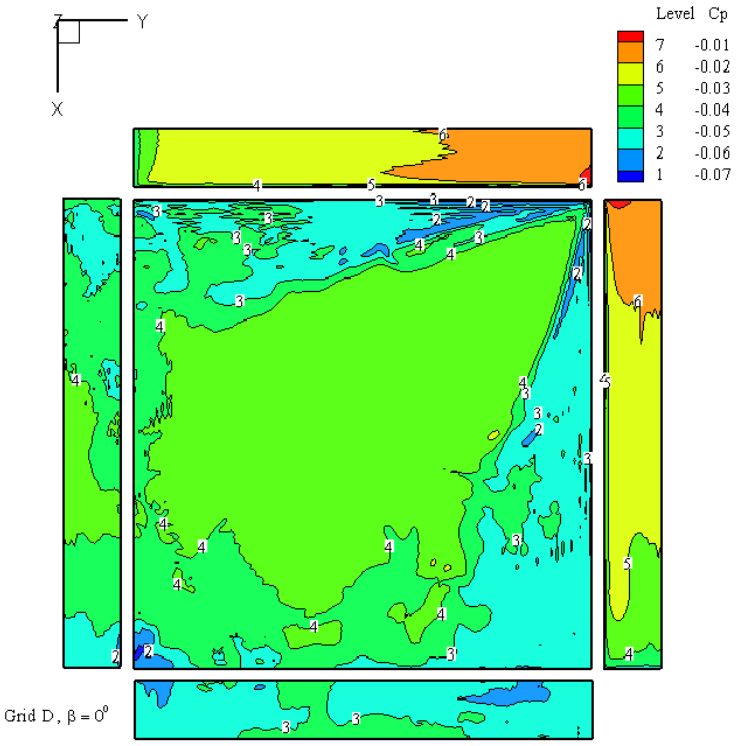

Figure 5.29 Structure plan area (8h x 8h), exploded faces of the pressure coefficients ($\beta = 0^0$)

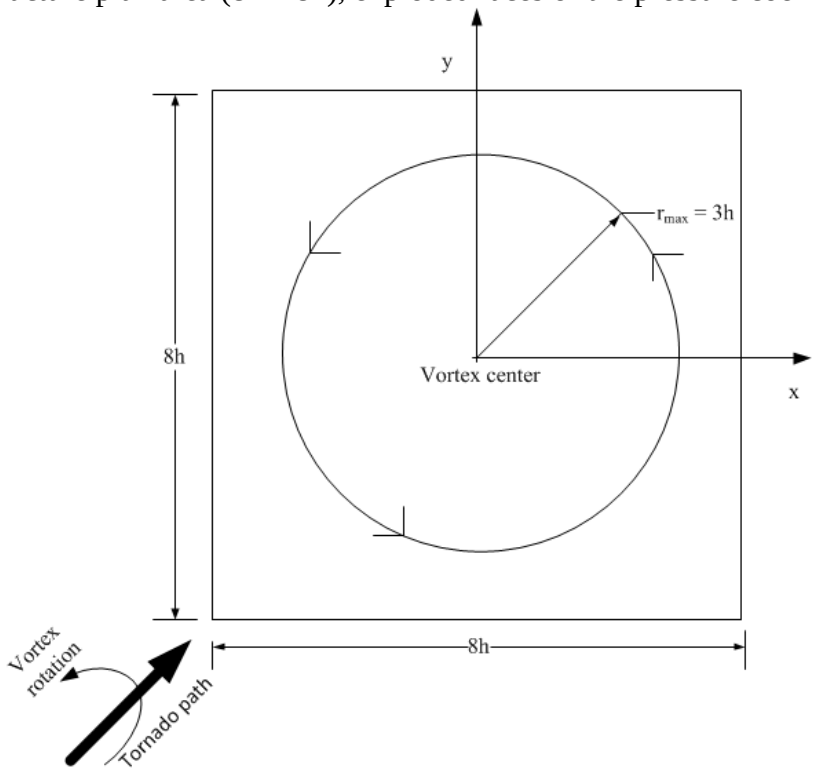

Figure 5.30 x-y plane schematic of the structure plan area (8h x8h) vs. tornado vortex ($\beta = 45^0$)

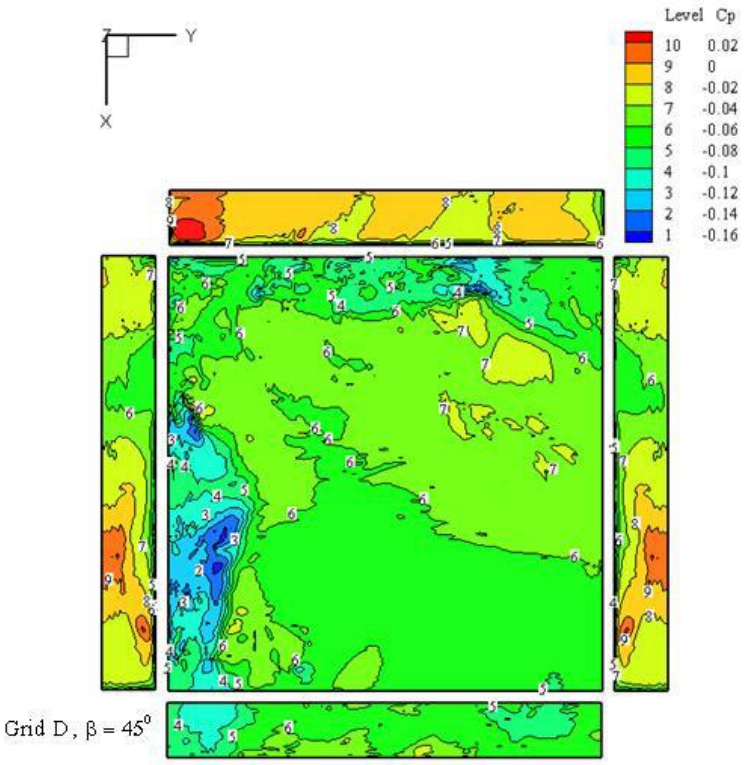

Figure 5.31 Structure plan area (8h x 8h), exploded faces of the pressure coefficients ($\beta = 45^0$)

From the pressure coefficient study on the LSPA, we conclude that the size of the tornado, the SPA and the orientation of the tornado path are significant on determining where the maximum pressure coefficients occurred on the LSPA. For the three-dimensional visualization of the pressure coefficient contour plot on the large structure plan areas see Appendix (B-3).

5.5.3 COMPARISON OF THE SAME USE OF (Vtran.) IN A TORNADO AND A SL WIND

The use of the same maximum translating reference velocity ($V_{trans.}$) in a tornado and in a SL flow allows us to examine the values of force coefficient in the x-direction and maximum pressure coefficient on a structure compared to SL flow. The $V_{trans.}$ is the non-dimensional unit velocity as specified in Table 5.2. The tornado and the SL wind flow approach the structure with two angles of attack ($\beta = 0^0, \beta = 45^0$).

The force coefficient in the x-direction and pressure coefficient for $\beta = 0^0$ and $\beta = 45^0$ are summarized separately in Table 5.7 and Table 5.8. Figure 5.32 and Figure 5.33 illustrate the force coefficient comparison in the x-direction between tornado and SL flow for the abovementioned angles. Likewise, the pressure coefficient comparison between the tornado and the SL flow are shown separately in FigS.5.34 and 5.35.

Table 5.7 Comparison force coefficient and pressure coefficient for $\beta = 0^0$

Grid name	Structure Plan Area	C_x SL flow	C_x Tornado	C_p SL flow	C_p Tornado
A	h x h	0.75	25.11	-0.05	-28
B	2h x 2h	0.74	15.43	-0.6	-18
C	4h x 4h	0.71	4.24	-0.7	-5
D	8h x 8h	0.69	0.90	-1.12	-1.117

Table 5.8 Comparison force coefficient and pressure coefficient for $\beta = 45^0$

Grid name	Structure Plan Area	C_x SL flow	C_x Tornado	C_p SL flow	C_p Tornado
A	h x h	0.87	27.53	-0.1	-24
B	2h x 2h	0.81	21.8	-0.7	-16
C	4h x 4h	0.55	8.17	-0.9	-6.5
D	8h x 8h	0.29	2.12	-1.15	-2.4

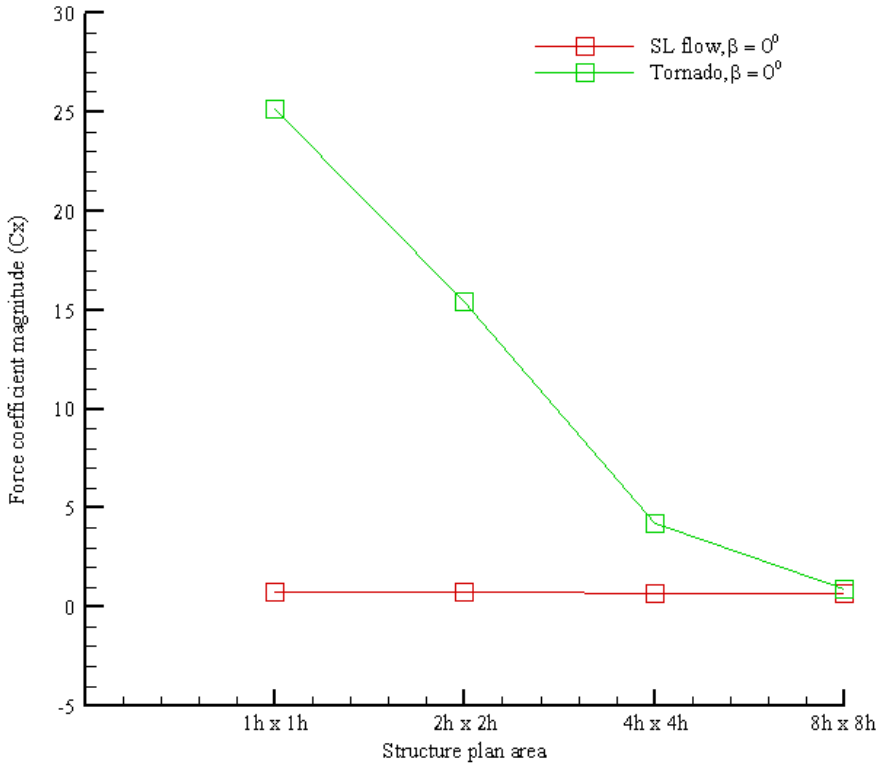

Figure 5.32 Force coefficient (Cx) comparison on large structure plan area ($\beta = 0^0, V_{trans.}=1$)

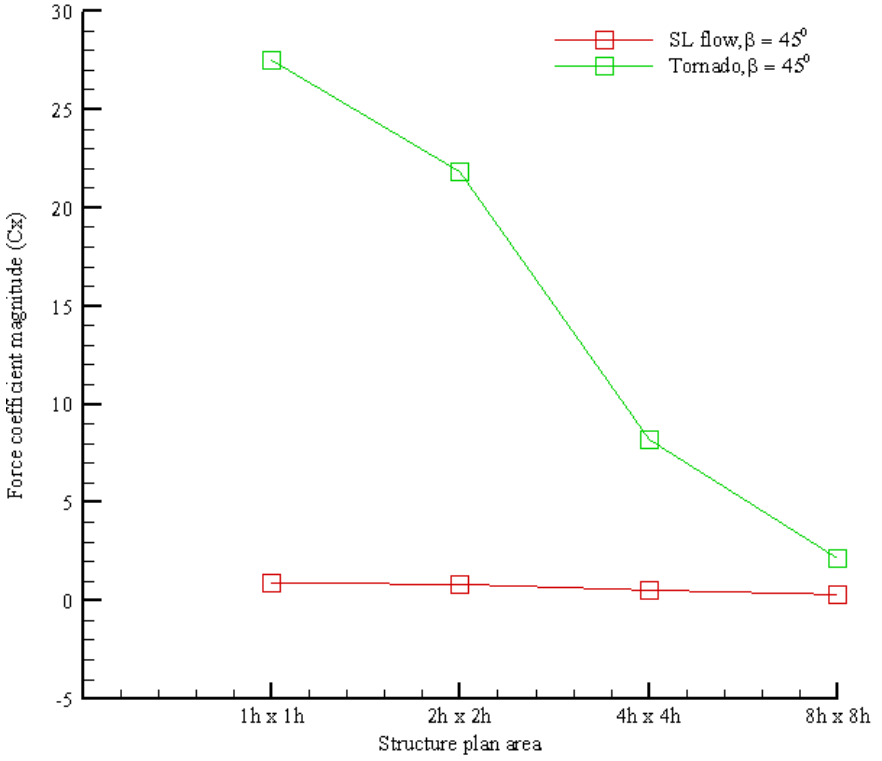

Figure 5.33 Force coefficient (Cx) comparison on large structure plan area ($\beta = 45^0, V_{trans.}=1$)

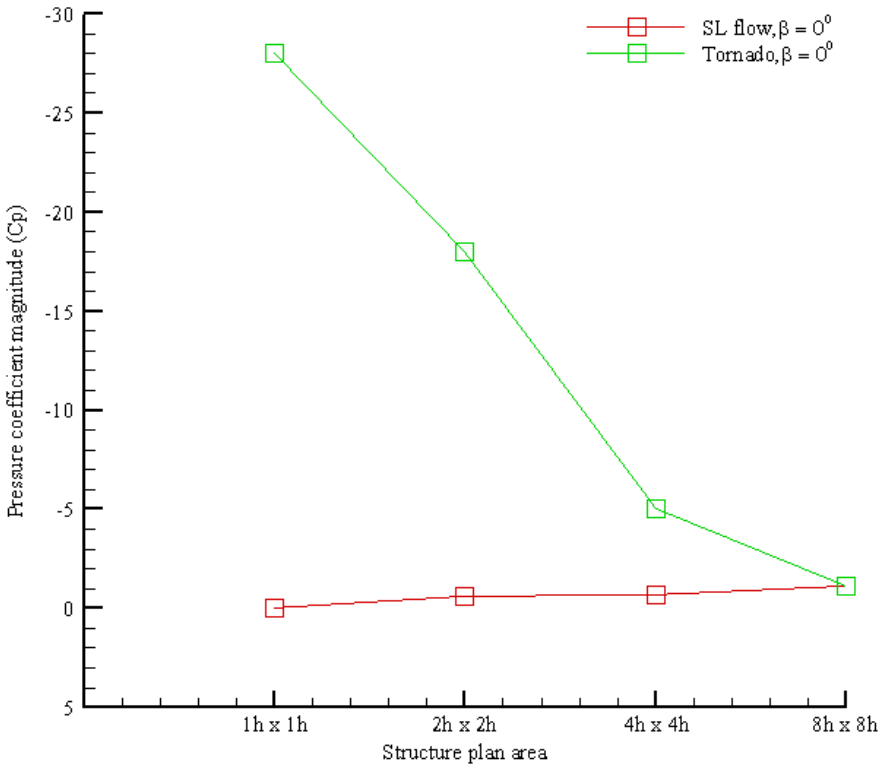

Figure 5.34 Pressure coefficient comparison on large structure plan area ($\beta = 0^0, V_{trans.}=1$)

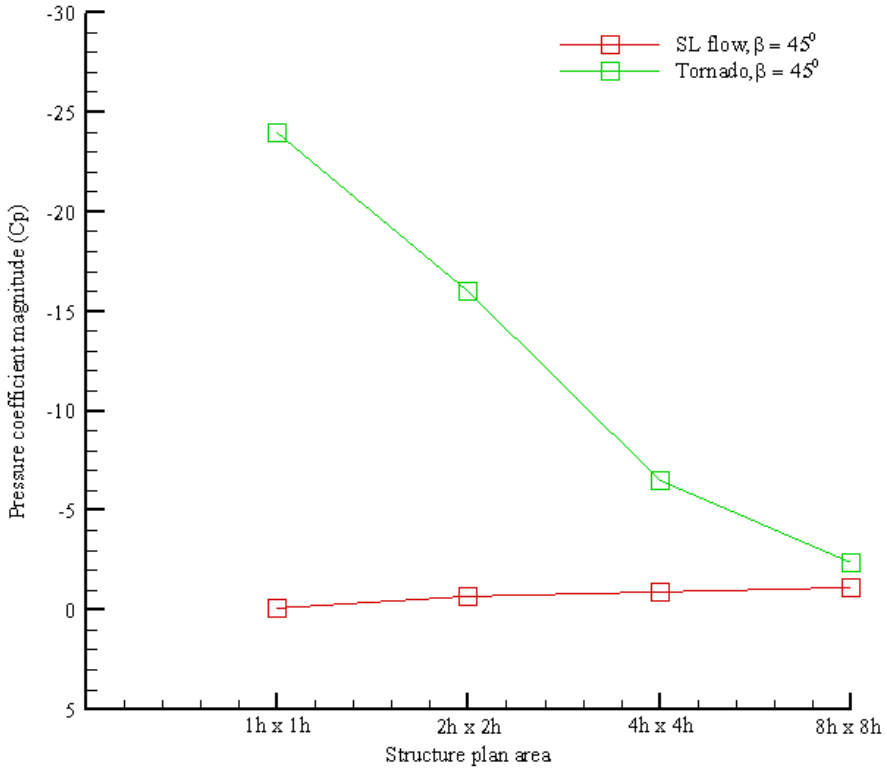

Figure 5.35 Pressure coefficient comparison on large structure plan area ($\beta = 45^0, V_{trans.}=1$)

For the same V_{trans}., and for $\beta = 0^0$, the tornado force coefficient in the x-direction was approximately 25 times that of the SL force coefficient on the SPA (1h x 1h). Similarly, the tornado and SL flow approached the structure with the same V_{trans}., and $\beta = 45^0$, the tornado created almost 27 times the force coefficient in the x-direction compared to the force coefficient in the x-direction for the SL flow on SPA (1h x 1h).

Figures 5.36 and 5.37 illustrate the three-dimensional pressure coefficient (Cp) distributions of the tornado and the SL flow on the SPA (1h x 1h) for $\beta = 0^0$. The pressure coefficient distributions on the SPA (1h x 1h) showed that the tornado generated a 28 times greater pressure coefficient on the roof compared to the SL flow pressure coefficient. Equivalently for the same V_{trans}., and $\beta = 45^0$, the tornado induced a 24 times higher pressure coefficient on the roof of SPA (1h x 1h) compared to the SL flow pressure coefficient, see Figs. 5.38 and 5.39.

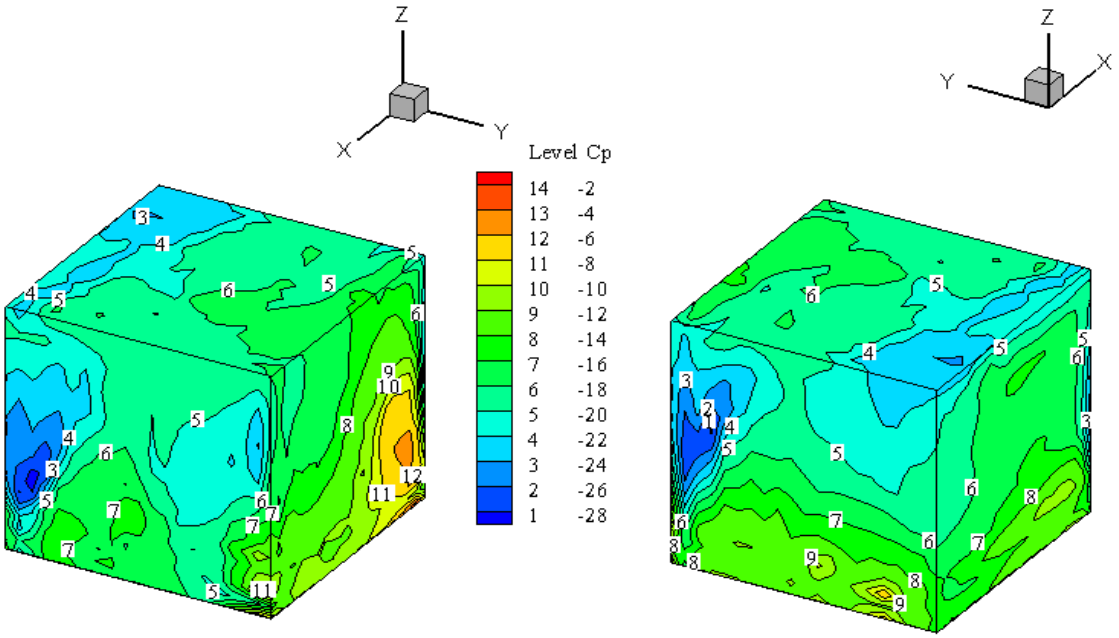

Figure 5.36 Structure plan area (1h x 1h), tornado pressure coefficient contour plot, $\beta = 0^0$

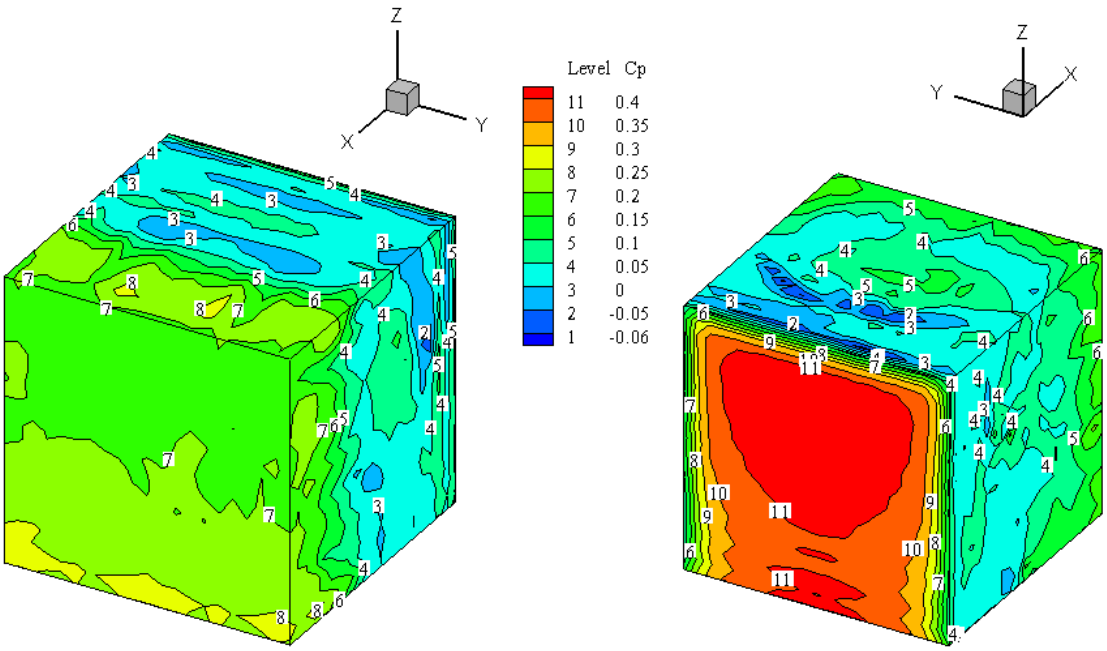

Figure 5.37 Structure plan area (1h x 1h), SL flow pressure coefficient contour plot, $\beta = 0^0$

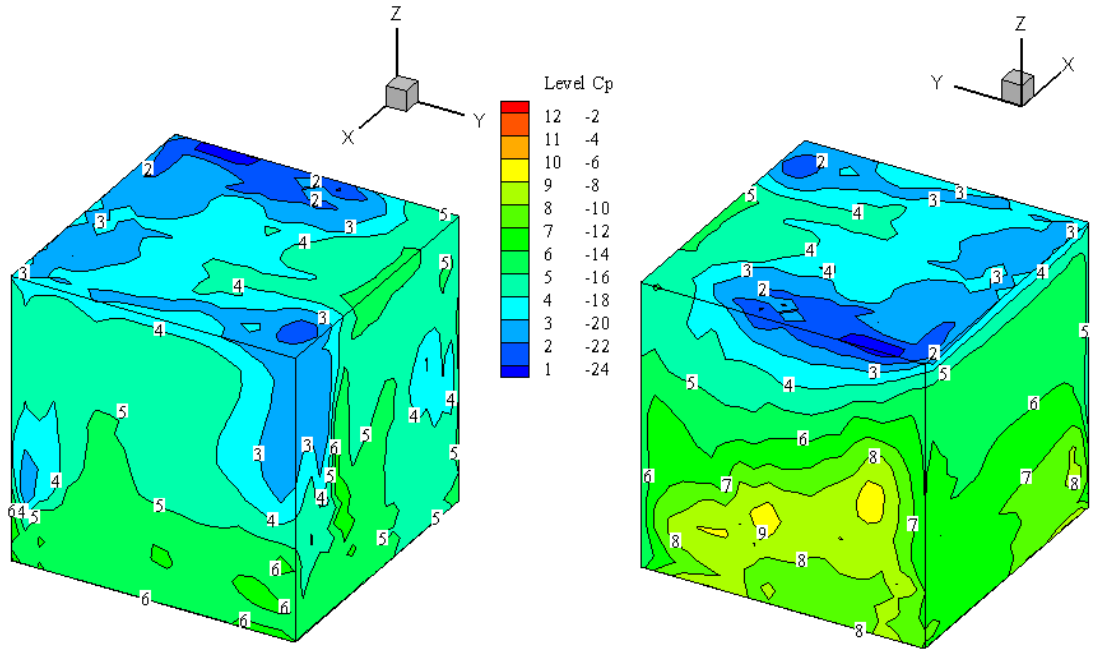

Figure 5.38 Structure plan area (1h x 1h), tornado pressure coefficient contour plot, $\beta = 45^0$

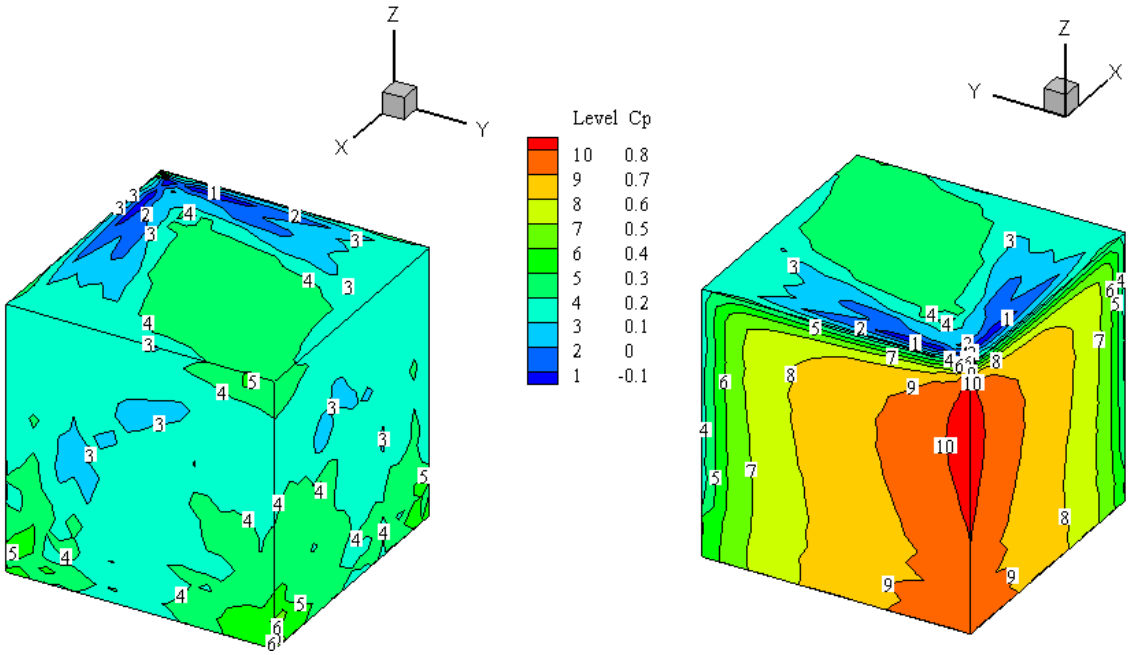

Figure 5.39 Structure plan area (1h x 1h), SL flow pressure coefficient contour plot, $\beta = 45^0$

For the same maximum reference velocity with two different angles of approach, the tornado generated approximately two to twenty-seven times higher force coefficient and pressure coefficients on structures plan areas (1h x 1h , 2h x 2h and 4h x 4h). When the SPA (8h x 8h) and tornado approach with $\beta = 0^0$ or $\beta = 45^0$, the tornado can be treated as a SL flow, see Figs.5.40 and 5.41 . The three-dimensional view of the Cp contour plot distribution on structures plan areas (2h x 2h and 4h x 4h) for $\beta = 0^0$ or $\beta = 45^0$ and on structure plan area (8h x 8h) for $\beta = 45^0$ are in Appendix (B-4).

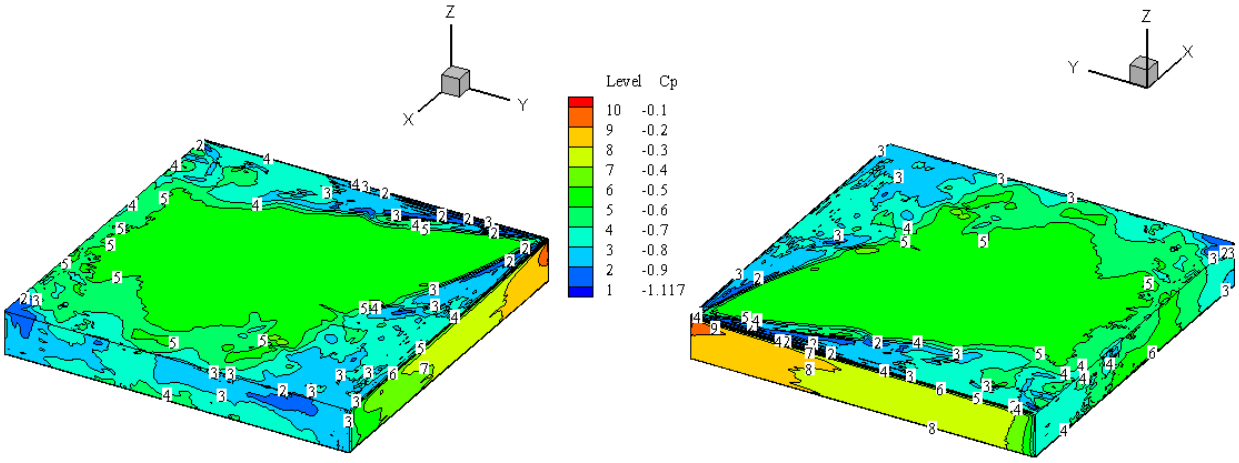

Figure 5.40 Structure plan area (8h x 8h), tornado pressure coefficient contour plot, $\beta = 0^0$

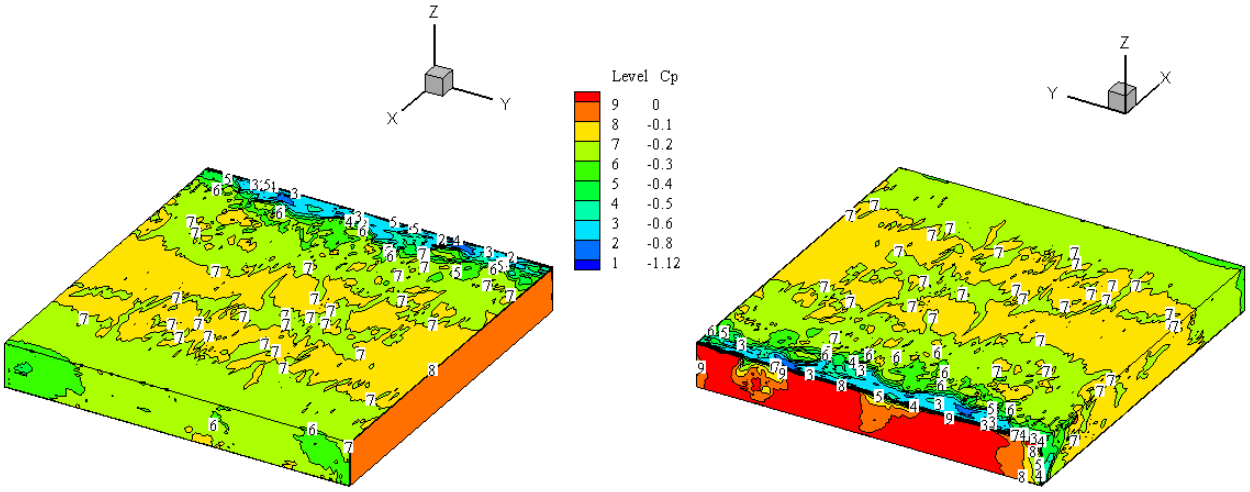

Figure 5.41 Structure plan area (8h x 8h), SL flow pressure coefficient contour plot, $\beta = 0^0$

Using the same reference velocity ($V_{trans.}$), the tornado produced three to twenty-seven times greater force coefficients and the pressure coefficients on the plan areas that the tornado can completely cover compared to the SL flow for both angles approached. However, when the ratio between d_L and d_{max} was approximately two, the pressure coefficient and force coefficient were almost the same as the SL flow.

The tornado created a higher force coefficient on the structures plan areas (1h x 1h, 2h x 2h and 4h x 4h) because the tornado has translational, rotational and vertical velocities, whereas the SL flow has only a translational velocity. The structure plan area, the tornado orientation, the same use of the same reference maximum velocity, and the tornado size are critical in differentiating between tornado forces and SL wind forces.

Selvam and Millett (2003) have provided a benchmark study on the mesh refinement for a cubic structure (h x h x h) and found that the spacing in the x, y and z –directions must be 0.005h normal to the structure in each direction, and on the structure edges 0.025h. However, the goal of this Chapter is to show how increasing structure plan areas affect tornado forces. For further investigation refinement mesh on the structure edges would increase the accuracy in the result of the force coefficients and pressure distributions on the large structure plan areas.

CHAPTER 6

COMPUTING TORNADO FORCES ON A STRUCTURE WITH THIN PLAN AREAS

6.1 INTRODUCTION

The goal of this Chapter is to examine tornado force coefficients on a Thin Structure Plan Areas (TSPA). To obtain the TSPA, the Large Structure Plan Areas (LSPA) were divided by a factor of 10. The TSPA are (0.1h x 0.1 h, 0.2h x 0.2h, 0.4h, 0.4h and 0.8h x 0.8h). The structure height (h) is the same as the height of the LSPA. The Structure Plan Area (SPA), which is (0.1h x 0.1h), is almost in the eye of the tornado when the two centers coincide in the computational fluid domain. The fluid computational domain has been designed based on the discussion in Chapter 4. The focus of this Chapter is to answer, what will happen to the tornado forces when the TSPA increases in size?

In the numerical simulation, the tornado and SL flow approach the structure with $\beta = 0^0$ and $\beta = 45^0$, and the force coefficients are compared for the same angle approaches. When $\beta = 0^0$ and $\beta = 45^0$, the tornado pressure coefficient (Cp) on the TSPA are compared. The same maximum translating reference velocity ($V_{trans.}$) in a tornado and a SL flow will be used to compare the pressure coefficient and the force coefficient in the x-direction for the same angle of attack on the TSPA.

6.2 GRID PROPERTIES AND TORNADO PARAMETERS

The TSPA have the same grid layout in the x, y and z-directions. The grids were generated by FORTRAN code. 0.005h minimum grid spacing normal to the structure and 0.01h spacing on the structure edges were used throughout the study. The grid spacing layout in the

computational domain increases by 1.25 times the assigned minimum grid spacing in each direction. When the spacing between two nodes reaches half of the structure height in each direction, the spacing is limited to half of the structure height. The TSPA and grid properties are tabulated in Table 6.1.

Table 6.1 Thin structure plan areas grid properties

Grid name	TSPA	Grid size	Total # of points on Structure edges	Total # of points in domain
E	0.1h x 0.1h	122 x 122 x 81	11 x 11 x 11	1,205,604
F	0.2h x 0.2h	142 x 142 x 81	21 x 21 x 11	1,633,284
G	0.4h x 0.4h	180 x 180 x 81	41 x 41 x 11	2,624,400
H	0.8h x 0.8h	260 x 260 x 81	81 x 81 x 11	5,475,600

Mesh, or grid points, in the computational domain is visualized by TecPlot software. Figure 6.1 shows the mesh in the x-y plane for SPA (0.1h x0.1h). In addition, Fig.6.2 shows a close up of the mesh around the structure edges in the x-y plane for the same SPA. The mesh of the TSPA (0.2h x 0.2h, 0.4h x 0.4h and 0.8h x 0.8h) are found in Appendix (C-1).

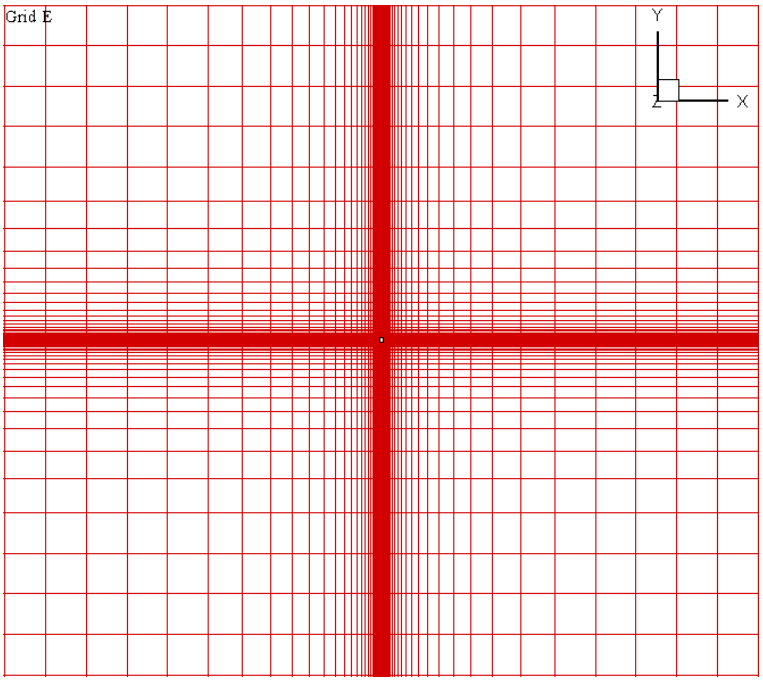

Figure 6.1 Structure plan area (0.1h x0.1h), the x-y plane mesh

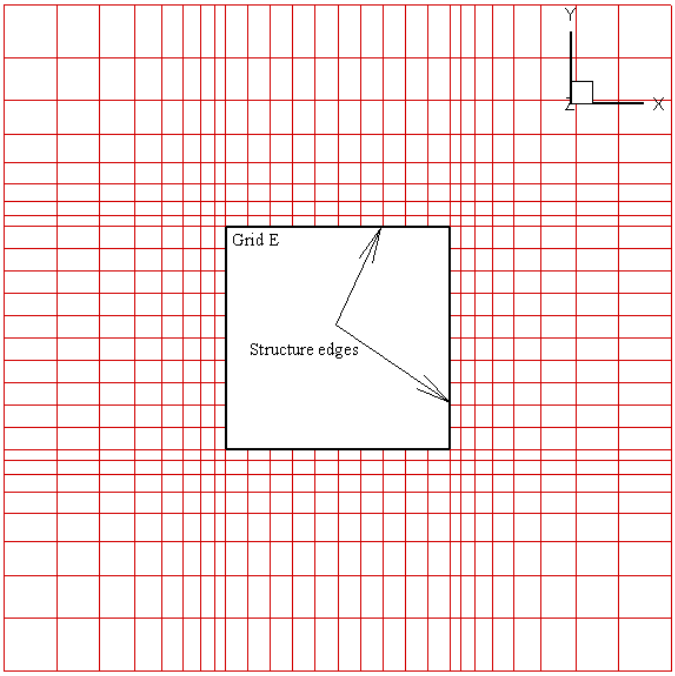

Figure 6.2 Structure plan area (0.1h x 0.1h), the x-y plane close up in the mesh

Figures 6.3 and 6.4 illustrate a top view of a tornado path approaching a structure with $\beta = 0^0$ and $\beta = 45^0$ respectively. The structure geometry is dimensionalized by the structure height (h) and the flow velocity fields are dimensionalized by the translation velocity ($V_{trans.}$). The maximum velocity (V_{max}) in a tornado is the sum of two velocity components and they are the tangential (V_θ) and the translation ($V_{trans.}$) velocities. The maximum velocity is calculated from the Rankine-Combined Vortex (RCV) velocities as described in Chapter 4. The tornado vortex strength (α) is the same for $\beta = 0^0$ and $\beta = 45^0$. The tornado parameters are the same as the tornado parameters were given in Chapter 5, see Table 6.2.

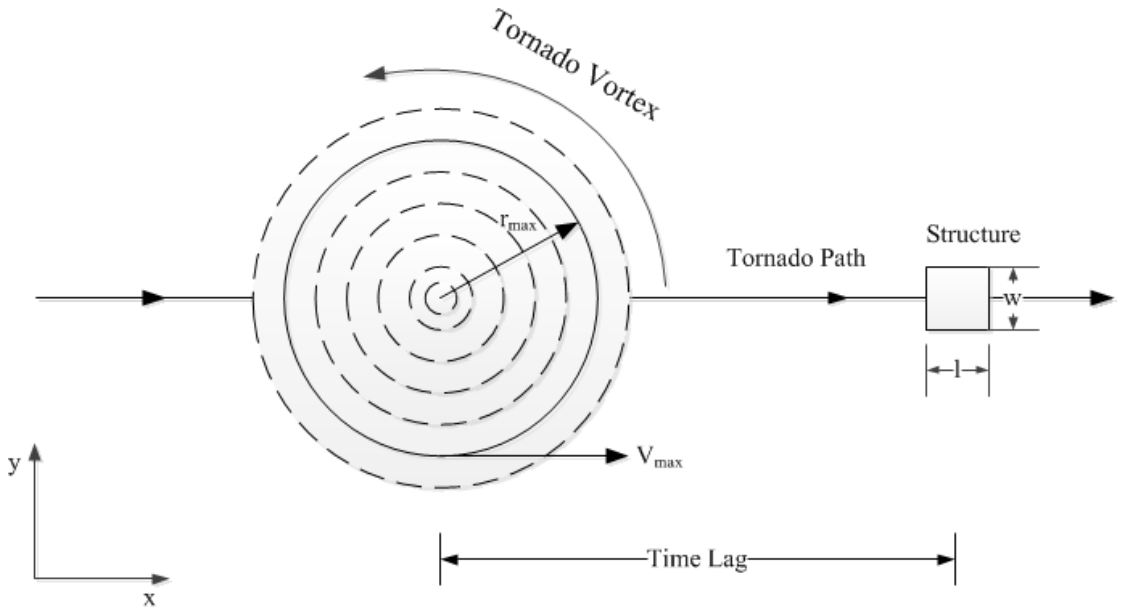

Figure 6.3 Top view of a tornado path approaches a structure with 0^0

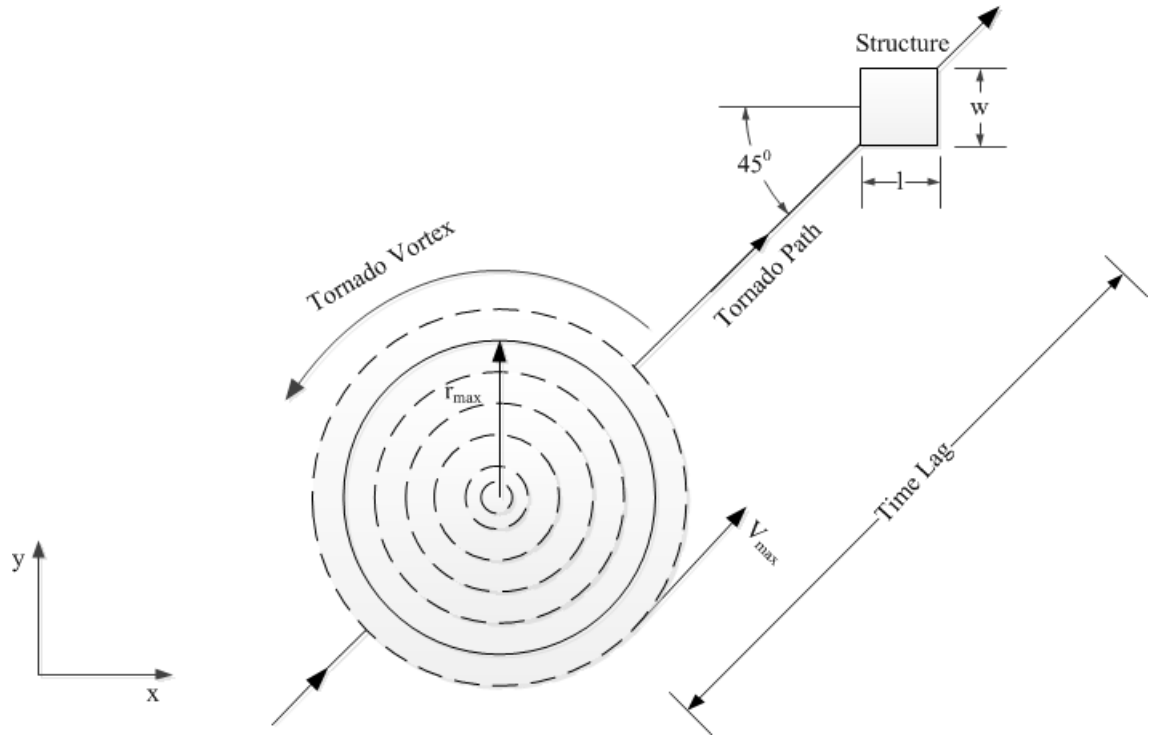

Figure 6.4 Top view of a tornado path approaches a structure with 45^0

Table 6.2 Tornado parameters of thin structure plan areas

	h	α	r_{max}	$V_{trans.}$	V_{θ}	V_{max}
English units	66.6 (ft)	1.5 (1/s)	200 (ft)	45.5 (mph)	205 (mph)	250.5 (mph)
SI units	20.3 (m)	1.5 (1/s)	61.0 (m)	20.3 (m/s)	91.5 (m/s)	111.8 (m/s)
Non-Dimensional units	1	1.5	3.0	1.0	4.5	5.5

6.3 GEOMETRY AND BOUNDARY CONDITIONS

The structure center starts at the origin axis and has the dimensions l for length, w for width and h for height. The computational fluid domain has the dimensions L for length, W for width and H for height. Figure 6.5 illustrates an isometric view of the structure and the computational fluid domain. The computational fluid domain is located approximately ten times the inner maximum tornado core radius (r_{max}) in each direction, as suggested by the design of the computational fluid domain in Chapter 4. The dimensions of the computational domain and the TSPA are specified in Table 6.3.

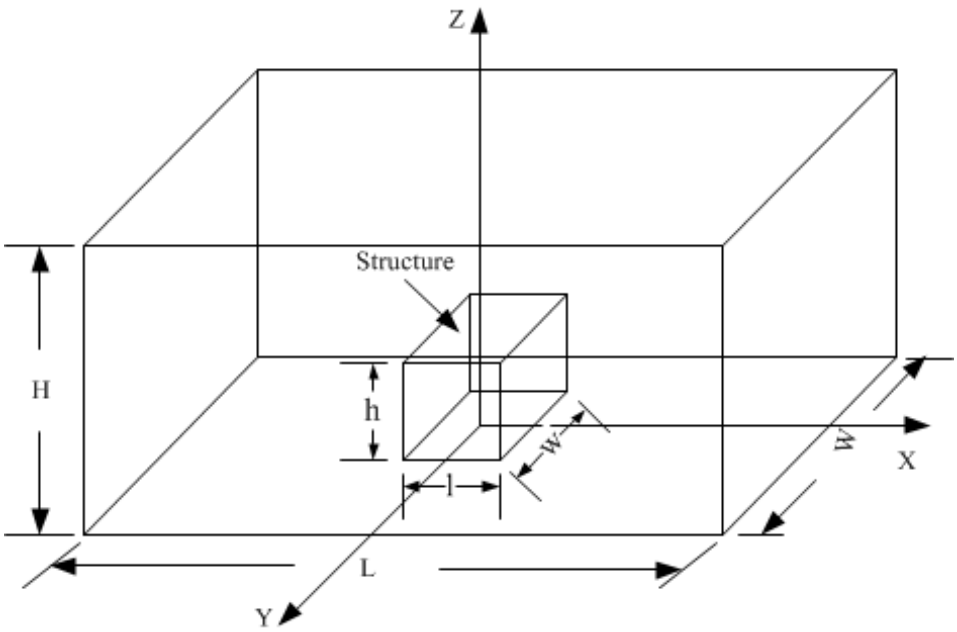

Figure 6.5 Isometric views of the TSPA and the computational fluid domain

Table 6.3 Computational domain and structure dimensions

Grid name	Domain size in h	Structure size
E	59 x 59 x 30	0.1h x 0.1h x h
F	60 x 60 x 30	0.2h x 0.2h x h
G	60.5 x 60.5 x 30.5	0.4h x 0.4h x h
H	61 x 61 x 31	0.8h x 0.8h x h

The specified boundary conditions on each face of the TSPA are zero velocities (no slip boundary condition). The boundary conditions applied on the exterior faces of the computational fluid domain are the RCV model velocities. Equations (6.1, 6.2, 6.3 and 6.4) give the RCV velocity components in a Cartesian form. The RCV model velocities applied on each grid point in the computational domain and these velocities change in time based on the location of the vortex core. The RCV model is discussed in detail in Chapter 3 and Chapter 4.

$$V_x = (V_t - y\alpha)Zf \qquad \text{if } r \le r_{max} \tag{6.1}$$

$$V_y = (x - V_t t)\alpha\, Zf \qquad if\ r \le r_{max} \tag{6.2}$$

$$V_x = (V_t - Cy)Zf \qquad \text{if } r > r_{max} \tag{6.3}$$

$$V_y = (x - V_t t)C\, Zf \qquad \text{if } r > r_{max} \tag{6.4}$$

The growth in the boundary layer along the z-axis (Zf) in the computational fluid domain is given in Eq.(6.5) as discussed in Chapter 4.

$$Zf = \frac{u}{k} \ln\left(\frac{h+h_0}{h_0}\right) \tag{6.5}$$

6.4 FORCE COEFFICIENTS AND PRESSURE COEFFICIENT

Forces on the TSPA are computed from integrating the pressure on each surface area in x,y and z-directions. The reported maximum tornado force coefficients on each TSPA are for the specified time lag in each simulation. The time lag is the period from the start time of the

simulation and when the center of the tornado coincides with the center of the structure. The force coefficients and pressure coefficient are calculated from the following equations:

$$Cx = \frac{F_x}{0.5\rho V^2 A} \tag{6.6}$$

$$Cy = \frac{F_y}{0.5\rho V^2 A} \tag{6.7}$$

$$Cz = \frac{F_z}{0.5\rho V^2 A} \tag{6.8}$$

$$Cp = \frac{\Delta p}{0.5\rho V^2} \tag{6.9}$$

The reference velocity (V) has an assigned value based on the numerical study. If a tornado is simulated in the computational domain, the reference velocity is the maximum velocity (V_{max}). On the other hand, if a SL wind flow is simulated in the computational domain, the reference velocity is the translating velocity ($V_{trans.}$). The definition of the force coefficient and pressure coefficient were given in Chapter 4 and Chapter 5.

6.5 THIN STRUCTURE PLAN AREAS RESULTS AND DISCUSSION

The UA-CFD wind code was used to compute the tornado and SL flow force coefficients and pressure coefficient on the TSPA (0.1h x 0.1h, 0.2h x 0.2h, 0.4h x 0.4h and 0.8h x 0.8h). The Tornado and SL flow approached the structure with 0^0 and 45^0 angles of attack. The force coefficient and pressure coefficients on TSPA are computed when the tornado center coincides with the structure center. The two centers coincide when the time (t) is equal to the specified time lag in each simulation.

Here we define the Thin Structure Plan Area Characteristic Length Ratio (TSPACLR) as d_{ratio} , the Thin Structure Plan Areas Characteristic diagonal length (TSPACDL) as d_L, and the Tornado Maximum Characteristic Diameter (TMCD) as d_{max}. The TSPACLR is the ratio

between the TSPACDL to TMCD. The TSPACLR is calculated form Eq. (6.10). Table 6.4 gives the values of the TSPACLR for each TSPA. Figure 6.6 illustrates the TMCD and the TSPACDL in the x-y plane for the TSPA.

$$d_{ratio} = \frac{d_L}{d_{max}} \tag{6.10}$$

Table 6.4 Thin Structure plan area characteristic length ratio

Grid Name	d_L	d_{max}	d_{ratio}
E	$0.1\sqrt{2}$	6	0.024
F	$0.2\sqrt{2}$	6	0.047
G	$0.4\sqrt{2}$	6	0.094
H	$0.8\sqrt{2}$	6	0.189

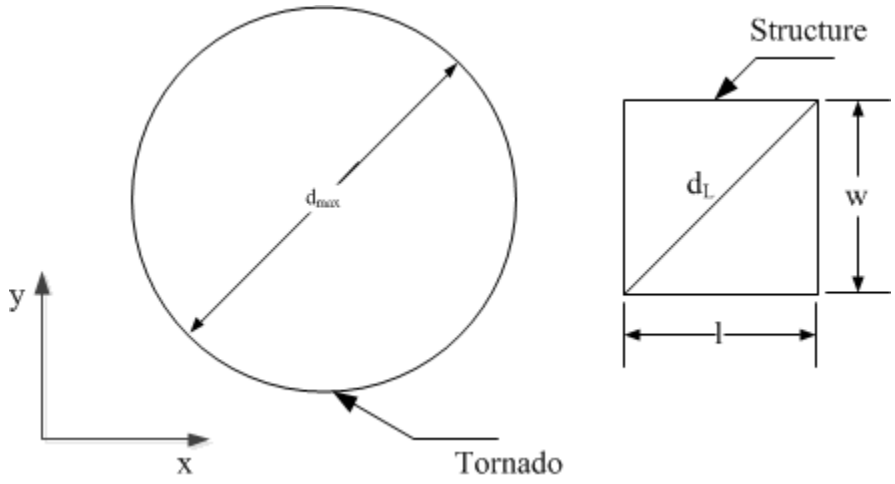

Figure 6.6 Tornado and structure characteristic length in the x-y plane

The following sections will discuss first, how the TSPA influences tornado force coefficients and compared to SL flow force coefficients, second the tornado pressure coefficient for two different angles approaches, third the use of the same maximum reference velocity ($V_{trans.}$) in both tornado and SL flow to compare the pressure coefficient on the structure roof and the force coefficient in the x-direction, and lastly the vortex shedding.

6.5.1 TORNADO FORCE COEFFICIENTS VS. SL FORCE COEFFICIENTS

Tornado and SL flow forces on the TSPA are computed by integrating the pressure on each surface. The force coefficients and pressure coefficient on TSPA are calculated from Eq. (6.6, 6.7, 6.8, and 6.9). The maximum force coefficients on TSPA are obtained at the specified time lag in each simulation. At the specified time lag, the tornado center coincides with the structure center as shown in Fig. 6.7 for SPA (0.1h x 0.1h). The force coefficients on the TSPA are tabulated in Table 6.5. When the TSPA increases in size, the tornado and the SL flow force coefficients are decreased as shown in Table 6.5 for $\beta = 0^0$ and $\beta = 45^0$.

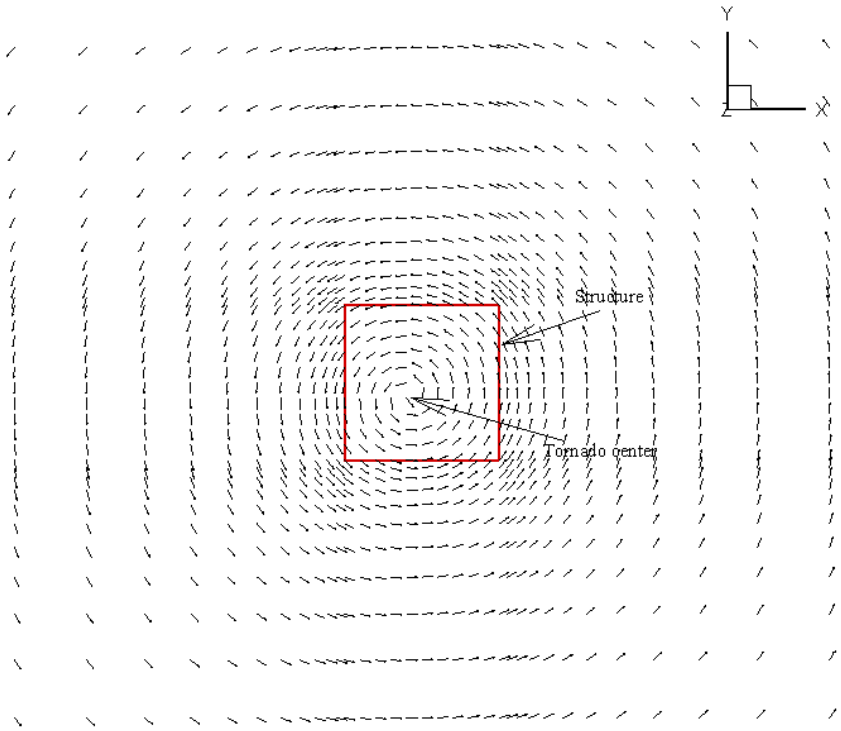

Figure 6.7 Tornado center and structure plan area (0.1h x 0.1h) center at 0.1h above the roof

Table 6.5 Tornado and SL force coefficients on thin structure plan areas

Flow types	Grid Name	Structure plan areas	Angle of attack β	C_x	C_y	C_z
Tornado flow	E	0.1h x 0.1h	0^0	1.55	1.40	2.48
			45^0	**1.83**	**1.66**	**2.25**
	F	0.2h x 0.2h	0^0	1.51	1.17	2.12
			45^0	**1.68**	**1.22**	**1.79**
	G	0.4h x 0.4h	0^0	1.42	1.08	1.91
			45^0	**1.34**	**1.01**	**1.61**
	H	0.8h x 0.8h	0^0	1.38	0.90	1.76
			45^0	**1.06**	**0.81**	**1.48**
SL flow	E	0.1h x 0.1h	0^0	1.06	0.02	1.41
			45^0	**0.82**	**0.78**	**1.21**
	F	0.2h x 0.2h	0^0	0.84	0.02	1.15
			45^0	**0.79**	**0.75**	**1.02**
	G	0.4h x 0.4h	0^0	0.80	0.01	0.91
			45^0	**0.77**	**0.70**	**0.90**
	H	0.8h x 0.8h	0^0	0.75	0.01	0.75
			45^0	**0.76**	**0.66**	**0.79**

When the tornado approached the TSPA with $\beta = 0^0$, it created approximately 10 % - 30 % greater force coefficients on the structure roof compared to $\beta = 45^0$. On the SPA (0.1h x 0.1h), the tornado force coefficient in the z-direction (on the roof) has the highest force coefficient compared to all other TSPA. The eye of the tornado is associated with a high suction pressure as shown by the tornado pressure probe measurement (Lee et al., 2004). Therefore, when the center of the SPA (0.1h x 0.1h) and the tornado center are coincided in the computational fluid domain, the tornado created a high suction force on the roof of the SPA (0.1h x 0.1h). Figures 6.8 and 6.9 show that the tornado generated twice force coefficient on the roof and 50 % higher on the side walls (in the x and y-directions) on the TSPA compared to the SL flow for the same angle approaches.

Force coefficients were plotted in time as the tornado translates and then engulfs the TSPA at the specified time lag in each simulation. Figures 6.10 and 6.11 show the tornado force

coefficients time history for $\beta = 0^0$ and $\beta = 45^0$ on the SPA (0.1h x0.1h). Similarly, the SL flow force coefficients time histories are plotted in Figs. 6.12 and 6.13 for the same SPA and same angle of approach. Figure 6.10 or 6.11 indicated that when the tornado engulfed the SPA (0.1h x 0.1h) with $\beta = 0^0$ or $\beta = 45^0$, it exerted high suction force on all side walls and lifting force on the structure roof. However, Fig. 6.12 and 6.13 illustrated that the SL flow force coefficient on the SPA (0.1h x0.1h) showed a fluctuation for both angles approach. The fluctuations in the force coefficients occurred because the structure is thin, tall and the flow is highly turbulent. For all other TSPA, the force coefficients time history are found in Appendix (C-2) for $\beta = 0^0$, $\beta = 45^0$.

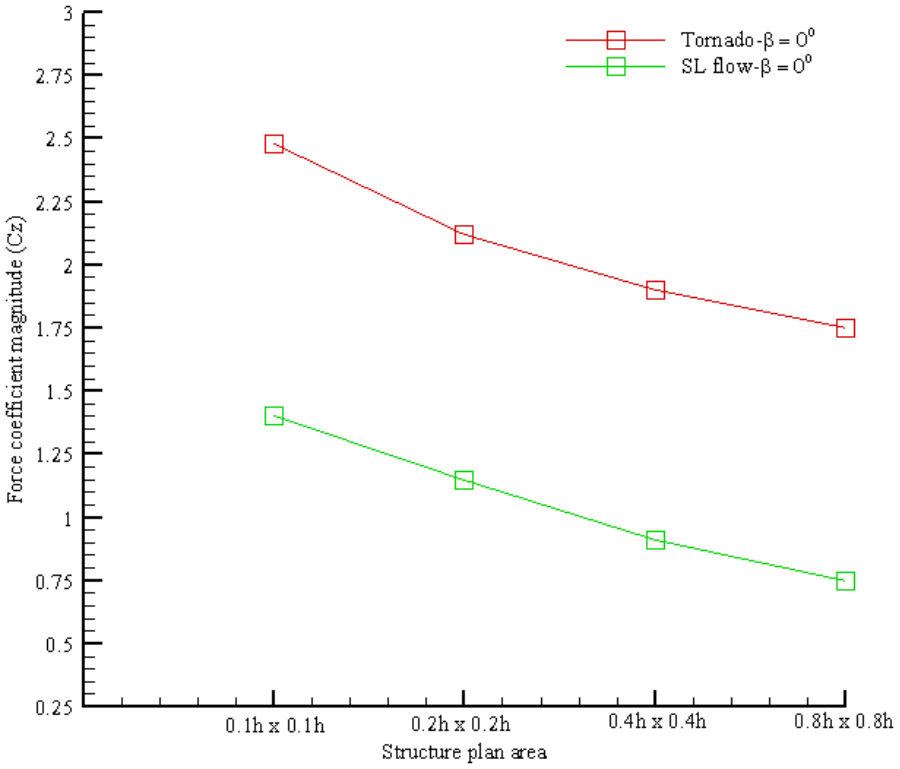

Figure 6.8 Thin structure plan areas roof force coefficient comparison, $\beta=0^0$

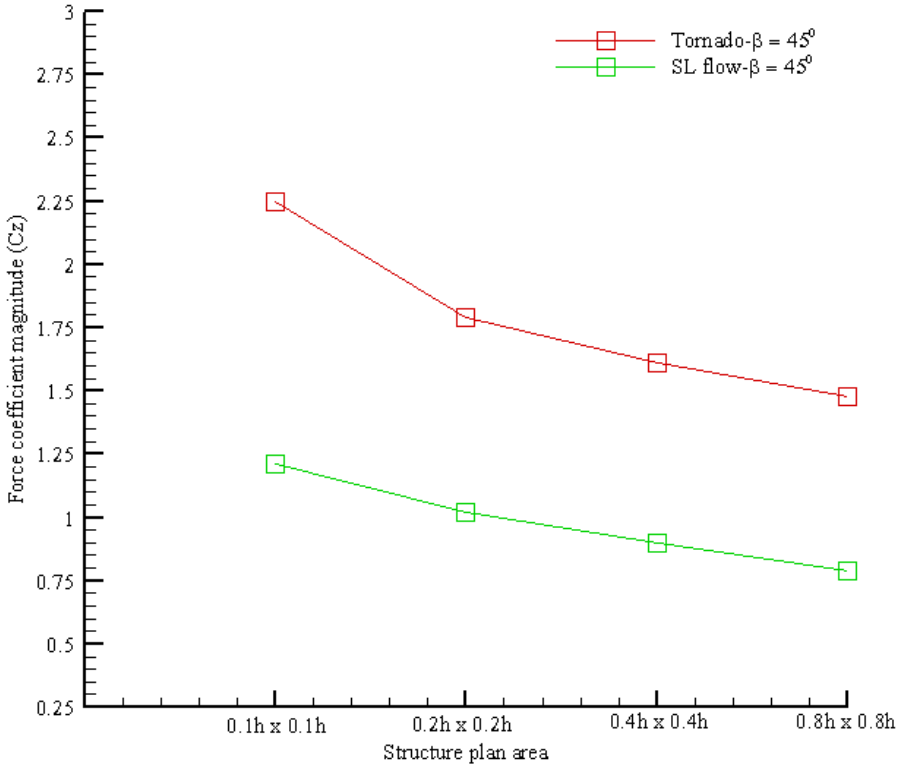

Figure 6.9 Thin structure plan areas roof force coefficient comparison, $\beta=45^0$

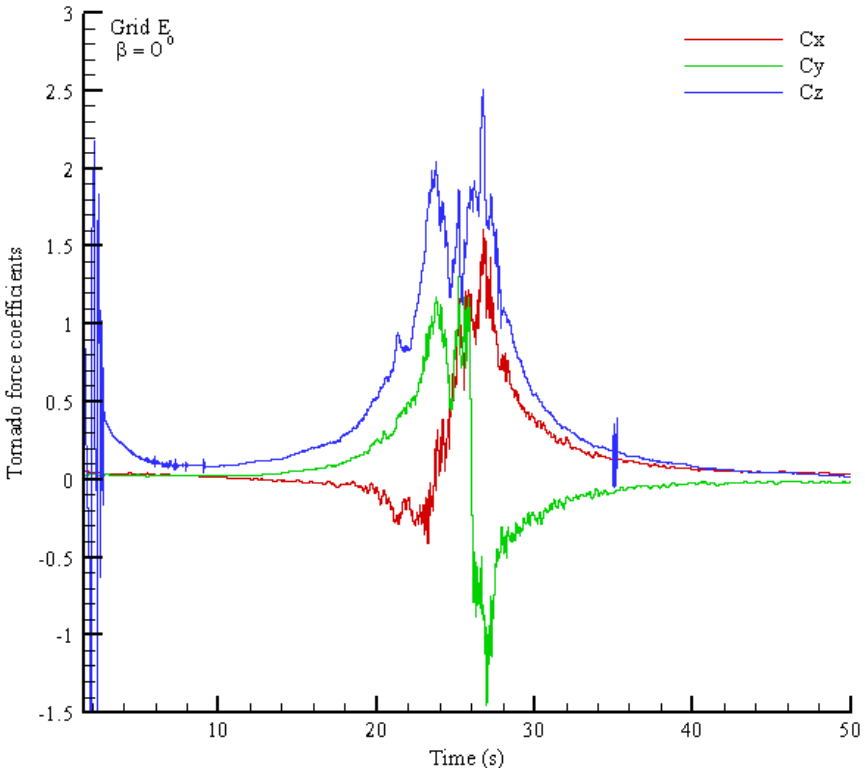

Figure 6.10 Structure plan area (0.1h x 0.1h), Tornado force coefficients,$\beta = 0^0$

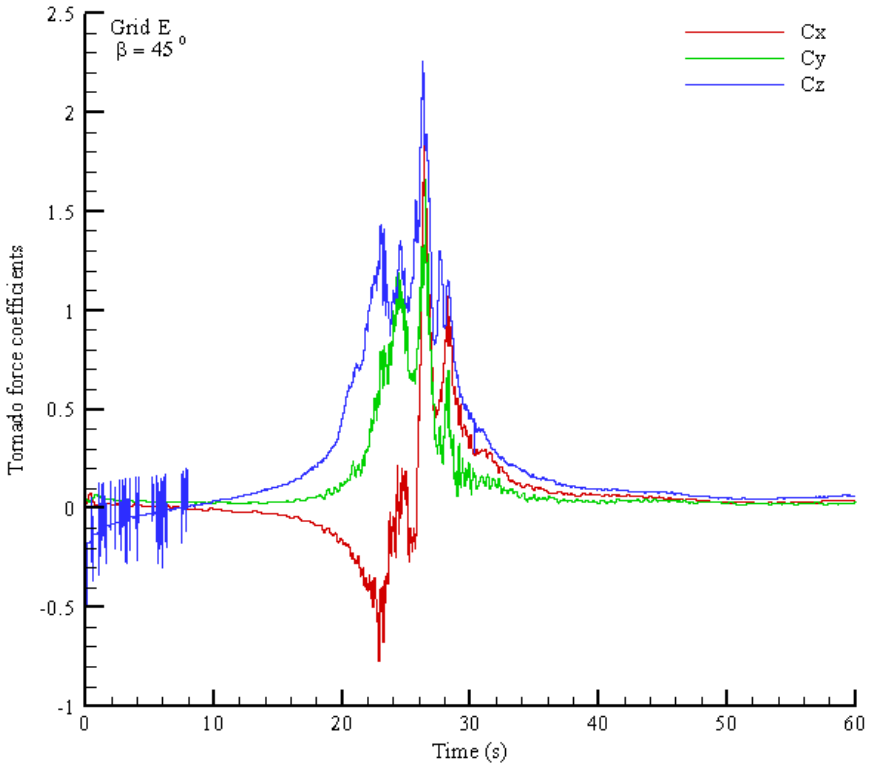

Figure 6.11 Structure plan area (0.1h x 0.1h), Tornado force coefficients, $\beta = 45^0$

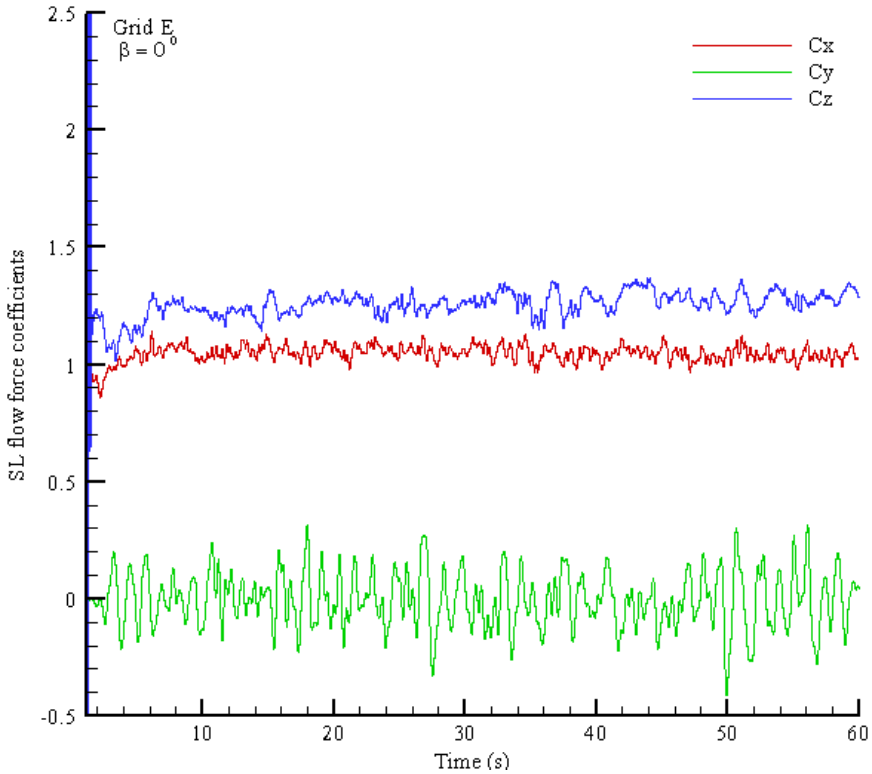

Figure 6.12 Structure plan area (0.1h x 0.1h), SL wind force coefficients, $\beta = 0^0$

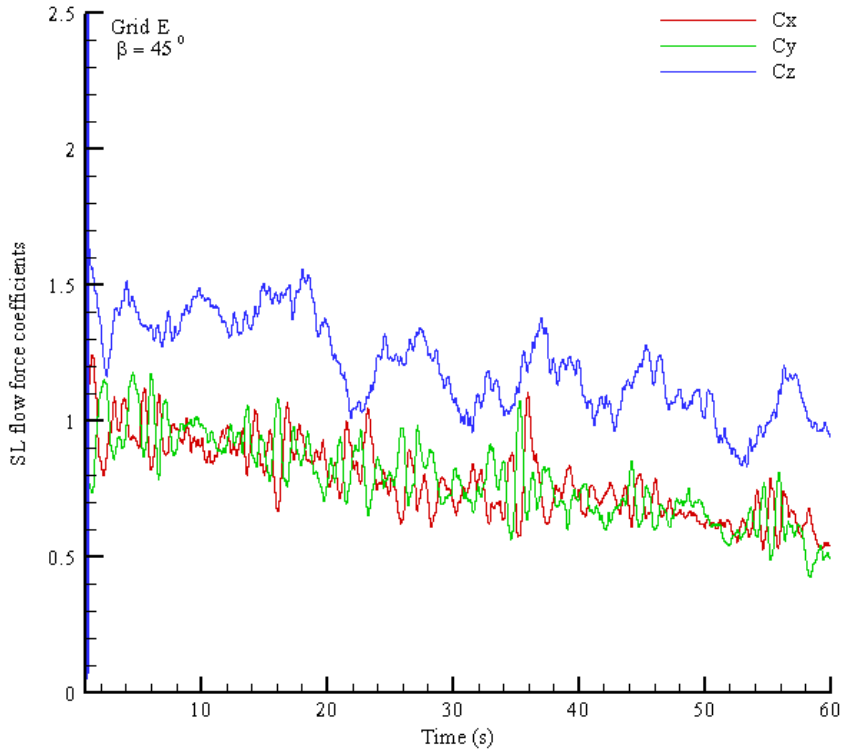

Figure 6.13 Structure plan area (0.1h x 0.1h), SL wind force coefficients, $\beta = 45^0$

6.5.2 TORNADO PRESSURE COEFFICIENT

The NSEs are iterated numerically by using Finite Difference Method (FDM) in order to solve the pressure and velocities at each grid point in the computational fluid domain in the x, y and z-directions. The pressure was integrated on each surface, and then the pressure coefficient (Cp) on the structure was computed from Eq. (6.9). Table 6.6 summarizes the tornado maximum pressure coefficient (Cp_{max}) study on the TSPA roof for two angles of tornado approach. Figure 6.14 shows the tornado maximum pressure coefficient (Cp) on the TSPA roof for $\beta = 0^0$ and $\beta = 45^0$.

Table 6.6 Tornado maximum pressure coefficient

Grid name	Structure plan areas	$C_{p,max}$ $\beta = 0^0$	$C_{p,max}$ $\beta = 45^0$
E	0.1h x 0.1h	-0.87	-0.84
F	0.2h x 0.2h	-1.0	-0.98
G	0.4h x 0.4h	-1.37	-1.31
H	0.8h x 0.8h	-1.67	-1.57

When the tornado surrounded the TSPA with $\beta = 0^0$, the tornado generated high suction pressure on the roof and the edges compared to a tornado approaching with $\beta = 45^0$. When the TSPA increases in size, the pressure coefficients increases as shown in Table 6.6 and in Fig.6.13. The three-dimensional C_p contour plots on the TSPA are shown in Figs. 6.15, 6.16, 6.17, 6.18, 6.19, 6.20, 6.21 and 6.22 for $\beta = 0^0$ and $\beta = 45^0$, respectively. The pressure coefficients contour plot on the TSPA showed that the tornado created high suction pressure on the roof and side walls except the windward wall. Therefore, the TSPA may experience failure because the tornado creates a small positive pressure value on the windward wall and a negative pressure on the roof, leeward wall, and side walls for $\beta = 0^0$ and $\beta = 45^0$.

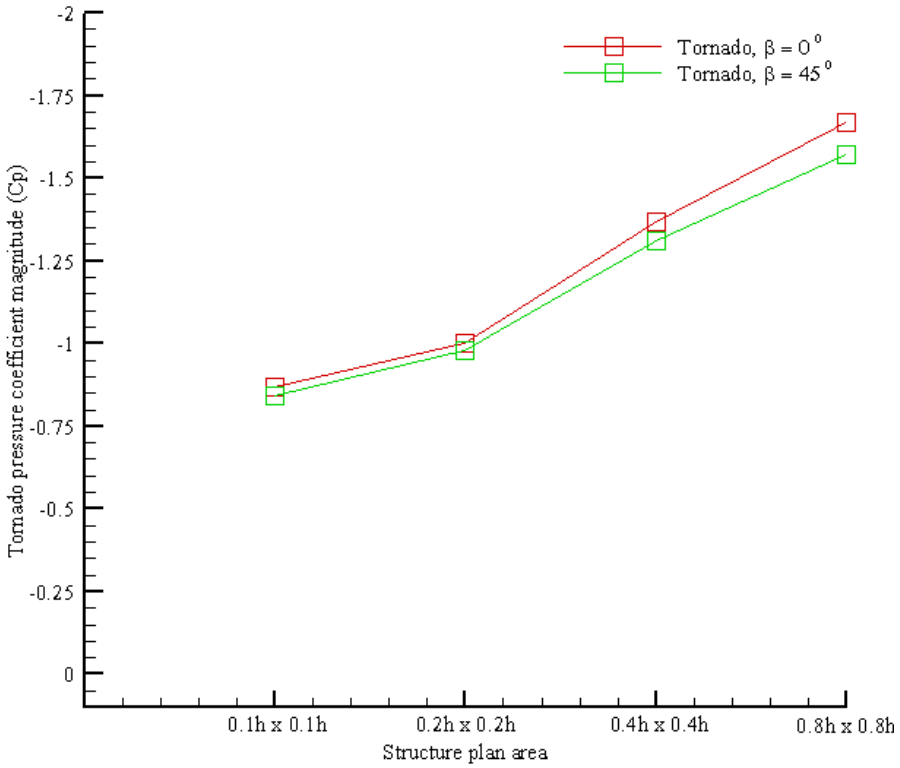

Figure 6.14 Tornado pressure coefficient (Cp) comparisons on thin structure plan areas

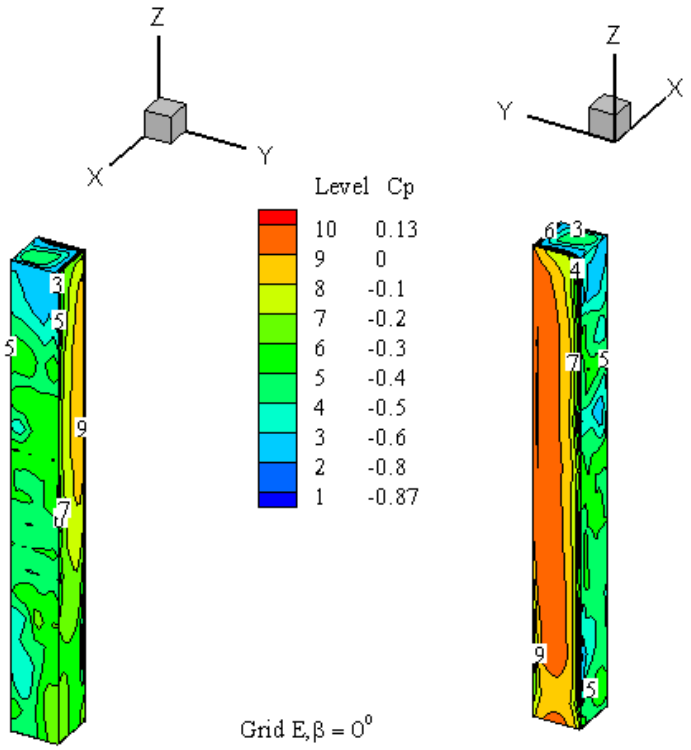

Figure 6.15 Structure plan area (0.1h x 0.1h), tornado pressure coefficient for $\beta = 0^0$

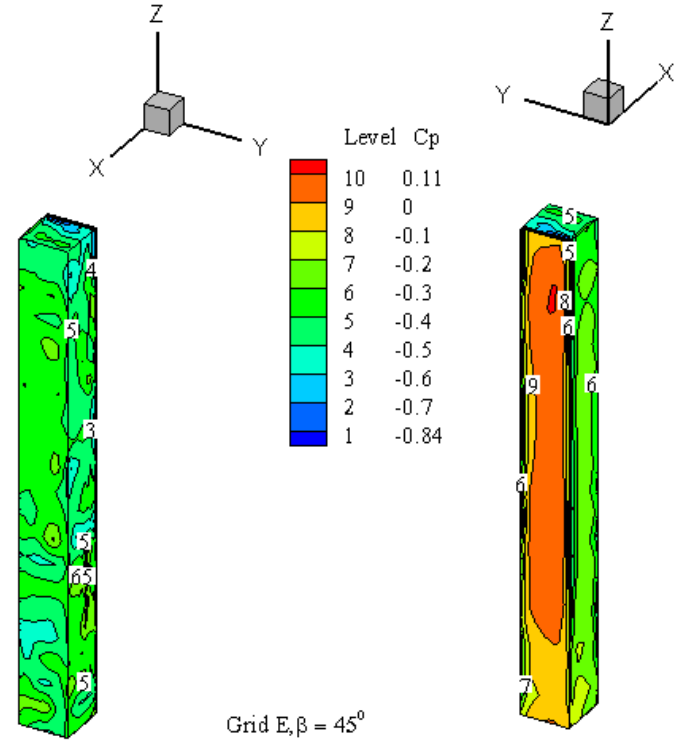

Figure 6.16 Structure plan area (0.1h x 0.1h), tornado pressure coefficients for $\beta = 45^0$

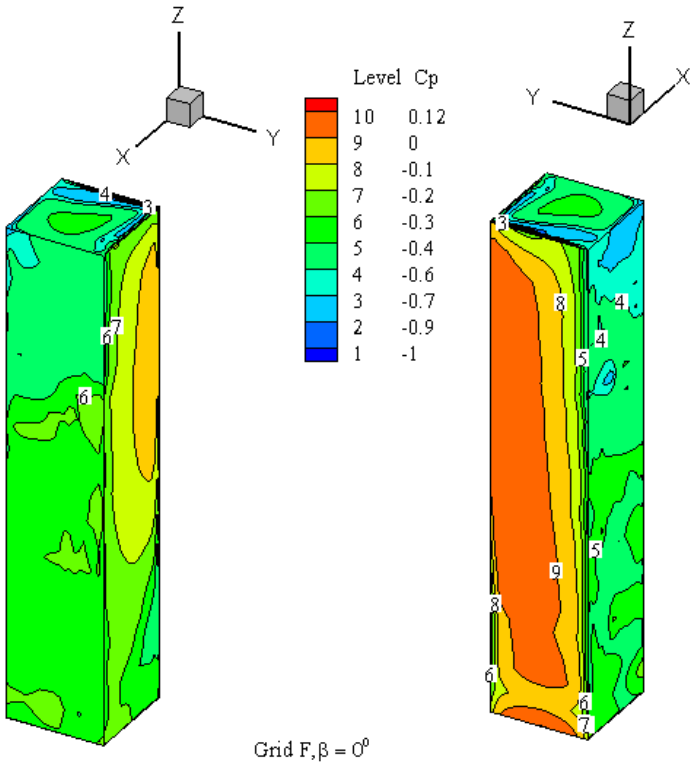

Figure 6.17 Structure plan area (0.2h x 0.2h), tornado pressure coefficient for $\beta = 0^0$

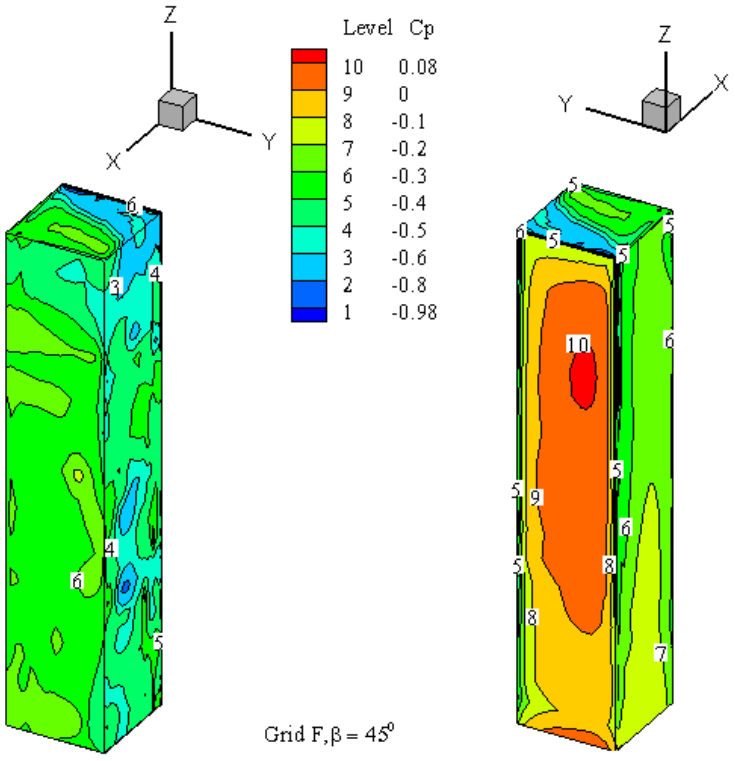

Figure 6.18 Structure plan area (0.2h x 0.2h), tornado pressure coefficients for $\beta = 45^0$

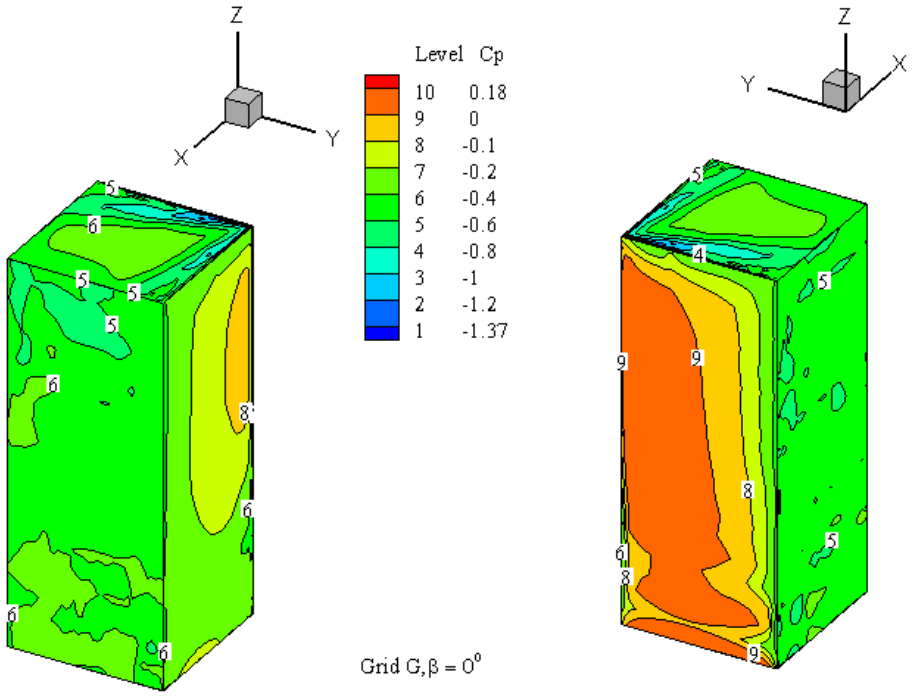

Figure 6.19 Structure plan area (0.4h x 0.4h), tornado pressure coefficient for $\beta = 0^0$

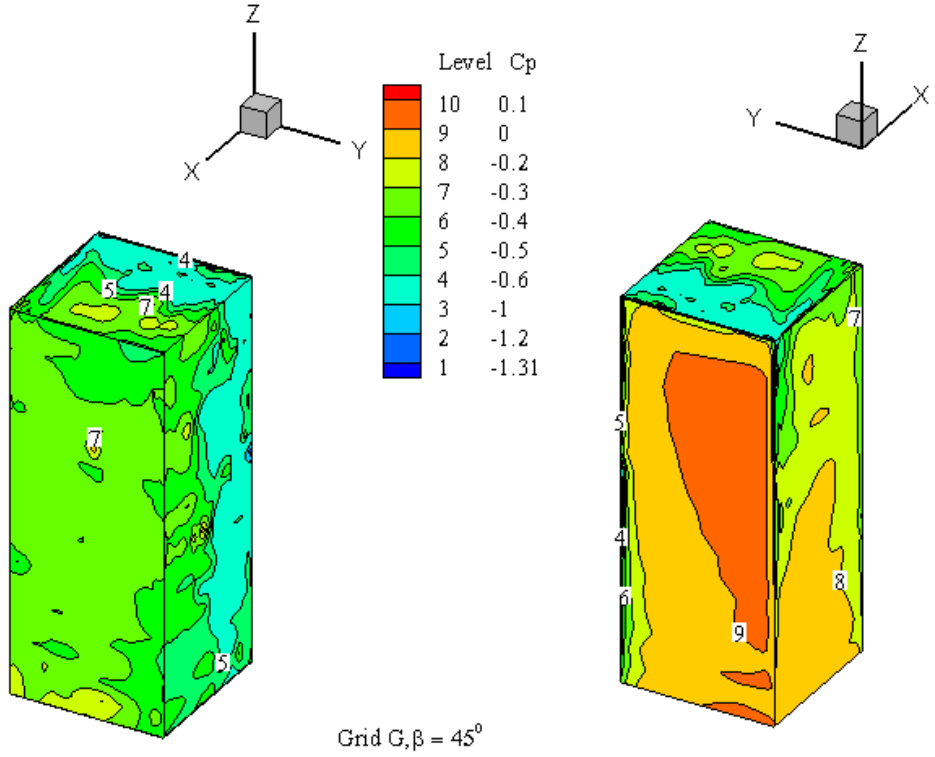

Figure 6.20 Structure plan area (0.4h x 0.4h), tornado pressure coefficients for $\beta = 45^0$

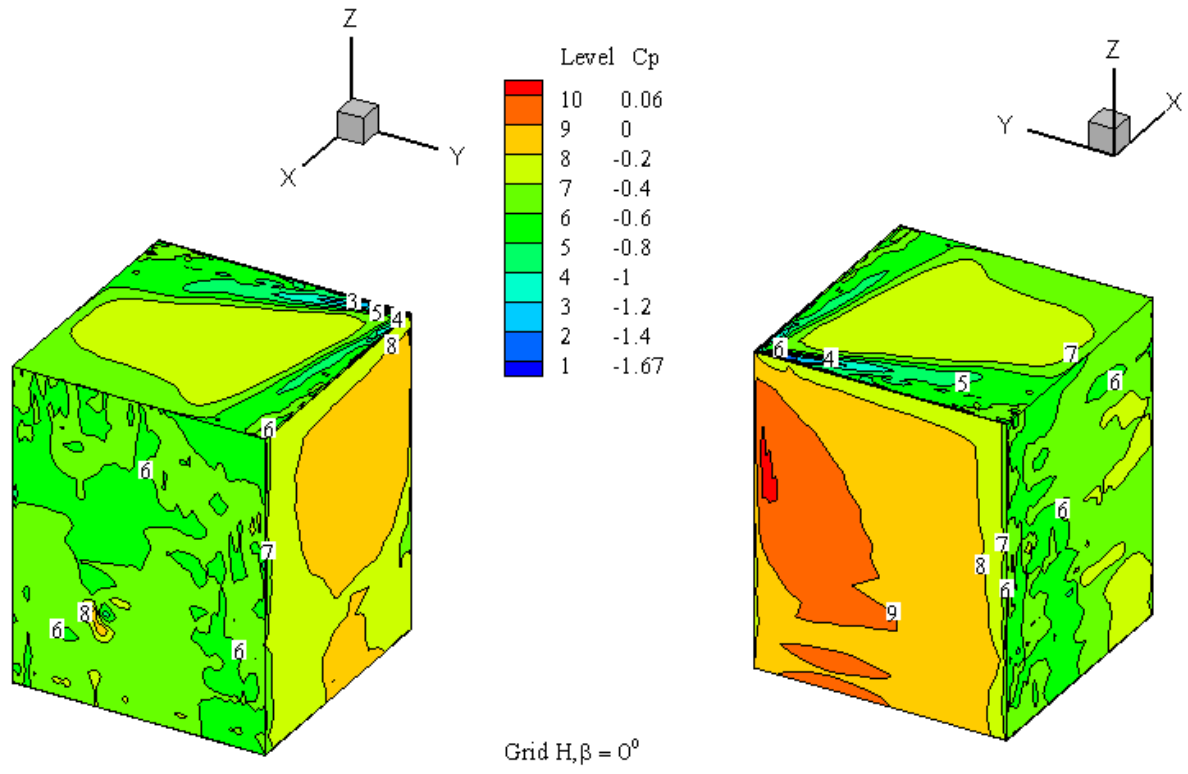

Figure 6.21 Structure plan area (0.8h x 0.8h), tornado pressure coefficient for $\beta = 0^0$

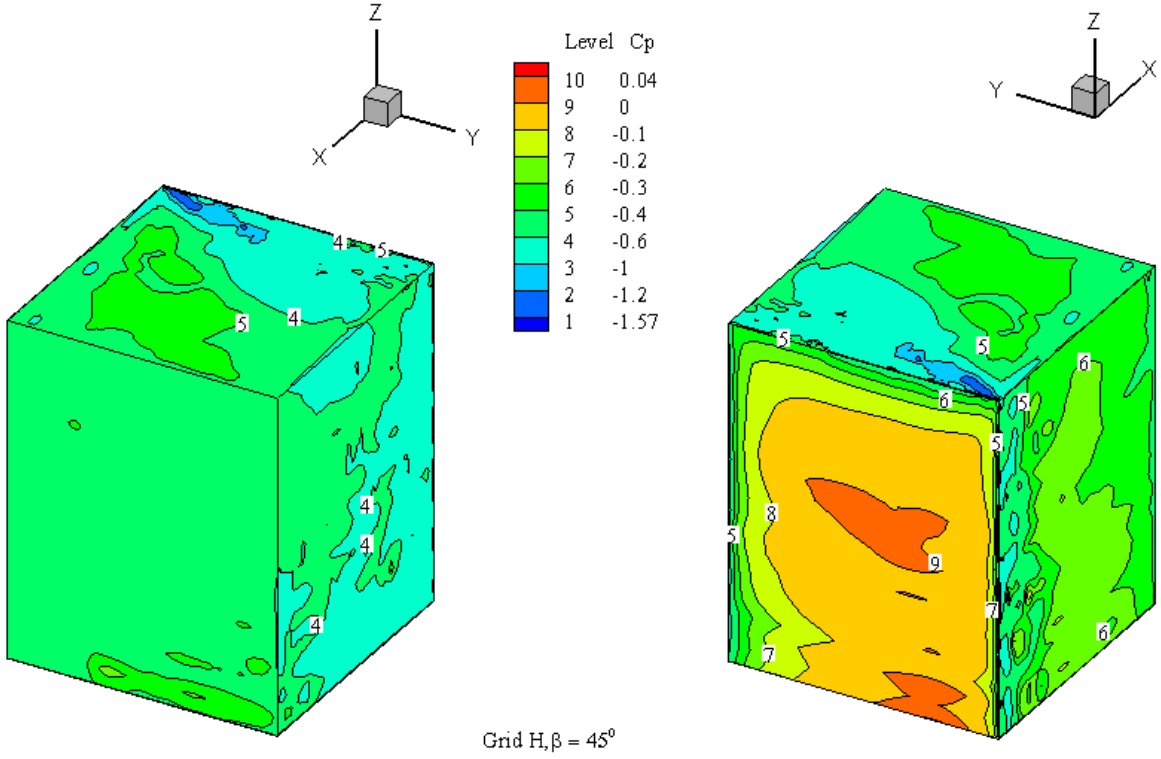

Figure 6.22 Structure plan area (0.8h x 0.8h), tornado pressure coefficients for $\beta = 45^0$

6.5.3 COMPARISON OF THE SAME USE OF ($V_{tran.}$) IN A TORNADO AND A SL WIND

The use of the same maximum translating reference velocity ($V_{trans.}$) in a tornado and in a SL flow allows us to examine the values of force coefficients in the x-direction, the maximum pressure coefficients on TSPA, and these coefficients compared to SL flow. The $V_{trans.}$ is the non-dimensional unit velocity as specified in Table 6.2. The tornado and the SL wind flow approach the structure with two angles of attack ($\beta = 0^0, \beta = 45^0$).

The force coefficient in the x-direction and pressure coefficient on the TSPA for $\beta = 0^0$ and $\beta = 45^0$ are summarized separately in Table 6.7 and Table 6.8. Figures 6.23 and 6.24 compare the maximum value of the pressure coefficient on the TSPA roof between the tornado and the SL flow for the abovementioned angles.

Table 6.7 Tornado and SL force and pressure coefficients comparison for $\beta = 0^0$

Grid name	Structure Plan Area	C_x SL flow	C_x Tornado	C_p SL flow	C_p Tornado
E	0.1h x 0.1h	1.06	46.89	-1.2	-13
F	0.2h x 0.2h	0.84	45.68	-1.29	-16
G	0.4h x 0.4h	0.80	42.96	-1.5	-20
H	0.8h x 0.8h	0.75	41.74	-1.3	-25

Table 6.8 Tornado and SL force and pressure coefficients comparison for $\beta = 45^0$

Grid name	Structure Plan Area	C_x SL flow	C_x Tornado	C_p SL flow	C_p Tornado
E	0.1h x 0.1h	0.82	55.36	-0.7	-12.3
F	0.2h x 0.2h	0.79	50.82	-0.9	-14.3
G	0.4h x 0.4h	0.77	40.53	-1.2	-19
H	0.8h x 0.8h	0.76	32.06	-1.3	-23

For the same $V_{trans.}$, and for $\beta = 0^0$, the tornado exerted on the TSPA approximately 40 to 46 times higher force coefficient in the x-direction compared to the SL flow as shown in Table 6.7. In addition, the tornado generated a nearly 13 to 25 times greater suction pressure on the roof of the TSPA compared to the SL pressure coefficient as shown in Fig.6.23. Similarly, for

same V_{trans}., and $\beta = 45^0$, the tornado created approximately 32 to 55 times higher force coefficient in the x-direction on the TSPA compared to the SL flow as shown in Table 6.7. In addition, the tornado generated a nearly 12 to 23 times higher suction pressure coefficient on the roof of the TSPA compared to the SL pressure coefficient (see Fig.6.24).

Figures 6.25 and 6.26 show a three-dimensional view of the pressure coefficient distributions on the SPA (0.1h x 0.1h) for the tornado and the SL flow approaching the structure with $\beta = 0^0$. Likewise, Figs. 6.27 and 6.28 show a three-dimensional view of the pressure coefficient distributions on the SPA (0.1h x 0.1h) for the tornado and the SL flow approaching the structure with $\beta = 45^0$.

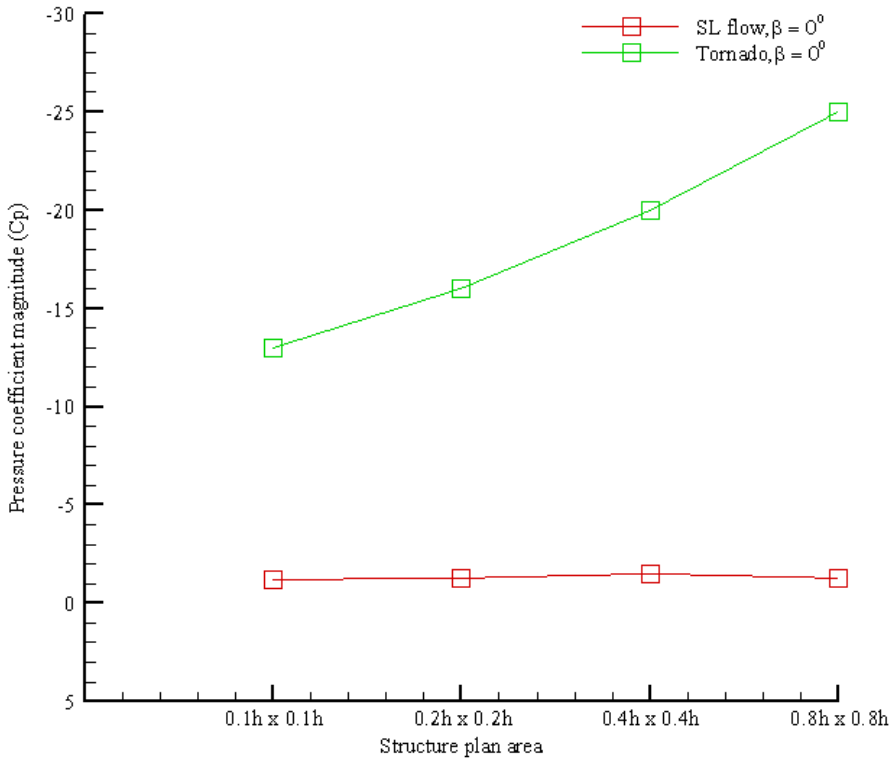

Figure 6.23 Pressure coefficient comparison on thin structure plan areas roof

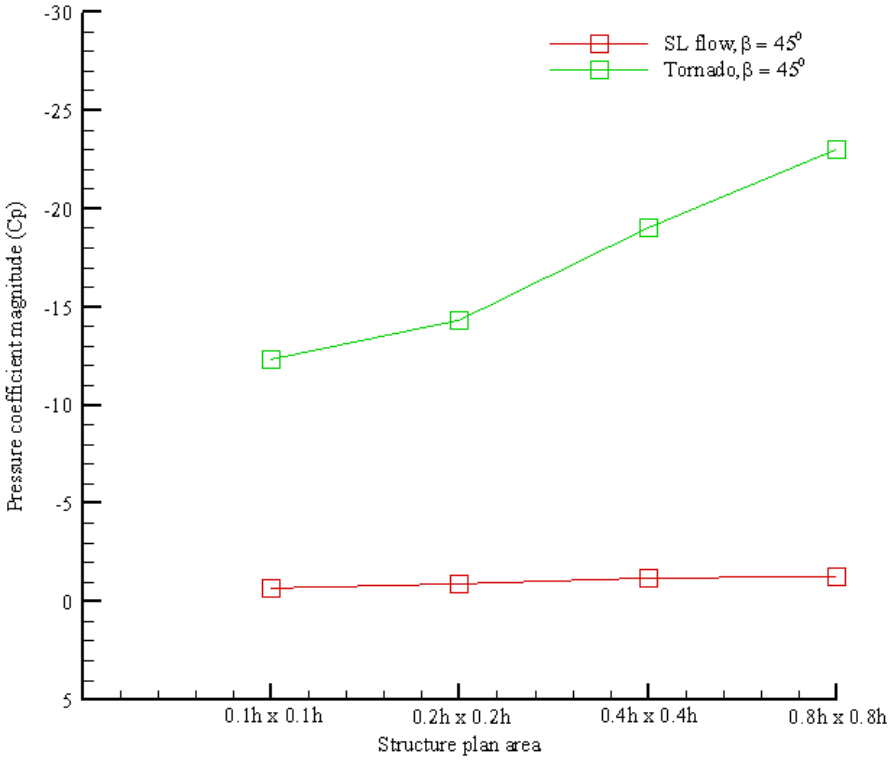

Figure 6.24 Pressure coefficient comparison on thin structure plan areas roof

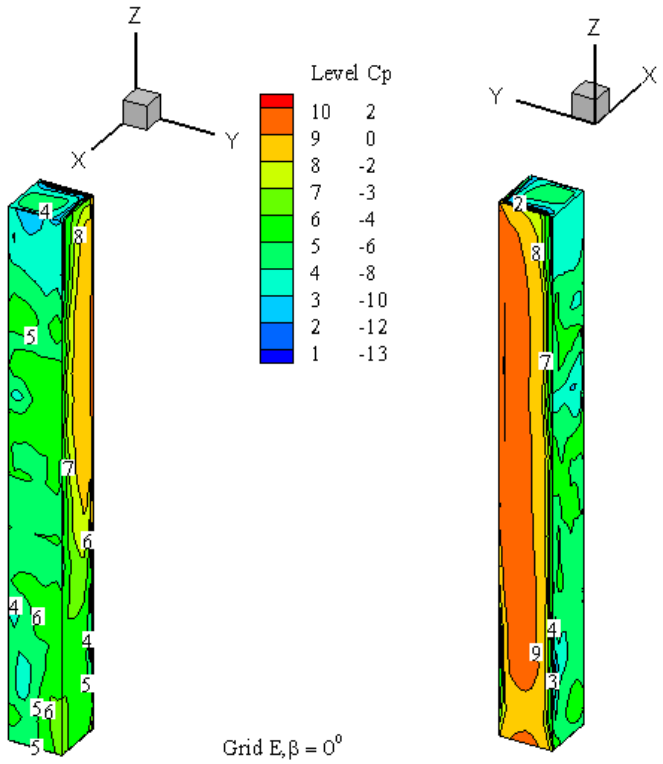

Figure 6.25 Structure plan area 0.1h x 0.1h, tornado pressure coefficients contour plot

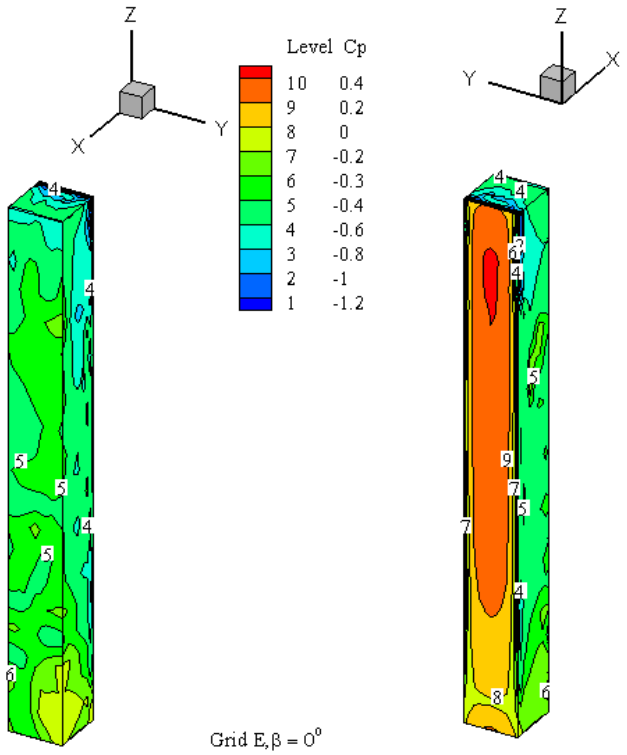

Figure 6.26 Structure plan area (0.1h x 0.1h), SL flow pressure coefficients contour plot

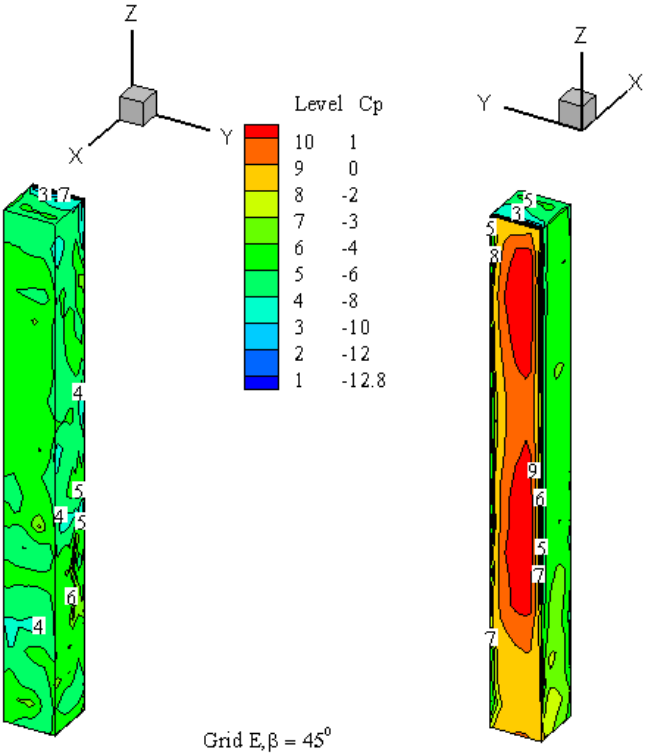

Figure 6.27 Structure plan area (0.1h x 0.1h), tornado pressure coefficients contour plot

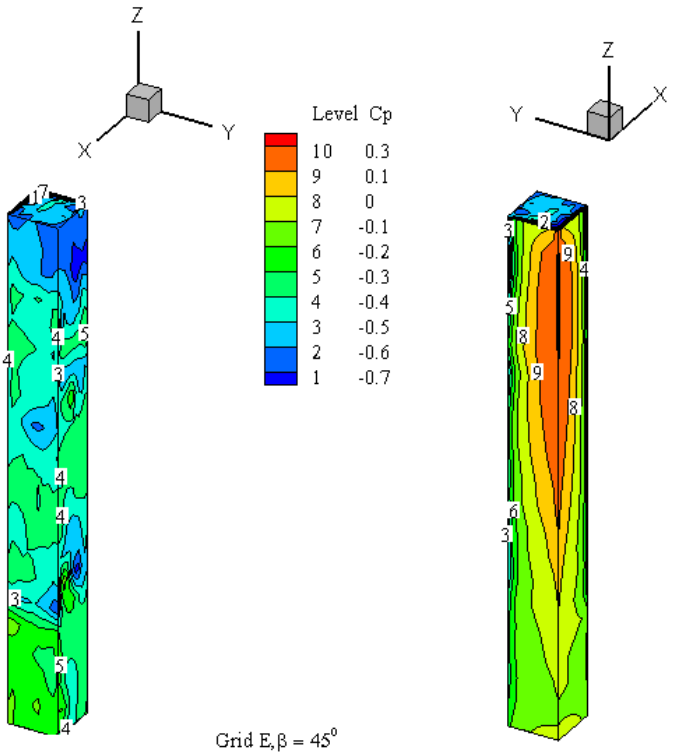

Figure 6.28 Structure plan area (0.1h x 0.1h), SL flow pressure coefficients contour plot

When the same V_{trans}. and same angle of approach was used in a tornado and SL flow, the tornado generated high suction pressure on the roof of the TSPA compared to the SL flow. In addition, when the TSPA increased, the pressure coefficient increased for the tornado and SL flow. On the TSPA, the structure was prone to collapse due to the differential pressure created by the tornado on the windward and leeward walls.

For $\beta = 0^0$ and $\beta = 45^0$,the three-dimensional of the tornado and SL flow pressure coefficients (Cp) contour plot on the rest of the TSPA can be found in the Appendix (C-3).

6.5.4 VORTEX SHEDDING

Vortex shedding occurs at critical wind velocities, and these wind velocities generate vortices at the leeward wall where low pressure develops. Thin structures and tall buildings are bluff bodies. When $\beta = 0^0$ and the flow is SL wind flow, separation in the flow occurs at the

leeward wall as shown in Fig. 6.29. The differential in the dynamic pressure distributions around the thin structure result in a transverse force normal to the wind direction with a torsion, as described by Mendis et al., (2007). In addition, if the frequency of the vortex shedding coincides with the thin structure frequency, a resonance will occur and the structure will fail. Equation (6.11) defines the frequency of the vortex shedding ($f_{sh.}$).

$$f_{sh.} = \frac{SU}{w} \tag{6.11}$$

Where:

S = Strouhal number

U= Maximum wind speed

W= Structure width

Mendis et.al (2007) has numerically studied the vortex shedding on a rectangular tall structure and the pressure distribution is illustrated in Fig. 6.29. Their CFD result was for a SL wind flow approaching the tall structure with $\beta = 0^0$. The CFD result here shows similar trends with Mendis et.al of the pressure distribution on the TSPA (0.1h x 0.1h) as shown in Fig.6.30. In addition, Fig. 6.31 shows the SL flow velocity vector plot where the vortex shedding occurs at the leeward wall.

In contrast, when $\beta = 0^0$, the velocity vector plot and pressure distributions on the SPA (0.1h x 0.1h) due to tornado-interaction are presented in Figs.6.32 and 6.33, respectively. The velocity vector plot of a translating tornado shows that the tornado created higher suction pressure, and complex vortices at the leeward wall and the side wall compared to the SL flow for the SPA (0.1h x 0.1h). Therefore, the tornado created complex weak vortices on two walls of all TSPA compared to the SL flow, and the structure is likely to fail or collapse faster in the

presence of the tornado because the tornado has translational and rotational velocities compared to the SL wind.

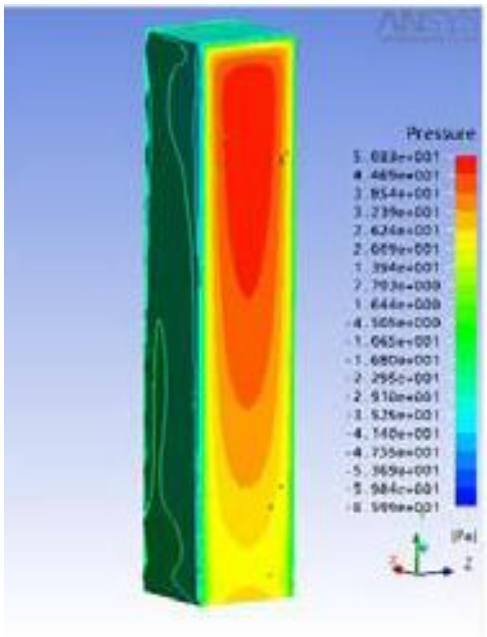

Figure 6.29 Pressure distributions of SL flow on a tall rectangular structure (Mendis, 2007)

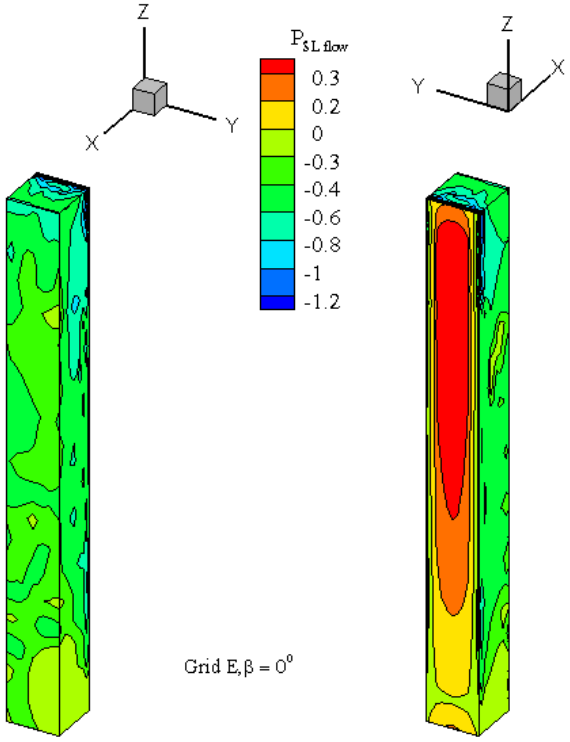

Figure 6.30 Structure plan area (0.1h x 0.1h), SL flow pressure coefficients contour plot

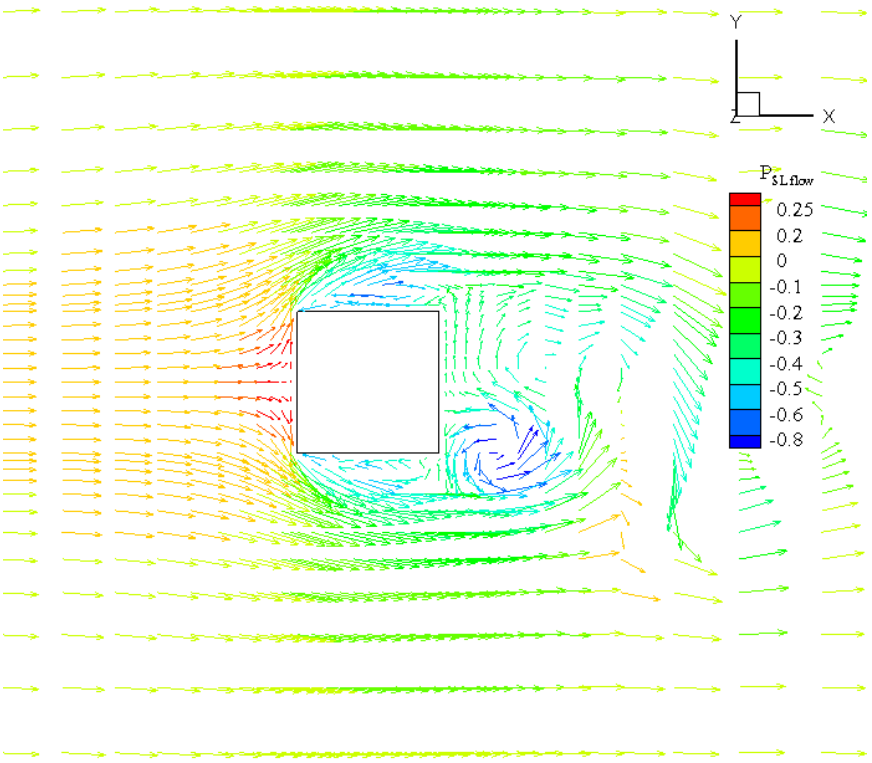

Figure 6.31 Structure plan area (0.1h x 0.1h), SL flow velocity vector plot ($\beta = 0^0$)

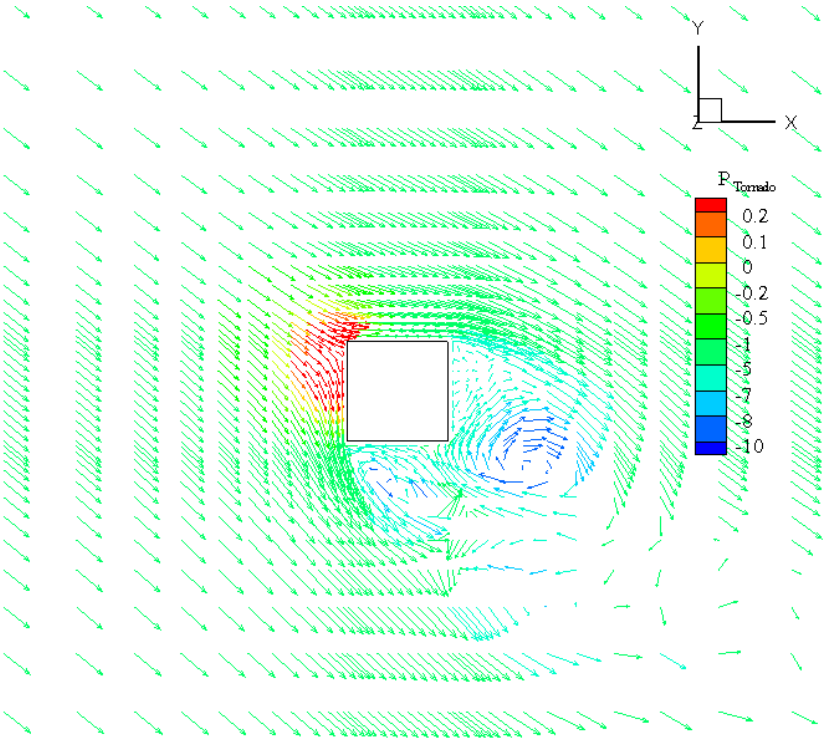

Figure 6.32 Structure plan area 0.1h x 0.1h, tornado velocity vector plot ($\beta = 0^0$)

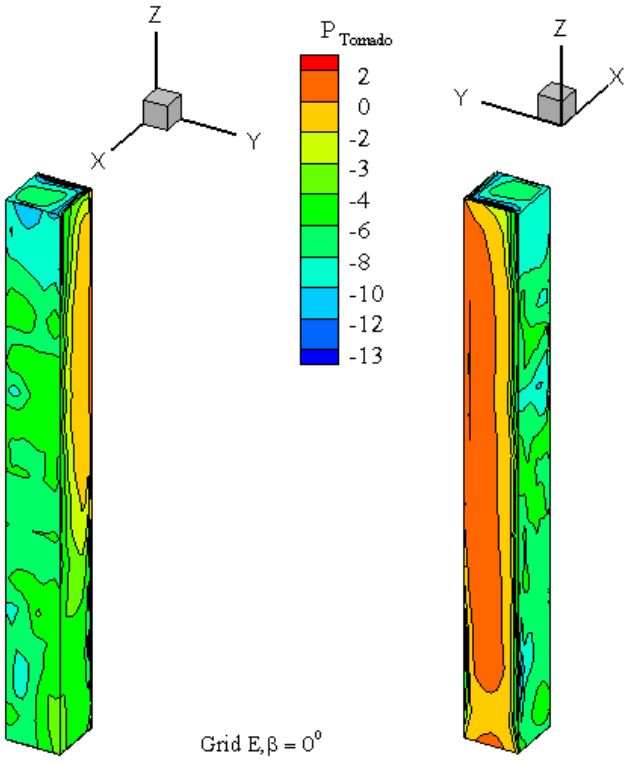

Figure 6.33 Structure plan area 0.1h x 0.1h, tornado pressure contour plot ($\beta = 0^0$)

Vortex shedding is a complex phenomenon, which required a refinement mesh on each TSPA to provide more accurate results on the pressure and force coefficients on each structure plan area. However, it was not feasible to provide a mesh refinement independent study for each structure plan area because of the computer resource limitations and limitation study length. A coarse mesh was used on the structure edges (0.01h) and normal to the structure edges (0.005h). However, Selvam and Millett (2003) have provided a benchmark study on the mesh refinement for a cubic structure (h x h x h) and found that the spacing in the x, y and z –directions mut be 0.005h normal to the structure in each direction. They also found that the minimum spacing on the structure edges must be 0.025h. Therefore, to achieve more precise result the mesh on the edges of the smallest structure plan area (0.1h x 0.1h) should be 0.0025h. In future studies refinement mesh is necessary to achieve the most accurate results on the force coefficients and pressure coefficient.

CHAPTER 7

EFFECT OF VARYING TORNADO VORTEX STRENGTH ON TORNADO FORCES

7.1 INTRODUCTION

The goal of this Chapter is to determine the relationship between increasing vortex strength values (α) in a tornado and the tornado force coefficients on a cubic structure (h x h x h). Since the tangential velocity (V_θ) increases every time the vortex strength increases, the tangential velocity increases linearly as described by the RCV model. It might be expected that tornado forces double every time the vortex strength value doubles, or vice versa.

In the numerical simulation, the tornado approaches the structure with $\beta = 0^0$ and with vortex strength values ($\alpha_1 = 0.75, \alpha_2 = 1.5, \alpha_3 = 2.25$ and $\alpha_4 = 3.0$). The grid points in the computational domain will remain the same for each case study and the force coefficients on the cubic structure will be tabulated for each simulation. The next sections will discuss in detail the grid properties and tornado parameters, geometry and boundary conditions and the computational result of tornado force coefficients.

7.2 GRID PROPERTIES AND TORNADO PARAMETERS

The grid layout in the x, y and z-directions in the computational domain are the same for each simulation. The grid points were generated by FORTRAN code. The minimum spacing normal to the structure in each direction is 0.005h and on the structure edges is 0.01h. The grid spacing layout in the computational domain increases by 1.25 times the assigned minimum spacing. When the spacing between two nodes reaches the structure length in each direction, the spacing restricted to the structure's length. In Chapter 4, the grid properties assigned for the

cubic structure (h x h x h) were enough to simulate the tornado in the computational domain and the tornado force coefficients did not change within increasing the computational domain dimensions. Therefore, the structure (grid A5) was selected to study the effect of increasing the tornado vortex strength (α) on the tornado forces and force coefficients. The grid property is tabulated in Table 7.1.

Table 7.1 Grid properties

Grid name	Domain size in h	Structure size	Grid Size	Grid spacing normal to bldg.	Total #of points in domain
A5	64 x 64 x 32	h x h x h	82 x 82 x 68	0.01 h	457,232

Mesh, or grid points, in the computational domain is visualized by TecPlot software. Figure 7.1 shows the mesh in the x-y plane for the cubic structure.

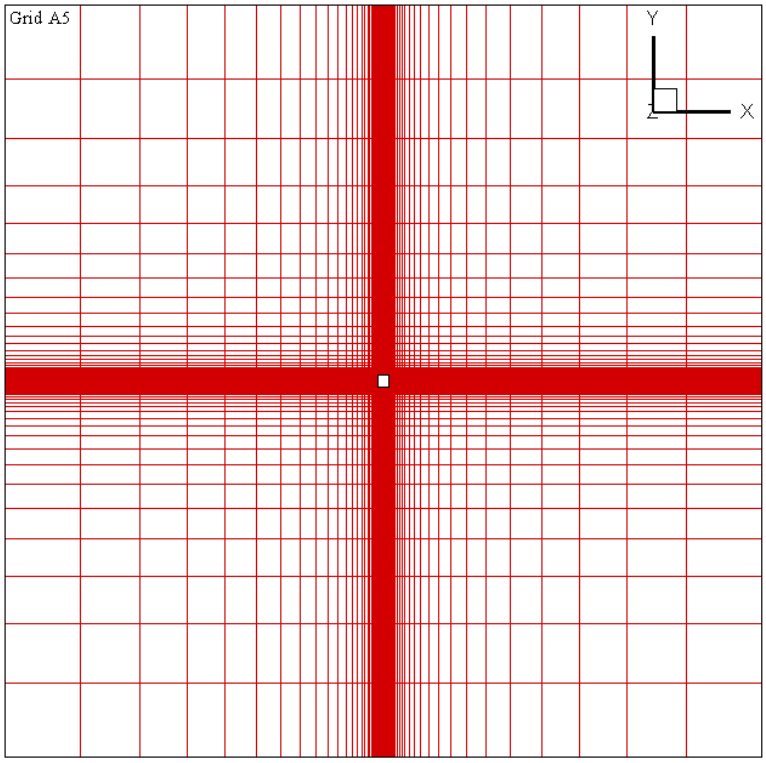

Figure 7.1 structure (h x h x h), the x-y plane mesh

Figure 7.2 illustrates a top view of a tornado path approaching the cubic structure with β = 0^0. The structure geometry dimensionalizes by the structure height (h) and the translation velocity ($V_{trans.}$) dimensionalizes the flow velocities fields. The maximum velocity (V_{max}) in a tornado is the sum of two velocity components and they are the tangential (V_θ) and the translation ($V_{trans.}$) velocities. The maximum velocity is calculated from the Rankine-Combined Vortex (RCV) velocities as described in Chapter 4. The tornado physical parameters used in this study are specified in Table 7.2.

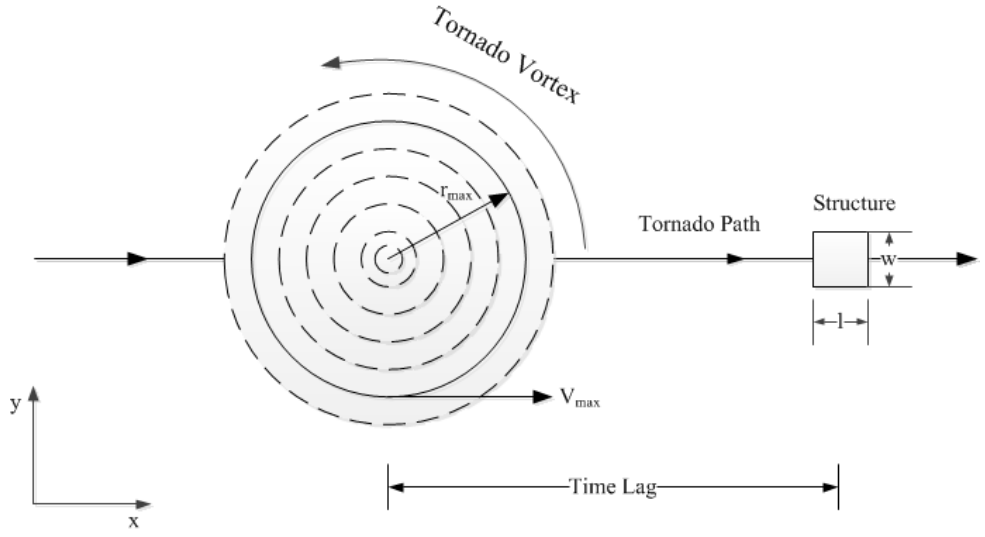

Figure 7.2 Top view of a tornado path approaching a structure with 0^0

Table 7.2 Tornado parameters

Case Study	Units	h	α	r_{max}	$V_{trans.}$	V_{θ}	V_{max}
Case # 1	SI units	20.3 (m)	0.75 (1/s)	61.0 (m)	20.3 (m/s)	45.75 (m/s)	66.05 (m/s)
	Non-Dimensional units	1.0	0.75	3.0	1.0	2.25	3.25
Case # 2	SI units	20.3 (m)	1.5 (1/s)	61.0 (m)	20.3 (m/s)	91.5 (m/s)	111.8 (m/s)
	Non-Dimensional units	1.0	1.5	3.0	1.0	4.50	5.50
Case # 3	SI units	20.3 (m)	2.25 (1/s)	61.0 (m)	20.3 (m/s)	137.25 (m/s)	157.55 (m/s)
	Non-Dimensional units	1.0	2.25	3.0	1.0	6.76	7.76
Case # 4	SI units	20.3 (m)	3.0 (1/s)	61.0 (m)	20.3 (m/s)	183 (m/s)	203.3 (m/s)
	Non-Dimensional units	1.0	3.0	3.0	1.0	9	10

7.3 GEOMETRY AND BOUNDARY CONDITIONS

The structure center starts at the origin axis and has the dimensions l for length, w for width and h for height. The computational fluid domain has the dimensions L for length, W for width and H for height. Figure 7.3 illustrates an isometric view of the structure and the computational fluid domain. The computational fluid domain is located approximately ten times the inner maximum tornado core radius (r_{max}) in each direction, as suggested by the design of the computational fluid domain in Chapter 4. The dimensions of the computational domain and the cubic structure are specified in Table 7.3.

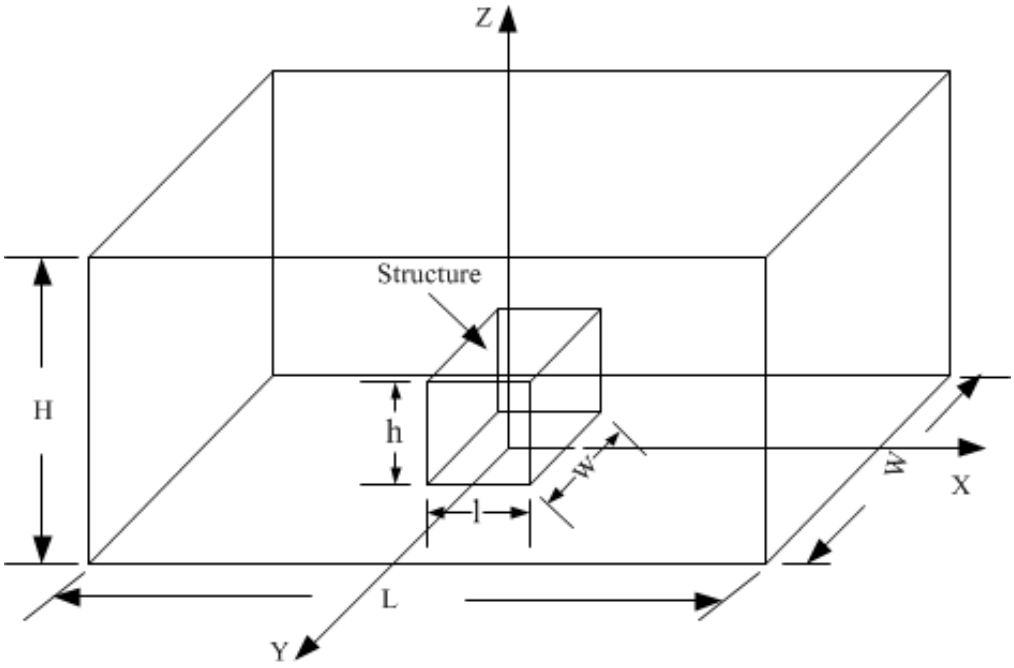

Figure 7.3 Isometric view of the computational fluid domain with the structure

Table 7.3 Computational domain and structure dimensions

Grid name	Domain size in h	Structure size
A5	64 x 64 x 32	h x h x h

The specified boundary conditions on each face of the modeled structure are zero velocities (no slip boundary condition). The boundary conditions applied on the exterior faces of the computational fluid domain are the RCV model velocities. Equations (7.1, 7.2, 7.3 and 7.4) give the RCV velocity components in a Cartesian form. The RCV model velocities were applied to each grid point in the computational domain, and these velocities changed over time based on the location of the vortex core. The RCV model is discussed in detail in Chapter 3 and Chapter 4.

$$V_x = (V_t - y\alpha)Zf \qquad \text{if } r \le r_{max} \qquad (7.1)$$

$$V_y = (x - V_t t)\alpha\, Zf \qquad if\ r \le r_{max} \qquad (7.2)$$

$$V_x = (V_t - Cy)Zf \qquad \text{if } r > r_{max} \qquad (7.3)$$

$$V_y = (x - V_t t)C\ Zf \qquad \text{if } r > r_{max} \tag{7.4}$$

The growth in the boundary layer along the z-axis (Zf) in the computational fluid domain is given in Eq.(7.5) as discussed in Chapter 4.

$$Zf = \frac{u}{k} \ln\left(\frac{h+h_0}{h_0}\right) \tag{7.5}$$

7.4 TORNADO FORCE COEFFICIENTS

Forces on the cubic structure are calculated by integrating the pressure on each surface area in x,y and z-directions. The reported maximum force coefficients in a tornado are for the specified time lag in the simulation. The time lag is the period from the start time of the simulation and when the center of the tornado coincides with the center of the structure. The force coefficients are calculated from the following equations:

$$Cx = \frac{F_x}{0.5\rho V^2 A} \tag{7.6}$$

$$Cy = \frac{F_y}{0.5\rho V^2 A} \tag{7.7}$$

$$Cz = \frac{F_z}{0.5\rho V^2 A} \tag{7.8}$$

The reference velocity (V) in a tornado is the maximum velocity (V_{max}). The definitions of the force coefficients were given in Chapter 4 and Chapter 5.

7.5 TORNADO VORTEX STRENGTH RESULTS AND DISCUSSION

The UA-CFD wind code was used to compute the tornado force coefficients on the structure (h x h x h) for three different tornado vortex strengths. The tornado approached the structure with a 0^0 angle of attack. Tornado forces on the cubic structure were computed by integrating the pressure on each surface, and then the force coefficients are calculated from Eqs. (7.6, 7.7, and 7.8). The reported maximum force coefficients are for the specified time lag in the

simulation. At the specified time lag, the tornado center coincides with the structure center as shown in Fig. 7.4 for structure (h x h x h). The force coefficient in the x, y and z-directions for each case study are summarized in Table 7.4. In addition, the force coefficients were plotting in time for α_1 = 0.75,α_2 = 1.5 ,α_3 = 2.25 and α_4 = 3.0 as illustrated in Figs. 7.5,7.6,7.7 and 7.8, respectively.

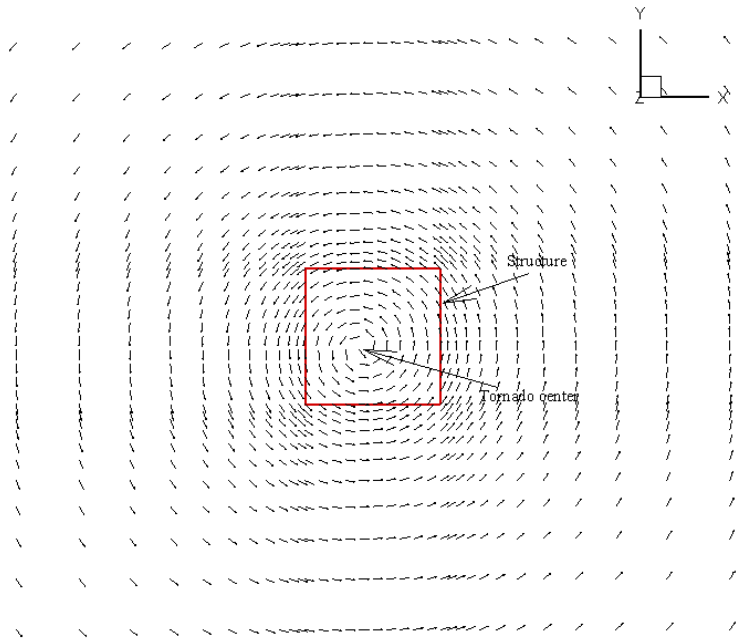

Figure 7.4 Structure (h x h x h) center coincides with tornado center at 1h above the roof

Table 7.4 Tornado absolute maximum force coefficients

Case Study	Structure Size	Vortex strength (α)	Angel of attack (β)	C_x	C_y	C_z
Case #1	h x h x h	0.75	0^0	0.67	0.42	0.86
Case #2	h x h x h	1.50	0^0	1.08	1.05	1.61
Case #3	h x h x h	2.25	0^0	1.98	1.56	2.71
Case #4	h x h x h	3.0	0^0	3.98	2.01	4.41

When the tornado vortex strength increases, the force coefficients in the x, y and z-directions increase as shown in Table 7.4. The tornado force coefficients in the x and z-directions increase exponentially when we use the maximum reference velocity (V_{max}) in the tornado as shown in Fig.7.9. However, the force coefficient in the y-direction increase linearly when the

vortex strength increase every time. To examine the force coefficient (Cz) and the force (F_{roof}) on the structure roof, it is required to integrate the pressure on each cell for each vortex strength.

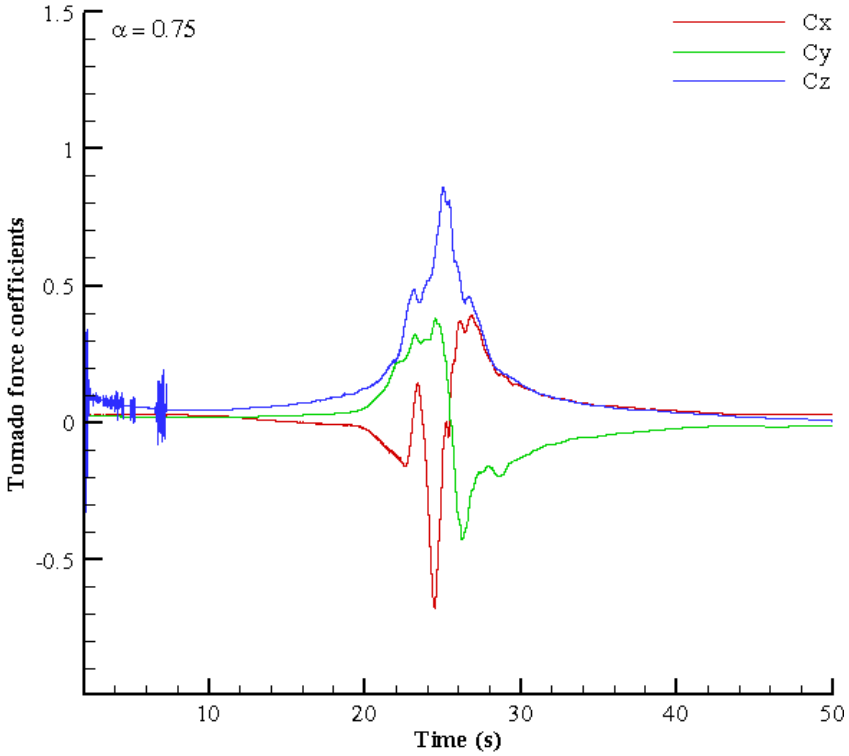

Figure 7.5 Tornado force coefficients, $\alpha_1 = 0.75$

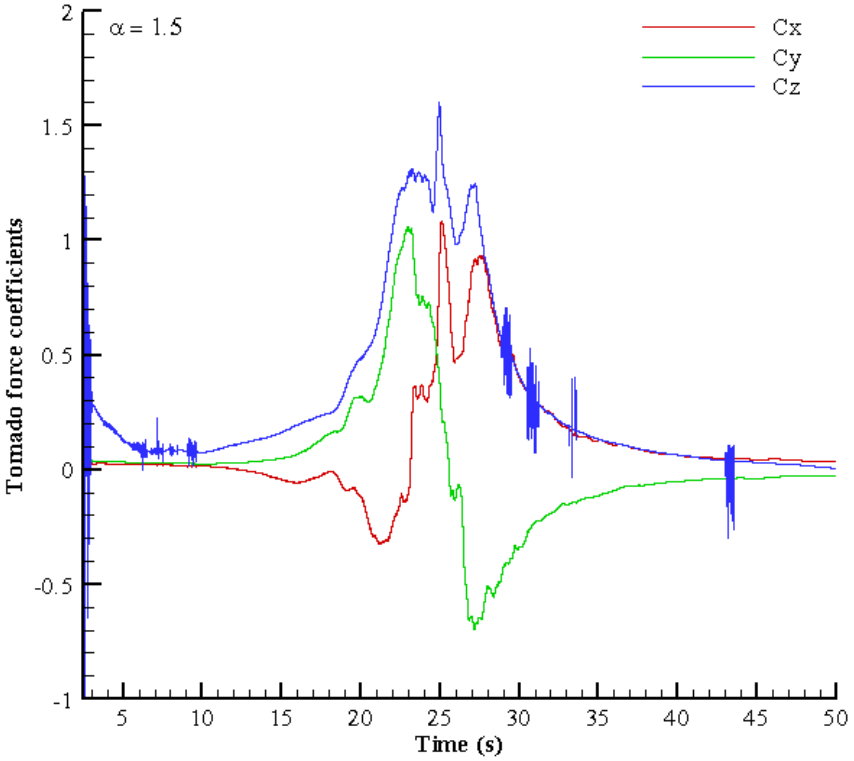

Figure 7.6 Tornado force coefficients, $\alpha_2 = 1.5$

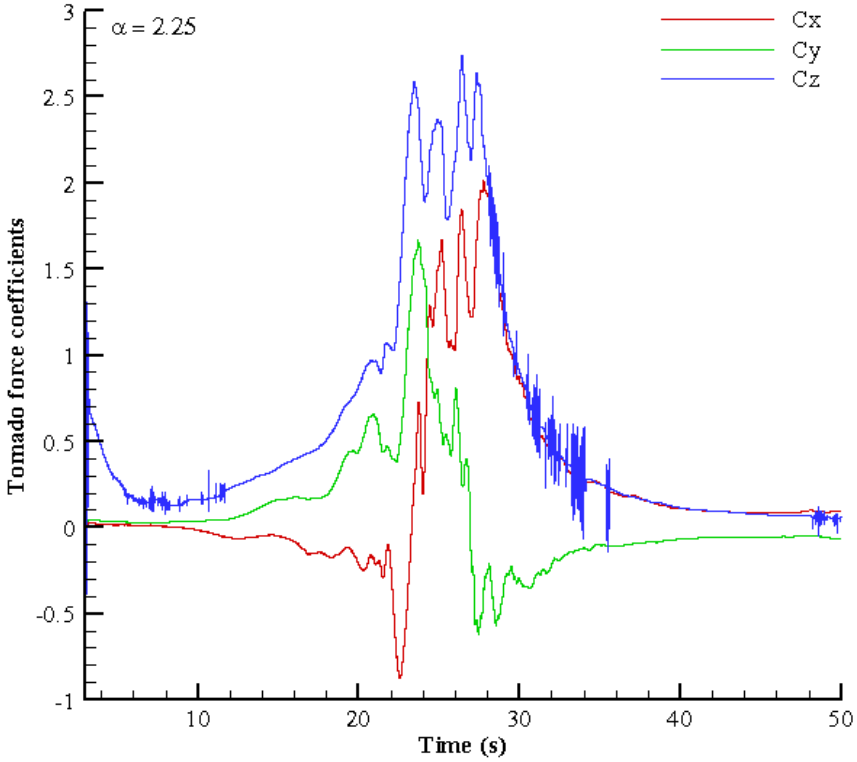

Figure 7.7 Tornado force coefficients, $\alpha_3 = 2.25$

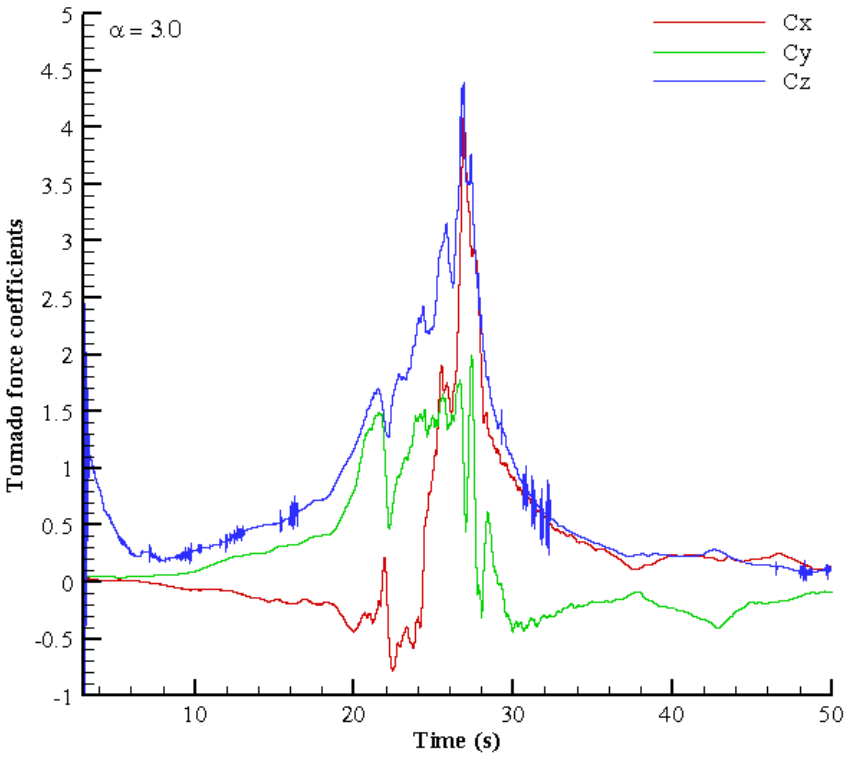

Figure 7.8 Tornado force coefficients, $\alpha_4 = 3.0$

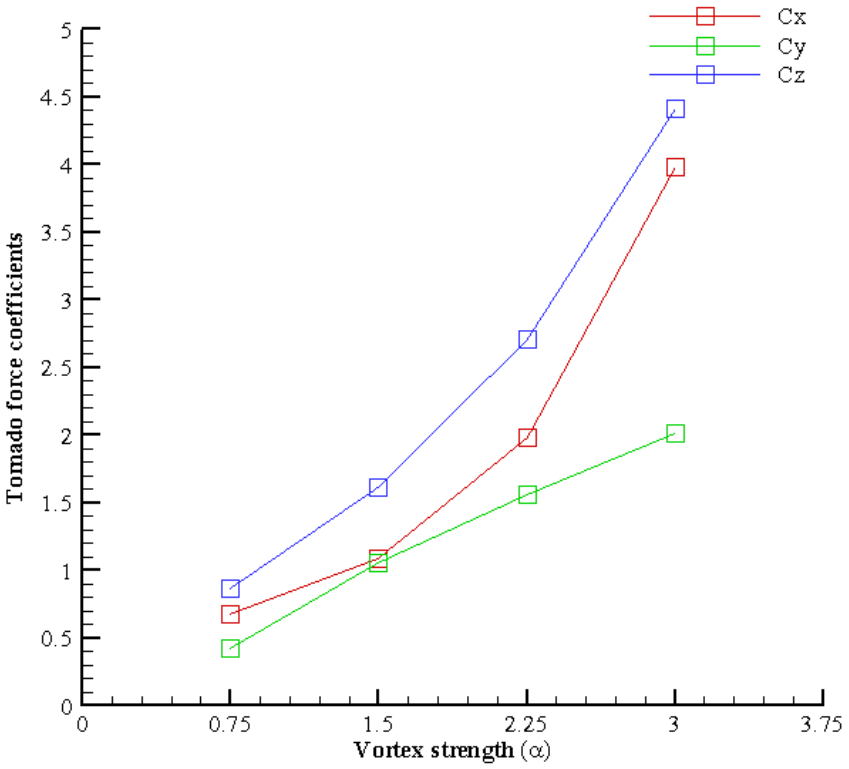

Figure 7.9 Tornado force coefficients vs. vortex strength

The force on the structure roof can be calculated by taking the summation of the average pressure at each grid cell and multiplying that by the area of the grid cell, divided by the total number of grid cells as shown in Eq. 7.9.

$$F_{roof} = \frac{1}{total\ numbers\ of\ cells} \times \sum (P_{avg})_{per/cell} \times \Delta x \times \Delta y \qquad (7.9)$$

The cell dimensions are Δx in the x-direction and Δy in the y-direction. In the numerical simulation, we kept Δx equal to Δy in spacing and both have a fixed value of 0.01 units. The average pressure in each cell on the structure roof can be visualized from a feature in TecPlot software. Figures 7.10, 7.11, 7.12 and 7.13 show the pressure average in each grid cell for α = 0.75, 1.5, 2.25 and 3.0 respectively. The force on the structure roof (F_{roof}) and the corresponding force coefficient (Cz) are summarized in Table 7.5 for each case study.

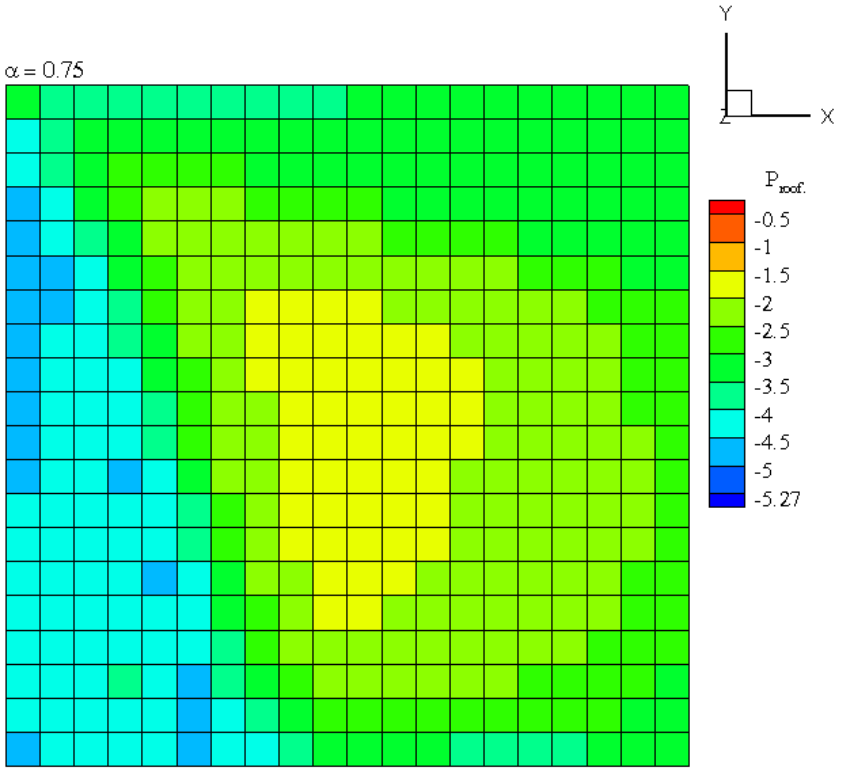

Figure 7.10 Tornado average pressure on each grid cell, α_1 = 0.75

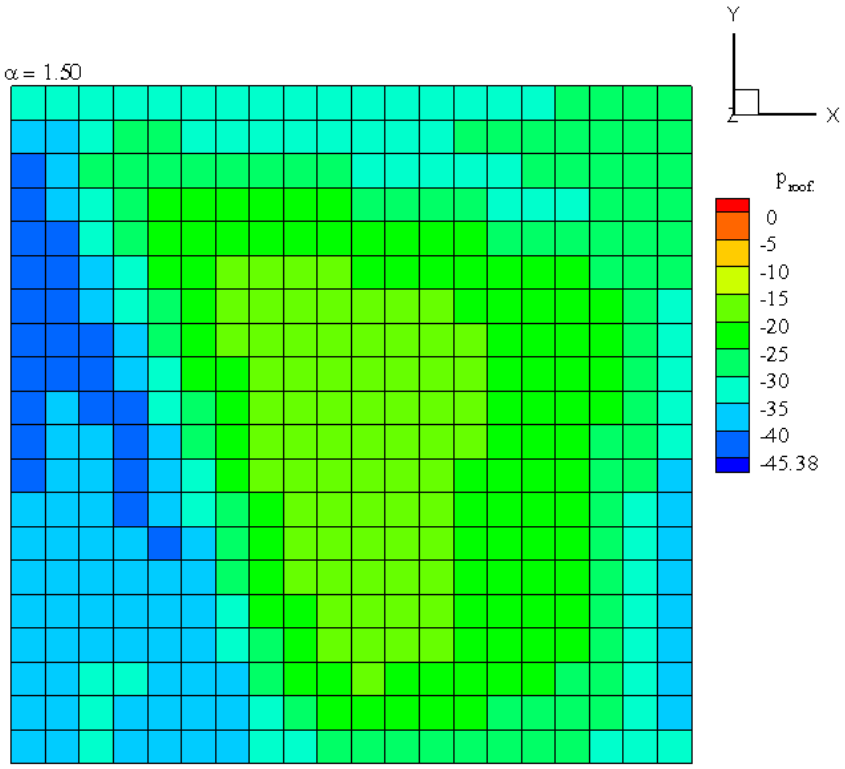

Figure 7.11 Tornado average pressure on each grid cell, $\alpha_2 = 1.5$

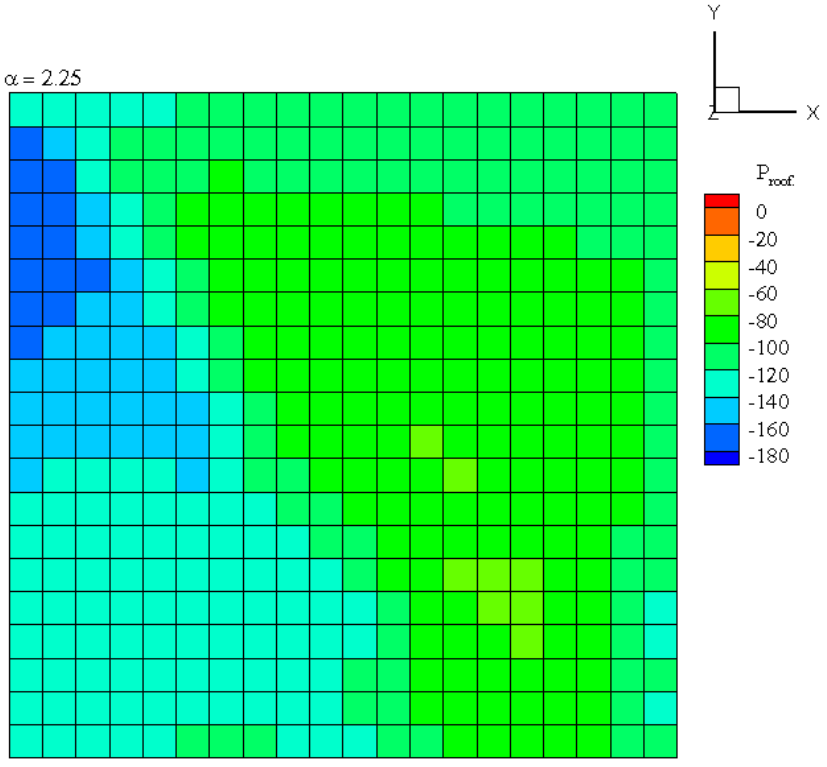

Figure 7.12 Tornado average pressure on each grid cell, $\alpha_3 = 2.25$

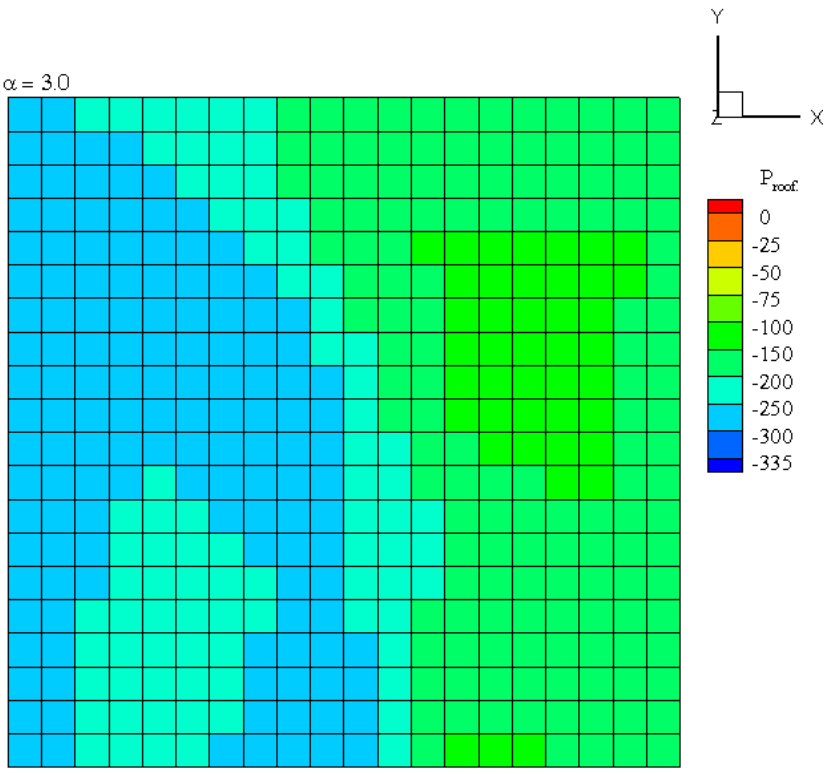

Figure 7.13 Tornado average pressure on each grid cell, $\alpha_4 = 3.0$

Table 7.5 Tornado absolute force and force coefficient on the structure roof

Case Study	Structure Size	Vortex strength (α)	Angel of attack (β)	F_{roof}	C_z
Case #1	h x h x h	0.75	0^0	4.54	0.859
Case #2	h x h x h	1.50	0^0	24.4	1.613
Case #3	h x h x h	2.25	0^0	84.56	2.80
Case #4	h x h x h	3.0	0^0	222	4.44

The tornado generated high suction pressure on the cubic structure roof when the strength of the vortex increased. When $\alpha_2 = 2\alpha_1$, the force coefficient on the structure roof approximately doubled. However, the force on the structure roof was approximately six times in value when $\alpha_2 = 2\alpha_1$, compared to α_1 as shown in Table 7.5. Figure 7.14 illustrates the relationship between the vortex strength and the force on the structure roof. In addition, Fig. 7.15 shows the relationship between the vortex strength and the force coefficient on the structure roof.

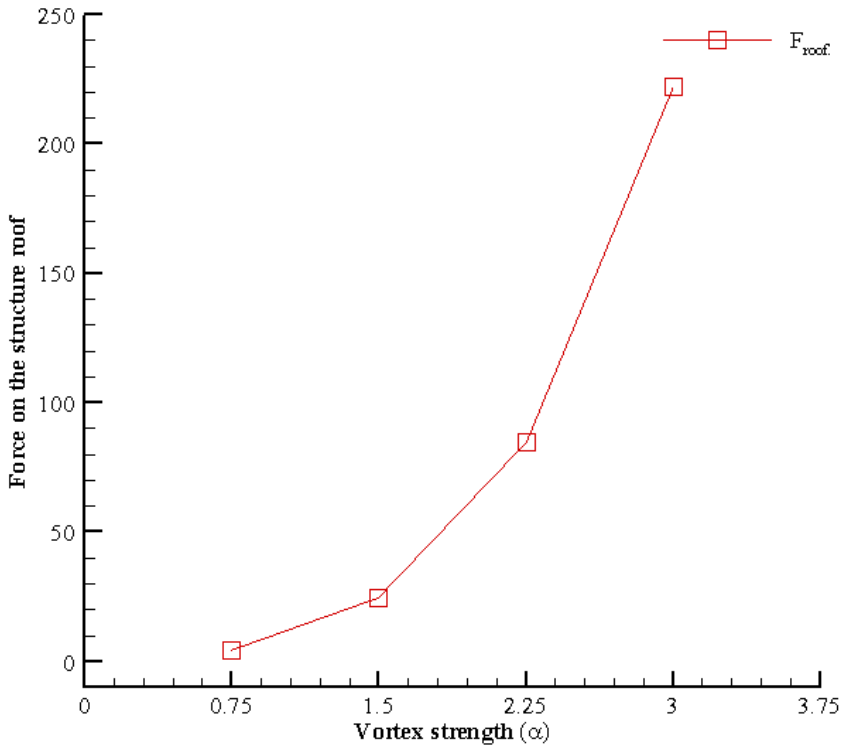

Figure 7.14 Force on the structure roof

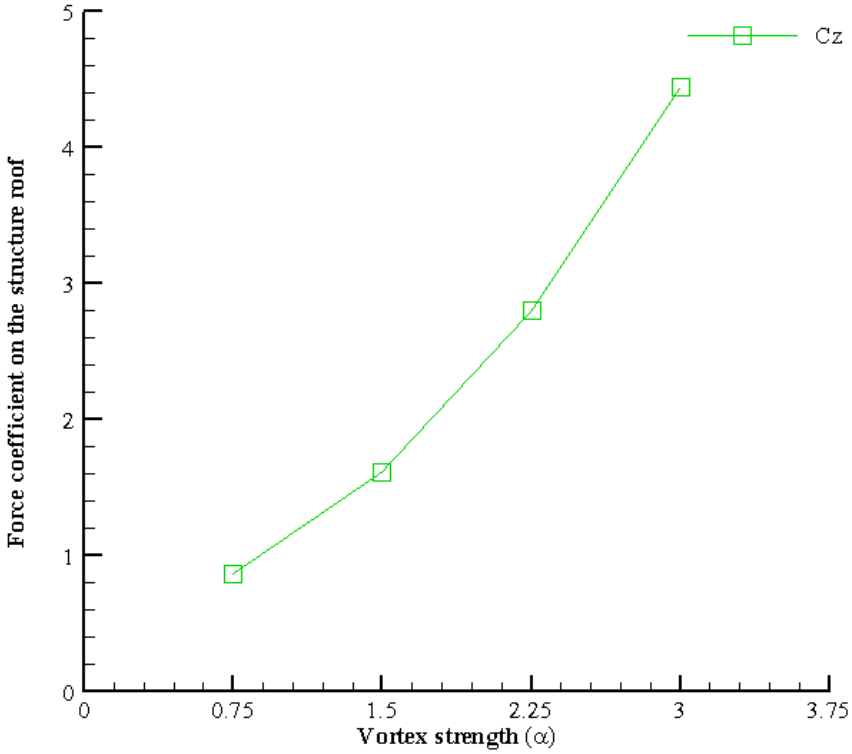

Figure 7.15 Force coefficient on the structure roof

It can be concluded that when the vortex strength increases in a tornado, the tornado force coefficients in the x and z-directions increase exponentially. However, the force coefficient in the y-direction only increases linearly when the tornado vortex strength increase. The force coefficient in the y-direction increases linearly because the tangential velocity increases linearly with increasing the tornado vortex strength as described by the tornado model (RCV model). In addition, when $\alpha_2 = 2\ \alpha_1$, the force on the structure roof was approximately four and half times the force produced by the weaker strength vortex (α_1). In general, increasing the tornado vortex strength will result in increasing the tornado forces on a structure, but the force coefficients on the structure will not double every time the vortex strength doubles. This can be visible when $\alpha_4 = 4\ \alpha_1$, the force coefficient on the structure roof increased to five times the tornado force coefficient created on the structure roof when compared to α_1. In addition, when $\alpha_4 = 4\ \alpha_1$, the tornado force on the structure roof was nearly forty four times comparing to the weaker vortex strength (α_1). While a refinement mesh could provide more accuracy in the results, the scope of this Chapter is limited to showing the relationship between increasing the vortex strength in a tornado and the force coefficients on a cubic structure.

CHAPTER 8

PRACTICAL RELEVANCE OF THE RESEARCH

8.1 INTRODUCTION

On May 22, 2011, a devastating EF5 rated tornado occurred in and around Joplin, Missouri, killing 166 people. The winds reportedly exceeded 200 mph. More recently, on February 29, 2012, an EF2-tornado with wind speeds estimated at 111 mph struck Branson, Missouri. A comparison between the results obtained from this study and the wind effects from these two tornados was developed to verify the conclusions reached in this work, with a hope of preventing tragedies such as those experienced in Joplin and Branson.

8.2 FAILURE AT THE EDGE OF THE TORNADO PATH

The purpose of this research was to determine the force coefficients on structures with various plan areas with heights. From the computer simulations, when the structure plan area was approximately twice the tornado size, the force coefficients at the edge of the tornado (the free vortex region) were similar to the SL flow force coefficients. Therefore, in the free vortex region the study indicated that tornado forces caused less damage to structures. The damage in these free vortex regions would then mostly be caused by flying debris. An illustration of this phenomenon is shown in a photograph taken after the Joplin tornado. The roof of the structure in the background was only partially damaged, while the structure in the foreground, approximately 10 (ft), away was completely destroyed as shown in Fig. 8.1. Other structures damaged by Joplin tornado is shown in Figs. 8.2 and 8.3. Based on the results from the computer model simulation of the tornado, when the structure is larger than the tornado size, or when a part of the structure was in the free vortex region, the force coefficients were much less. Furthermore, the tornado has

similar effect on the structure as the SL wind flow. The pictures from Joplin will compare favorably with the conclusion reached from this research.

Figure 8.1 Roof and wall partially damage at the outer edge of the Joplin tornado path

Figure 8.2 Wall and roof partially damaged at the outer edge of the Joplin tornado path

Figure 8.3 Roof and wall partially damage at the outer edge of the Joplin tornado path

8.3 FAILURE AT THE MIDDLE OF THE TORNADO PATH

In the numerical simulation of the tornado, the structure was positioned in the middle of the tornado path. From the computer simulation, the tornado generated higher suction forces on the small structure sizes compared to the large structure sizes. Therefore, the small structure plan areas were more likely destroyed because of the higher suction pressure associated with the tornado. In addition, from the numerical simulation, the large structure plan area reduced the tornado effect, creating reduced force coefficients.

A photo of the St. John hospital in Joplin, which has a larger plan area compared to the surrounding structures, is shown in Fig. 8.4. The engineered hospital structure was able to better withstand the tornado winds, whereas the small surrounding structures were completely demolished. A close up of the hospital is shown in Fig. 8.5. The windows were due to flying debris and high winds. Photos from the Joplin and Branson tornados are shown in Figs. 8.6, 8.7 and 8.8 to highlight how large structure plan areas reduced the tornado impacts.

A photo of a signal post is shown in Fig. 8.9 which was destroyed by the Joplin tornado. The signal post can be an example of a tall thin structure. The photos also provide evidence that the tornados generate high suction forces on small plan areas structures in the tornado path, possibly resulting in the destruction of the structure. The photos also confirm the computer simulation that tornados generate less force on large structure plan areas, reducing the tornado impacts on these structures.

Figure 8.4 Joplin tornados, John's Regional Medical Center

Figure 8.5 John's Regional Medical Center close up, author in foreground

Figure 8.6 Joplin tornado, large structure plan area

Figure 8.7 Branson tornado, Hilton hotel

Figure 8.8 Joplin tornado, small structures completely destroyed

Figure 8.9 Joplin tornado, signal post

Branson and Joplin tornados were used to verify the conclusions drawn from this research as discussed in Chapter 9. One should keep in mind that the tornado forces on engineered structures behave differently from these same forces on non-engineered structures. More detailed analysis is needed for further verification. In future work, an attempt will be taken to relate the location of the tornado maximum inner core radius to the location of the structure, as well as the position of the building in relation to the center of the tornado. These careful observations of the failure of structures to engineering analysis will point towards a better design procedure, and may reduce tornado effect on structures.

CHAPTER 9

CONCLUSIONS AND RECOMMENDATIONS

9.1 SUMMARY OF CURRENT WORK

Past research has focused on tornado-interaction with single structure plan areas, such as gable-roofed structures, rectangular structures, and cubic structures or tall buildings interacting with a translating or a stationary vortex either by computer modeling or in laboratory simulators. Since past research has had this limited focus, this research investigated this limitation and focused on tornado-interaction with different structure plan areas. A Large Eddy Simulation (LES) turbulence model and Rankine Combined Vortex (RCV) model were used to investigate tornado forces on structures. The structure height (h) remained constant for all structure plan areas and used a reference length to dimensionalize the structure geometry. The structure height is 20.3 (m) and the tornado inner maximum core radius is 3h (m).

First, the influence of Large Structure Plan Areas (LSPA) on tornado force coefficients and compared force coefficients to SL flow were investigated for the direction of tornado approach from $\beta = 0$ degree and $\beta = 45$ degree angles. Second, the influence of Thin Structure Plan Areas (TSPA) on tornado force coefficients and compared to SL flow were investigated for the direction of tornado approach from $\beta = 0$ degree and $\beta = 45$ degree angles. Lastly, a study on how the vortex strength affects tornado forces on a structure for $\beta = 0$ degree angle was investigated.

The LSAP are (1h x 1h), (2h x 2h), (4h x 4h) and (8h x 8h), where h is the height of the structure. The maximum reference velocity (V_{max}) in a tornado is the sum of the translation and the tangential velocities. Therefore, when the V_{max} was used and with $\beta = 0$ degree and $\beta = 45$

degree angles, the tornado force coefficients decrease when the Structure Plan Area (SPA) increases. On SPA (1h x 1h and 2h x 2h), the tornado force coefficients were twice the SL flow because the tornado completely overlaid the SPA. In addition, on SPA (4h x 4h and 8h x 8h), the tornado force coefficients were lesser than the SL flow force coefficients because the tornado had a localized vortex effect on the affected region. When the same maximum reference velocity ($V_{trans.}$) was used in a tornado and SL flow, the tornado produced force coefficients three to twenty-seven times greater on the plan areas that the tornado can completely cover, compared to the SL flow. In addition, on the large structure plan area (8h x 8h), which is larger than the tornado size, the tornado force coefficients were the same as the SL flow force coefficients. Therefore, the tornado has the same forces as a SL flow when the large structure plan areas characteristic length is twice the tornado maximum radius.

The LSPA were divided by a factor of ten to obtain the TSPA. When V_{max} was used in the tornado, the tornado force coefficients were twice the SL force coefficients on all TSPA. Unlike on LSPA, the tornado created a positive pressure on the windward wall. Therefore, the TSPA are more likely prone to collapse due to differentials in tornado pressure between the windward wall and the leeward wall.

Finally, when the vortex strength increases in a tornado, the tornado force coefficients in the x and z-directions increase exponentially. However, the force coefficient in the y-direction increase linearly when the tornado vortex strength increase. The force coefficient in the y-direction increases linearly because the tangential velocity increases linearly with increasing the tornado vortex strength as described by the tornado model (RCV model). In addition, when $\alpha_2 = 2\ \alpha_1$ the force on the structure roof was approximately four and half times the force produced by the weaker strength vortex (α_1). In general, increasing the tornado vortex strength will result in

increasing the tornado forces on a structure, but the force coefficients on the structure will not double when the vortex strength doubles. This is visible when $\alpha_3 = 4\ \alpha_1$, the force coefficient on the structure roof was about five times that the tornado force coefficient created on the structure roof when compared to α_1. In addition, when $\alpha_3 = 4\ \alpha_1$, the tornado force on the structure roof was nearly forty four times comparing to the weaker vortex strength (α_1).

9.2 RECOMMENDATIONS FOR FUTURE WORK

Understanding the interaction between all possible structures and all possible tornadoes will enable us to understand the most destructive phenomena in nature. Based on the research provided in this dissertation and in order to understand the proper tornadic wind induced loads on a structure, I recommend the following:

- Fix the structure plan area, change the structure height, and compare tornado forces on the structure to SL flow.
- Model a residential house, change tornado maximum radius, and compare tornado force to SL flow.
- Model a residential house, change the translation velocity in tornado, and compare tornado force to SL flow.
- Use different turbulence models and compare tornado forces on a structure to SL flow.

REFERENCES

ASCE 7-05, 2006, "Minimum Design Loads for Buildings and Other Structures", ASCE Standard, SEI/ASCE7-05, American Society of Civil Engineers.

Church, C. R., Snow, J. T., and Agee, E. M., 1977, "Tornado vortex simulation at Purdue University", Bulletin American Meteorological Society, Vol. 58, pp. 900-908.

Davies-Jones, R. P., 1973,"The Dependence of Core Radius on Swirl Ratio in a Tornado Simulator", Journal of the Atmospheric Sciences,Vol. 30, pp. 1427-1430.

Davies-Jones, R. P., 1986, "Tornado Dynamics, In Thunderstorm Morphology and Dynamics", 2nd ed., edited by E. Kessler, pp. 197-236, University of Oklahoma Press, Norman.

Dutta, P.K., Ghosh, A.K., and Agarwal, B.L., 2002, "Dynamic Response of Structures Subjected to Tornado Loads by FEM", Journal of Wind Engineering and Industrial Aerodynamics, Vol.90, pp. 55-69.

Fiedler, B. H., 1994, "The Thermodynamic Speed Limit and its Violation in Axisymmetric Numerical Simulations of Tornado-Like Vortices", Atmosphere-Ocean,Vol. 32, pp. 335–359.

Fiedler, B. H., 1998, "Wind-Speed Limits in Numerically Simulated Tornadoes with Suction Vortices ", Quarterly Journal of the Royal Meteorological Society,Vol. 124,pp. 2377-2392.

Haan, F. L, Sarkar, P.P, and Gallus, W.A., 2008, "Design, Construction and Performance of a Large Tornado Simulator for Wind Engineering Applications", Engineering Structures, Vol.30, pp. 1146–1159.

Haan, F. L., Balaramudu,V.K., and Sarkar, P. P.,2010, "Tornado-Induced Wind Loads on a Low-Rise Building", ASCE Journal of Structure Engineering ,Vol. 136, pp.106 -116.

Hangan, H., and Kim, J., 2008, "Swirl Ratio Effects on Tornado Vortices in Relation to Fujita Scale", Journal Wind Engineering and Structures, Vol.11, pp. 291-302.

Hu, H., Yang, Z., Sarkar, P. and Hann, F. , 2011, "Characterization of the Wind Loads and Flow Fields Around a Gable-Roof Building Model in Tornado-like Winds", Experiments in Fluids, Vol.51, pp. 835-851.

Ishihara, T., Oh, S., and Tokuyama, Y., 2011,"Numerical Study on Flow Fields of Tornado-Like Vortices Using the LES Turbulent Model", Journal of Wind Engineering and Industrial and Aerodynamics, Vol.99, pp. 239-248.

Jischke, M.C., and Light, B.D., 1983, "Laboratory Simulation of Tornadic Wind Loads on a Rectangular Model Structure", Journal of Wind Engineering and Industrial and Aerodynamics, Vol.13, pp. 371-382.

Kuai, L., Hann, F. L., Gallus, W. A., and Sarkar, P. P., 2008. "CFD Simulations of the Flow Field of a Laboratory-Simulated Tornado for Parameter Sensitivity Studies and Comparison with Field Measurements", Wind and Structures,Vol.,11,75-96.

Lee, J., Samaras, T.M., and Young, C.R, 2004, " Pressure measurements at the ground in an F4 tornado",Preprints,22nd Conference on Severe Local Storms, Hyannis, MA, American Meteorology Society., CD-ROM, 15.4.

Lewellen, W. S., 1976, "Theoretical Models of the Tornado Vortex", Proceedings of the Symposium on Tornadoes", Edited by: R.E. Peterson, Texas Tech University, Lubbock, June 22-24, pp. 107-143.

Lewellen, D.C., Lewellen, W.S., and Sykes, R.I., 1997, "Large-Eddy Simulation of a Tornado's Interaction with the Surface", Journal of the Atmospheric Sciences,Vol. 54,pp. 581–605.

Lewellen, D. C., Lewellen, W. S., and Xia, J., 2000, "The Influence of a Local Swirl Ratio on Tornado Intensification Near the Surface", Journal of the Atmospheric Sciences,Vol. 57,pp. 527–544.

Mendis, P., Ngo, T., Haritos, N., and Hira, A., 2007, "Wind loadings on Tall buildings", Electronic Journal of Structural Engineering, Special Issue: Loading on Structures, pp.41-54.

Millett, P.C., 2003, "Computer Modeling of the Tornado-Structure Interaction: Investigation of Structural Loading on a Cubic Building", Master's Thesis, University of Arkansas, Fayetteville, AR.

Mishra, A.R., James, D.L., and Letchford, C.W., 2008a,"Physical Simulation of a Single-Celled Tornado-Like Vortex, Part A: Flow Field Characterization", Journal of Wind Engineering and Industrial and Aerodynamics, Vol. 96, pp.1243–1257.

Mishra, A.R., James, D.L., and Letchford, C.W., 2008b,"Physical Simulation of a Single-Celled Tornado-Like Vortex, Part A: Flow Field Characterization", Journal of Wind Engineering and Industrial and Aerodynamics, Vol. 96, pp. 1258–1273.

Mitsuta, Y., Monji, N., 1984, "Development of a Laboratory Simulation for Small Scale Atmospheric Vortices", Journal of Natural Disaster Science, Vol.6, pp.43-54.

Nolan, S. D., and Farrell, B. H., 1999, "The Structure and Dynamics of Tornado Like Vortices", Journal of the Atmospheric Sciences, Vol.56, pp. 2908-2936.

Ogawa, A., 1993,"Vortex Flow" 1st ed., in Anonymous Boca Raton, Fla: CRC Press, pp.198.

Sabareesh, G.R., Matsui, M., Yoshida, A. and Tamura, Y., 2009, "Pressure Acting on a Cubic Model in Boundary-Layer and Tornado-Like Flow Fields", 11th Americas Conference On Wind Engineering.

Sarkar, P.P., Haan, F.L., Gallus, W.A., Le, K., and Wurman, J., 2005, "A Laboratory Tornado Simulator: Comparison of Laboratory, Numerical and Full-Scale Measurements", In Proceedings of the 10th Americas Conference on Wind Engineering, Baton Rouge, LA, pp.197-211.

Selvam, R. P., 1993, "Computer Modeling of Tornado Forces on Buildings", Proceedings: The 7th US National Conference on Wind Engineering, Edited by: Gary C. Hart, Los Angeles, June 27-30, pp.605-613.

Selvam, R. P., 1997, "Computation of Pressures on Texas Tech Building Using Large Eddy Simulation", Journal of Wind Engineering and Industrial Aerodynamics,Vol. 67 & 68,pp. 647-657.

Selvam, R.P., 2002 a. "Computer Modeling of Tornado Forces on Buildings", in Proceedings of the Second International Symposium on Advances in Wind & Structures, C.K. Choi et. al. (Ed.), Techno-Press, Korea, 2002, pp. 105-114.

Selvam, R.P., Roy, U.K., and Jung, Y., 2002b, "Investigation of Tornado Forces on 2D Cylinder Using Computer Modeling", in Wind Engineering, Proceedings of NCWE 2002, Edited by: K. Kumar, Phoenix Publishing House, New Delhi, pp. 342-353.

Selvam R.P., and Millett, P.C., 2002c, "Computer Modeling of the Tornado-Structure Interaction: Investigation of Structural Loading on Cubic Building", Second International Conference on Fluid Mechanics and Fluid Power, Indian Institute of Technology-Roorkee, Dec.12-14.

Selvam R.P., Millett, P.C., 2003,"Computer Modeling of the Tornado Forces on Buildings", Journal of Wind Engineering and Structures, vol. 6, pp. 209-220.

Selvam R.P., Millett, P.C., 2005. "Large Eddy Simulation of the Tornado-Structure Interaction to Determine Structural Loadings", Journal of Wind Engineering and Structures, Vol. 8,pp. 49-60.

Sengupta, A., Haan, F.L., Sarkar, P.P., Balaramudu, V., 2008, "Transient Loads on Buildings in Microbursts and Tornado Winds" Journal of Wind Engineering and Industrial and Aerodynamics,Vol. 96,pp.2173-2187.

Thampi, H., Dayal, V., and Sarkar, P.P., 2010, "Finite Element Modeling of Interaction of Tornado with a Low-Rise Timber Building", In: Fifth International Symposium on Computational Wind Engineering, Chapel Hill, North Carolina, USA.

Thampi, H., Dayal, V. and Sarkar, P. P., 2011, "Finite Element Analysis of Interaction of Tornados with a Low-rise Timber Building", Journal of Wind Engineering and Industrial Aerodynamics", Vol. 99, pp. 369-377.

Wan, C.A., and Chang, C.C., 1972, "Measurement of the Velocity Field in a Simulated Tornado-Like Vortex Using a Three Dimensional velocity Probe", Journal of Atmospheric Science,Vol. 29,pp.116-127.

Ward, N.B., 1964, "The Newton ,Kansas ,Tornado cyclone of May 24,1962", in Preprints: 11th Weather Radar Conference, pp. 410-415.

Ward, N. B., 1972, "The Exploration of Certain Features of Tornado Dynamics Using a Laboratory model", Journal of the Atmospheric Sciences,Vol. 29,pp. 1194-1204.

Wilson T., 1977, "Tornado Structure Interaction: A Numerical Simulation", Report: UCRL-52207, Distribution Category: UC-11, 80, Lawrence Livermore Laboratory, University of California, Livermore.

Yang, Z., Sarkar, P.P, and Hu, H., 2009, "Flow Structures Around a High-Rise Building Model in Tornado-Like Winds", 46th AIAA Aerospace Sciences Meeting and Exhibit, Orlando, Florida, 7- 10 Jan.

Ying, S.J., and Chang, C.C., 1970, "Exploratory Model Study of Tornado-Like Vortex Dynamics", Journal of Atmospheric Science, Vol. 27, No.1, pp. 3-14.

Zhang, W., and Sarkar, P.P., 2010, "Influence of Surrounding Buildings on the Flow Around a Low-Rise Building in ABL and Tornado-Like Winds", In: Fifth International Symposium on Computational Wind Engineering, Chapel Hill, North Carolina, USA.

APPENDIX A: LARGE EDDY SIMULATION (LES)

Selvam and Millett (2003) have used the LES turbulence model to compute the tornado forces on a cubic structure. The NSEs are filtered by using the LES turbulence model in space and the FD is applied. Selvam and Millet (2003) presented the Large Eddy Simulation (LES) turbulence model in tensor notations for the incompressible fluid flow in three dimensions. The continuity and momentum equations are as follows:

Continuity Equation:

$$U_{i,i} = 0 \tag{A-1}$$

Momentum Equation:

$$U_{i,t} + \left(U_j - V_j\right)U_{i,j} + \left(\frac{p}{\rho} + \frac{2k}{3}\right)_i = \left[(\upsilon + \upsilon_t)\left(U_{i,j} + U_{j,i}\right)\right]_j \tag{A-2}$$

Control volume spacing (h_1 h_2 h_3):

$$h = (h_1 h_2 h_3)^{1/3} \tag{A-3}$$

h_1 h_2 h_3 are the control spacing in the x, y and z-directions, respectively.

C_s and C_k are empirical constants values:

$$C_s = 0.1 \qquad C_k = 0.094 \tag{A-4}$$

Turbulence eddy viscosity (ν_t):

$$\upsilon_t = (C_s h)^2 \left(\frac{S_{i,j}^2}{2}\right)^{0.5} \tag{A-5}$$

Turbulence kinetic energy (k):

$$k = \left(\frac{\upsilon_t}{C_k h}\right)^2 \tag{A-6}$$

Where U_i is the mean velocity and p is the pressure. The velocity at the grid is V_i and ρ is the fluid density. The time is represented by the subscript t. i= 1, 2 and 3 denote to the variables in the x, y and z-directions. For more discussion see Selvam (1998) and Selvam and Millett (2003)

APPENDIX B: LARGE STRUCTURE PLAN AREAS

B-1 Grids (Meshes) on LSPA (2h x 2h, 4h x 4h and 8h x 8h)

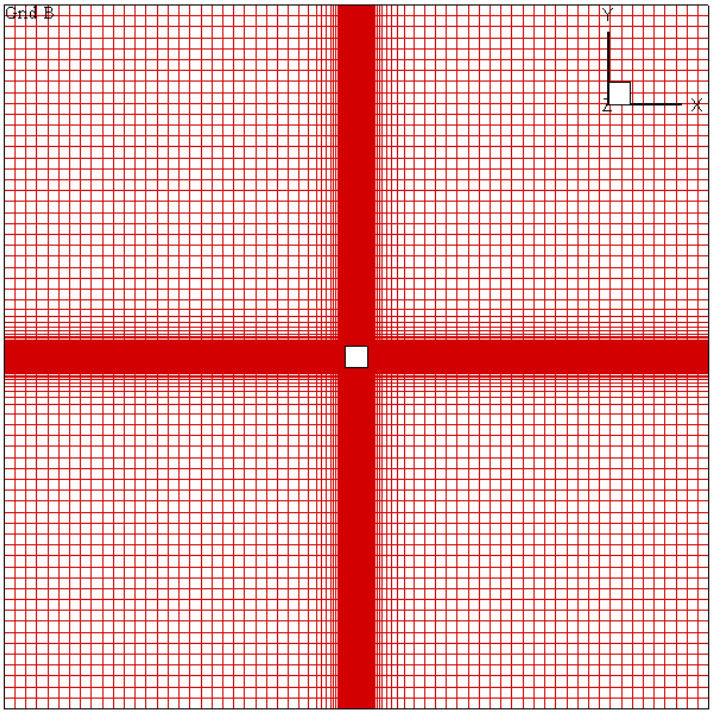

Figure B-1.1 Structure plan area (2h x 2h) mesh in the x-y plane

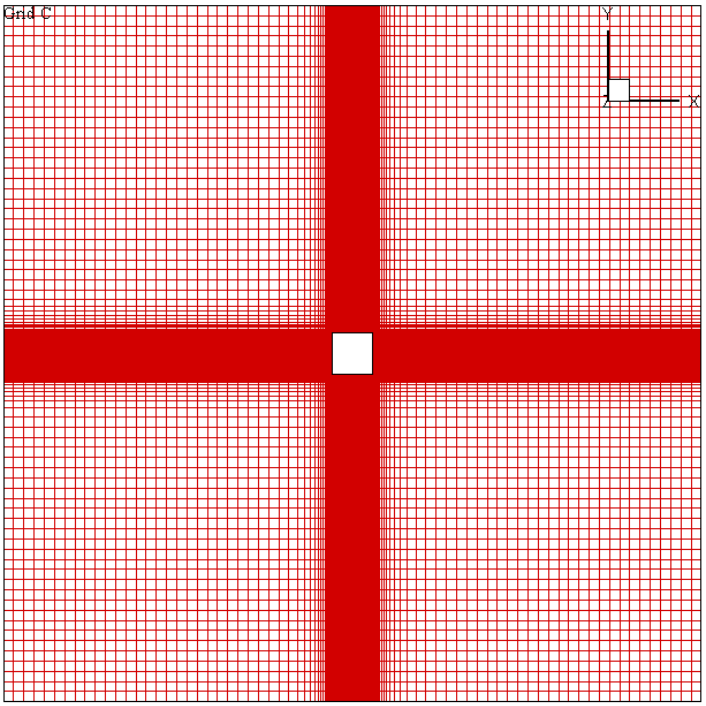

Figure B-1.2 Structure plan area (4h x 4h) mesh in the x-y plane

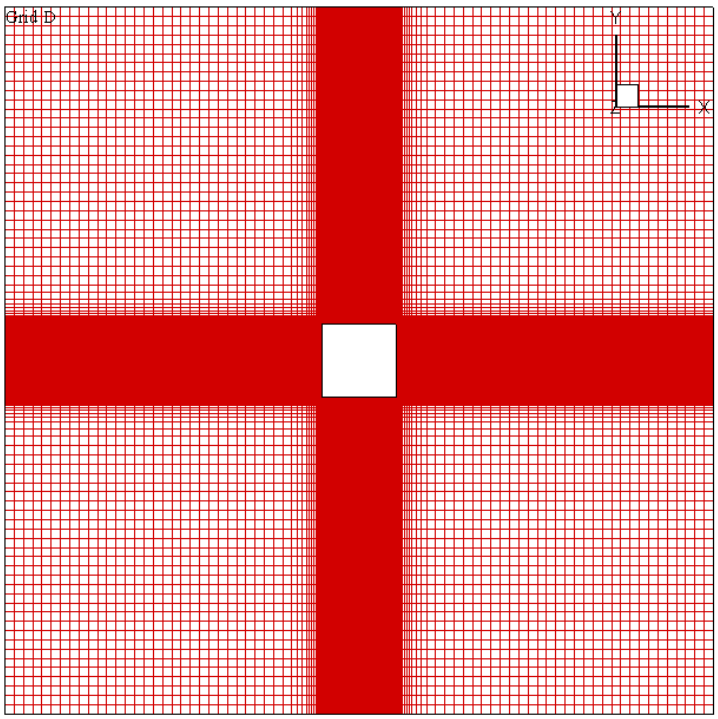

Figure B-1.3 Structure plan area (8h x 8h) mesh in the x-y plane

B -2 Tornado force coefficients time history

1. Tornado force coefficients and SL flow force coefficients for $\beta = 0^0$

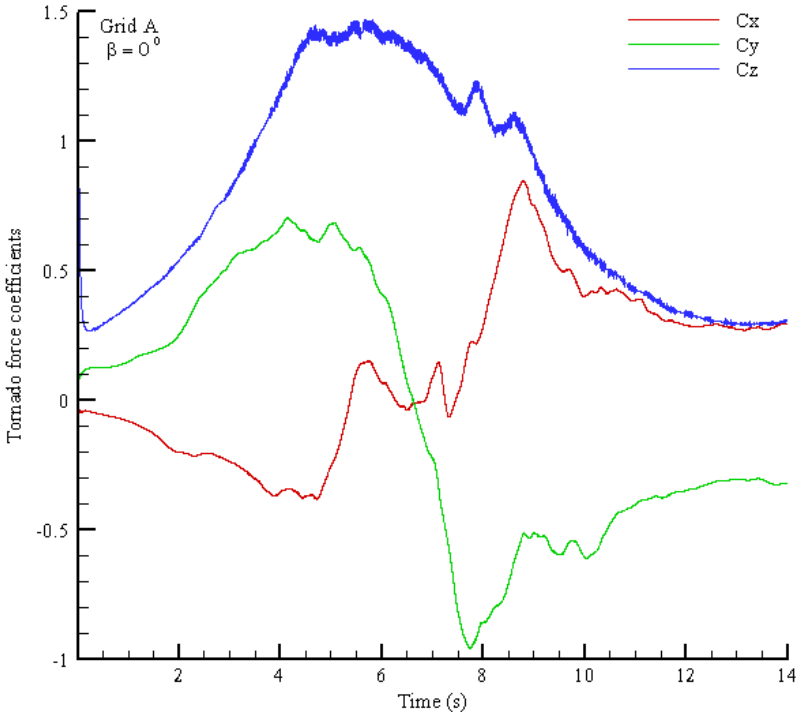

Figure B-2.1 Tornado force coefficients on structure plan area (2h x 2h)

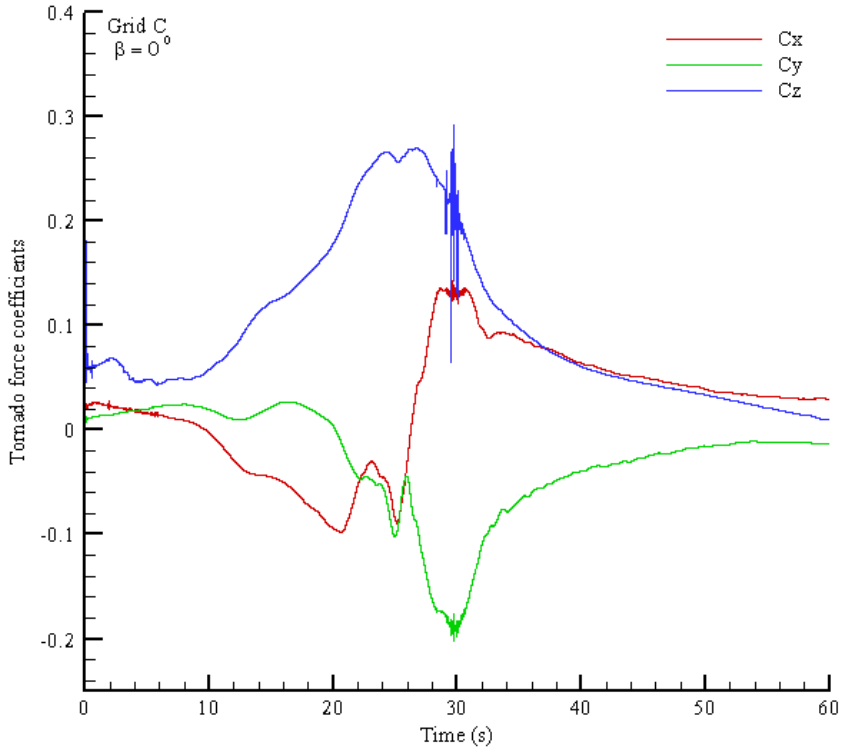

Figure B-2.2 Tornado force coefficients on structure plan area (4h x 4h)

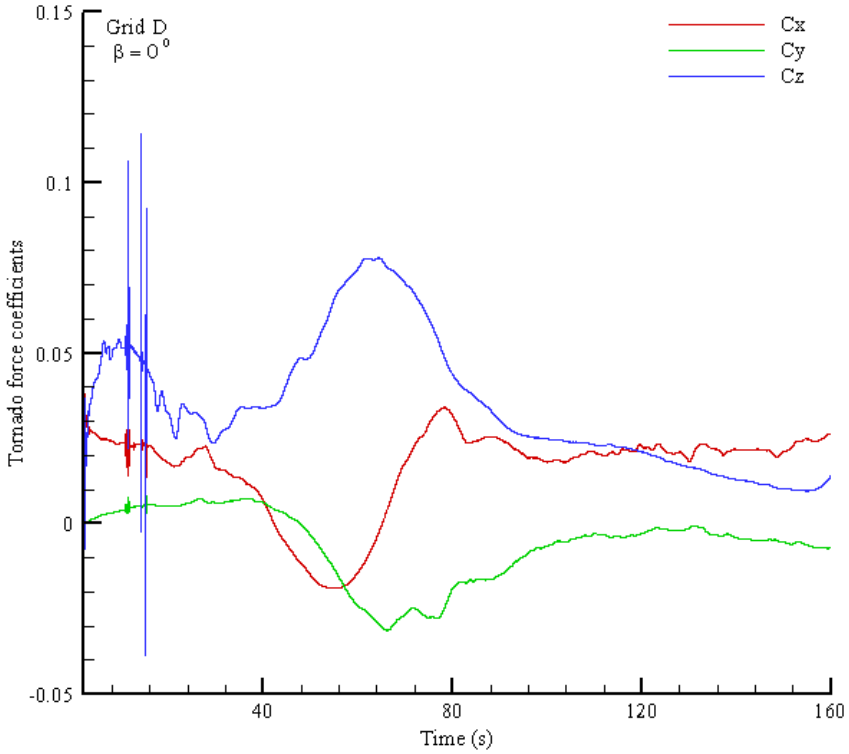

Figure B-2.3 Tornado force coefficients on structure plan area (4h x 4h)

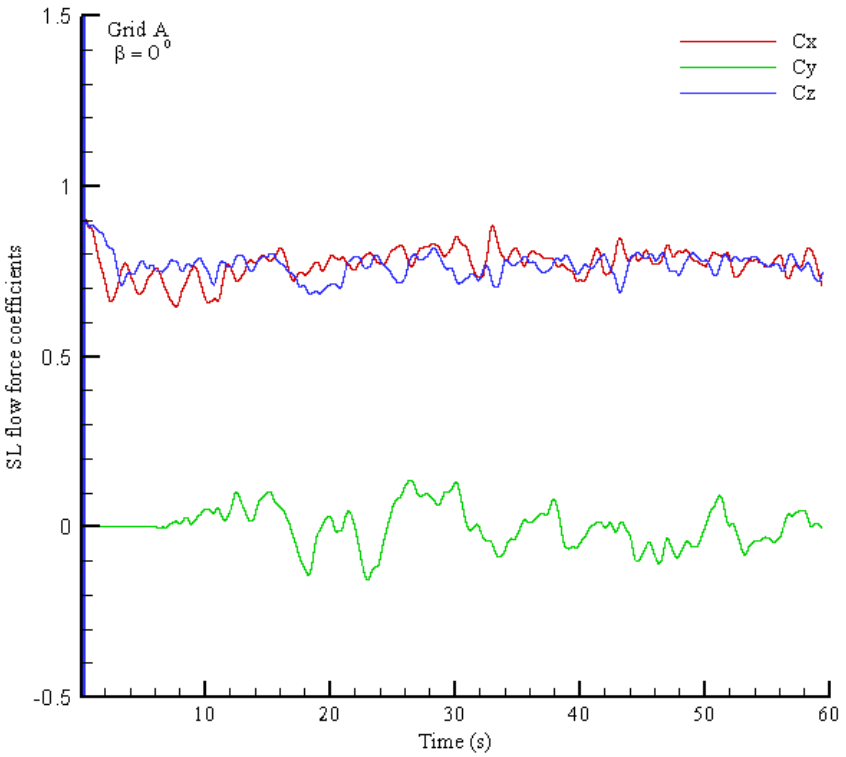

Figure B-2.4 SL flow force coefficients on structure plan area (1h x 1h)

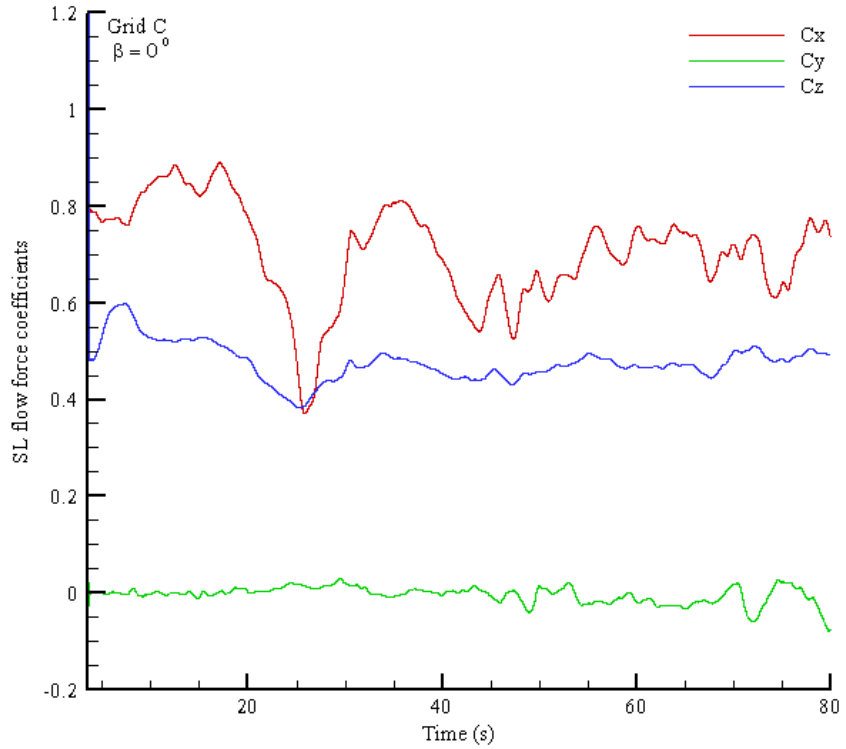

Figure B-2.5 SL flow force coefficients on structure plan area (4h x 4h)

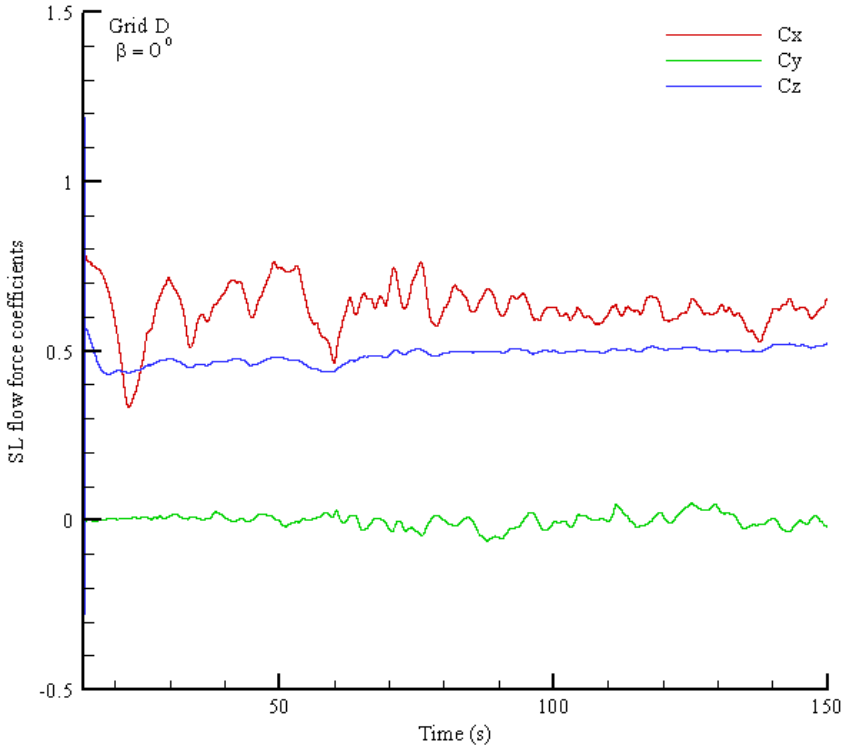

Figure B-2.6 SL flow force coefficients on structure plan area (8h x 8h)

2. Tornado force coefficients and SL flow force coefficients for $\beta = 45^0$

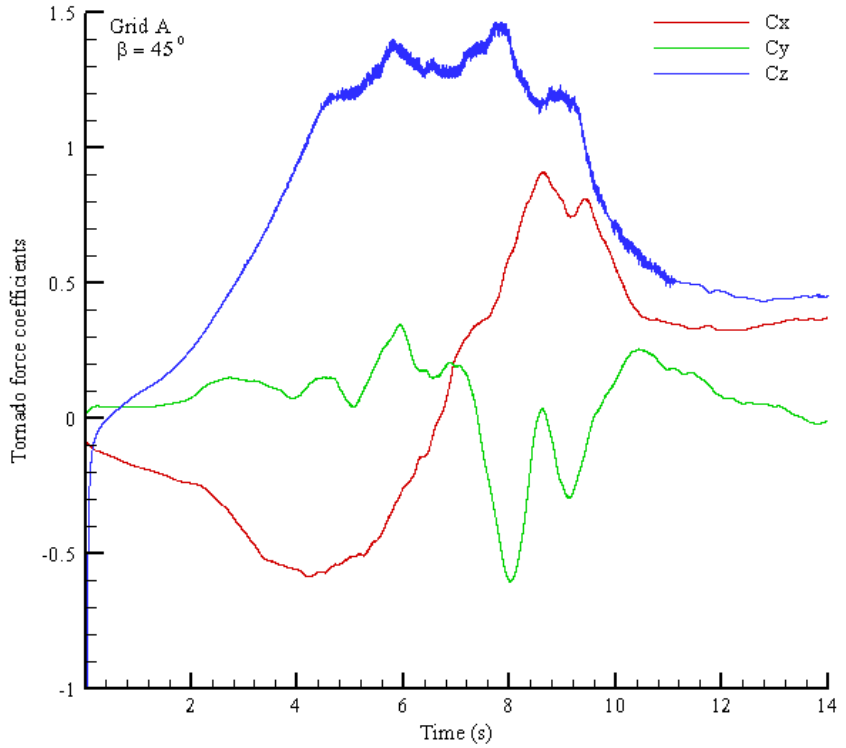

Figure B-2.7 Tornado force coefficients on structure plan area (1h x 1h)

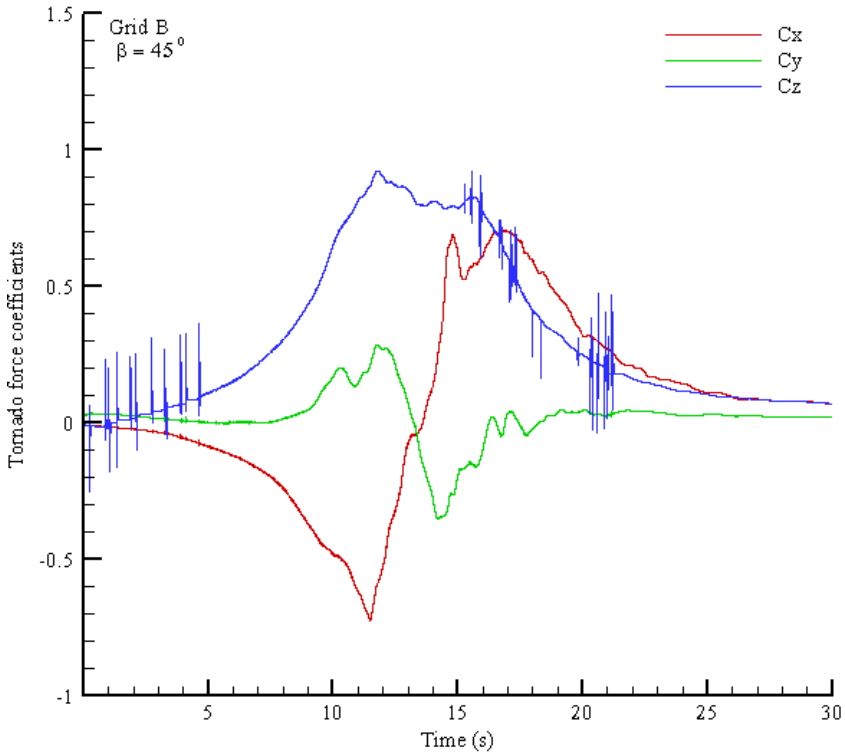

Figure B-2.8 Tornado force coefficients on structure plan area (2h x 2h)

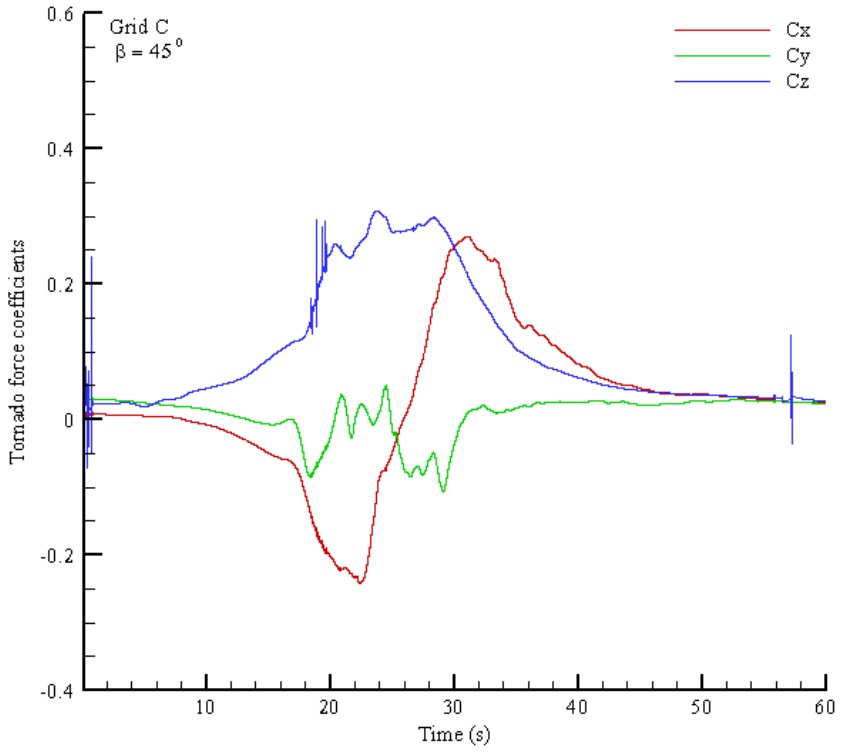

Figure B-2.9 Tornado force coefficients on structure plan area (4h x 4h)

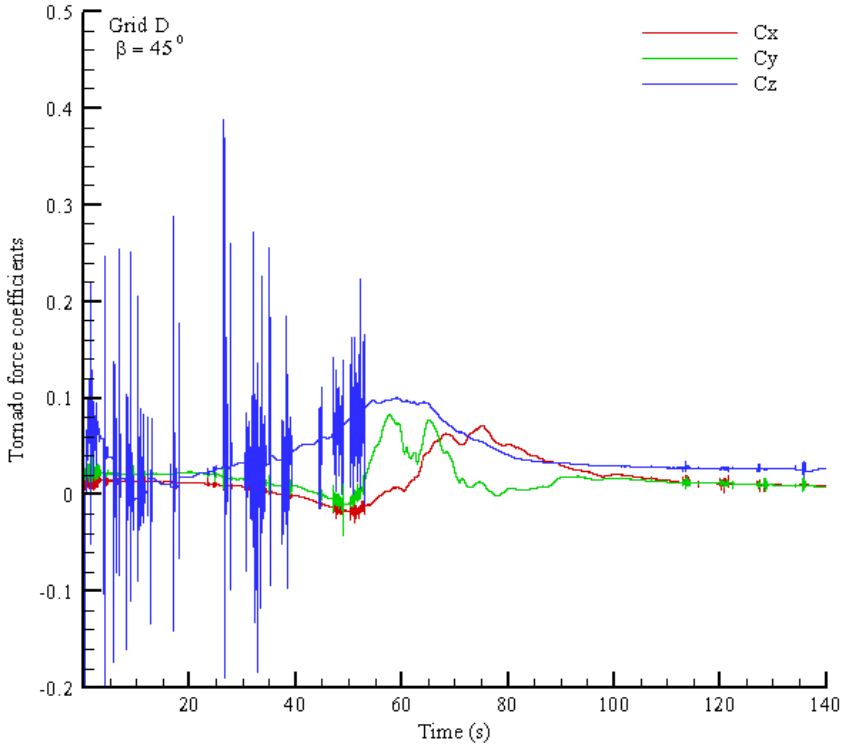

Figure B-2.10 Tornado force coefficients on structure plan area (8h x 8h)

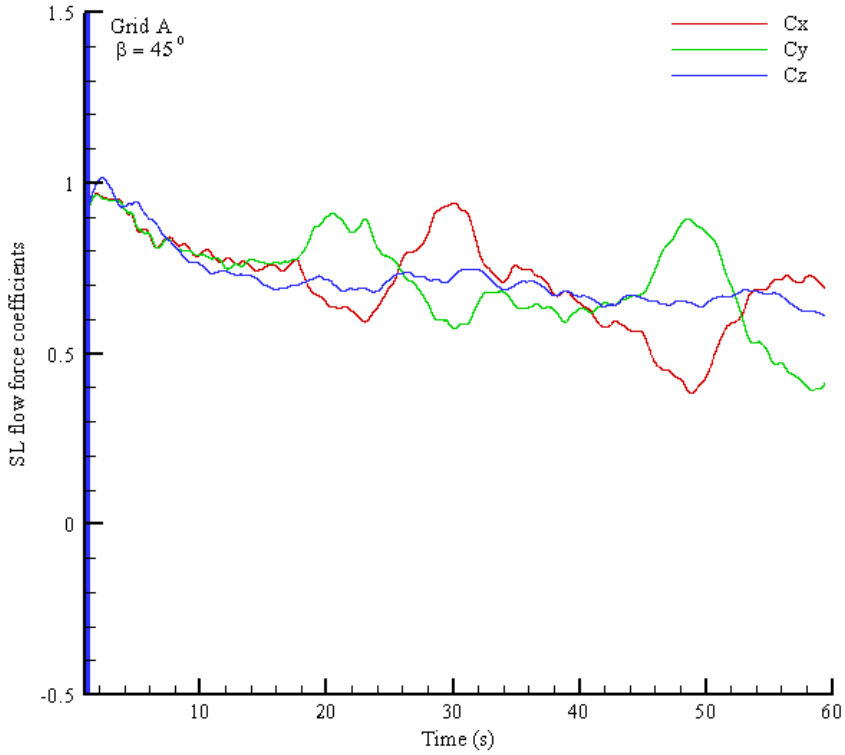

Figure B-2.11 SL flow force coefficients on structure plan area (1h x 1h)

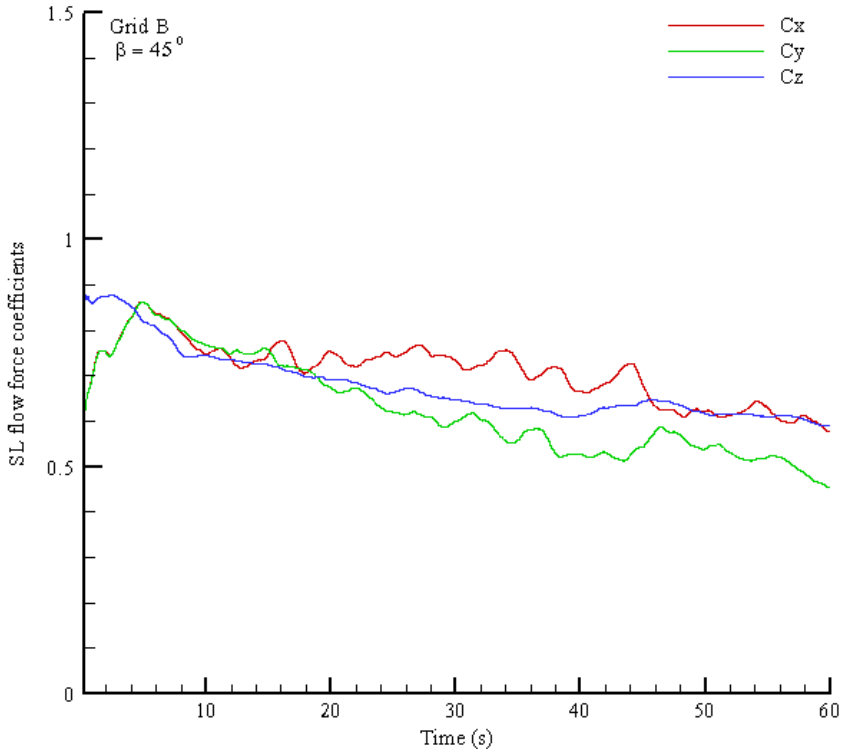

Figure B-2.12 SL flow force coefficients on structure plan area (2h x 2h)

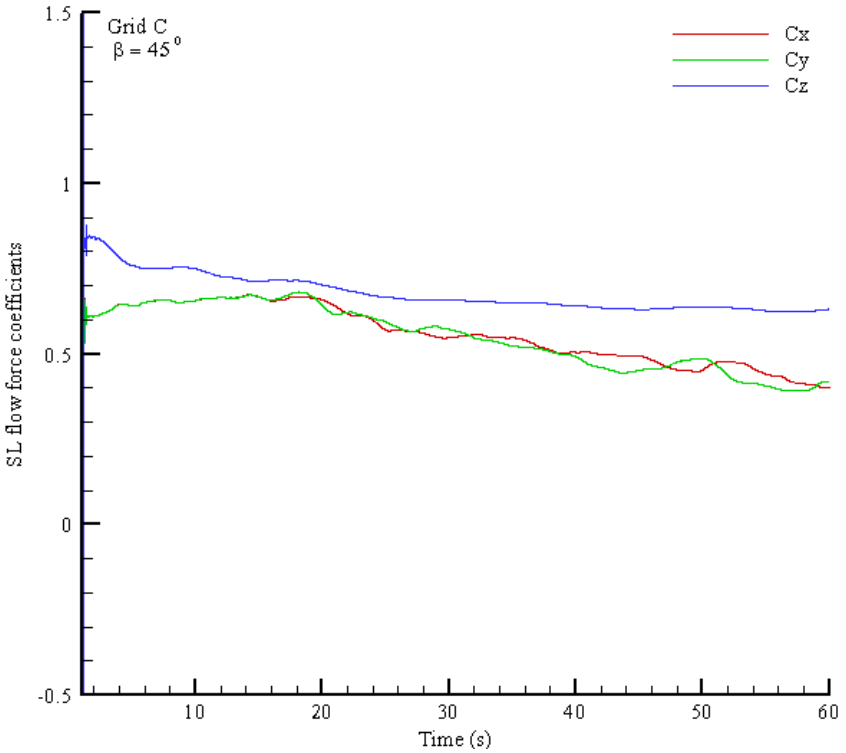

Figure B-2.13 SL flow force coefficients on structure plan area (4h x 4h)

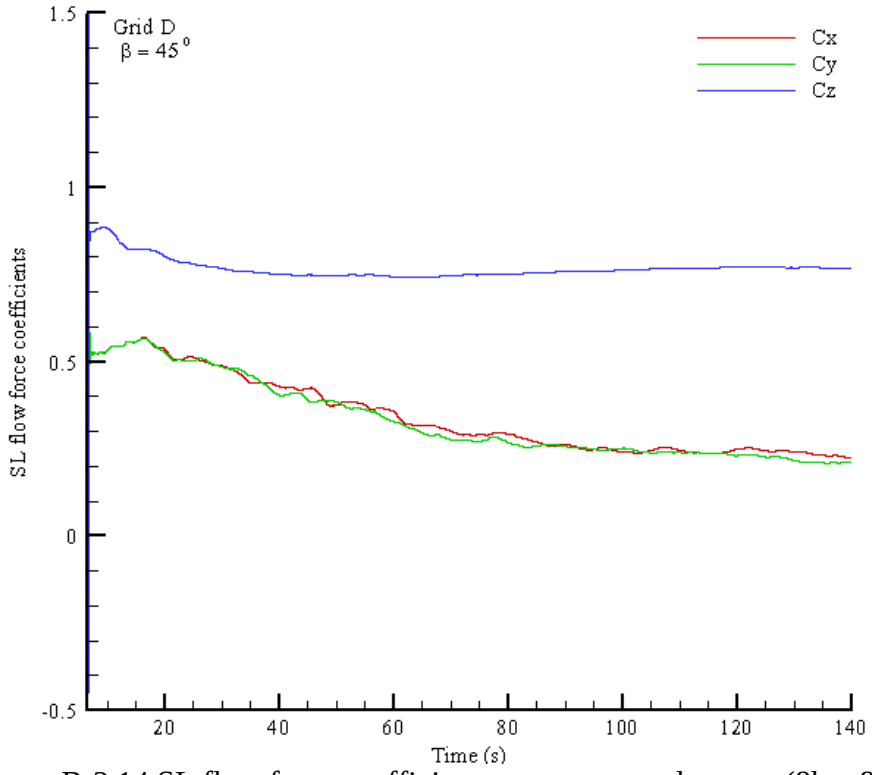

Figure B-2.14 SL flow force coefficients on structure plan area (8h x 8h)

B-3 Three dimensional view of the pressure contour plot on the large structures plan areas

1- Pressure Contour plot for $\beta = 0^0$

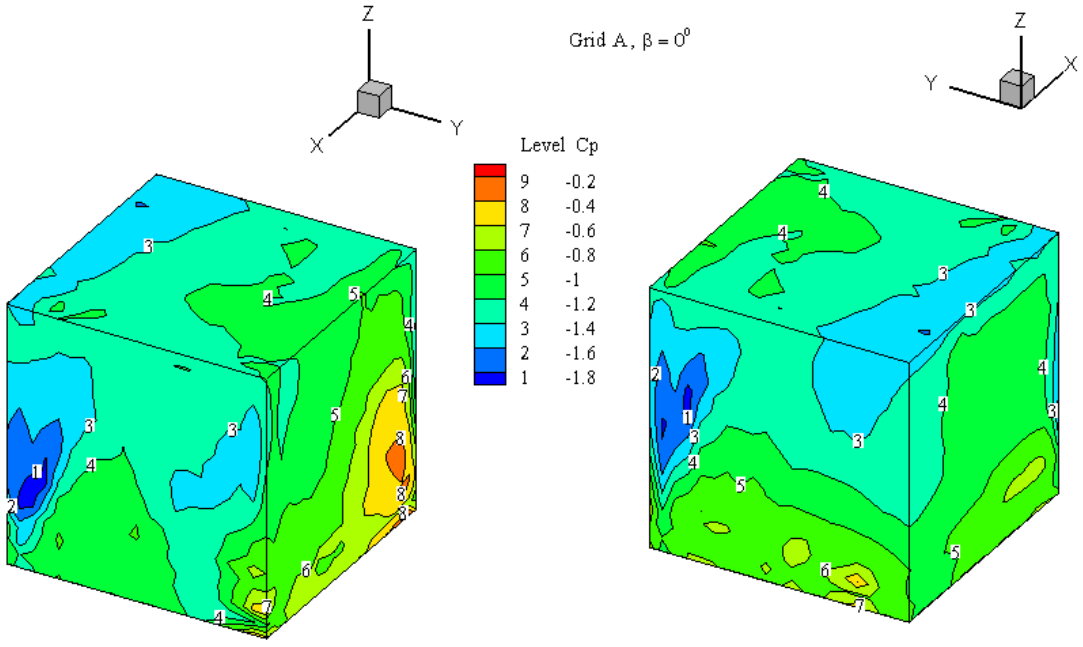

Figure B-3.1 Tornado pressure contour plot on structure plan area (1h x 1h)

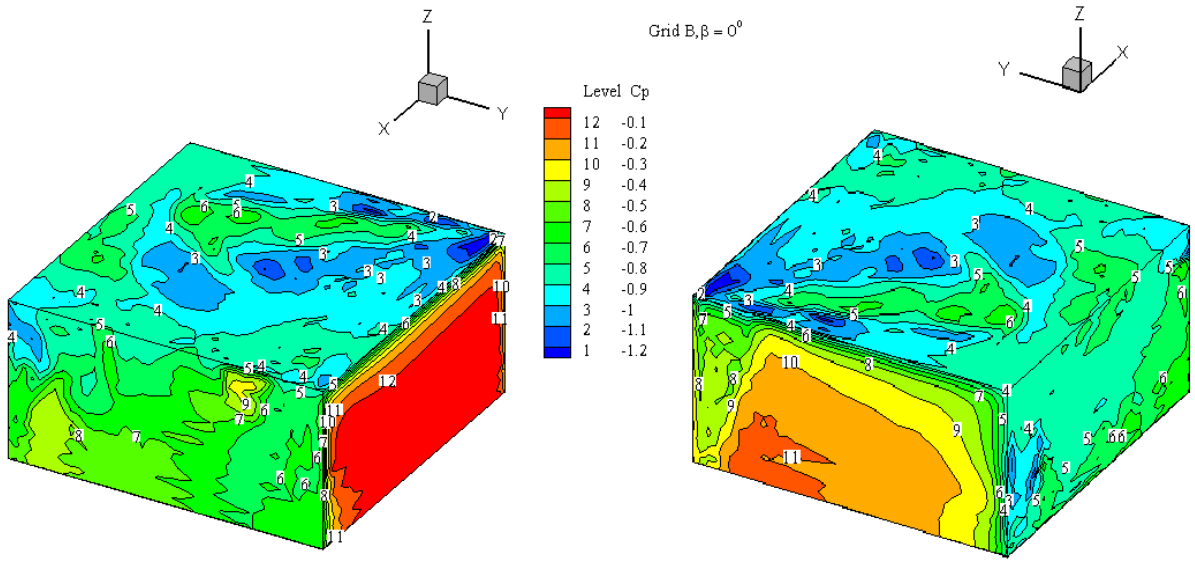

Figure B-3.2 Tornado pressure contour plot on structure plan area (2h x 2h)

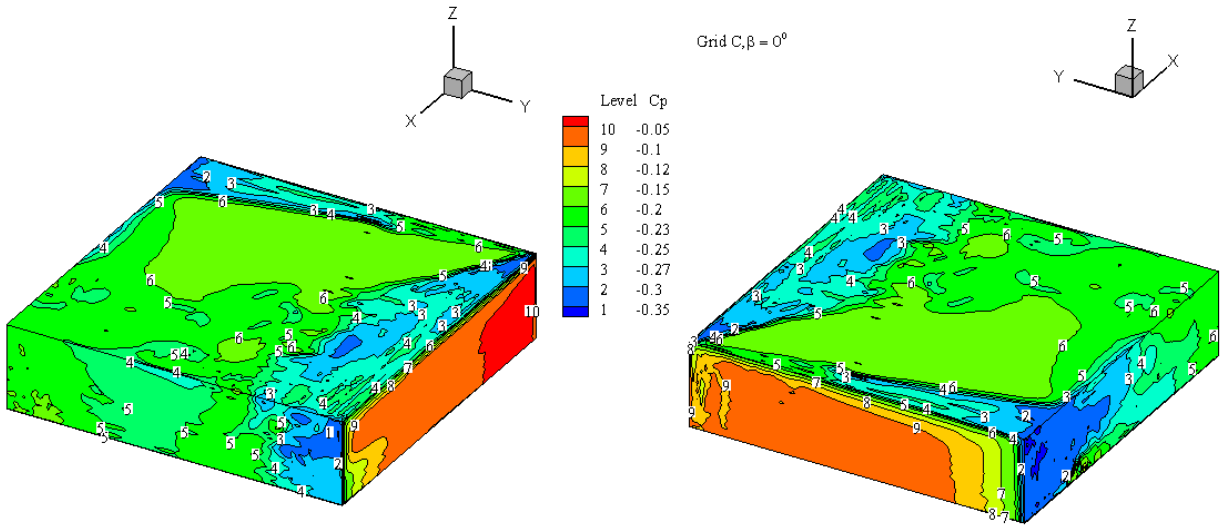

Figure B-3.3 Tornado pressure contour plot on structure plan area (4h x 4h)

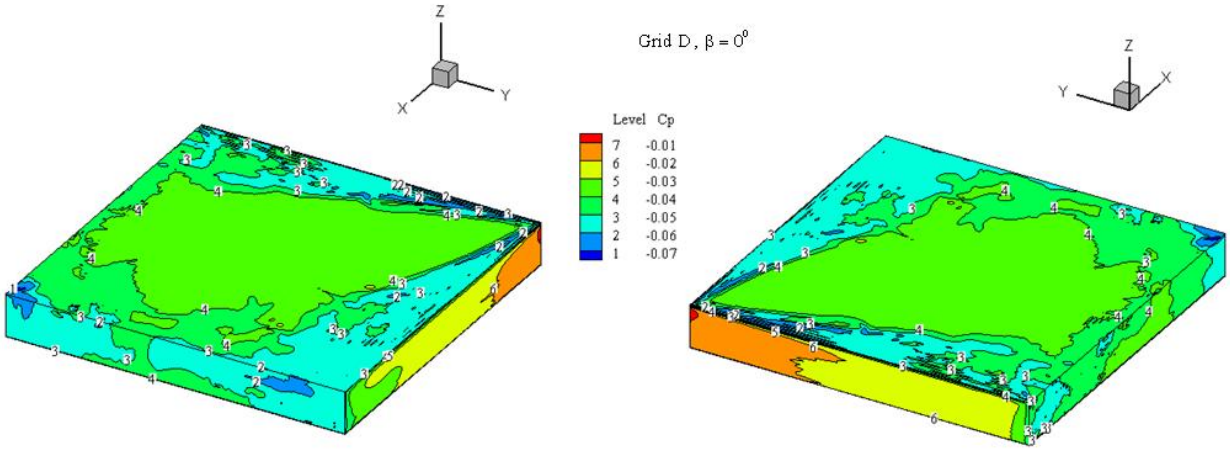

Figure B-3.4 Tornado pressure contour plot on structure plan area (8h x 8h)

2- Pressure Contour plot for $\beta = 45^0$

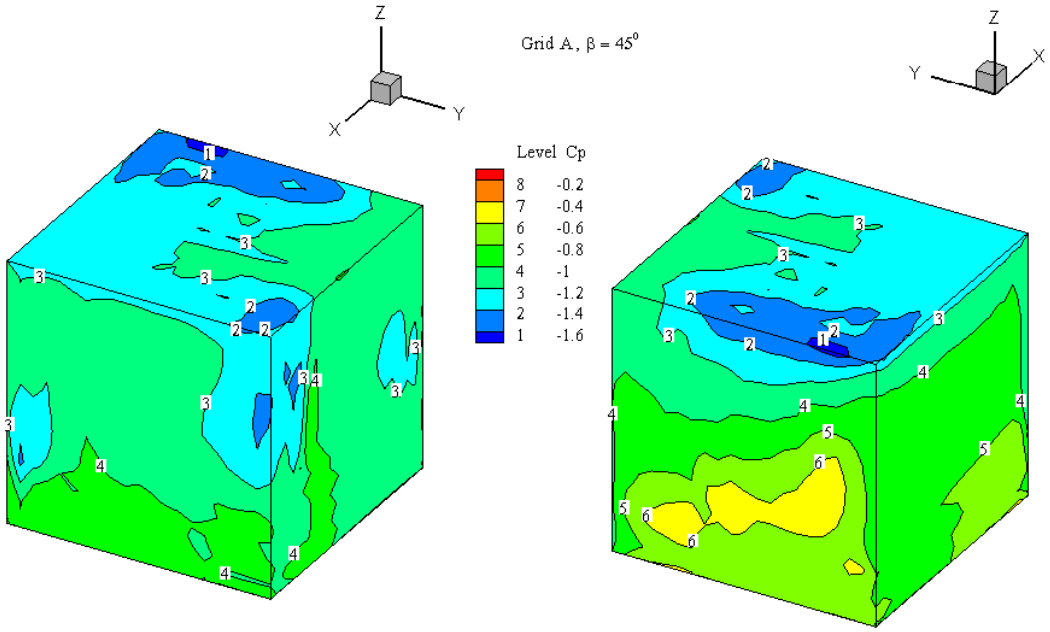

Figure B-3.5 Tornado pressure contour plot on structure plan area (1h x 1h)

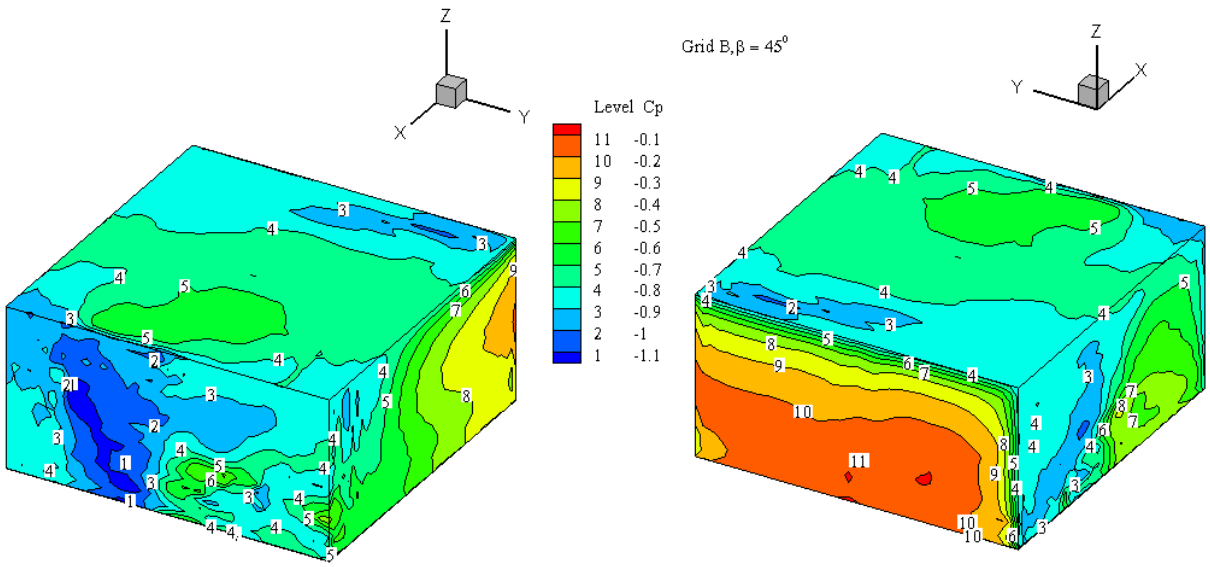

Figure B-3.6 Tornado pressure contour plot on structure plan area (2h x 2h)

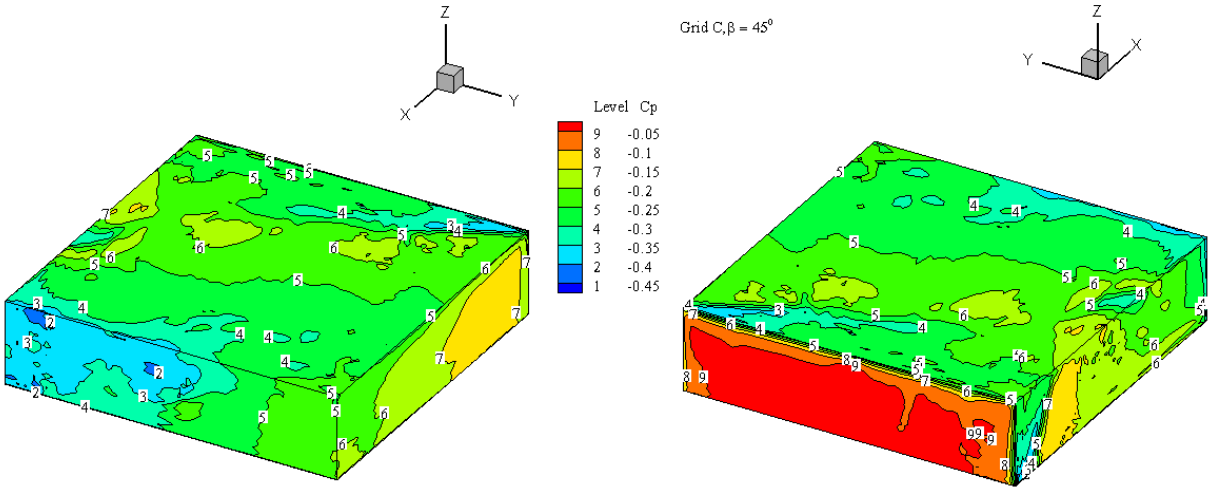

Figure B-3.7 Tornado pressure contour plot on structure plan area (4h x 4h)

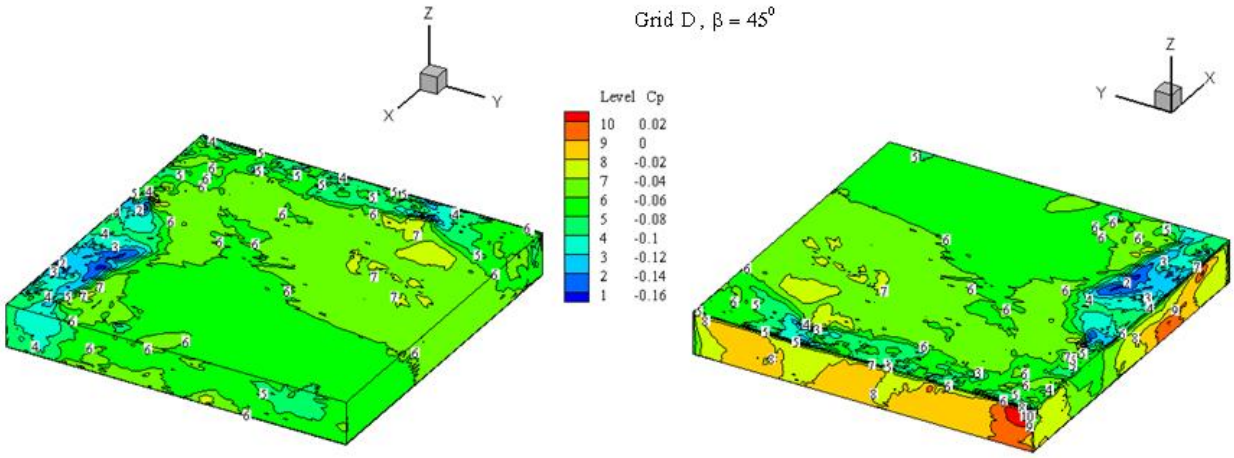

Figure B-3.8 Tornado pressure contour plot on structure plan area (8h x 8h)

B-4 Three dimensional view of the pressure coefficient contour plot for same maximum reference translating velocity

1- Tornado and SL flow approaching the structure with $\beta = 0^0$ and same reference velocity

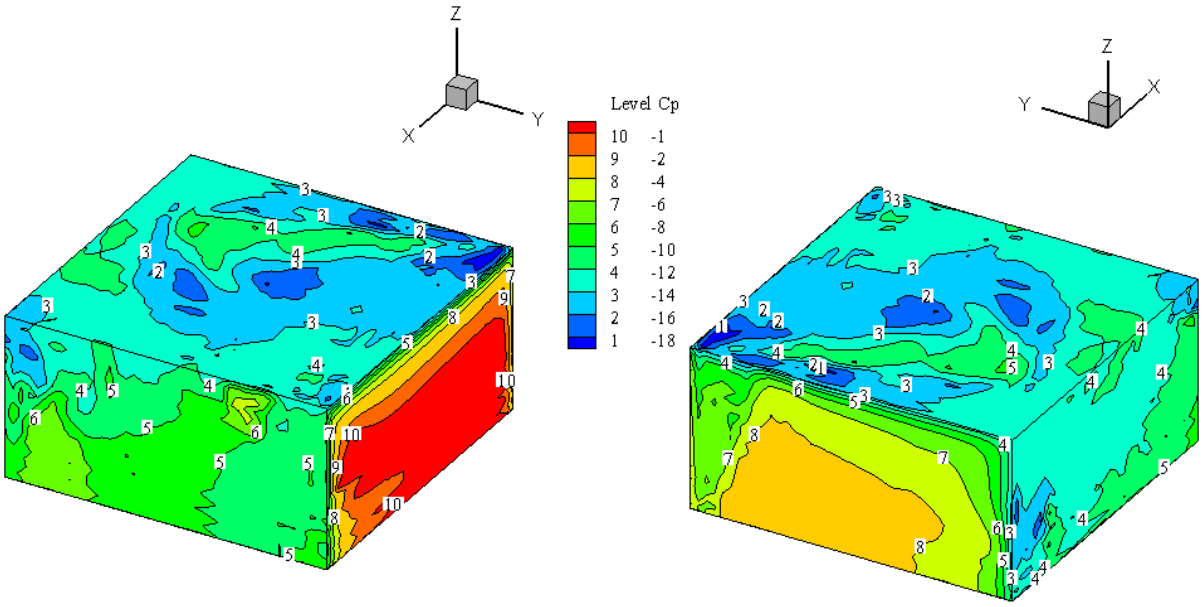

Figure B-4.1 Tornado pressure contour plot on structure plan area (2h x 2h) for same $V_{trans.}$

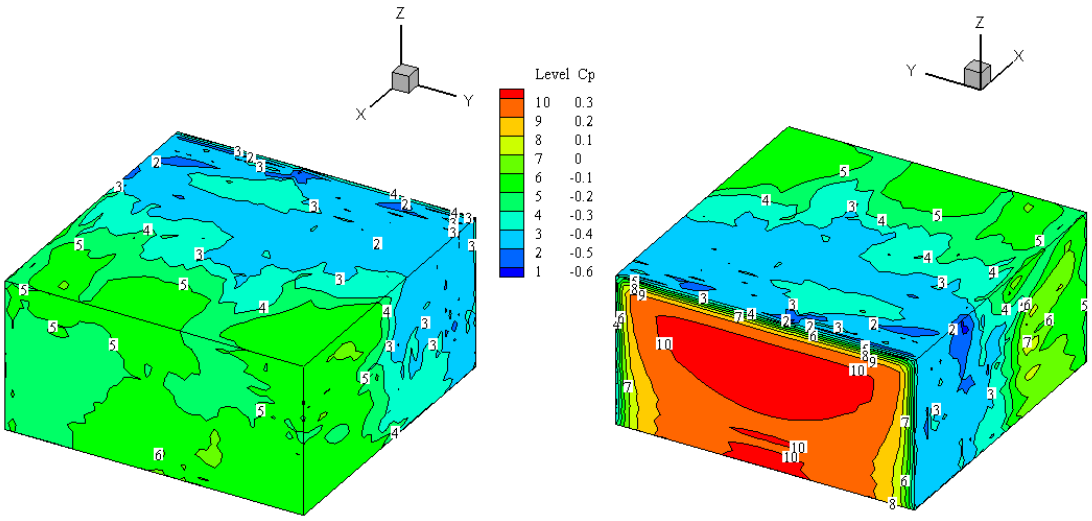

Figure B-4.2 SL flow pressure contour plot on structure plan area (2h x 2h) for same $V_{trans.}$

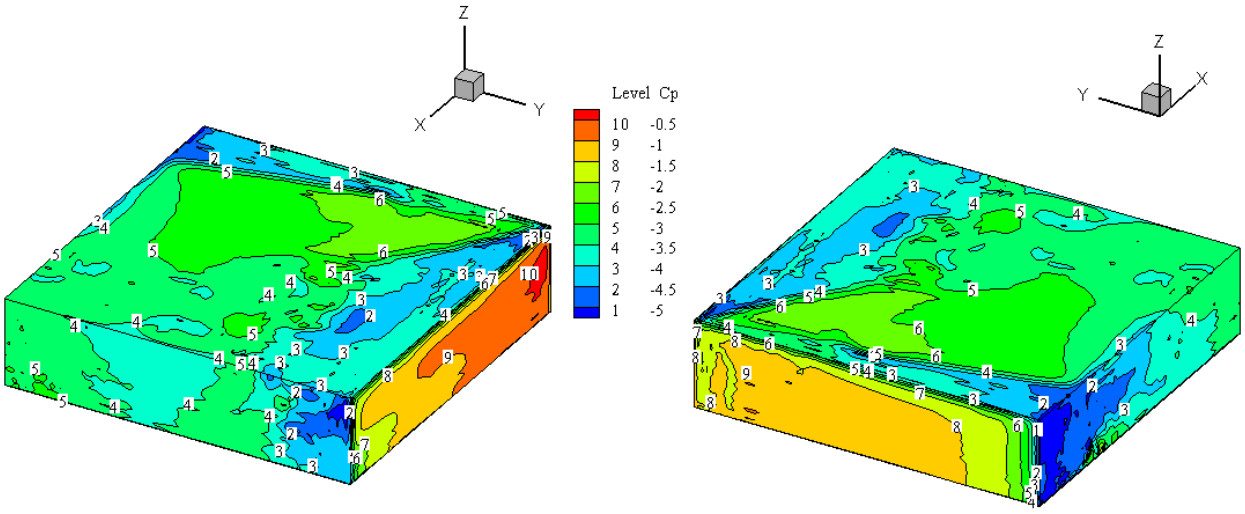

Figure B-4.3 Tornado pressure contour plot on structure plan area (4h x 4h) for same $V_{trans.}$

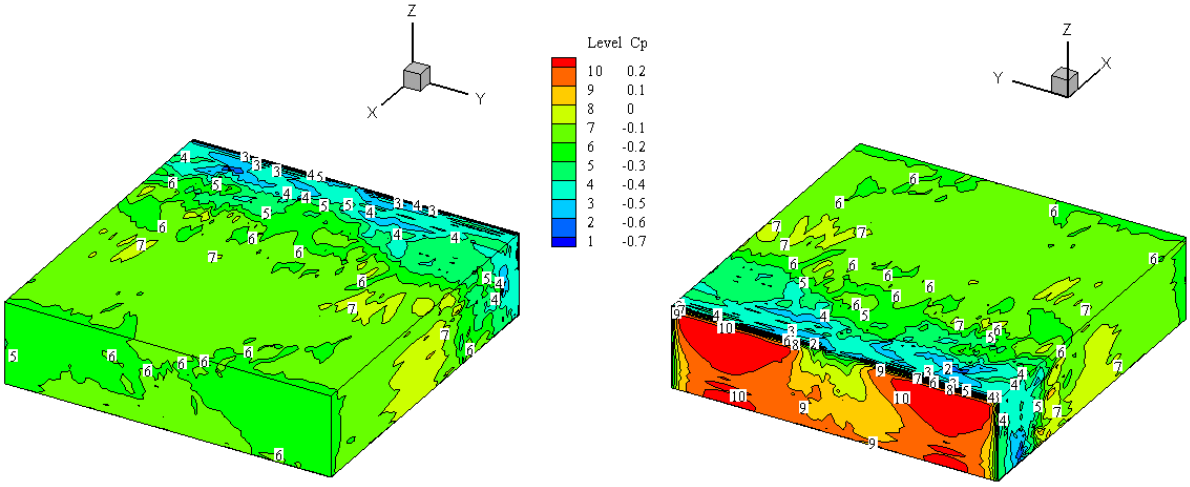

Figure B-4.4 SL flow pressure contour plot on structure plan area (4h x 4h) for same $V_{trans.}$

2- Tornado and SL flow approaching the structure with $\beta = 45^0$

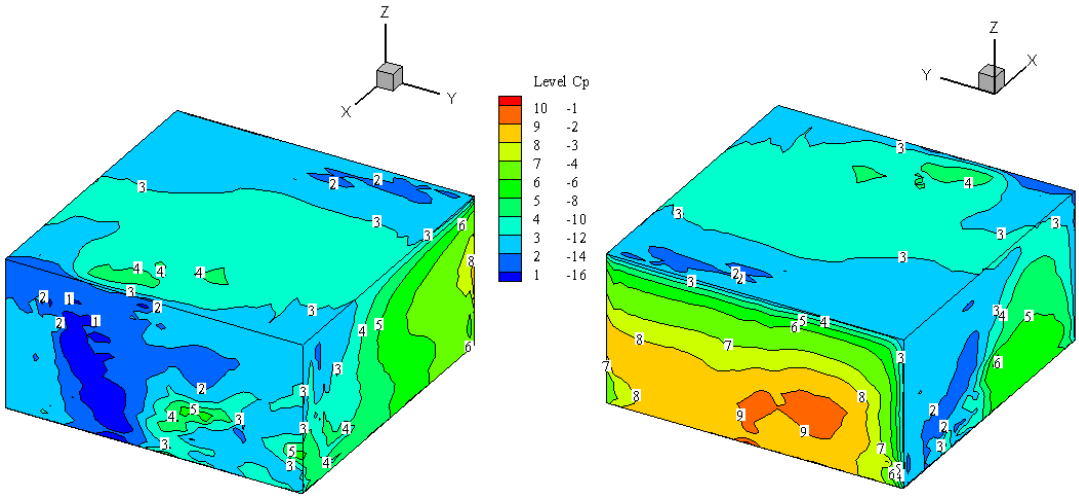

Figure B-4.5 Tornado pressure contour plot on structure plan area (2h x 2h) for same $V_{trans.}$

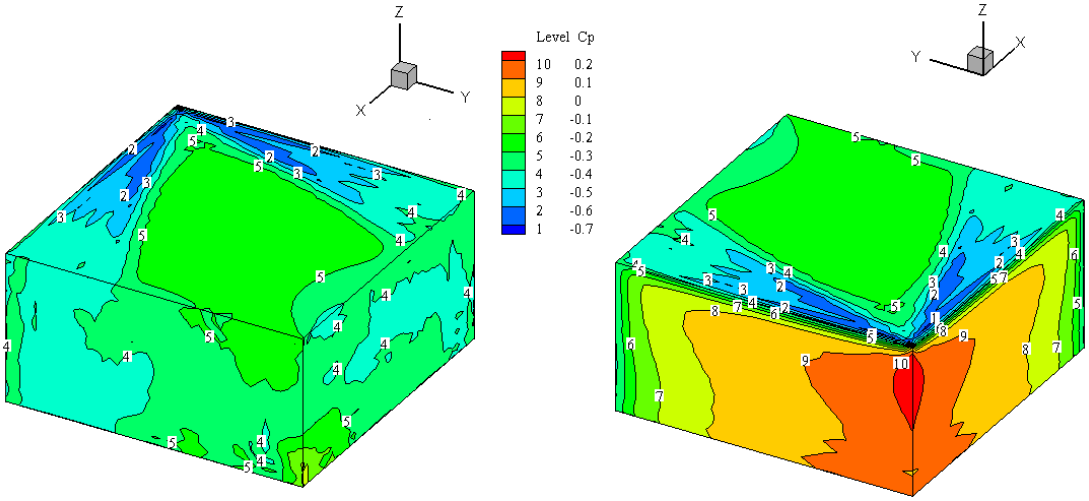

Figure B-4.6 SL flow pressure contour plot on structure plan area (2h x 2h) for same $V_{trans.}$

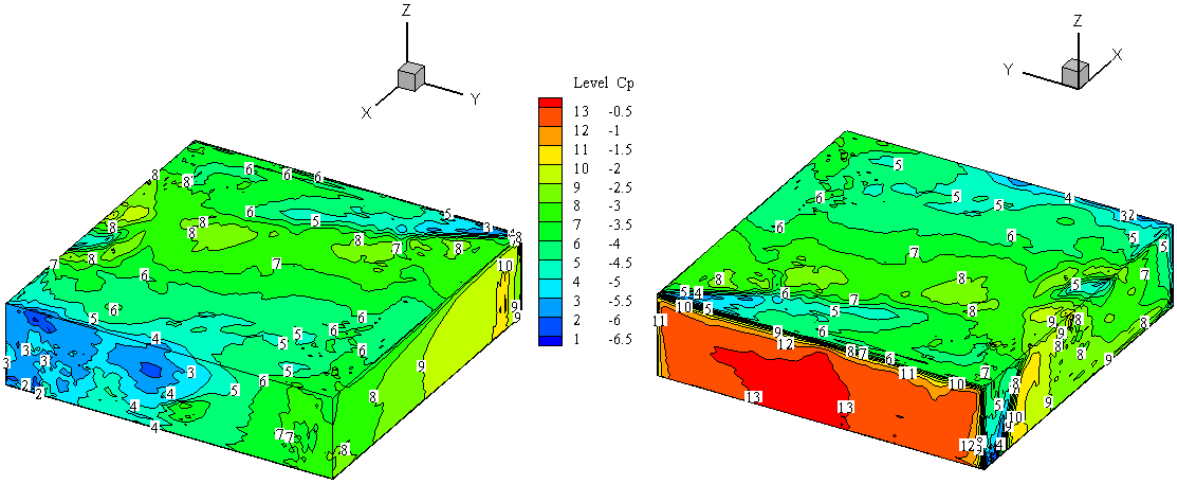

Figure B-4.7 Tornado pressure contour plot on structure plan area (4h x 4h) for same $V_{trans.}$

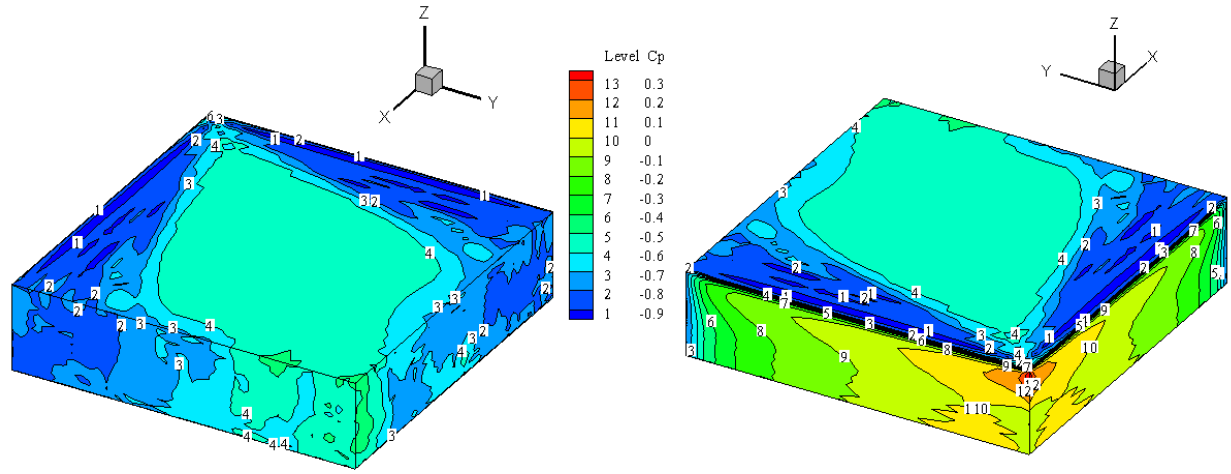

Figure B-4.8 SL flow pressure contour plot on structure plan area (4h x 4h) for same $V_{trans.}$

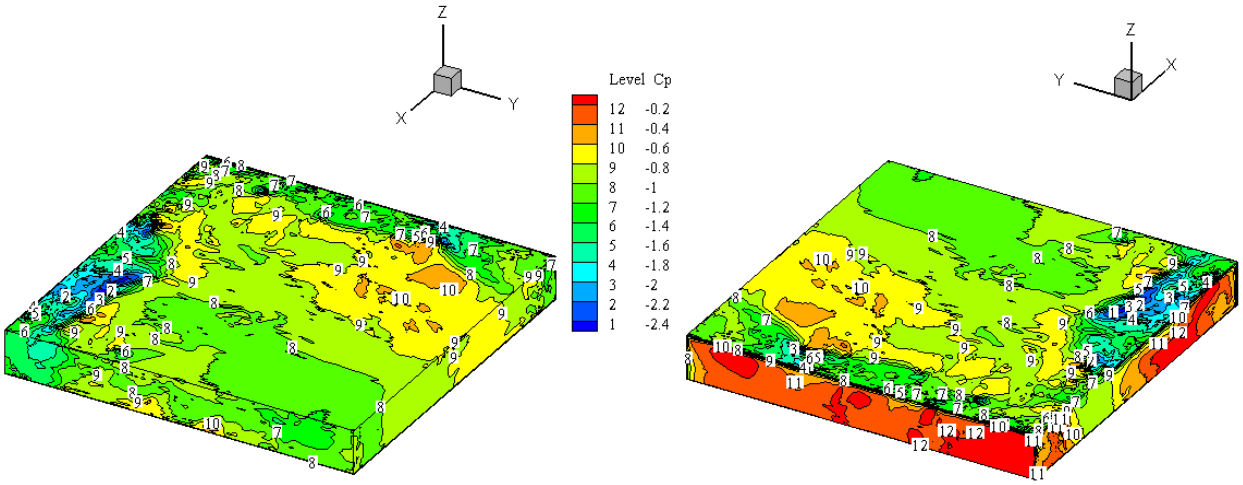

Figure B-4.9 Tornado pressure contour plot on structure plan area (8h x 8h) for same $V_{trans.}$

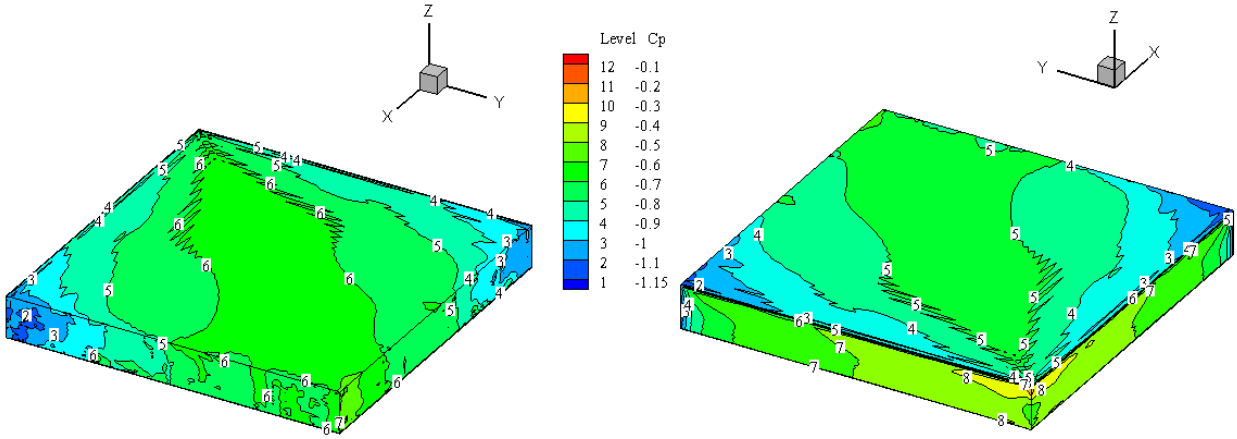

Figure B-4.10 SL flow pressure contour plot on structure plan area (8h x 8h) for same $V_{trans.}$

APPENDIX C: THIN STRUCTURE PLAN AREAS

C-1 Grids (Meshes) on TSPA (0.2h x 0.2h, 0.4h x 0.4h and 0.8h x 0.8h)

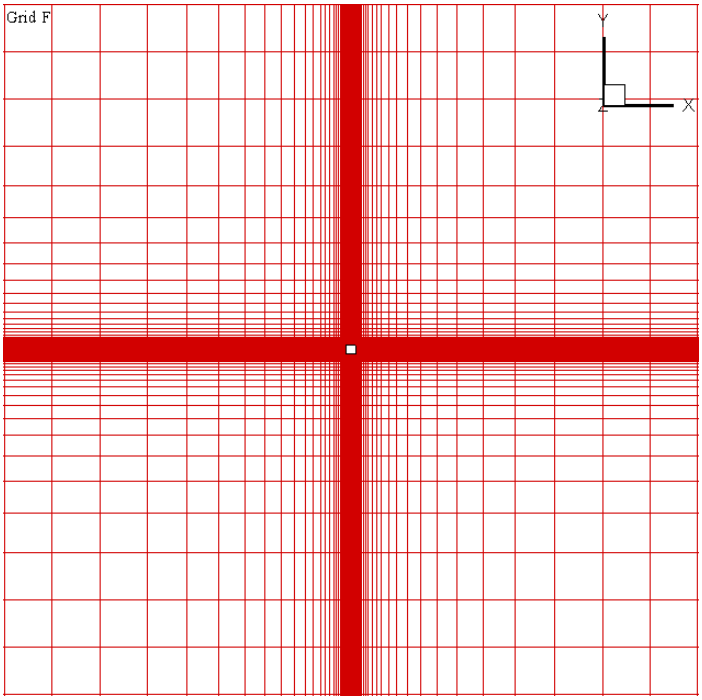

Figure C-1.1 Grid F x-y plane mesh

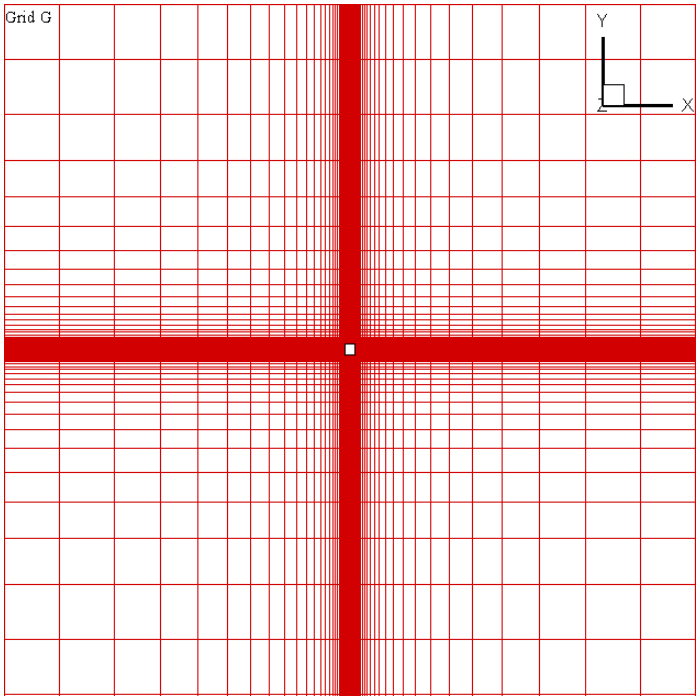

Figure C-1.2 Grid G x-y plane mesh

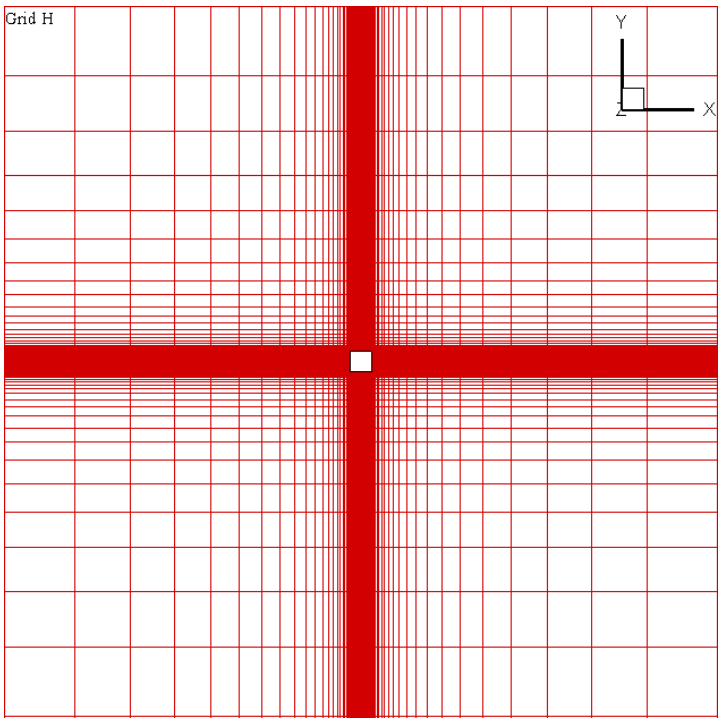

Figure C-1.3 Grid H x-y plane mesh

C-2 Tornado and SL flow force coefficients time history

1. Tornado force coefficients and SL flow force coefficients for $\beta = 0^0$

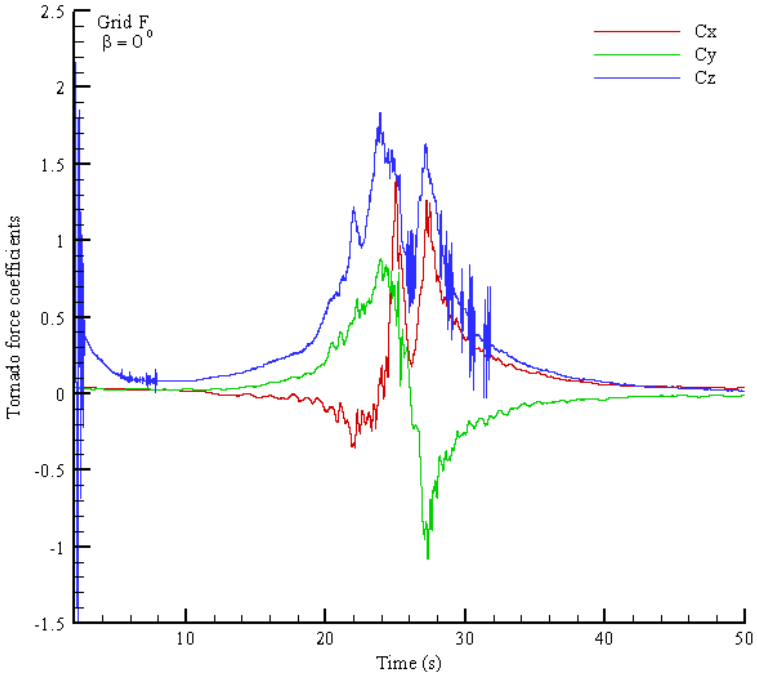

Figure C-2.1 Structure plan area (0.2h x 0.2h), Tornado force coefficients,$\beta = 0^0$

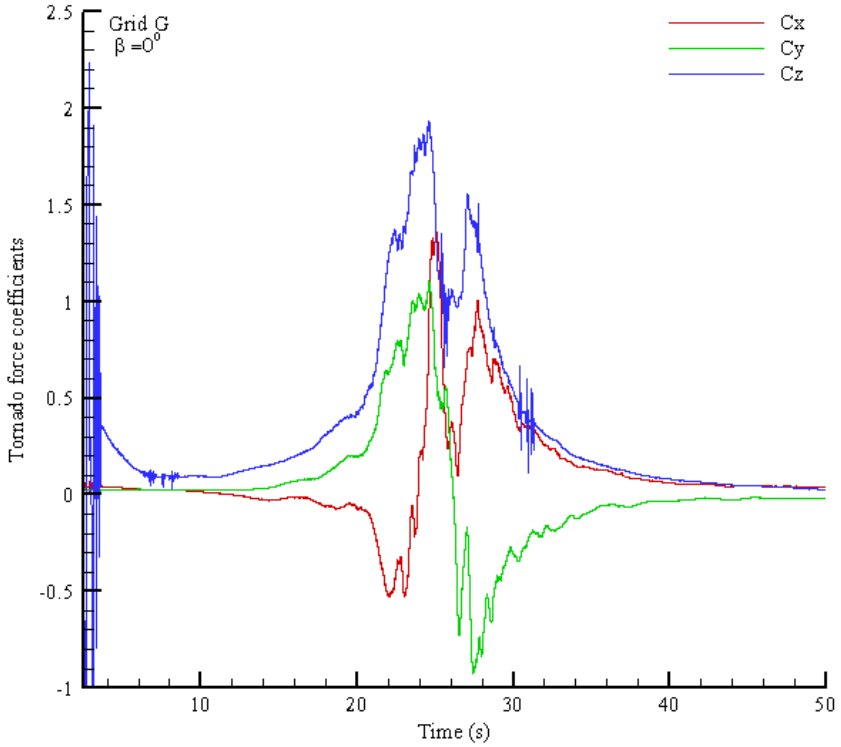

Figure C-2.2 Structure plan area (0.4h x 0.4h), Tornado force coefficients,$\beta = 0^0$

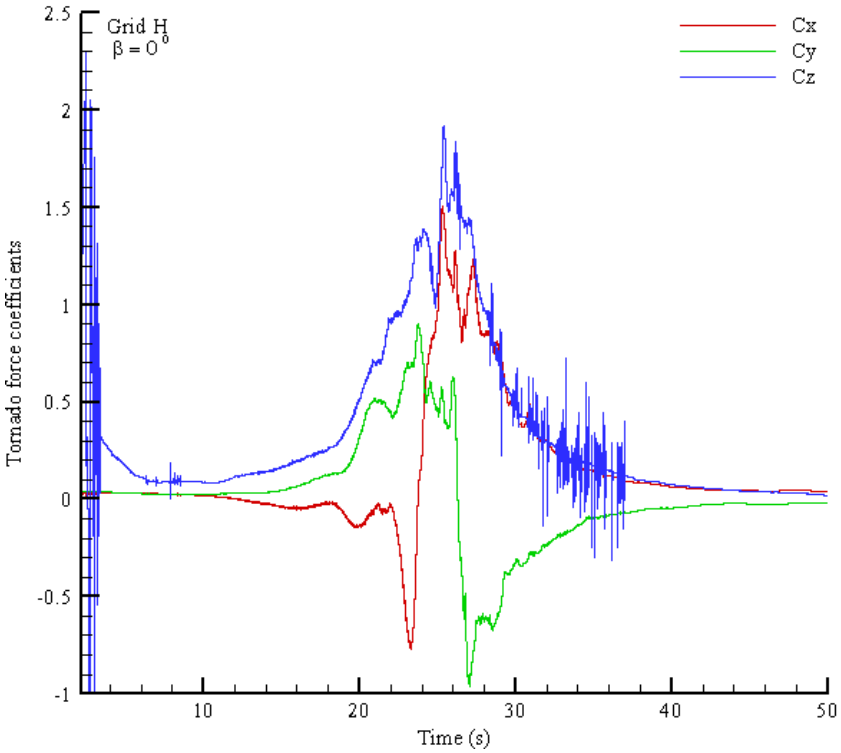

Figure C-2.3 Structure plan area (0.8h x 0.8h), Tornado force coefficients,$\beta = 0^0$

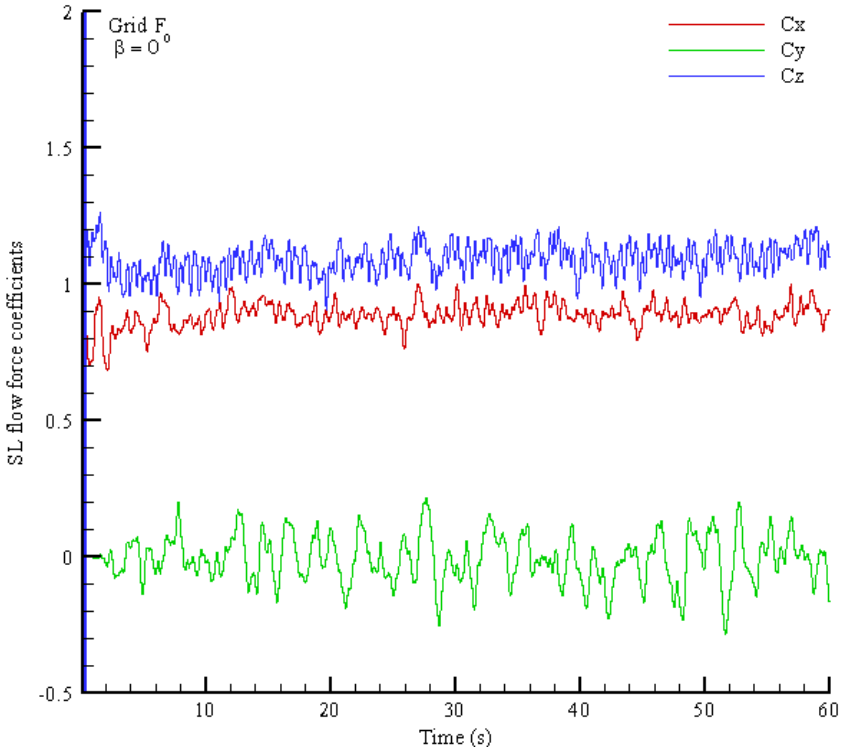

Figure C-2.4 Structure plan area (0.2h x 0.2h), SL flow force coefficients,$\beta = 0^0$

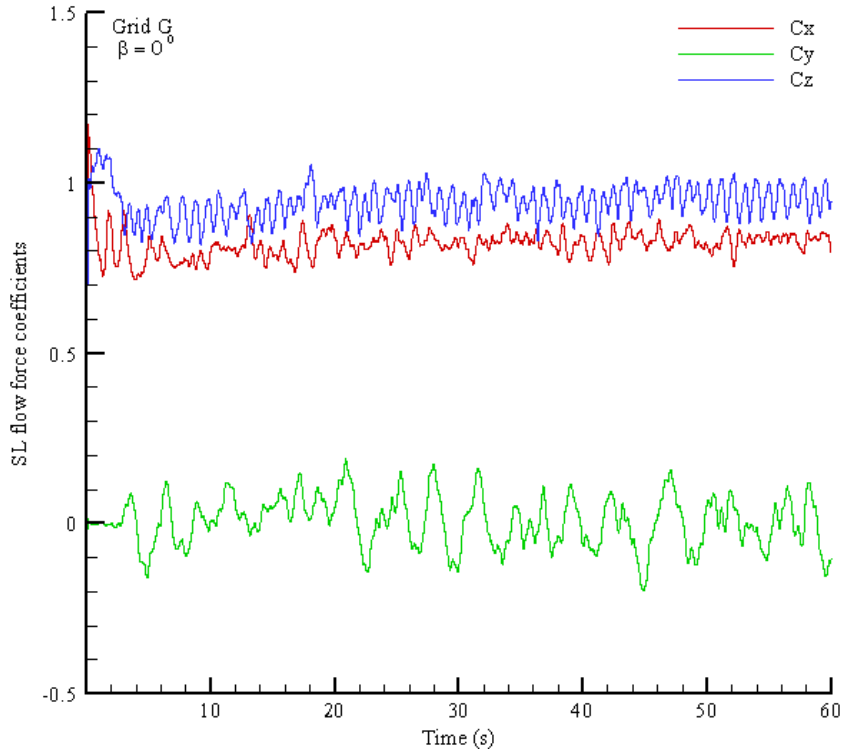

Figure C-2.5 Structure plan area (0.4h x 0.4h), SL flow force coefficients,$\beta = 0^0$

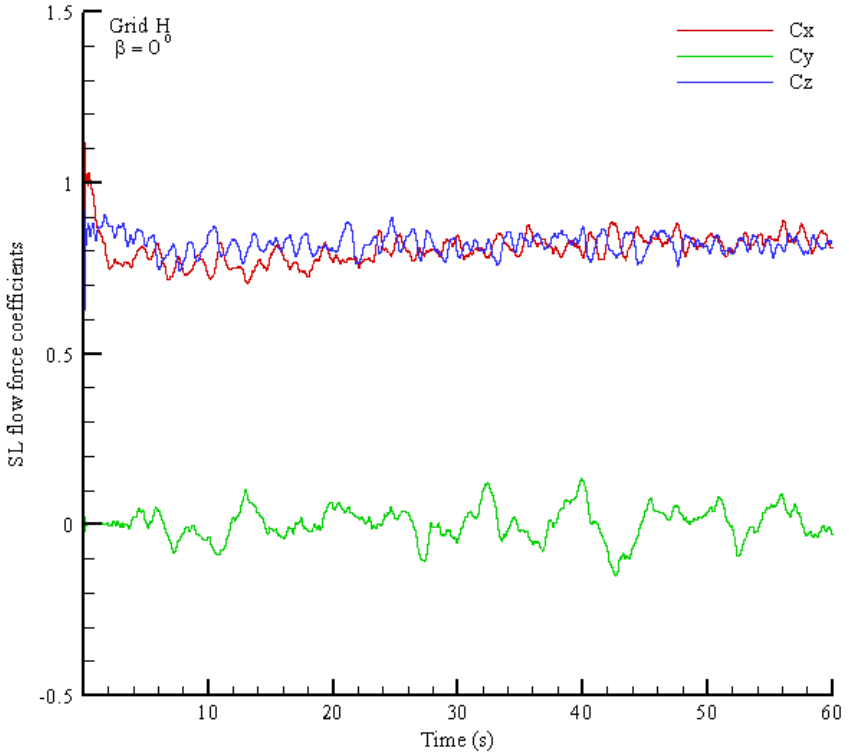

Figure C-2.6 Structure plan area (0.8h x 0.8h), SL flow force coefficients,$\beta = 0^0$

2. Tornado force coefficients and SL flow force coefficients for $\beta = 45^0$

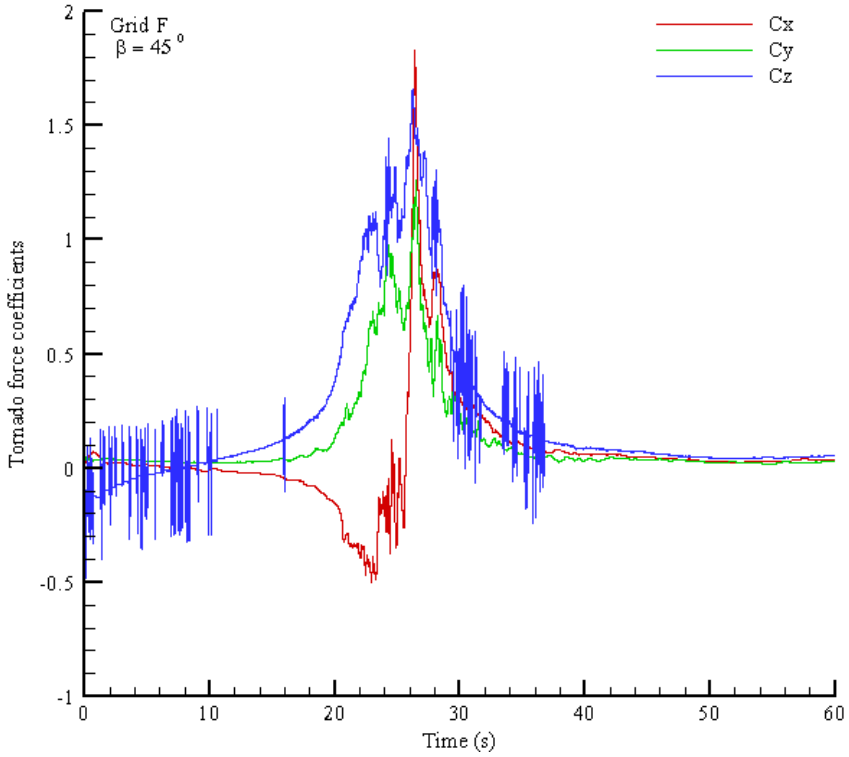

Figure C-2.7 Structure plan area (0.2h x 0.2h), Tornado force coefficients,$\beta = 45^0$

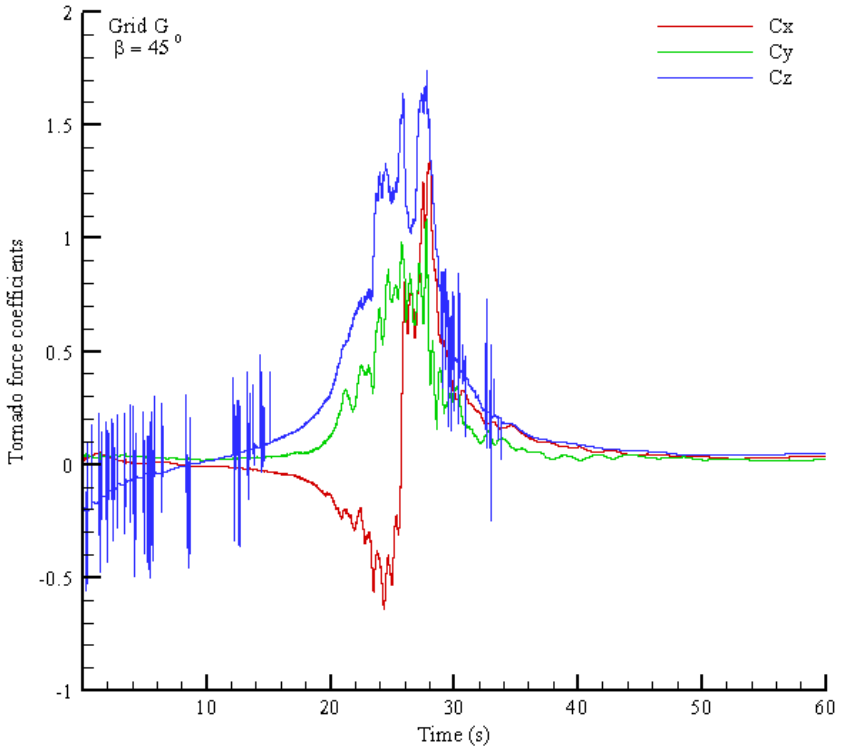

Figure C-2.8 Structure plan area (0.4h x 0.4h), Tornado force coefficients,$\beta = 45^0$

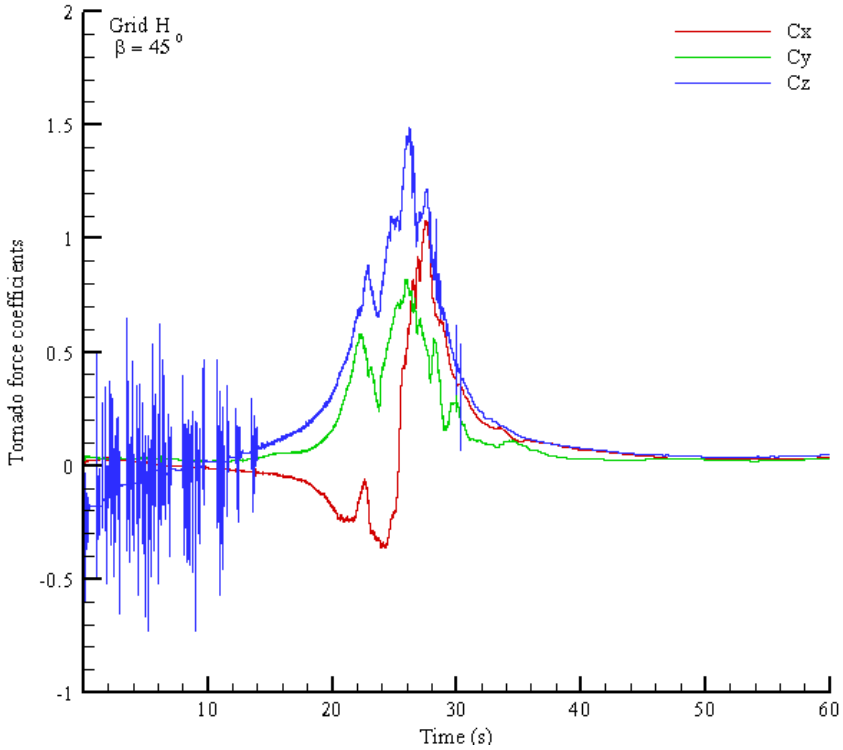

Figure C-2.9 Structure plan area (0.8h x 0.8h), Tornado force coefficients,$\beta = 45^0$

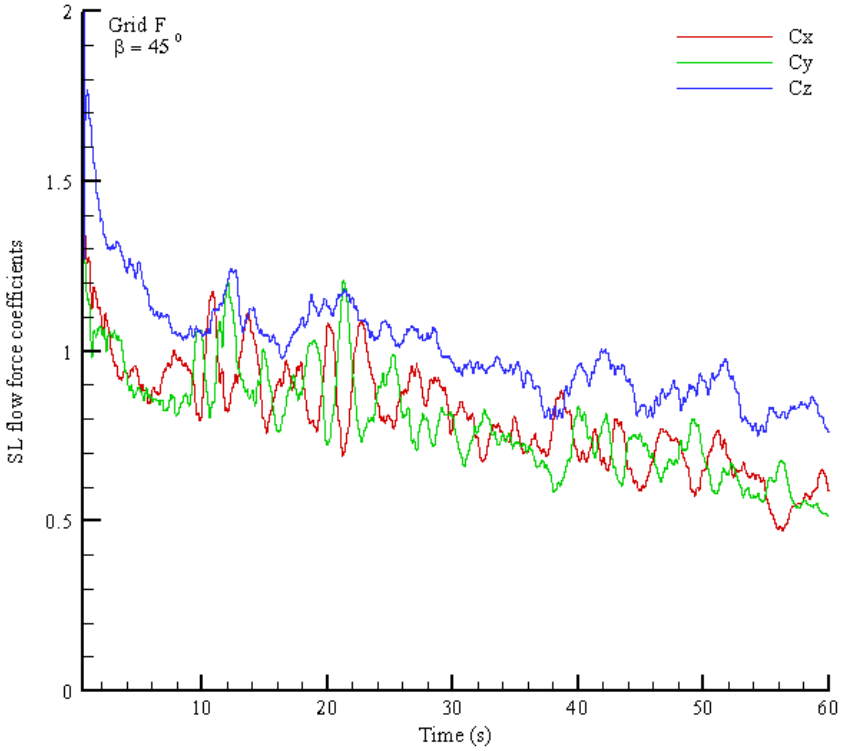

Figure C-2.10 Structure plan area (0.2h x 0.2h), SL flow force coefficients,$\beta = 45^0$

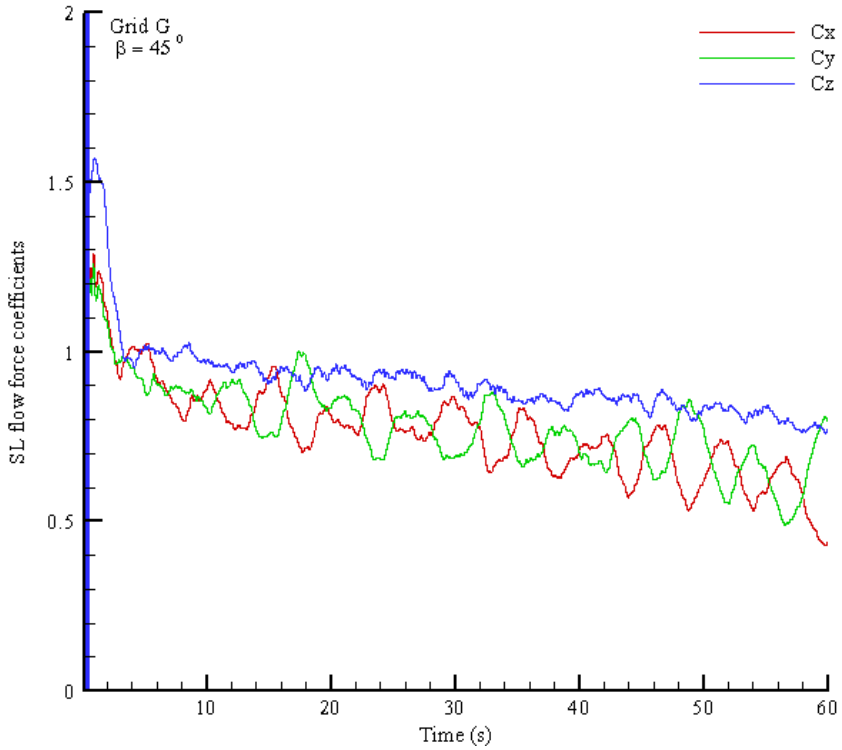

Figure C-2.11 Structure plan area (0.4h x 0.4h), SL flow force coefficients,$\beta = 45^0$

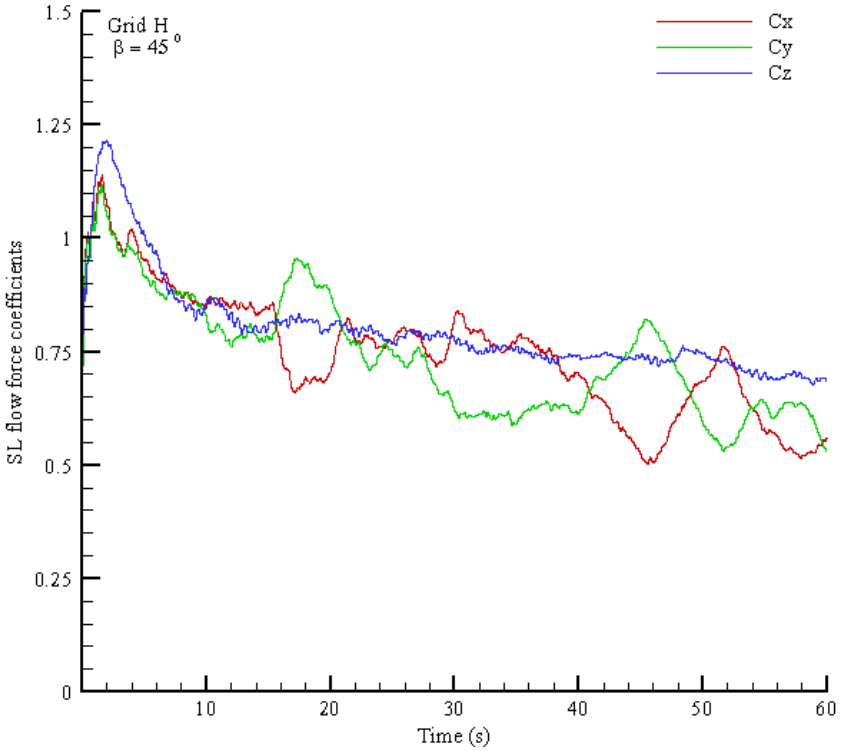

Figure C-2.12 Structure plan area (0.8h x 0.8h), SL flow force coefficients,β = 45^0

C-3 Pressure coefficients (Cp) contour plot on thin structure plan areas

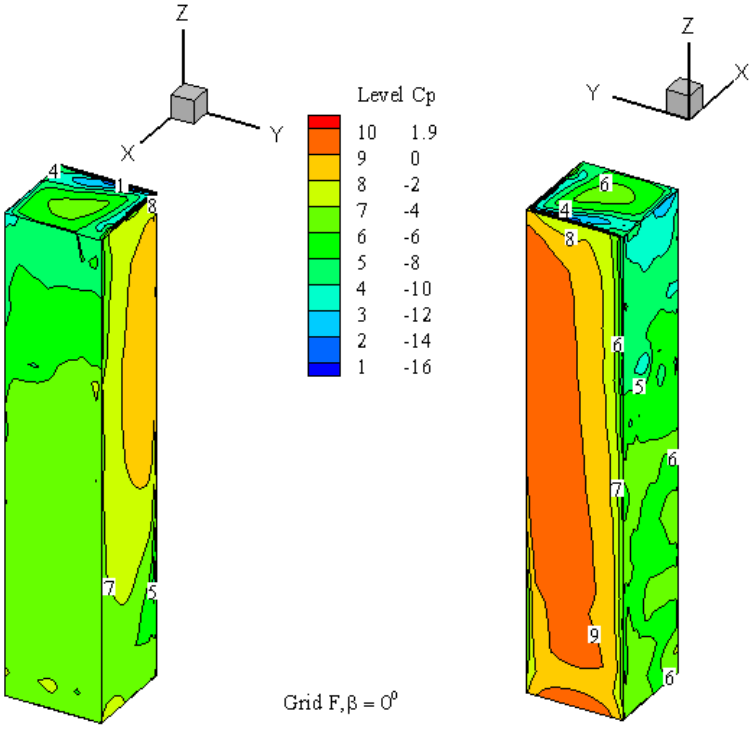

Figure C-3.1 Structure plan area (0.2h x 0.2h), tornado pressure coefficients contour plot, β =0^0

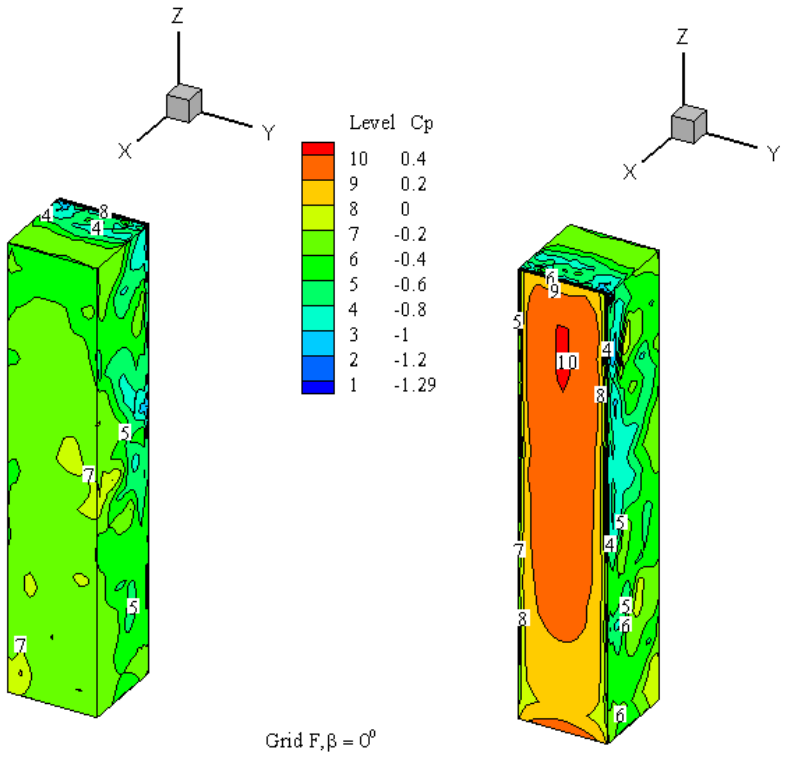

Figure C-3.2 Structure plan area (0.2h x 0.2h), SL flow pressure coefficients contour plot, $\beta = 0^0$

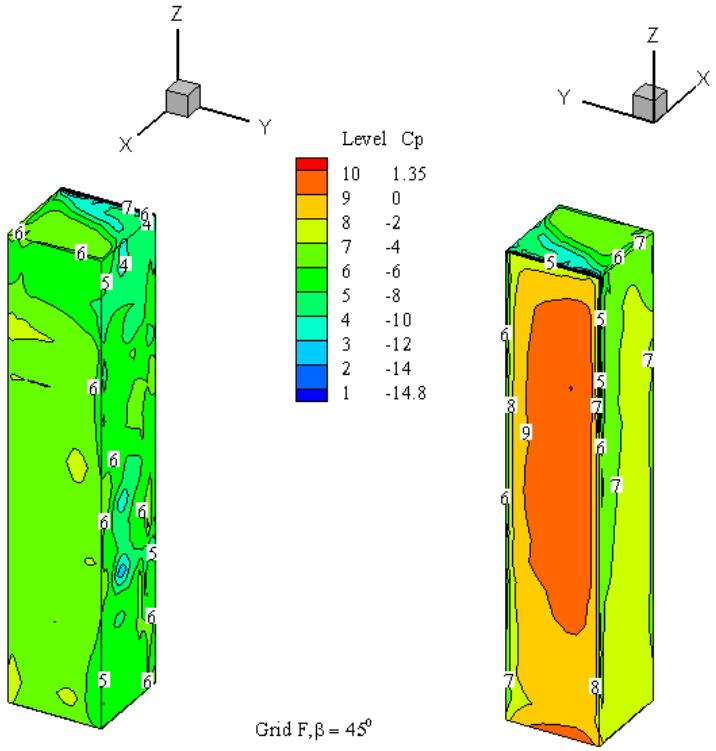

Figure C-3.3 Structure plan area (0.2h x 0.2h), tornado pressure coefficients contour plot, $\beta = 45^0$

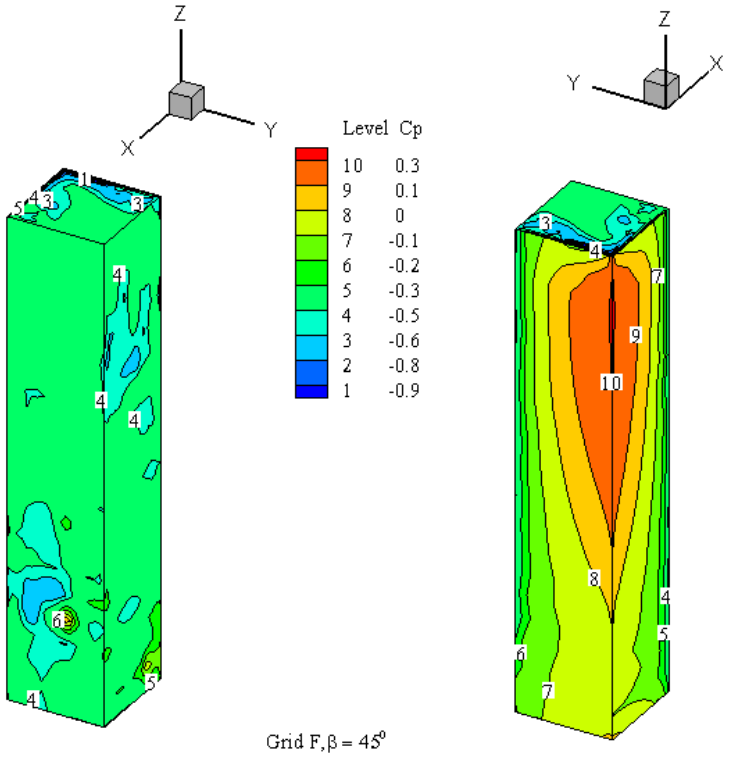

Figure C-3.4 Structure plan area (0.2h x 0.2h), SL flow pressure coefficients contour plot, β =45^0

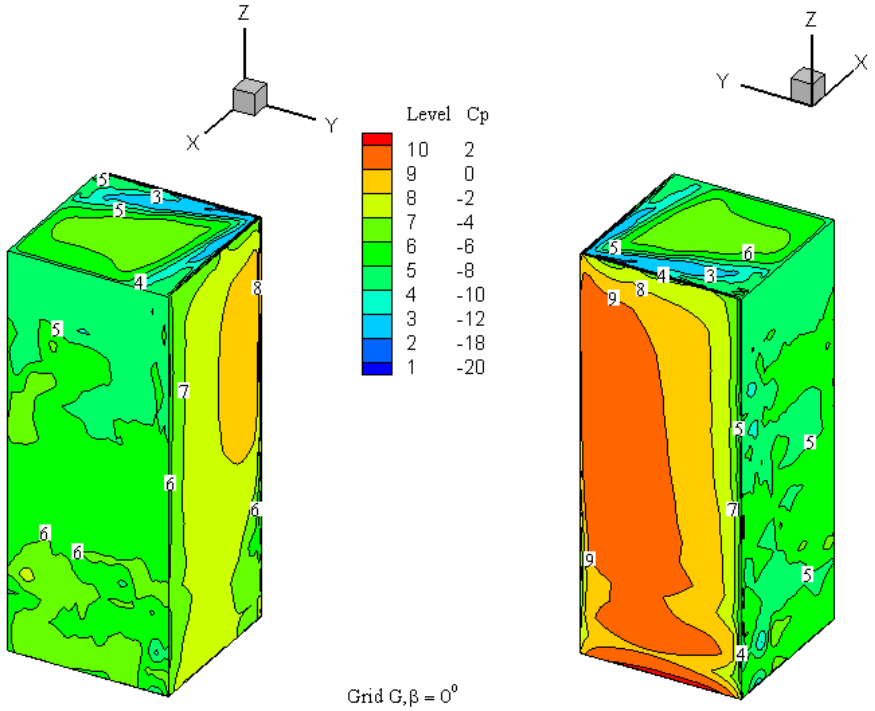

Figure C-3.5 Structure plan area (0.4h x 0.4h), tornado pressure coefficients contour plot, β =0^0

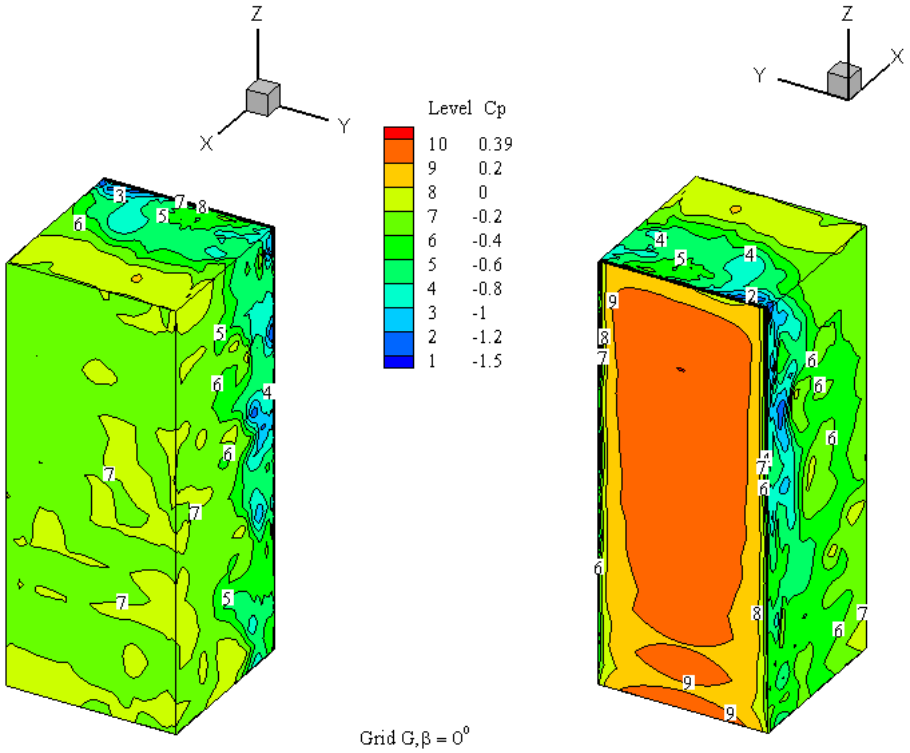

Figure C-3.6 Structure plan area (0.4h x 0.4h), SL flow pressure coefficients contour plot, $\beta = 0^0$

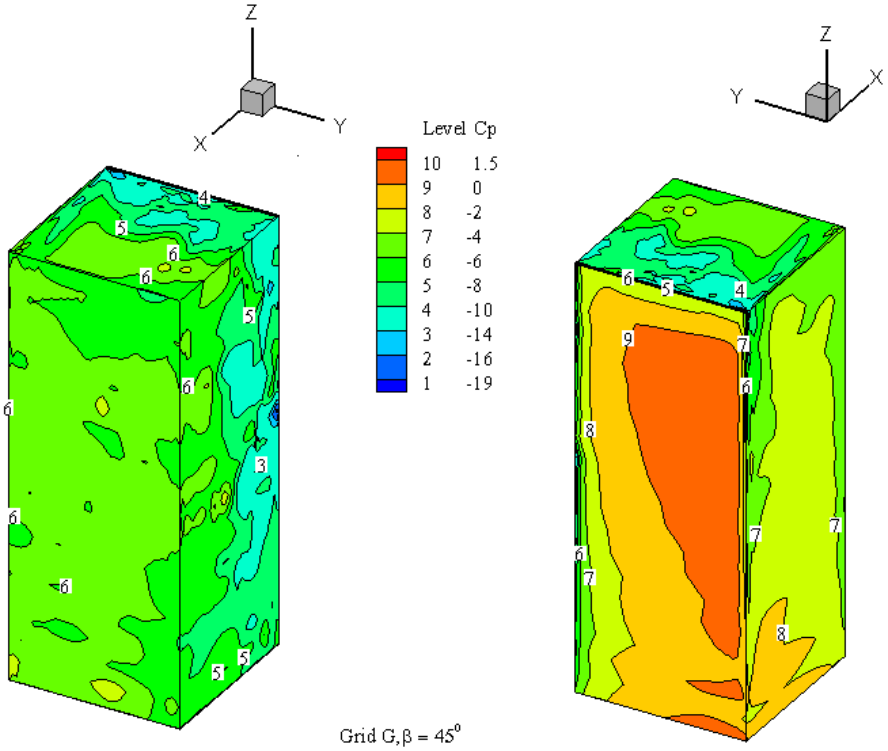

Figure C-3.7 Structure plan area (0.4h x 0.4h), tornado pressure coefficients contour plot, $\beta = 45^0$

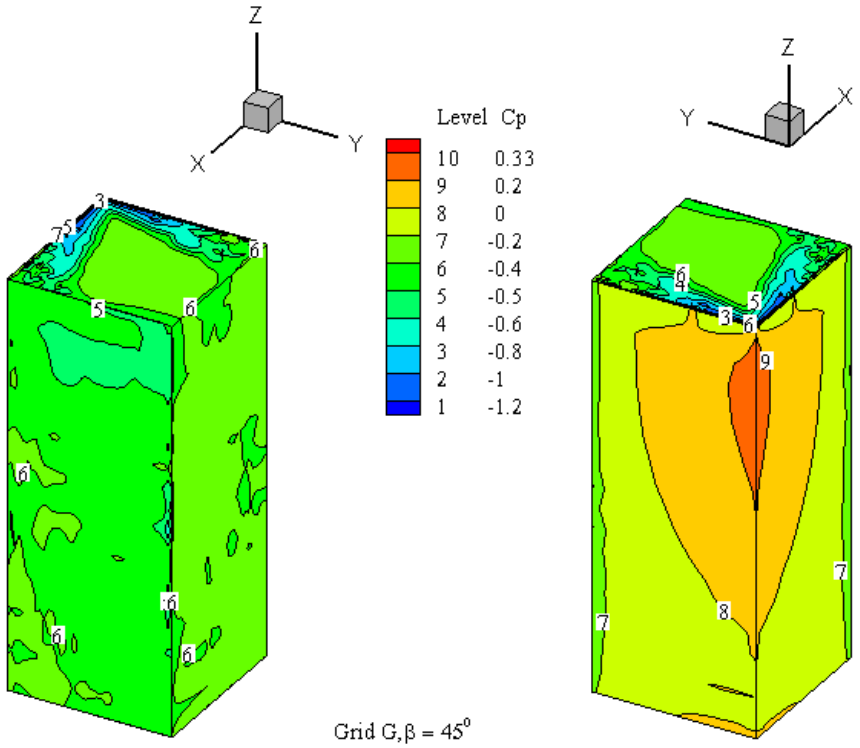

Figure C-3.8 Structure plan area (0.4h x 0.4h), SL flow pressure coefficients contour plot, $\beta = 45^0$

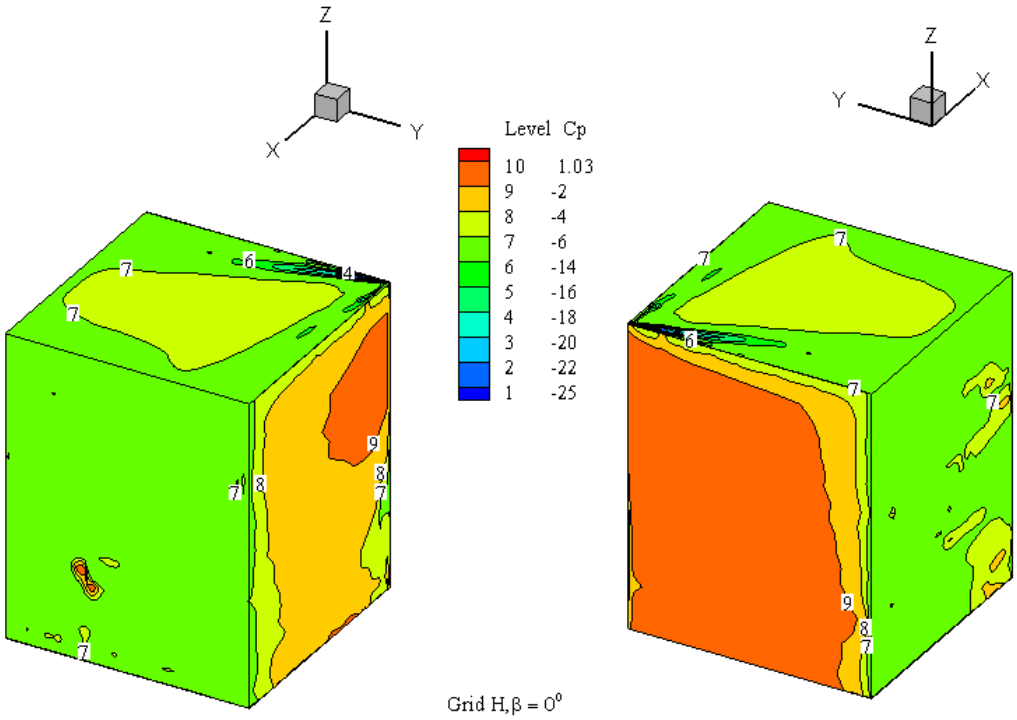

Figure C-3.9 Structure plan area (0.8h x 0.8h), tornado pressure coefficients contour plot, $\beta = 0^0$

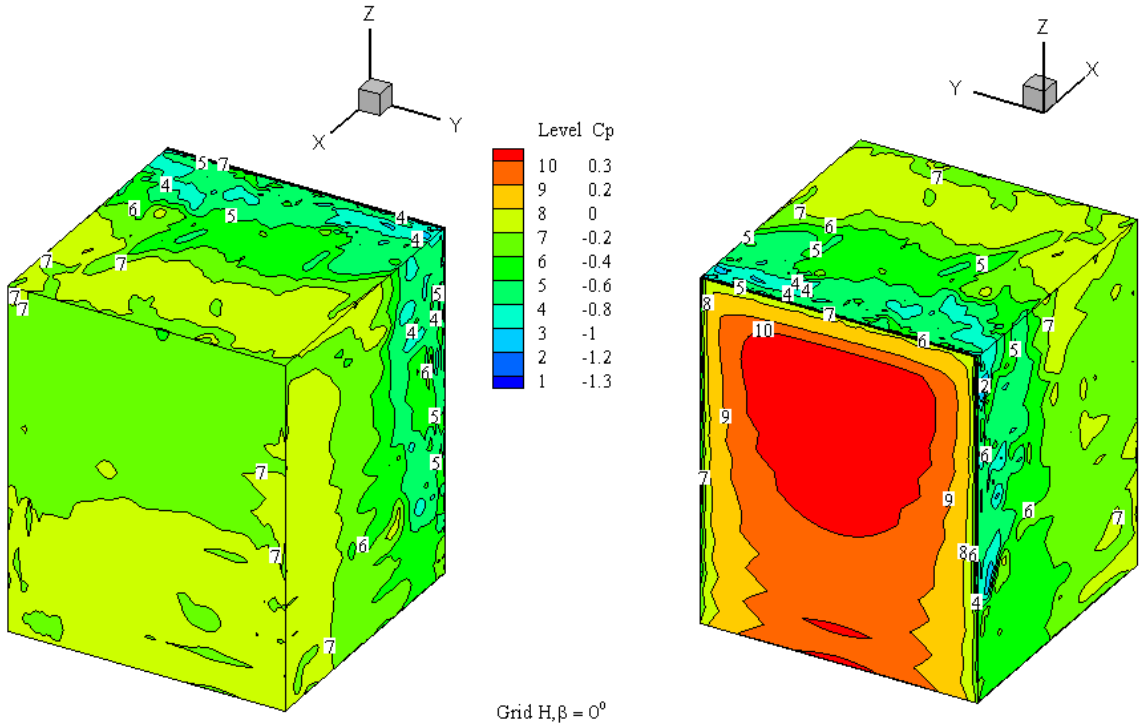

Figure C-3.10 Structure plan area (0.8h x 0.8h), SL flow pressure coefficients contour plot,β=45^0

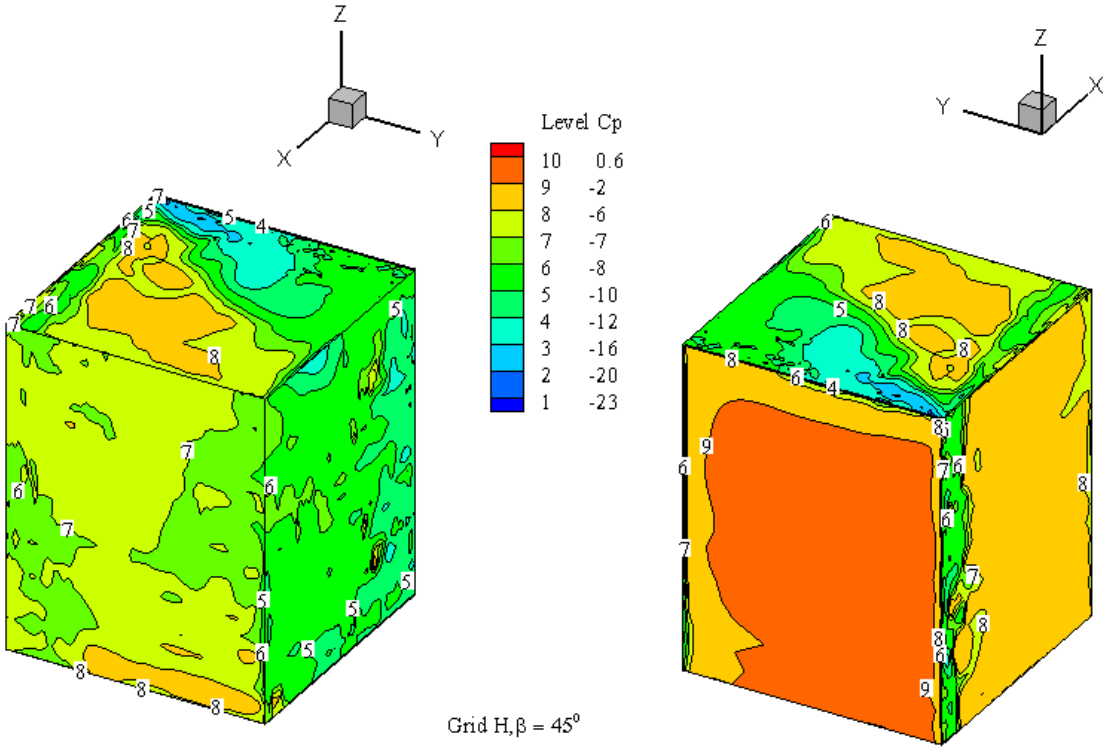

Figure C-3.11 Structure plan area (0.8h x 0.8h), tornado pressure coefficients contour plot, β=45^0

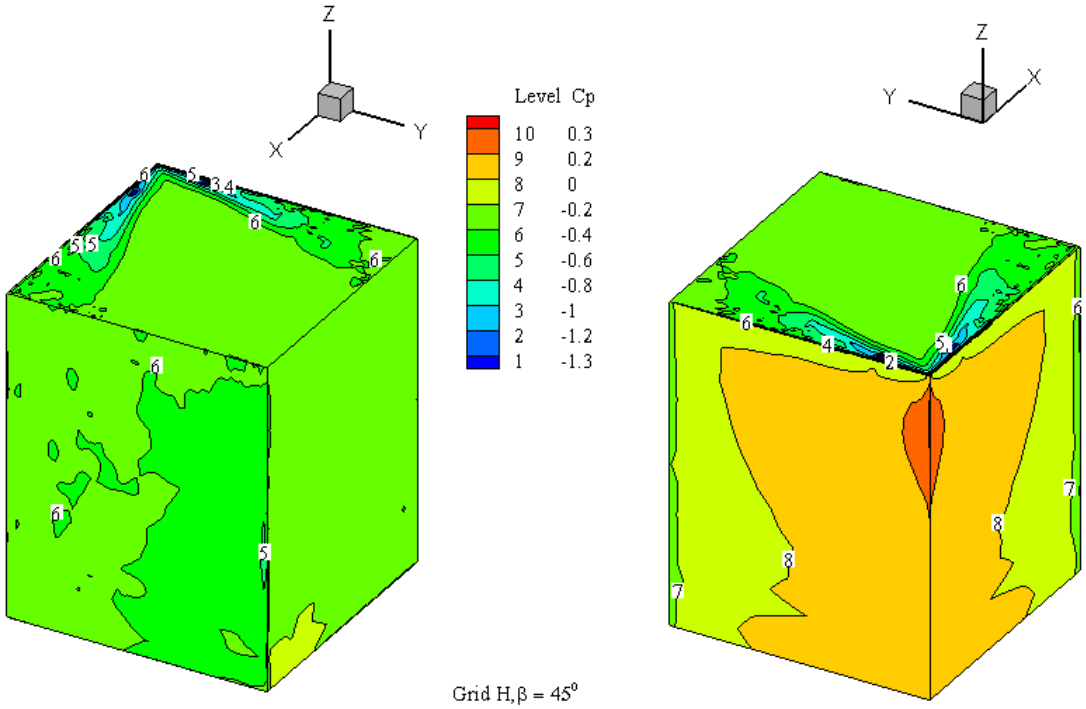

Figure C-3.12 Structure plan area (0.8h x 0.8h), SL flow pressure coefficients contour plot,β=45^0